



SAPIENZA
UNIVERSITÀ DI ROMA

**DOCTORAL RESEARCH IN PHARMACOLOGY AND
TOXICOLOGY: XXXIV^A CYCLE**

Department of Physiology and Pharmacology V. Erspamer

Pharmacological characterization of new compounds
and herbal derivatives for pain and inflammation
treatment

Academic Tutor: Prof. Roberta Lattanzi

Department of Physiology and Pharmacology "Vittorio Erspamer", Sapienza University
of Rome, 00185 Rome, Italy.

Supervisor: Dr. Stefano Pieretti

National Center for Drug Research and Evaluation, Italian National Institute of Health,
00161 Rome, Italy.

PhD Candidate: Paola Minosi

2018-2021

Disclosure

This PhD dissertation has been reviewed by:

Prof. Adriano Mollica

Department of Pharmacy, University of Chieti-Pescara "G. d'Annunzio", 66100 Chieti, Italy.

Prof. Francesco Maione

Department of Pharmacy, School of Medicine and Surgery, University of Naples Federico II, 80131 Naples, Italy.

The work described in this thesis was carried out at National Center for Drug Research and Evaluation, Italian National Institute of Health, Viale Regina Elena 299, 00161 Rome, Italy.

To my loving husband Daniele

And if there is a secret
to do as
you see only the sun
and not
something that doesn't exist.

(Elisa, an Italian Singer-songwriter)

CONTENTS

GENERAL INTRODUCTION	1
CHAPTER 1: Long-Lasting Anti-Inflammatory and Antinociceptive Effects of Acute Ammonium Glycyrrhizinate Administration: Pharmacological, Biochemical, and Docking Studies	15
Abstract.....	16
Introduction	17
Materials and Methods	18
Results	22
Discussion.....	33
CHAPTER 2: Ammonium Glycyrrhizinate Prevents Apoptosis and Mitochondrial Dysfunction Induced by High Glucose in SH-SY5Y Cell Line and Counteracts Neuropathic Pain in Streptozotocin-Induced Diabetic Mice.....	45
Abstract.....	46
Introduction	47
Materials and Methods	49
Results	54
Discussion.....	62
CHAPTER 3: Plant-derived peptides rubiscolin-6, soymorphin-6 and their C-terminal amide derivatives: Pharmacokinetic properties and biological activity	71
Abstract.....	72
Introduction	73
Materials and Methods	75
Results	80
Discussion.....	87
CHAPTER 4: Selective MOR activity of DAPEA and Endomorphin-2 analogues containing a (R)-γ-Freidinger lactam in position two	95
Abstract.....	96
Introduction	97

Materials and Methods	99
Results and Discussion	100
CHAPTER 5: <i>In silico</i> identification of Tripeptides as Lead Compound for the design of KOR.....	119
Abstract.....	120
Introduction	121
Results and Discussion	125
Methods and Materials	136
CHAPTER 6: Discovery of Orexant and Anorexant Agents With Indazole Scaffold Endowed With Peripheral Antiedema Activity	154
Abstract.....	155
Introduction	156
Materials and Methods	161
Results	169
Discussion.....	174
CHAPTER 7: Long-Lasting, Antinociceptive Effects of pH-Sensitive Niosomes Loaded With Ibuprofen in Acute and Chronic Models of Pain.....	185
Abstract.....	186
Introduction	187
Materials and Methods	189
Results	193
Discussion.....	197
GENERAL DISCUSSION.....	204
FINAL CONCLUSION	210
CURRICULUM VITAE	215
ACKNOWLEDGEMENTS.....	222

GENERAL INTRODUCTION

The International Association for the Study of Pain (IASP) define pain as “*An unpleasant sensory and emotional experience associated with, or resembling that associated with, actual or potential tissue damage*” [1].

The perception of pain is subjective and is influenced by many factors [2]. An identical sensory stimulus can elicit quite distinct responses in the same individual under different conditions. Many wounded soldiers, for example, do not feel pain until they have been removed from the battlefield; injured athletes are often not aware of pain until a game is over. Simply put, there are no purely “painful” stimuli, sensory stimuli that invariably elicit the perception of pain in all individuals [2].

When pain is experienced, it can be acute, persistent, or in extreme cases chronic. Persistent pain characterizes many clinical conditions and is usually the reason that patients seek medical attention. In contrast, chronic pain appears to have no useful purpose; it only makes patients miserable [3]. Pain’s highly individual and subjective nature is one of the factors that make it so difficult to define objectively and to treat clinically [4]. Increased pain induced by mild painful stimuli is termed *hyperalgesia*, while pathological pain induced by non-painful stimuli is termed *allodynia* [5]. Both mechanical and thermal allodynia and hyperalgesia can occur as a result of inflammation and central or peripheral nerve injury of various origins (traumatic, toxic), which can occur at any level of the somatosensory or spinothalamic-cortical system [6].

Every pain syndrome has an inflammatory profile consisting of the inflammatory mediators that are present in the pain syndrome. Activation of pain receptors, transmission and modulation of pain signals, neuroplasticity and central sensitization are all one continuum of inflammation and the inflammatory response [7]. Inflammatory events induced by nerve injury play a central role in the pathogenesis of neuropathic pain. These involve inflammatory cells (eg, macrophages), the production of molecules that mediate inflammation (cytokines/interleukins), and the production of nerve growth factor (NGF) [8]. Irrespective of the type of pain whether it is acute or chronic pain, peripheral or central pain, nociceptive or neuropathic pain, the underlying origin is inflammation and the inflammatory response. Activation of pain receptors, transmission and modulation of pain signals, neuro-plasticity and central sensitization

are all one continuum of inflammation and the inflammatory response. Irrespective of the characteristic of the pain, whether it is sharp, dull, aching, burning, stabbing, numbing or tingling, all pain arise from inflammation and the inflammatory response [9]. When peripheral inflammation triggers a neuroinflammatory response involving blood–brain barrier, glia and neurons, that is neuroinflammation [10]. Neuroinflammation is a term used to describe the broad range of immune responses of the central nervous system, differing from peripheral inflammation in a number of ways, primarily concerning the principle cells involved (such as microglia and astrocytes). The blood brain barrier, a highly specialised form of endothelium, was previously thought to completely separate the central nervous system from the peripheral immune system. However, it is not only permeable to pro-inflammatory mediators derived from peripheral inflammation, but can also be stimulated to both release and transmit these mediators and allow leucocyte migration into the brain [11]. This neuroinflammatory response results in synaptic impairment, neuronal death and an exacerbation of several disease pathologies within the brain [12].

Chronic pain due to tissue inflammation, nerve lesion, tumor invasion, or chemotherapy represents a major health problem in the health care system [13]. Chronic pain is among the most common complaints in outpatient clinic [14]. It is estimated that 11–40% of adult population suffers from chronic pain [13,15,16]. Moreover, chronic pain is usually accompanied with emotional changes, including anxiety, depression, or even suicidal tendencies [14].

Therefore, chronic pain dramatically affects the life quality and posts heavy economic and social burdens to the suffering patients. This is partly due to the increase in average life and the consequent aging of the population, and partly to incorrect lifestyles that can lead to obesity, with a consequent increase in other pathologies, such as diabetes which, as a side effect, can lead to the development of neuropathies [17]. Chronic pain patients are at risk of facing pain aggravation due to constrained spatial mobility to seek treatment, shortage of medication supply, access to rehabilitation facilities, which increases pandemic-related stress and mood symptoms. In Italy, there was a light but sustained increase in the prescription of pain medications in the last five years, with a total 2019 expenditure of about 400 million euros for the Italian National Health System [18].

Population estimates for the prevalence of pain, both acute and chronic conditions, vary widely according to age, sex, and hospital or outpatient populations, as well as in the definition of methods [19]. Regarding the hospital population in Italy, the FADOI-DOMINO study, carried out by the Italian Scientific Society FADOI [20], has revealed that pain affected 4 out of 10 patients admitted to Internal Medicine Departments during the hospitalization. Costantini et al [21] performed in 30 public hospitals of the Liguria region, have encountered a 43.1% of pain patients at the time of the interview, and 56.6% of patients declared pain during the previous 24 hours from the survey. Regarding the outpatient population, an observational, multicenter, cross-sectional study from Latina et al [22], conducted in the Latium Region, has shown severe pain in 54% of the 1606 patients of the study sample. Besides, in daily clinical practice, we often witness both situations of chronic pain, and acute-on-chronic pain, as shown from some studies carried out in Emergency Departments [23,24,25].

But added to these problems, there may be new-onset pain associated with the COVID-19 infection itself [26]. In fact, the pandemic has impacted significantly on people who suffer chronic pain. In this case, new-onset chronic pain patients would be added to the health care system, with potential human, ethical, logistical and financial challenges to society. Pain has been proposed to be the result of indirect mechanisms, such as muscle wasting and critical illness neuropathy due to prolonged immobilisation and mechanical ventilation, as well as corticosteroid and neuromuscular blocking drugs use; painful sequelae from neurological complications of the disease (e.g. Guillain-Barre syndrome and stroke); and psychological aspects, specially intensive care-related post-traumatic stress disorder [27,28].

Pharmacologic treatment of pain is complex and requires specific education and clinical training since there are important clinical considerations that physicians may face in daily practice. To achieve optimal outcomes, prescribing decisions should be individualized to ensure the best match between the drug properties and the patient's characteristics [29].

Two types of treatments can be used to treat inflammatory and chronic pain: nonsteroidal anti-inflammatory drugs (NSAIDs) and opioids. In particular, despite the frequency and severity of pain, the available pharmacologic options for inflammatory

pain treatment are not satisfactory, and most of the analgesics currently in use are quite old. Drugs for pain fall into four main categories:

- weak analgesics;
- non-steroidal antiinflammatory drugs (NSAIDs);
- opioids;
- adjuvant drugs (Table 1) [30].

Different drugs with different mechanism(s) of action may be combined for enhanced efficacy.

Table 1: Drugs used in inflammatory pain pharmacologic treatment.

Weak analgesics	Paracetamol
NSAIDs	Ibuprofen, diclofenac, ketoprofen
Opioids	Morphine, Hydrocodone, Fentanyl, Tramadol, Methadone, Oxymorphone
Adjuvant drugs	Antidepressant, antiepileptic medications, corticosteroids, colchicine, neurotrophine, biologic drugs

Paracetamol is the most widely used of the “weak analgesics” and its mechanism of action has not been fully elucidated yet. The analgesic and antipyretic actions of paracetamol are comparable to those of aspirin, but paracetamol is devoid of any antiinflammatory activity. In many guidelines, paracetamol is still considered the analgesic of first choice, and it is usually the preferred drug for long-term treatment [29]. A recent review of clinical guidelines for the management of non-specific low back pain pointed out that paracetamol is not recommended as the first-choice analgesic, as it was for many years, and NSAIDs are preferable [30]. The broad utilization of paracetamol for pain management is mainly due to its allegedly favorable safety profile, especially on the gastrointestinal (GI) tract, and low cost. New evidence increasingly points out a cardiovascular (CV) and GI safety concern in addition to the drug’s well-documented hepatotoxicity [31]. Paracetamol is frequently combined with

opioids for pain relief, and even if combination products offer beneficial incremental pain relief, available clinical studies have demonstrated that this was not superior to NSAIDs in the control of post-surgery pain and correlated with more adverse events [32].

NSAIDs are considered as first choice and effective drugs for inflammatory pain [33,34]. NSAIDs are: analgesic, antipyretic, antiinflammatory and platelet aggregation inhibitors. All actions are mediated by the same mechanism of action: they block prostaglandin production by inhibiting both forms of cyclooxygenase (COX1 and COX2) essential for the synthesis of prostaglandins (PGs) [35]. NSAIDs represent an important pharmacologic choice in the management of inflammatory pain. This class of drugs includes many compounds with clinically relevant differences regarding efficacy and safety. Among the many NSAIDs available, ibuprofen, diclofenac and ketoprofen remain the most frequently used [35]. Primary indications for NSAID treatment include postoperative pain, traumatic pain, acute arthritis, rheumatoid arthritis (RA) and other rheumatic disorders.

However, when NSAIDs and paracetamol are used for a long time, there are several side effects, such as gastrointestinal lesions [36] and nephrotoxicity [37]. Furthermore, some of them, such as ibuprofen, have pharmacokinetic problems. In fact, while ibuprofen is completely absorbed after oral administration [38], the plasma level is still low several hours after topical application [39].

Among the adjuvant agents we find: antidepressant, antiepileptic medications, corticosteroids, colchicine, neurotrophine, biologic drugs [3]. In particular, antiepileptic medications are frequently used as adjuvants for chronic painful conditions; in particular, they address neuropathic pain [40]. Many antiepileptic drugs have been demonstrated to be efficacious in the treatment of post-herpetic neuralgia and the treatment of trigeminal neuralgia, conditions with an inflammatory component [41]. However, most antiepileptic drugs cause some degree of adverse drug reactions. Behavioral side effects associated with antiepileptic drugs are often overlooked, but are a significant consideration. Agitation, aggression, psychosis, behavioral disorders, hyperactivity, and restlessness are some antiepileptic drugs-related behavioral side effects [42].

Finally, opioids remain a mainstay of pain therapy, in particular severe pain, as in the postsurgical setting, and other situations in which NSAIDs or other treatments provide inadequate pain relief [43]. Common side effects of opioid administration include sedation, dizziness, nausea, vomiting, constipation, physical dependence, tolerance, and respiratory depression. Physical dependence and addiction are clinical concerns that may prevent proper prescribing and in turn inadequate pain management. Less common side effects may include delayed gastric emptying, hyperalgesia, immunologic and hormonal dysfunction, muscle rigidity, and myoclonus. The most common side effects of opioid usage are constipation (which has a very high incidence) and nausea. These two side effects can be difficult to manage and frequently tolerance to them does not develop; this is especially true for constipation. In addition, there have been widespread concerns that the use of opioids is increasing at an unwarranted and possibly hazardous rate [44].

Despite the availability of several analgesic options, the effective treatment of pain and inflammation is still a challenge for clinicians, and the balance between efficacy and safety aspects remains both crucial and difficult [29].

In view of this, it is necessary to increase research activities aimed at discovering new drugs and therapies which to provide the patient with the best care and a reasonable quality of life. Thus, the identification of new potential targets which may affect pain and inflammatory processes is becoming an urgent clinical and therapeutic need.

Outline

This thesis aimed at investigating pharmacological profile of novel structures, as part of our program in search for new antinociceptive and anti-inflammatory agents to be used for the treatment of pain and inflammation.

In recent years, in close collaboration with various national (Department of Pharmacy University di Chieti-Pescara “G. D’Annunzio”, Chieti; Department of Medicine, Surgery and Neuroscience, University of Siena; Department of Pharmacy, University of Naples “Federico II”, Naples; Department of Medical Sciences, Section of Pharmacology, University of Ferrara; Department of Drug Chemistry and Technology, Sapienza University of Rome, 00185 Rome, Italy; Department of Pharmacy (DIFAR), University of Genova; NGN Healthcare, Mercogliano) and foreign research groups (Department of Biomolecular Chemistry, Medical University of Lodz, Poland; Jiangxi University of Traditional Chinese Medicine, Chin; Department of Biology, Science Faculty, Konya, Turkey; Institute of Cardiovascular Sciences (ICVS), College of Medical and Dental Sciences, University of Birmingham; Institute of Biochemistry, Biological Research Centre of the Hungarian Academy of Sciences, Hungary; Department of Biochemistry, Sanandaj, Iran; Advanced Pharmaceutics and Drug Delivery Laboratory, University of Toronto, Canada), we have established a systematic, synergistic and highly multidisciplinary approach to study the pharmacological profile of new compounds and herbal derivatives with significant antinociceptive and anti-inflammatory effects.

In fact, in order to discover new drugs and therapies which to provide the patient with the best care and a reasonable quality of life, our work has been based on analyzing the possible antinociceptive and anti-inflammatory activities of natural and synthetic compounds and on alternative drug delivery systems, using *in vitro* and *in vivo* studies. In particular, our national and foreign colleagues worked on molecular modeling, new synthetic methods and chemical profiling, *in silico* and *in vitro* studies (such as antioxidant, enzyme inhibitory studies and docking experiments) for the identification of new compounds’ natural or of synthetic origin. On the other hand, my colleagues and I conducted *in vivo* studies of new compounds and herbal derivatives, using murine models of pain and nociception (CD-1 male mice), under the supervision of Dott.

Stefano Pieretti at National Center for Drug Research and Evaluation of Istituto Superiore di Sanità in Rome.

In the following chapters, we will see you can achieve interesting results using products of different derivation as possible treatments for pain and inflammation: natural, semi-synthetic and synthetic compounds.

Among natural compounds, our attention has been focused on ammonium glycyrrhizinate (AG), glycyrrhizic acid ammonium salt derived from liquorice root, and plant-derived peptides rubiscolin-6, soymorphin-6 and their c-terminal amide derivatives. In **Chapter 1** and in **Chapter 2** we evaluated the potential use of AG for clinical treatment of pain and/or inflammatory-related diseases. In particular, in Chapter 1 we analysed the long-lasting effects induced by AG after a single administration in mice, using murine models of pain and inflammation [45]. In Chapter 2, we analysed the *in vivo* effects of AG in preventing or fighting neuropathic pain in streptozotocin-induced diabetic mice [46].

Then, we evaluated the antinociceptive activities of rubiscolin-6 and soymorphin-6, two natural products, and their C-terminal amides derivatives. In order to investigate the biological and antinociceptive activities of opioid plant-derived peptides soymorphin-6, rubiscolin-6 and their novel C-terminal amides derivatives, my colleagues and I conducted *in vivo* studies using murine models of pain and inflammation, as described in **Chapter 3** [47].

In **Chapter 4** we point our attention to the evaluate pharmacological profile of synthetic novel structures. In particular, we analysed the *in vivo* pharmacological profile of selective MOR activity of DAPEA and Endomorphin-2 analogues containing a (R)- γ -Freidinger lactam in position two [48]. We then tested two synthetic products obtained from *in silico* studies, as reported in **Chapter 5**. In particular, the two compounds obtained in modest yields and excellent purity were also tested *in vivo* using murine models of pain and inflammation [49].

In later time, we have focused our full attention on the endocannabinoid system, that plays an important role in several processes, including feeding behaviour and pain processing [50]. In particular, with the aim to stabilize the CB1 agonist activity we have tested *in vivo* the orexic/anorexic and antinociceptive profiles of a series of lonidamine

joined Leu, tert-Leu and Val amino acids with different C-terminal functional groups (LONI 1-4,11) as reported in **Chapter 6** [51].

Finally, in order to overcome the difficulties associated with the distribution and effectiveness of analgesic drugs, we have focused on alternative drug delivery systems, as described in **Chapter 7**. In particular, we evaluated the analgesic activity of a new pH-sensitive formulation of niosomes containing Polysorbate-20 derivatized by Glycine and loaded with ibuprofen (NioIbu) in several animal models of pain and inflammation [52].

References

1. Raja SN, Carr DB, Cohen M, et al. The revised International Association for the Study of Pain definition of pain: concepts, challenges, and compromises. *Pain*. 2020 Sep 1;161(9):1976-1982.
2. Fenton BW, Shih E, Zolton J. The neurobiology of pain perception in normal and persistent pain. *Pain Manag*. 2015;5(4):297-317.
3. Kandel ER, Schwartz JH, Jessell TM, et al. Principles of neural science, Fifth Edition, Chapter 24/Pain, 530-553.
4. Allegri M, Clark MR, De Andrés J, Jensen TS. Acute and chronic pain: where we are and where we have to go. *Minerva Anesthesiol*. 2012 Feb;78(2):222-35.
5. Jensen TS, Finnerup NB. Allodynia and hyperalgesia in neuropathic pain: clinical manifestations and mechanisms, *Lancet Neurol*. 2014; (13)924–935.
6. Lolignier S, Eijkelkamp N, Wood JN. Mechanical allodynia, *Pflügers Arch. - Eur. J. Physiol*. 2015; (467)133–139.
7. Omoigui S. The biochemical origin of pain: the origin of all pain is inflammation and the inflammatory response. Part 2 of 3 - inflammatory profile of pain syndromes. *Med Hypotheses*. 2007;69(6):1169-78.
8. Tal M. A Role for Inflammation in Chronic Pain. *Curr Rev Pain*. 1999;3(6):440-446.
9. Omoigui S. The biochemical origin of pain: the origin of all pain is inflammation and the inflammatory response. Part 2 of 3 - inflammatory profile of pain syndromes. *Med Hypotheses*. 2007;69(6):1169-1178.
10. Lyman Monty, Lloyd Dafydd G., Ji Xunming, et al. Neuroinflammation: The role and consequences. *Neuroscience Research*. 2014; 79,1-12.
11. Laflamme N, Lacroix S, Rivest S. An essential role of interleukin-1beta in mediating NF-kappaB activity and COX-2 transcription in cells of the blood-brain barrier in response to a systemic and localized inflammation but not during endotoxemia. *The Journal of Neuroscience*. 1999; 19,10923-10930.
12. Kitazawa M, Oddo S, Yamasaki TR, et al. Lipopolysaccharide-induced inflammation exacerbates tau pathology by a cyclin-dependent kinase 5-mediated pathway in a transgenic model of Alzheimer's disease. *The Journal of Neuroscience*. 2005; 25,8843-8853.
13. Dahlhamer J, Lucas J, Zelaya C, et al. Prevalence of chronic pain and high-impact chronic pain among adults - United States, 2016. *MMWR Morb Mortal Wkly Rep*. 2018;67(36):1001–6.
14. Dydyk AM, Conermann T. Chronic pain. Treasure Island (FL): In StatPearls; 2020.
15. Sá KN, Moreira L, Baptista AF, et al. Prevalence of chronic pain in developing countries: Systematic review and meta-analysis. *PAIN Reports*. 2019; (4)e779.
16. GBD (2016). Disease and injury incidence and prevalence collaborators (2017). Global, regional, and national incidence, prevalence, and years lived with disability for 328 diseases and injuries for 195 countries, 1990–2016: A

- systematic analysis for the Global Burden of Disease Study 2016. *Lancet*, 390, 1211– 1259.
17. Okifuji A, Hare BD. The association between chronic pain and obesity. *J Pain Res.* 2015 Jul 14;8:399-408.
 18. Italian Medicines Agency (AIFA). The medicines utilisation monitoring centre. National Report on Medicines use in Italy. Year 2019. Rome, 2020. Available at:<https://www.aifa.gov.it/documents/20142/1205984/rapporto-osmed-2019.pdf/f41e53a4-710a-7f75-4257-404647d0fe1e>.
 19. Mills SEE, Nicolson KP, Smith BH. Chronic pain: a review of its epidemiology and associated factors in population-based studies. *Br J Anaesth.* 2019; 123: 273-283.
 20. Civardi G, Zucco F, Valerio A, et al. Pain management in internal medicine and effects of a standardised educational intervention: the FADOI-DOMINO Study. *Int J Clin Pract.* 2015; 69: 33-40.
 21. Costantini M, Viterbori P, Flego G. Prevalence of pain in Italian Hospitals: results of a regional cross-sectional survey. *J Pain Symptom Manage.* 2002; 23: 221-230.
 22. Latina R, De Marinis MG, Giordano F, et al. Epidemiology of chronic pain in the Latium Region, Italy: a cross-sectional study on the clinical characteristics of patients attending pain clinics. *Pain Manag Nurs.* 2019; 20: 373-381.
 23. Chen E, Tsoy D, Upadhve S, Chan TM. The acute care of chronic pain study: perceptions of acute care providers on chronic pain, a social media-based investigation. *Cureus.* 2018; 10:e2399.
 24. Todd KH, Cowan P, Kelly N, Homel P. Chronic or recurrent pain in the emergency department: national telephone survey of patient experience. *West J Emerg Med.* 2010; 11: 408-415.
 25. Paulin PA, Nelli J, Tremblay S, et al. Chronic pain in the emergency department: a pilot mixed-methods cross-sectional study examining patient characteristics and reasons for presentations. *Pain Res Manag* 2016; 2016: 3092391.
 26. Karos K, McParland JL, Bunzli S, et al. The social threats of COVID-19 for people with chronic pain. *Pain.* 2020; 161, 2229– 2235.] [Treede RD, Rief W, Barke A, et al. A classification of chronic pain for ICD-11. *Pain.* 2015; 156, 1003–1007.
 27. Kemp HI, Corner E, Colvin LA. Chronic pain after COVID-19: Implications for rehabilitation. *British Journal of Anaesthesia.* 2020; 125, 436– 440.
 28. Vittori A, Lerman J, Cascella M, et al. COVID-19 pandemic acute respiratory distress syndrome survivors: Pain after the storm? *Anesthesia and Analgesia.* 2020; 131, 117– 119.
 29. Varrassi G, Alon E, Bagnasco M, et al. Towards an Effective and Safe Treatment of Inflammatory Pain: A Delphi-Guided Expert Consensus. *Adv Ther.* 2019;36(10):2618-2637.

30. Oliveira CB, Maher CG, Pinto RZ, et al. Clinical practice guidelines for the management of non-specific low back pain in primary care: an updated overview. *Eur Spine J.* 2018;27(11):2791–2803.
31. Roberts E, Delgado Nunes V, Buckner S, et al. Paracetamol: not as safe as we thought? A systematic literature review of observational studies. *Ann Rheum Dis.* 2016;75:552–559.
32. Nauta M, Landsmeer ML, Koren G. Codeine-acetaminophen versus nonsteroidal anti-inflammatory drugs in the treatment of post-abdominal surgery pain: a systematic review of randomized trials. *Am J Surg.* 2009;198:256–261.
33. Scarpignato C, Lanas A, Blandizzi C, et al. Safe prescribing of non-steroidal anti-inflammatory drugs in patients with osteoarthritis—an expert consensus addressing benefits as well as gastrointestinal and cardiovascular risks. *BMC Med.* 2015;13:55.
34. Tramér MR, Williams JE, Carroll D, et al. Comparing analgesic efficacy of non-steroidal anti-inflammatory drugs given by different routes in acute and chronic pain: a qualitative systematic review. *Acta Anaesthesiol Scand.* 1998;42:71–79.
35. Sarzi-Puttini P, Atzeni F, Lanata L, Bagnasco M. Efficacy of ketoprofen vs. ibuprofen and diclofenac: a systematic review of the literature and meta-analysis. *Clin Exp Rheumatol.* 2013;31:731–738.
36. Sinha M, Gautam L, Shukla PK, et al. Current perspectives in NSAID-induced gastropathy. *Mediat. Inflamm.* 2013;2013:258209.
37. Musu M, Finco G, Antonucci R, et al. Acute nephrotoxicity of NSAID from the foetus to the adult. *Eur. Rev. Med. Pharmacol. Sci.* 2011;15:1461–1472.
38. Moffat AC, Osselton MD, Widdop B. *Clarke's Analysis of Drugs and Poisons: In Pharmaceuticals, Body Fluids and Postmortem Material*, 2. Pharmaceutical Press and American Pharmacists' Association; London, UK: 2004. p. 1125.
39. Berner G, Engels B, Vögtle-Junkert U. Percutaneous ibuprofen therapy with Trauma-Dolgit gel: Bioequivalence studies. *Drugs Exp. Clin. Res.* 2004;XV:559–564.
40. Attal N, Cruccu G, Haanpää M, et al. EFNS guidelines on pharmacological treatment of neuropathic pain. *Eur J Neurol.* 2006;13:1153–1169.
41. Dickenson AH, Ghandehari J. Anti-convulsants and anti-depressants. *Handb Exp Pharmacol.* 2007;177:145–177.
42. Thigpen J, Miller SE, Pond BB. Behavioral Side Effects of Antiepileptic Drugs. *Pharmacist.* 2013;38(11):HS15-HS20.
43. Rawal N. Current issues in postoperative pain management. *Eur J Anaesthesiol.* 2016 Mar;33(3):160-71.
44. Benyamin R, Trescot AM, Datta S, et al. Opioid complications and side effects. *Pain Physician.* 2008 Mar;11(2 Suppl):S105-20.
45. Maione F, Minosi P, Di Giannuario A, et al. Long-Lasting Anti-Inflammatory and Antinociceptive Effects of Acute Ammonium Glycyrhizinate Administration: Pharmacological, Biochemical, and Docking Studies. *Molecules.* 2019 Jul 4;24(13):2453.

46. Ciarlo L, Marzoli F, Minosi P, et al. Ammonium Glycyrrhizinate Prevents Apoptosis and Mitochondrial Dysfunction Induced by High Glucose in SH-SY5Y Cell Line and Counteracts Neuropathic Pain in Streptozotocin-Induced Diabetic Mice. *Biomedicines*. 2021 May 26;9(6):608.
47. Stefanucci A, Dimmito MP, Tenore G, et al. Plant-derived peptides rubiscolin-6, soymorphin-6 and their c-terminal amide derivatives: Pharmacokinetic properties and biological activity. *Journal of Functional Foods*. 2020; 73, 104154.
48. Della Valle A, Stefanucci A, Scioli G, et al. Selective MOR activity of DAPEA and Endomorphin-2 analogues containing a (R)- γ -Freidinger lactam in position two. *Bioorg Chem*. 2021 Jul 28;115:105219.
49. Stefanucci A, Iobbi V, Della Valle A, et al. In silico Identification of Tripeptides as Lead Compounds for the Design of KOR Ligands. *Molecules*. 2021 Aug 6;26(16):4767.
50. Woodhams SG, Sagar DR, Burston JJ, Chapman V. The role of the endocannabinoid system in pain. *Handb Exp Pharmacol*. 2015;227:119-43.
51. Dimmito MP, Stefanucci A, Pieretti S, et al. Discovery of Orexant and Anorexant Agents with Indazole Scaffold Endowed with Peripheral Antiedema Activity. *Biomolecules*. 2019 Sep 16;9(9).
52. Marzoli F, Marianecchi C, Rinaldi F, et al. Long-Lasting, Antinociceptive Effects of pH-Sensitive Niosomes Loaded with Ibuprofen in Acute and Chronic Models of Pain. *Pharmaceutics*. 2019 Feb 1;11(2).

CHAPTER 1: Long-Lasting Anti-Inflammatory and Antinociceptive Effects of Acute Ammonium Glycyrrhizinate Administration: Pharmacological, Biochemical, and Docking Studies

Francesco Maione¹, Paola Minosi², Amalia Di Giannuario², Federica Raucci¹, Maria Giovanna Chini³, Simona De Vita³, Giuseppe Bifulco³, Nicola Mascolo¹, Stefano Pieretti²

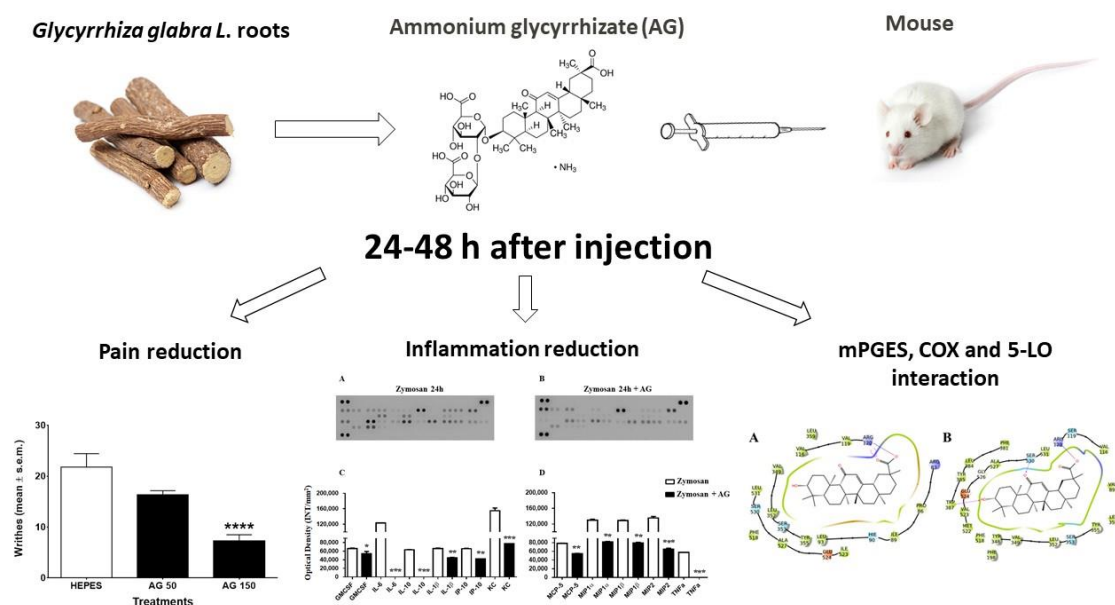
¹ Department of Pharmacy, School of Medicine and Surgery, University of Naples Federico II, 80131 Naples, Italy.

² National Center for Drug Research and Evaluation, Italian National Institute of Health, 00161 Rome, Italy.

³ Department of Pharmacy, University of Salerno, 84084 Fisciano (SA), Italy.

Abstract

The object of the study was to estimate the long-lasting effects induced by ammonium glycyrrhizate (AG) after a single administration in mice using animal models of pain and inflammation together with biochemical and docking studies. A single intraperitoneal injection of AG was able to produce anti-inflammatory effects in zymosan-induced paw edema and peritonitis. Moreover, in several animal models of pain, such as the writhing test, the formalin test, and hyperalgesia induced by zymosan, AG administered 24 h before the tests was able to induce a strong antinociceptive effect. Molecular docking studies revealed that AG possesses higher affinity for microsomal prostaglandin E synthase type-2 compared to type-1, whereas it seems to locate better in the binding pocket of cyclooxygenase (COX)-2 compared to COX-1. These results demonstrated that AG induced anti-inflammatory and antinociceptive effects until 24-48 h after a single administration thanks to its ability to bind the COX/mPGEs pathway. Taken together, all these findings highlight the potential use of AG for clinical treatment of pain and/or inflammatory-related diseases.



Introduction

The most prevalent medical issues strongly affecting people in terms of health and quality of life are acute and chronic pain [1]. Acute and chronic pain are different clinical entities. Acute pain resolves with healing of the underlying injury and it is usually nociceptive, whereas chronic pain is a pathophysiological state connected with the alteration of the peripheral and/or central nervous systems and it is commonly coupled with inflammation caused by tissue trauma, chemical stimuli, and infectious agents. A considerable number of studies have demonstrated that several mediators, including cytokines (Interleukin (IL) -1β , IL-6, IL-17, IL-10, tumor necrosis factor (TNF) $-\alpha$), chemokines (chemokine (CXCL1), Motif Chemokine Ligand (CCL2), C-X-C chemokine receptor type 2 (CXCR2)), lipid mediators (prostaglandins and leukotrienes) and growth factors (nerve growth factor (NGF), and brain-derived neurotrophic factor (BDNF)), play an important role in inflammatory pain [2].

Two types of treatments can be used to treat inflammatory pain: nonsteroidal anti-inflammatory drugs (NSAIDs) and opioids. Very often there are several side effects, such as gastrointestinal lesions [3] and nephrotoxicity [4], in the case of treatment with NSAIDs, when they are used for a long time, and respiratory depression, tolerance, and physical dependence for opioids [5]. Thus, the identification of new potential targets to treat pain without inducing side effects is crucial.

Glycyrrhiza glabra L., commonly known as liquorice, is a perennial, herbaceous shrub, belonging to the family of Leguminosae. This plant is endemic to Mediterranean countries, such as Greece, Spain, and Southern Italy [6]. Liquorice root has been used since prehistoric times. It contains triterpenoid saponins (3–5%), mainly glycyrrhizin, a mix of calcium and potassium salts of 18β -glycyrrhizic acid (also known as glycyrrhizic or glycyrrhizinic acid and a glycoside of glycyrrhetic acid) and flavonoids (1–1.5%) [7,8]. Responsible for the anti-inflammatory effect, owing an indirect strengthening of the glucocorticoid activity, are triterpenes [9]. Liquorice is a herb that people have used for thousands of years to treat a variety of ailments, such as dermatitis, psoriasis, and eczema, and shows comparable efficacy to that of corticosteroids [10,11,12]. In particular, the ammonium salt of glycyrrhizic acid (AG) has strong anti-inflammatory activity [13]. Furthermore it is clear that glycyrrhizin leads to a decrease in inflammatory events due to spinal cord injury (edema, tissue damage, apoptosis, inducible expression of nitric oxide synthase (iNOS)) and nuclear factor kappa-light-

chain-enhancer of activated B cells (NF κ B) activation, improving the recovery of limb function [14].

Antinociceptive effects were also reported for glycyrrhizic acid and derivatives. Disodium glycyrrhethinic acid hemiphthalate significantly suppressed acetic acid-induced writhing responses in mice, with a potency ~12 times higher than acetylsalicylic acid [15]. Glycyrrhizin in mice significantly inhibited the nociception induced by acetic acid and formalin, downregulating the expression levels of TNF- α , IL-6, iNOS, and COX-2 [16]. Recent evidence confirm the anti-inflammatory and antinociceptive effectiveness of glycyrrhizin and suggest that these effects depend upon the glycyrrhizin inhibition of microglial high-mobility group box 1 protein (HMGB1) [17].

The above-mentioned activities were observed in a short time range after administration of AG and AG derivatives. Therefore, in the present study, we investigated the long-lasting anti-inflammatory and antinociceptive effects of AG after a single administration and we have explored its mechanism of action by biochemical and molecular docking studies.

Materials and Methods

Reagents

Ethylenediaminetetraacetate (EDTA), enhanced chemiluminescence detection kit (ECL), and glycyrrhizic acid ammonium salt from glycyrrhiza root ($\geq 95\%$) were purchased from Sigma-Aldrich (Milan, Italy). The proteome profiler mouse cytokine array kit was from R&D System (Abingdon, UK). All the other reagents were from Carlo Erba (Milan, Italy), unless otherwise specified.

Animals and Ethical Statement

We used male CD-1 mice (Harlan, Italy) weighing 25 g in all of the experiments. Mice were housed in colony cages (seven mice per cage) under standard conditions of light, temperature, and relative humidity for at least one week before the start of experimental sessions. Food and water were available ad libitum. All experiments were performed according to Legislative Decree 26/14, which implements the European Directive 2010/63/UE on laboratory animal protection in Italy, and were approved by the local ethics committee. Animal studies are reported in accordance with the ARRIVE (Animal

Research: Reporting of *In vivo* Experiments) guidelines. The research protocol was approved by the Service for Biotechnology and Animal Welfare of the Istituto Superiore di Sanità and authorized by the Italian Ministry of Health.

Edema Induced by Zymosan

Edema was induced with a subcutaneous injection of 2.5% *w/v* zymosan A in saline, in the dorsal surface of the right hind paw (20 μ L/paw). Paw volume was measured three times before the injections and at 1, 2, 3, 4, 24, and 48 h thereafter by the use of hydroplethysmometer specially modified for small volumes (Ugo Basile, Italy). AG (50 or 150 mg/kg) and vehicle (Hepes, 10 mL/kg) were administered intraperitoneally (i.p.) 10 min before zymosan A. The increase in paw volume was evaluated as percentage difference between the paw volume at each time point and the basal paw volume [18].

Writhing Test

Mice were given an intraperitoneal injection of 0.6% *v/v* acetic acid in a volume of 10 mL/kg. Acetic acid induces a series of writhes, consisting in abdominal contraction and hind limb extension [19]. AG (50 or 150 mg/kg) and vehicle (Hepes, 10 mL/kg) were administered i.p. 24 h before acetic acid. After vehicle or AG administration, the number of writhes were recorded over a 20 min period beginning 5 min after acetic acid injection.

Formalin Test

Male mice were split into three groups of ten animals each: vehicle (10 mL/kg, i.p.), AG (50 mg/kg, i.p.) and AG (150 mg/kg, i.p.). One percent formalin in saline was injected into the right mouse hind paw, twenty-four hours after saline and AG i.p. administrations. Formalin aroused nociceptive behavioural responses, such as licking and/or biting the injected paw, which are considered indices of nociception [20]. The nociceptive response showed a biphasic trend: an early phase (from 0 to 10 min after formalin injection) produced by the direct stimulation of peripheral nociceptors, and a late prolonged phase (from 15 to 40 min) which reflected the response to inflammatory pain. The total time the animal spent licking or biting its paw during the early and late phase of formalin-induced nociception was recorded. During the test, the mouse was located in a Plexiglas observation cage (30 \times 14 \times 12 cm) 1 h before the formalin administration to allow it to acclimatize to its surroundings.

Zymosan-Induced Hyperalgesia

In these experiments, AG (50 or 150 mg/kg) and vehicle (Hepes, 10 mL/kg) were administered intraperitoneally (i.p.) 10 min before a subcutaneous injection (20 µL/paw) of zymosan A (2.5% w/v in saline) into the dorsal surface of the right hind paw. Then, hyperalgesia measurements were performed [21]. The plantar test (Ugo Basile, Italy) was used to measure the sensitivity to a noxious heat stimulus with the aim of assessing thermal hyperalgesia after zymosan-induced inflammation of the mouse hind paw. The animals are located in cages with a glass floor covered with transparent plastic boxes and allowed to habituate to their surroundings for at least 1 h in a temperature-controlled room (21 °C) for three consecutive days prior to testing. On the test day, the animals were acclimatized to their environment for at least 1 h before paw withdrawal latency (PWL) was measured. Care was taken to initiate the test when the animal was at rest, not walking, with its hind paw in contact with the glass floor of the test apparatus. A radiant heat source was constantly directed at the mouse footpad until paw withdrawal, foot drumming, licking, or any other aversive action was observed. A timer started automatically when the heat source was activated, and a photocell stopped the timer when the mouse withdrew its hind paw. The heat source on the plantar apparatus was set to an intensity of 30 and a cut-off time of 15 s was used to avoid tissue damage. Animals were first tested to determine their baseline PWL; after zymosan injection, the PWL (seconds) of each animal in response to the plantar test was determined again at 1, 2, 3, 4, 5, 24, and 48 h.

Zymosan Peritonitis

Zymosan peritonitis was induced as previously reported [22,23]. Mice were injected intraperitoneally with 500 mg/kg of zymosan. Animals were killed by CO₂ exposure, peritoneal cavities washed with 3 mL of PBS containing 3 mM EDTA, at different time points. Aliquots of the lavage fluids were then stained with Turk's solution (0.01% crystal violet in 3% acetic acid) and differential counts performed using a Neubauer haemocytometer counting chamber (Thermo Fisher Scientific, Rome, Italy) and a light microscope. Lavage fluids were collected and used to measure the relative expression levels of ~40 cytokines and chemokines using the Mouse Cytokine Array Panel A from R&D System.

Cytokines and Chemokines Protein Array

Equal volumes (1.5 mL) of the peritoneal inflammatory fluids obtained at different time points (4 and 24 h) after the treatment with zymosan (500 mg/kg) or zymosan plus AG (150 mg/kg) were incubated with the precoated proteome profiler array membranes according to the manufacturer's instructions. Dot plots were detected by using ECL detection kit and ImageQuant 400 GE Healthcare (GE Healthcare Europe GmbH, Milan, Italy) and successively quantified as optical density (INT/mm²) using GS 800 imaging densitometer software (Bio-Rad Laboratories, Milan, Italy) as previously described [24].

Molecular Docking Input Files Preparation

The crystal structure of mPGES1 in complex with inhibitors (5TL9) [25], mPGES-2 in complex with indomethacin (1Z9H) [24], COX-1 in complex with mofezolac (5WBE) [26], COX-2 in complex with meclofenamic acid (5IKQ) [27], and 5-lipoxygenase (3V99) [28] were used as molecular targets for the docking studies. All the protein 3D structures were produced using the Schrödinger Protein Preparation Wizard workflow [29]. First, all missing hydrogen atoms were added, bond orders were properly assigned, partial charges calculated, water molecules were eliminated, and protein termini were capped. Glycyrrhizic acid was built with Maestro's Build Panel (Maestro version 10.2, 2015), processed with LigPrep (LigPrep version 3.4, 2015) and, finally, minimized with the OPLS 2005 force field [30].

Docking Experiments

The cocrystallized inhibitors were used to generate the grid necessary for the molecular docking experiments, using the following coordinates: 10.75 (x), 15.07 (y), 28.45 (z) for mPGES-1; -21.10 (x), 54.51 (y), 11.75 (z) for mPGES-2; 19.34 (x), 2.67 (y), 31.22 (z) for COX-1; 24.25 (x), 3.52 (y), 33.07 (z) for COX-2; 9.21 (x), -82.00 (y), -32.69 (z) for 5-LO. The boundaries of the inner box were extended of 10 Å for COX-1 and mPGES1 and 13 Å for mPGES-2 and COX-2 in the three directions of space. Regarding 5-LO, in both calculations, the centre of the grid was set close to Asn544 and, in the rigid docking approach, the outer box boundaries were set at 40 Å from it. For the *in silico* docking experiments, the software Glide [31,32,33] was used. In the rigid docking approach, in a preliminary phase, in standard precision (SP) mode, 10,000 ligand poses were kept, and the best 800 poses were selected for energy minimization. Once the minimization was completed, only one output structure was saved for each ligand. After

this phase, a post-docking optimization of the obtained molecules was carried out, setting the rejection cut-off at 0.5 kcal/mol and a maximum of ten poses per ligand were kept. The poses generated in the initial phase, were submitted to a second optimizations phase in extra precision glide (XP) mode. In this last phase, the post-docking optimization of the docking poses was performed accounting for a maximum of ten poses with the same parameters for the selection of initial poses and rejection cut off used during the SP docking experiments. The induced fit docking was carried out using the same settings of the rigid docking XP mode, but allowing a certain degree of flexibility to amino acids of the catalytic pocket. The first step consists in docking the ligand in the binding site with Glide [31,32,33]; then, the protein side chains are re-oriented with Prime [34,35] with the aim of better accommodating the molecule. At the last stage, a second rigid docking inside the new cavity is carried out.

Data Analysis and Statistics

The results achieved are given as the mean \pm SEM. Statistical analysis was carried out by using one-way ANOVA followed by Dunnett's post-test when comparing more than two groups. In certain cases, one sample *t*-test was used to evaluate significance against the hypothetical zero value. Statistical analysis was conducted by using GraphPad Prism 6.0 software (San Diego, CA, USA). Data were considered statistically significant when a value of $p < 0.05$ was achieved. The data and statistical analysis comply with the recommendations on experimental design and analysis [36].

Results

Edema Induced by Zymosan

In animals treated with vehicle (Hepes, 10 mL/kg, i.p.) 10 min before zymosan, we discovered a rise in paw volume that achieved the maximal value 3–4 h after the injection, followed by a slight reduction in the following 48 h (Figure 1). In this set of experiments, we noticed significant differences in the behavioral responses between treatments ($F_{2,33} = 16.30, p < 0.0001$) and in the time elapsed after zymosan administration ($F_{5,165} = 38.59, p < 0.0001$). The i.p. administration of AG at the dose of 50 mg/kg 10 min before zymosan generated a considerable reduction of paw edema induced by zymosan injection, from 1 to 3 h after zymosan injection (Figure 1). The i.p. administration of AG at the dose of 150 mg/kg induced a robust reduction of paw edema starting from 1 h and lasting for the full course of treatment (Figure 1).

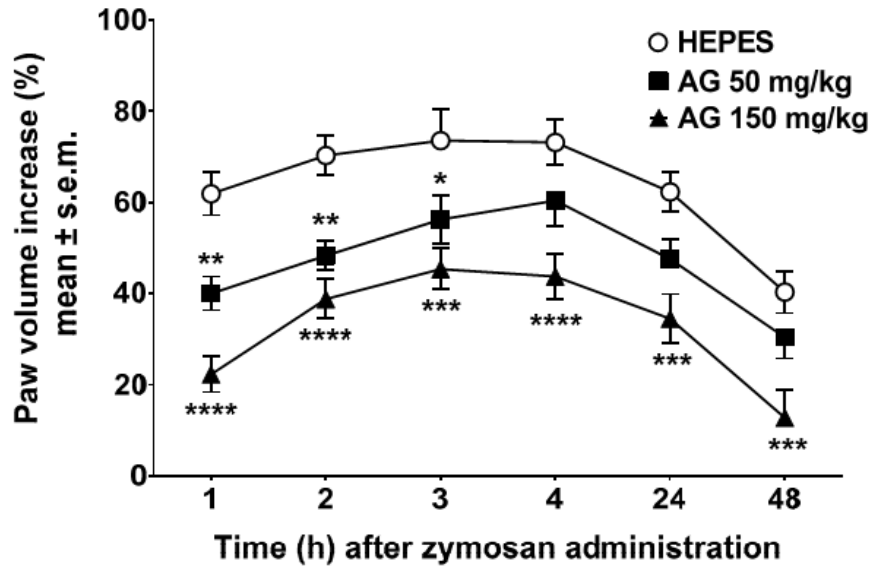


Figure 1. Zymosan-induced paw edema. Effects induced by vehicle (Hepes, 10 mL/kg, intraperitoneally (i.p.)) and ammonium glycyrrhizate (AG, 50 or 150 mg/kg, i.p.) administered 10 min before zymosan (2.5% *w/v* in saline, 20 μ L/paw). * denotes $p < 0.05$, ** denotes $p < 0.01$, *** denotes $p < 0.001$ and **** denotes $p < 0.0001$ vs. Vehicle. $n = 12$.

Writhing Test

The antinociceptive effect of AG in acetic acid writhing test is shown in Figure 2. Statistical analysis revealed significant differences between treatments ($F_{2,24} = 17.69$, $p < 0.0001$). In this test, AG administered i.p. at the dose of 50 mg/kg reduced writhes induced by acetic acid. Severe inhibition of the number of writhes was discovered when AG was administered at the dose of 150 mg/kg.

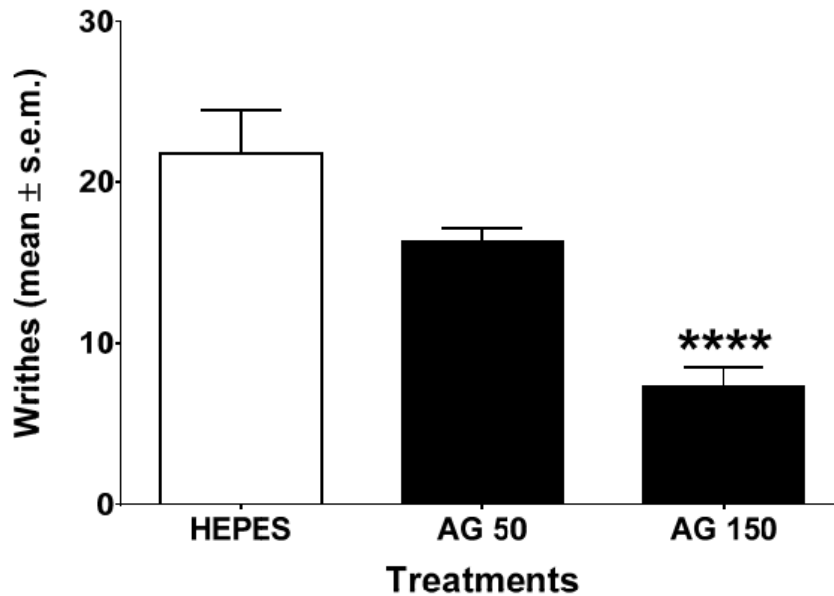


Figure 2. Writhing test. Effects induced by vehicle (Hepes, 10 mL/kg, intraperitoneally (i.p.)) and ammonium glycyrrhizate (AG, 50 or 150 mg/kg, i.p.) administered 24 h before acetic acid (0.6% *v/v* in salina, 10 mL/kg, i.p.). **** denotes $p < 0.0001$ vs. Vehicle. $n = 9$.

Formalin Test

Subcutaneous injection of formalin induced a nociceptive behavioural response that showed a biphasic trend. There was an early phase (from 0 to 10 min after formalin injection) produced by the direct stimulation of peripheral nociceptors, and a late prolonged phase (from 15 to 40 min) which reflected the response to inflammatory pain. The total time the animal spent licking or biting its paw during the early and late phase of formalin-induced nociception was recorded. The results obtained in these experiments are reported in Figure 3. The administration of AG at the dose of 50 or 150 mg/kg i.p. 24 h before formalin, did not modify the nociceptive response induced by aldehyde in the early phase of the test ($F_{2,27} = 2.903, p > 0.05$). A considerable decrease of the formalin-induced licking and biting activity was instead observed in the late phase of the test ($F_{2,27} = 24.69, p < 0.0001$). When the confront was restricted to two means, AG administered at the dose of 50 mg/kg induced a light but nonsignificant reduction of formalin-induced behaviour ($p > 0.05$) in the late phase. On the contrary, AG administered at the dose of 150 mg/kg strongly reduced the nociceptive behavior induced by formalin ($p < 0.0001$).

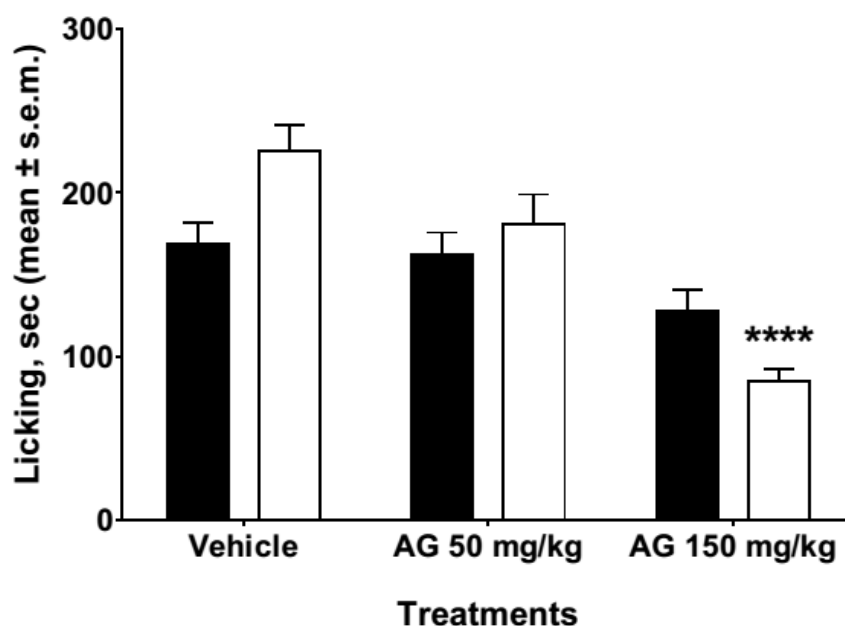


Figure 3. Formalin test. Effects induced by vehicle (Hepes, 10 mL/kg, i.p.) and ammonium glycyrrhizate (AG, 50 or 150 mg/kg, i.p.) administered 24 h before formalin (1% in saline, 20 μ L/paw) in the formalin test. Black bars represent the early phase and the white bars represent the late phase of the formalin test. **** is for $p < 0.0001$ vs. Vehicle. $n = 10$.

Zymosan-Induced Hyperalgesia

This experimental pain model is characterized by the measurements of time-dependent hyperalgesia after zymosan administration. This measurement is equivalent to time-dependent reduction in the latency to respond to the thermal stimuli applied to the injected paw compared with the baseline measurements. In particular, 20 μ L of zymosan A (2.5% w/v in saline) was administered s.c. into the dorsal surface of one hind paw.

In our experiments, treatments were given i.p. 10 min before the first measurement of the pain threshold, i.e., 1 h after zymosan administration. Figure 4 shows the results of these experiments. With the use of two-way ANOVA, we can notice that there are significant differences in treatments ($F_{2,27} = 6.901, p < 0.01$) and in the time point when pain threshold was recorded ($F_{5,135} = 30.51, p < 0.0001$). Tukey's multiple comparison test showed significant differences from 1 to 24 h after zymosan administration between animals treated with AG at the dose of 150 mg/kg, i.p. and those

deal with vehicle. AG administered at low dose (50 mg/kg, i.p) induced a light but nonsignificant increase in pain threshold (Figure 4).

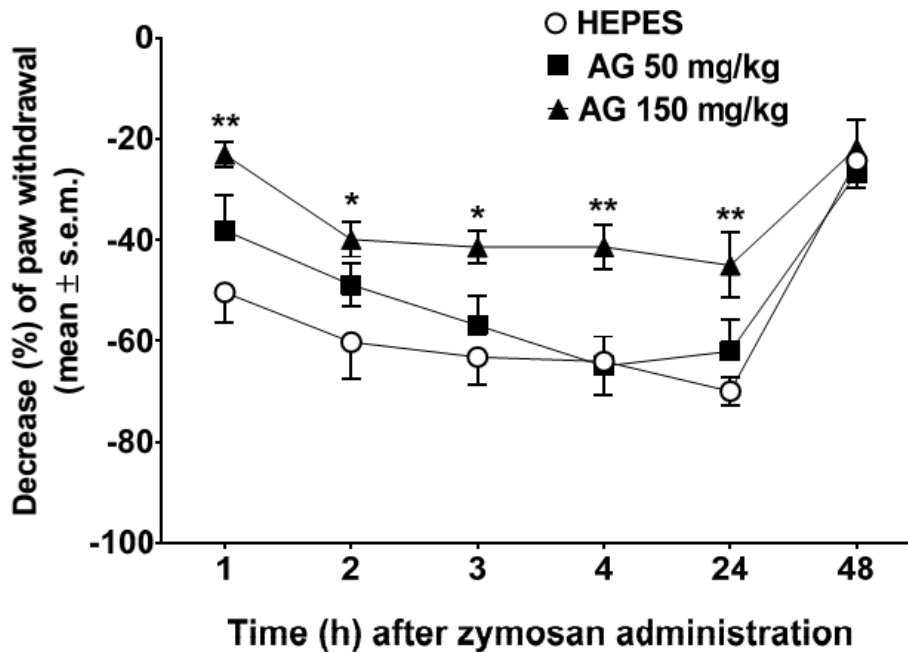


Figure 4. Zymosan-induced hyperalgesia. Effects induced by vehicle (Hepes, 10 mL/kg, intraperitoneally (i.p.)) and ammonium glycyrrhizate (AG, 50 or 150 mg/kg, i.p.) administered 10 min before zymosan (2.5% w/v in saline, 20 μ L/paw). * denotes $p < 0.05$ and ** denotes $p < 0.01$ vs. Vehicle. $n = 10$.

Zymosan Peritonitis and Cytokines-Chemokines Protein Array

To investigate the molecular mechanisms behind the selective long-lasting anti-inflammatory and antinociceptive effects of AG, we firstly compared the recruitment of total inflammatory cells and the cytokines and chemokines profiles of collected inflammatory fluids obtained from mice receiving zymosan and zymosan plus AG at 4 and 24 h. As shown in Figure 5a, 4 h after zymosan (500 mg/kg) or zymosan + AG (150 mg/kg) injection, mice exhibited no significant difference in the number of recruited inflammatory leukocytes. In contrast, at 24 h, mice receiving AG (150 mg/kg) showed a marked decrease ($p < 0.01$) in the number of inflammatory infiltrates compared to zymosan-treated mice (Figure 5b). Administration of AG at 50 and 150 mg/kg did not show any significant effect, both at 4 and 24 h (data not shown). Contingently, as shown in Figure 6, zymosan administration at 4 h caused a massive production of cyto/chemokines (Figure 6a) that was not counterbalanced in AG-treated mice (Figure 6b), except for macrophage inflammatory proteins (MIP)-1 α and keratinocyte

chemoattractant (KC) production and with a less extent IL-6, SDF-1 and TNF- α (Figure 6c). Interestingly, comparison of the inflammatory profile of fluids from zymosan (Figure 7a) and zymosan + AG (Figure 7b) at 24 h revealed a striking difference in the semiquantitative levels of IL-6, IL-10, IL-1 β , IP-10, KC, MCP-5, macrophage inflammatory proteins (MIP) 1- α , 1- β , 2, and TNF- α (Figure 7c,d).

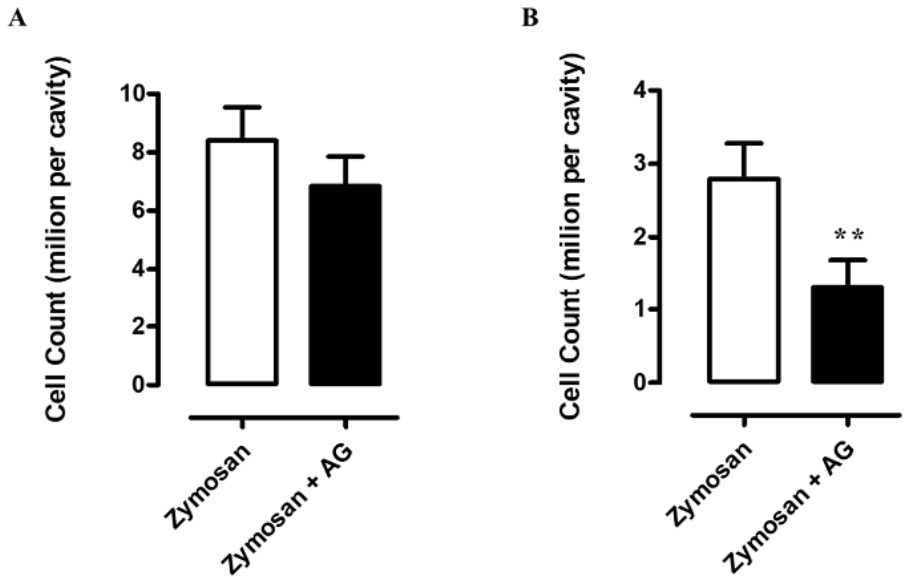


Figure 5. (A) Cell infiltration into mouse peritoneal cavity of mice that have received an intraperitoneal (i.p.) injection of zymosan (500 mg/kg) or zymosan + AG (150 mg/kg) at 4 and (B) 24 h. Bars represent group mean values \pm Standard Error of the Mean (S.E.M) of three separate experiments with $n = 7$ mice. ** $p < 0.01$ vs. zymosan-treated mice.

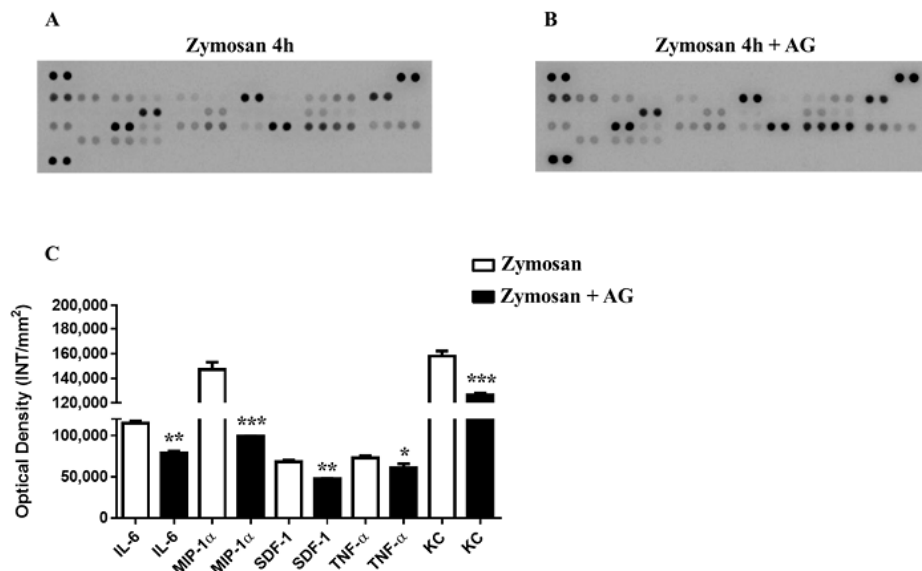


Figure 6. (A) Inflammatory fluids in zymosan and zymosan + AG-injected mice at 4 h. Inflammatory fluids obtained from peritoneal cavities were assayed using a proteome profiler cytokine array. Mean changes (\pm S.E.M) between zymosan (500 mg/kg) and (B) zymosan + AG-injected mice (150 mg/kg) of three separate experiments with $n = 7$ mice, (C) are expressed as increase in the optical density (INT/mm²) between the two groups. * $p < 0.05$, ** $p < 0.01$ and *** $p < 0.001$ vs. zymosan-treated mice.

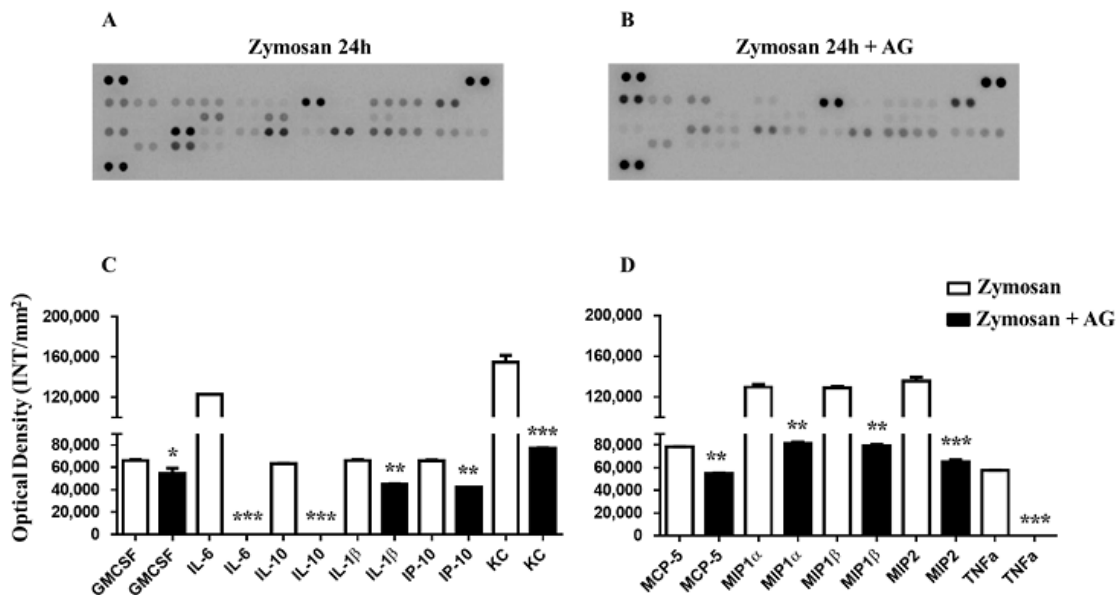


Figure 7. (A) Inflammatory fluids in zymosan and zymosan + AG-injected mice at 24 h. Inflammatory fluids obtained from peritoneal cavities were assayed using a proteome profiler cytokine array. (B) Mean changes (\pm S.E.M) between zymosan (500 mg/kg) and zymosan + AG-injected mice (150 mg/kg) of three separate experiments with $n = 7$ mice, (C, D) are expressed as increase in the optical density (INT/mm²) between the two groups. * $p < 0.05$, ** $p < 0.01$ and *** $p < 0.001$ vs. zymosan-treated mice.

Docking Experiments

The molecular docking studies were used to evaluate and to rationalize the anti-inflammatory activity of glycyrrhizic acid towards some key enzymes of the arachidonic acid cascade such as 5-lipoxygenase (5-LO), 5-lipoxygenase-activating protein (FLAP), microsomal prostaglandin E synthase 1 and 2 (mPGES-1 and mPGES-2), and COX-1 and COX-2, responsible for leukotrienes (LTs) and prostaglandin (PG) biosynthesis, respectively. These enzymes are involved in the generation of inflammatory mediators and their role in the progression of inflammation is well-established; therefore, they were suitable targets for the study of the glycyrrhizic acid anti-inflammatory activity.

mPGES-1 and mPGES-2

Prostaglandin E₂ (PGE₂) is one of the key mediators of inflammation and it is synthesized by members of the prostaglandin E synthase (PGESs) family from the unstable prostaglandin H₂ (PGH₂). The most known and studied isoforms are mPGES-1 and mPGES-2; the first one is an inducible isoform, whereas mPGES-2 is constitutively expressed [37]. They differ also in tissue localization, with mPGES-1 mainly expressed in lung, kidney, and reproductive organs and mPGES-2 mainly expressed in heart and brain [37,38]. Key amino acids for the binding are: Arg38, Asp49, Arg52, His53, Arg70, Arg73, Asn74, Glu77, Arg110, Leu121, Arg122, Arg126, Ser127, Ile125, Thr129, and Tyr130 for mPGES-1 [39,40,41,42], and Cys110, His241, His244, Ser247, Arg292, and Arg296 for mPGES-2 [43]. Molecular docking experiments involving both microsomal prostaglandin E synthase proteins revealed that AG has a higher affinity for mPGES-2 than mPGES-1. In particular, in the case of mPGES-1, the only interaction shown is one H-bond between the OH group and Arg52 and His53 on chain B. Regarding mPGES-2, instead, the three polar groups of AG are all involved in H-bonds with the target. In more detail:

- The OH group interacts both with the side chain and the backbone of Thr109,
- The carbonyl group interacts with Ser247, and
- The carboxyl group forms an H-bond and a salt bridge with Arg296 (Figure 8 and Figure 9).

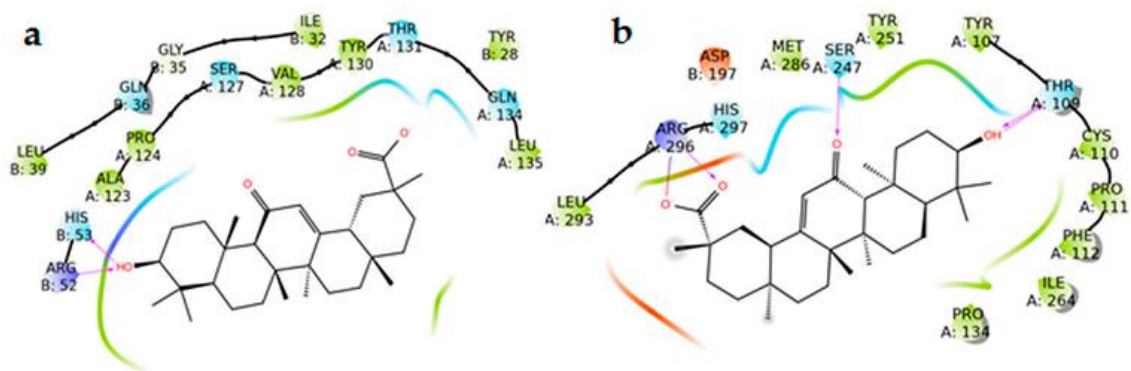


Figure 8. (a) 2D panels represent the interactions between AG with the microsomal prostaglandin E synthase 1 (mPGES-1) and 2 (mPGES-2) (b) binding sites. Positively charged residues are colored violet, negatively charged residues are colored red, polar residues are colored light blue, hydrophobic residues are colored green. Red-to-blue lines represent salt bridges and H-bonds (side chain) are reported as dotted pink arrows.

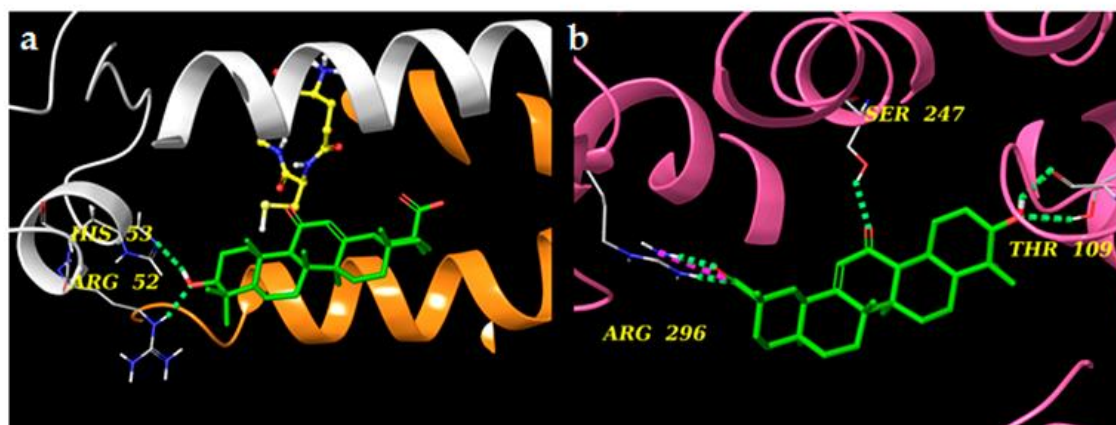


Figure 9. (a) 3D models of AG (colored by atom types: C green, O red, polar H white) in the binding site of microsomal prostaglandin E synthase 1 (mPGES-1) (panel a, chain A and chain B are reported in orange and white ribbons, respectively) and (b) microsomal prostaglandin E synthase 2 (mPGES-2) (chain A is reported in pink ribbons). Green dotted lines represent H-bonds and pink dotted lines represent salt bridges.

COX-1 and COX-2

Cyclooxygenases are the starting point in the production of eicosanoids, as they convert fatty acids into PGH₂. Like mPGESs, they are present in two main isoforms: COX-1, which is constitutively expressed, and COX-2, which is inducible [26,44]. COX-1 and COX-2 monomers consist of three different domains: the EGF domain, the membrane-

binding domain, and the catalytic domain containing the catalytic triad Arg120, Tyr355, and Glu524. Among these, the catalytic domain represents the main target for NSAID and, particularly, Arg120, Tyr355, Tyr385, Ser530, and Arg513 are essential for the inhibitory activity [45]. The study of the interaction between AG and the two isoforms of COX required a flexible docking approach (induced fit) [46] to allow the entrance of the ligand into the catalytic site of the enzymes. AG seems to locate better in the binding pocket of COX-2 as it interacts with key amino acids such as Trp387 and Ser530 (H-bonds) and Arg120 (salt bridge). In the case of COX-1, on the other hand, AG forms H-bonds and a salt bridge with Arg120 that do not reach the inner part of the binding pocket (Figure 10 and Figure 11). These data suggest a preference of glycyrrhetic acid (AG) for isoform 2 of COX.

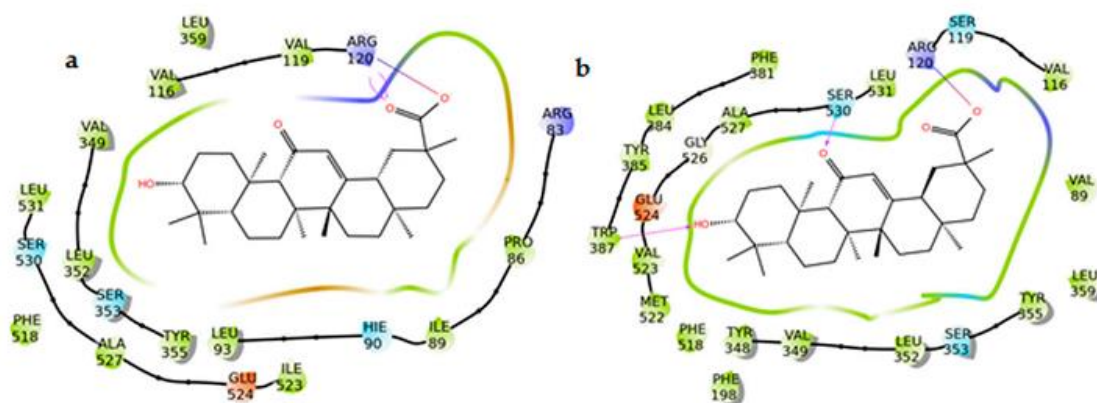


Figure 10. (a) 2D panels represent the interactions between AG with cyclooxygenase 1 (COX-1) and (b) cyclooxygenase 2 (COX-2) binding sites. Positively charged residues are colored violet, negatively charged residues are colored red, polar residues are colored light blue, hydrophobic residues are colored green. Red-to-blue lines represent salt bridges and H-bonds (side chain) are reported as dotted pink arrows. Neutral histidine with hydrogen on the δ nitrogen is shown as HIE.

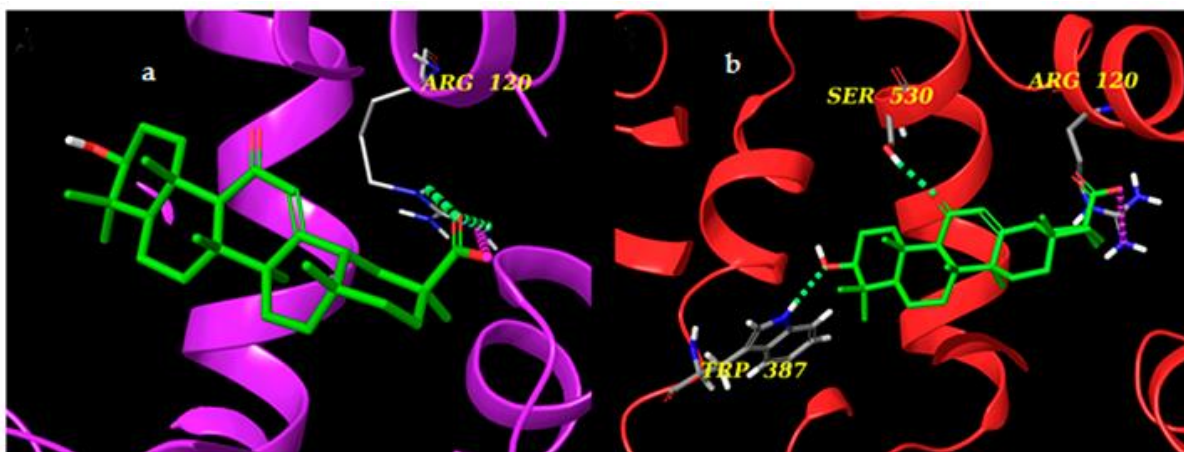


Figure 11. (a) 3D models of AG (colored by atom types: C green, O red, polar H white) in the binding site of cyclooxygenase 1 (COX-1) (purple ribbons) and (b) cyclooxygenase 2 (COX-2) (red ribbons). Green dotted lines represent H-bonds and pink dotted lines represent salt bridges.

5-LO

The mammalian 5-lipoxygenase (5-LO) pathway produces potent mediators, such as leukotriene B₄ (LTB₄) and peptide leukotrienes (LTC₄, LTD₄ or LTE₄), that have well-known functions and are involved in different pathologies and disorders [47,48,49]. To date, four different class of 5-LO direct inhibitors are classified: 1) iron-ligand inhibitors, 2) non-redox-active 5-LO inhibitors, which compete with arachidonic acid for binding to the enzyme 3) redox-active 5-LO inhibitors, interfering with the catalytic cycle of the enzyme, and 4) inhibitors that act with an unrecognized mechanism [48]. To computationally evaluate the binding of AG to 5-LO, a combined approach of rigid and flexible docking was used to predict its possible mechanism of action.

The human 5-LO structure (PDB ID: 3V99) [28] in complex with its substrate, arachidonic acid (AA), was used as the target for molecular docking studies [50]. The computational analysis highlighted two possible binding modes for the AG molecule (Figure 12), compatible with two different class of direct 5-LO inhibitors [48]. The results of the rigid docking approach are compatible with a non-redox type binding mode (Figure 12a), where AG was able to partially occupy the same binding site of AA and establishes hydrogen bonds with the side chain of Lys409 and with the backbone of Phe177. On the other hand, considering the induced fit molecular docking approach, the carboxylate group of AG was able to coordinate Fe²⁺ (Figure 12b) in a bidentate

manner, and the OH group formed a hydrogen bond with the backbone of Arg666, behaving as an iron-ligand inhibitor.

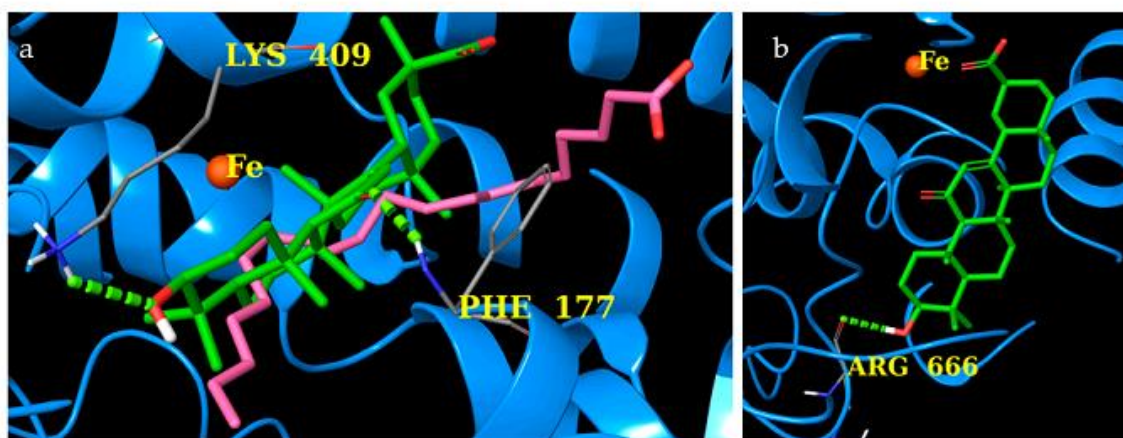


Figure 12. (a) Rigid docking and induced fit (b) of AG (colored by atom types: C green, O red, polar H white) in the binding site of 5-lipoxygenase (5-LO) (blue ribbons and Fe²⁺ as an orange sphere). Green dotted lines represent H-bonds, and original arachidonic acid (AA) molecule is in pink.

These computational data have suggested a probable binding between AG and 5-LO by one of the two proposed mechanisms, which could represent a novel finding regarding its biological activity profile, especially with respect to glycyrrhizin from *Glycyrrhiza glabra L.* as reported by Chandrasekaran et al. [51].

Discussion

Available therapy for the management of chronic and inflammatory pain is not fully adequate in most cases. Furthermore, the common treatments of inflammatory pain, NSAIDs and opioids, lead to severe toxicities, including gastrointestinal lesions and nephrotoxicity [4] in the case of NSAIDs and respiratory depression, tolerance, and physical dependence for opioids when they are used for a long time [52]. Thus, identification of new potential targets which may affect pain and inflammatory processes is becoming an urgent clinical and therapeutic need. In our present study, we investigated the possible long-lasting anti-inflammatory and antinociceptive effects of AG using pharmacological, biochemical, and *in silico* tools. Our experimental method demonstrated that AG caused significant long-lasting reduction of inflammation and nociception, revealing that effects are most likely due to the inhibition of different aspects and mediators of inflammation. Moreover, these effects were observed at AG doses which have already been demonstrated to be free of toxic effects [53].

Several investigators have reported that the anti-inflammatory mechanism of AG involves cytokines such as IFN- γ , TNF- α , IL-1 β , IL-4, IL-5, IL-6, IL-8, IL-10, IL-12, and IL-17 [27,54,55,56,57,58], intercellular cell adhesion molecule 1 (ICAM-1) and P-selectin, enzymes such as iNOS, and transcription factors such as NF-kappaB, signal transducer and activator of transcription (STAT)-3 and STAT-6 [50].

The anti-inflammatory efficacy of AG was evaluated using zymosan-induced paw edema and peritonitis. Zymosan consists of insoluble polysaccharides from yeast cell wall that induces an inflammatory reaction [59]. In this context, zymosan-induced ear or paw edema are preliminary models for screening potential anti-inflammatory drugs, characterized by pronounced dose- and time-dependent edema with moderate to severe infiltration of neutrophils and, to a lesser extent, macrophages and lymphocytes [60]. Furthermore, zymosan-induced paw edema is COX-2-dependent since it is significantly reduced in COX-2^{-/-} mice [61]. In this context, previous studies demonstrated that AG was able to reduce paw [15,16] or ear [16] edema formation and these effects were observed from 1 to 5 h after its administration [62]. After carrageenan injection in mouse paw, TNF- α , IL-6, iNOS, and COX-2 mRNA expressions increased and AG treatment (150 mg/kg, i.p.) markedly suppressed carrageenan's effects [16]. The results of our experiments demonstrated that AG had a significant long-lasting anti-inflammatory activity since AG reduced paw edema formation until 48 h after administration.

Accordingly, to better investigate the long-lasting anti-inflammatory effect of AG, we next aimed to assess its action using zymosan-induced peritonitis. Intraperitoneal injection of zymosan is a model of acute inflammation and has been widely used for the quantification of cell types and inflammation-related soluble factors [63]. It is well known that the use of zymosan as experimental model of inflammation results in a range of benefits: following the injection with zymosan, it is possible to collect a reasonable amount of exudate for the analysis of several inflammatory mediators; the normal inflammatory response of an immunocompetent individual is imitated by zymosan injection. Furthermore, injection into a serosal cavity instead of an artificially formed cavity, such as a sterile air pouch, means that leukocytes exit from the site of inflammation via their natural conduits to the draining lymph node [64,65]. This model is simple, accurate, and capable of being reproduced [63].

When administered in the mouse peritoneal cavity, zymosan-induced acute inflammation characterized by increased vascular permeability, leukocyte influx, and release of inflammatory mediators [66]. In mice receiving AG 24 h before zymosan, AG induced a high decrease in the number of inflammatory cells and a significant decrease in IL-6, IL-10, IL-1 β , IP-10, KC, MCP-5, MIP1- α , MIP1- β , MIP2, and TNF- α release in inflammatory fluids from zymosan-treated animals. This scenario was partially evoked even at 4 h post-AG administration. At this time-point, AG was able to reduce the levels of IL-6, MIP-1 α , SDF-1, TNF- α , and KC. No data have previously been reported, to our knowledge, on AG effects in a zymosan-peritonitis model. However, in a model of acute lung injury induced by intratracheal administration of lipopolysaccharide (LPS) from *Escherichia coli*, AG was able to reduce lung edema, total leukocyte number, and neutrophil percentage in the bronchoalveolar lavage fluid (BALF), and AG downregulated TNF- α level in the lung [67]. Further investigation using a similar model of lung inflammation indicated that AG was able to reduce the concentrations of pro-inflammatory cytokines IL-1 β in BALF and AG suppressed the expression of COX-2 and iNOS in lung tissue [68]. All reported data confirm the anti-inflammatory effects of AG, and these AG-related anti-inflammatory effects were until present 24–48 h after a single AG administration.

The writhing test, formalin test, and zymosan-induced hyperalgesia test were performed 24 h after AG administration to evaluate the possible long-lasting antinociceptive property of AG. Several studies have already demonstrated that AG is able to induce antinociceptive effects in the writhing test [15,16], formalin test, and thermal hyperalgesia [16] and these effects were observed from 1 to 5 h after AG administration. Our data demonstrated for the first time that AG exerts long-lasting antinociceptive effects, since AG-induced antinociception was observed until 24–48 h after a single administration.

To better investigate its analgesic profile, we finally tested the AG pharmacological profile in an acetic acid-induced writhing test, a commonly used method for monitoring preliminary antinociceptive activity, since in this test both central and peripheral analgesics are detected [69]. The injection of acetic acid directly activates the visceral and somatic nociceptors that innervate the peritoneum and induces inflammation not only in subdiaphragmatic visceral organs, but also in the subcutaneous muscle walls [70]. Furthermore, the nociceptive activity of acetic acid in the writhing model may be

due to the release of TNF- α , IL-1 β , and IL-8 by resident peritoneal macrophages and mast cells [71]. Our results revealed that AG administered 24 h before the test significantly reduced the number of writhes, suggesting that AG possessed long-lasting antinociceptive effects. Because of the lack of drug specificity, caution is required in interpreting the results obtained in the writhing test [69], and other tests could be conducted to scientifically assess the obtained results.

The formalin test for nociception, which is mainly used with rats and mice, involves moderate and continuous pain generated by injured tissue. This test in mice is a well-founded and trustworthy model of nociception and is sensitive for various classes of analgesic drugs [72]. Plantar injections of formalin in the mouse induce a characteristic behaviour evoked in two temporal phases. The first phase is observed immediately after the formalin injection, followed by a quiescent period, and then a second phase appears, which lasts until the end of the period of observation. The first phase depends upon direct stimulation of nociceptors, whereas the second involves a period of sensitization during which inflammatory phenomena occurs, involving the release of pain mediators such as histamine, serotonin, prostaglandins, bradykinin, and cytokines. Opioid analgesics appear to be antinociceptive for both phases, whereas NSAIDs seem to suppress only the second phase [69]. In our research, AG substantially diminished the second phase of the formalin test when administered 24 h before the test, thus confirming the results obtained in the writhing test.

Furthermore, *in vivo* tests of AG show the efficiency of the drug in terms of increase of nociceptive threshold after zymosan administration. Associated with paw edema, the injection of zymosan in the mouse paw produces a decrease of pain thresholds, which indicates a state of hyperalgesia [60,61]. In this pain model, a time-dependent hyperalgesia was noticed after zymosan administration and measured as a time-dependent reduction in the latency to respond to the thermal stimuli applied to the injected paw compared to the baseline measurements. We also have outstanding results in terms of the highest increase in pain threshold after AG administration. We observed that AG caused a significant reduction of zymosan-induced hyperalgesia until 48 h after administration.

It is well known that several components of liquorice can suppress COX-2 [73,74] and this seems to be true also for AG [16]. In addition to above-mentioned effects of AG on

COX-2 [67,68], in skin tumor, AG significantly inhibited NF- κ B, COX-2, prostaglandin E₂ (PGE₂), and nitric oxide (NO) levels [75]. Furthermore, in focal cerebral ischemic-reperfusion injury in mice, AG administered for seven days significantly improved neurofunction, decreased infarct size, and suppressed edema [76]. The neuroprotective effect of AG was associated with a significant reduction in IL-1, TNF- α , COX-2, iNOS, NF- κ B, and GFAP levels [76]. Further recent studies showed that AG downregulates the expression of iNOS and COX-2 in the inflamed kidney [77] and skin [78], blocking NF- κ B activation. In HaCaT cells, AG inhibited the UV-B-mediated increase in intracellular ROS and downregulated the release of IL-6, IL-1 α , IL-1 β , TNF- α , and PGE₂ [79]. In LPS-stimulated mouse endometrial epithelial cells, AG considerably repressed LPS-induced TNF- α , IL-1 β , NO, and PGE₂ production, attenuated LPS-induced iNOS, COX-2, and TLR4 expression and NF- κ B activation [80].

Our docking studies, for the first time, suggest that AG's effects on inflammation and nociception might also depend upon the interaction with mPGES-1/2, COX-1/2, and 5-LO. In fact, from the analysis of the results, it emerged that AG interacted with key amino acids of mPGES-2 and COX-2, highlighting a preferential binding with these two isoforms. AG seems to locate better in the binding pocket of COX-2 as it interacts with key amino acids like Trp387, Ser530 (H-bonds), and Arg120 (salt bridge). Moreover, by combined rigid and flexible molecular docking studies, two possible mechanisms of interaction between AG and 5-LO were proposed: non-redox competitive binding and Fe²⁺ complexation. Here, the binding energy calculated is lower compared to those obtained with the other proteins, namely mPGES-1 and 2, COX-1 and 2 (data not shown), but consistent with putative inhibitor activity. These data suggest that further experiments should be performed to evaluate the effects of AG's interaction with 5-LO.

Results of the present study indicated that AG possesses long-lasting anti-inflammatory and antinociceptive effects as observed 24–48 h after the administration. Our data also suggest that its anti-inflammatory and antinociceptive effects might be attributed to the inhibition of the levels of different pro-inflammatory cytokines and chemokines. Taken together, all these findings indicate that AG is a long-acting therapeutic agent for the treatment of painful conditions and inflammatory-related diseases.

References

1. Rahavard BB, Candido KD, Knezevic NN. Different pain responses to chronic and acute pain in various ethnic/racial groups. *Pain Manag.* 2017;7:427–453.
2. Baral P, Udit S, Chiu IM. Pain and immunity: Implication for host defence. *Nat. Rev. Immunol.* 2019;15:1.
3. Sinha M, Gautam L, Shukla PK., et al. Current perspectives in NSAID-induced gastropathy. *Mediat. Inflamm.* 2013;2013:258209.
4. Musu M, Finco G, Antonucci R, et al. Acute nephrotoxicity of NSAID from the foetus to the adult. *Eur. Rev. Med. Pharmacol. Sci.* 2011;15:1461–1472.
5. Benyamin R, Trescot AM, Datta S, et al. Opioid complications and side effects. *Pain Physician.* 2008;11:S105–S120.
6. Statti GA, Tundis R, Sacchetti G, et al. Variability in the content of active constituents and biological activity of *Glycyrrhiza glabra*. *Fitoterapia.* 2004;75:371–374.
7. Fu Y, Hsieh TC, Guo J, et al. Licochalcone-A, a novel flavonoid isolated from licorice root (*Glycyrrhiza glabra*), causes G2 and late-G1 arrests in androgen-independent PC-3 prostate cancer cells. *Biochem. Biophys. Res. Commun.* 2004;322:263–270.
8. Ignesti G, Maleci L, Medica A, Pirisino R. *Piante Medicinali. Botanica, Chimica, Farmacologia, Tossicologia.* Pitagora Editrice; Bologna, Italy: 1999.
9. Chen MF, Shimada F, Kato H, et al. Effect of oral administration of glycyrrhizin on the pharmacokinetics of prednisolone. *Endocrinol. Jpn.* 1991;38:167–174.
10. Herold A, Cremer L, Calugaru A, et al. Hydroalcoholic plant extracts with antiinflammatory activity. *Roum. Arch. Microbiol. Immunol.* 2003;62:117–129.
11. Fukai T, Satoh K, Nomura T, et al. Preliminary evaluation of antinephritis and radical scavenging activities of glabridin from *Glycyrrhiza glabra*. *Fitoterapia.* 2003;74:624–629.
12. Morteza-Semnani K, Saedi M, Shahnava B. Comparison of antioxidant activity of extract from roots of licorice (*Glycyrrhiza glabra* L.) to commercial antioxidants in 2% hydroquinone cream. *J. Cosmet. Sci.* 2003;54:551–558.
13. Paolino D, Lucania G, Mardente D, et al. Ethosomes for skin delivery of ammonium glycyrrhizinate: *In vitro* percutaneous permeation through human skin and *in vivo* anti-inflammatory activity on human volunteers. *J. Control. Release.* 2005;106:99–110.
14. Genovese T, Menegazzi M, Mazzon E, et al. Glycyrrhizin reduces secondary inflammatory process after spinal cord compression injury in mice. *Shock.* 2009;31:367–375.
15. Khaksa G, Zolfaghari ME, Dehpour AR, et al. Anti-inflammatory and anti-nociceptive activity of disodium glycyrrhetinic acid hemiphthalate. *Planta Med.* 1996;62:326–328.
16. Wang HL, Li YX, Niu YT, et al. Observing Anti-inflammatory and Anti-nociceptive Activities of Glycyrrhizin Through Regulating COX-2 and Pro-

- inflammatory Cytokines Expressions in Mice. *Inflammation*. 2015;38:2269–2278.
17. Sun X, Zeng H, Wang Q, et al. Glycyrrhizin ameliorates inflammatory pain by inhibiting microglial activation-mediated inflammatory response via blockage of the HMGB1-TLR4-NF- κ B pathway. *Exp. Cell. Res.* 2018;369:112–119.
 18. Colucci M, Maione F, Bonito MC, et al. New insights of dimethyl sulphoxide effects (DMSO) on experimental *in vivo* models of nociception and inflammation. *Pharmacol. Res.* 2008;57:419–425.
 19. Pieretti S, Dal Piaz V, Matucci R, et al. Antinociceptive activity of a 3(2H)-pyridazinone derivative in mice. *Life Sci.* 1999;65:1381–1394.
 20. Tjølsen A, Berge OG, Hunskaar S, et al. The formalin test: An evaluation of the method. *Pain.* 1992;51:5–17.
 21. Niederberger E, Schmidtke A, Gao W, et al. Impaired acute and inflammatory nociception in mice lacking the p50 subunit of NF- κ B. *Eur. J. Pharmacol.* 2007;559:55–60.
 22. Chatterjee BE, Yona S, Rosignoli G, et al. Annexin 1-deficient neutrophils exhibit enhanced transmigration *in vivo* and increased responsiveness *in vitro*. *J. Leukoc. Biol.* 2005;78:639–646.
 23. Damazo AS, Yona S, Flower RJ, et al. Spatial and temporal profiles for anti-inflammatory gene expression in leukocytes during a resolving model of peritonitis. *J. Immunol.* 2006;176:4410–4418.
 24. Maione F, Piccolo M, De Vita S, et al. Down regulation of pro-inflammatory pathways by tanshinone IIA and cryptotanshinone in a non-genetic mouse model of Alzheimer's disease. *Pharmacol. Res.* 2018;129:482–490.
 25. Partridge KM, Antonysamy S, Bhattachar SN, et al. Discovery and characterization of [(cyclopentyl) ethyl] benzoic acid inhibitors of microsomal prostaglandin E synthase-1. *Bioorg. Med. Chem. Lett.* 2017;27:1478–1483.
 26. Cingolani G, Panella A, Perrone MG, et al. Structural basis for selective inhibition of Cyclooxygenase-1 (COX-1) by diarylisoxazoles mofezolac and 3-(5-chlorofuran-2-yl)-5-methyl-4-phenylisoxazole (P6) *Eur. J. Med. Chem.* 2017;138:661–668.
 27. Sun Y, Cai TT, Shen Y, et al. Si-Ni-San a traditional Chinese prescription, and its active ingredient glycyrrhizin ameliorate experimental colitis through regulating cytokine balance. *Int. Immunopharmacol.* 2009;9:1437–1443.
 28. Gilbert NC, Rui Z, Neau DB, et al. Conversion of human 5-lipoxygenase to a 15-lipoxygenase by a point mutation to mimic phosphorylation at Serine-663. *FASEB J.* 2012;26:3222–3229.
 29. Sastry GM, Adzhigirey M, Day T, et al. Protein and ligand preparation: Parameters, protocols, and influence on virtual screening enrichments. *J. Comput. Aided Mol. Des.* 2013;27:221–234.
 30. D'Ambola M, Fiengo L, Chini MG, et al. Fusicoccane Diterpenes from *Hypoestes forsskaolii* as Heat Shock Protein 90 (Hsp90) Modulators. *J. Nat. Prod.* 2019;82:539–549.

31. Friesner RA, Murphy RB, Repasky MP, et al. Extra Precision Glide: Docking and Scoring Incorporating a Model of Hydrophobic Enclosure for Protein-Ligand Complexes. *J. Med. Chem.* 2006;49:6177–6196.
32. Halgren TA, Murphy RB, Friesner RA, et al. Glide: A New Approach for Rapid, Accurate Docking and Scoring. 2. Enrichment Factors in Database Screening. *J. Med. Chem.* 2004;47:1750–1759.
33. Friesner RA, Banks JL, Murphy RB, et al. Glide: A New Approach for Rapid, Accurate Docking and Scoring. 1. Method and Assessment of Docking Accuracy. *J. Med. Chem.* 2004;47:1739–1749.
34. Jacobson MP, Pincus DL, Rapp CS, et al. A hierarchical approach to all-atom protein loop prediction. *Proteins Struct. Funct. Bioinf.* 2004;55:351–367.
35. Jacobson MP, Friesner RA, Xiang Z, et al. On the Role of the Crystal Environment in Determining Protein Side-chain Conformations. *J. Mol. Biol.* 2002;320:597–608.
36. Curtis MJ, Bond RA, Spina D, et al. Experimental design and analysis and their reporting: New guidance for publication in *BJP. Br. J. Pharmacol.* 2015;172:3461–3471.
37. Koeberle A, Werz O. Perspective of microsomal prostaglandin E₂ synthase-1 as drug target in inflammation-related disorders. *Biochem. Pharmacol.* 2015;98:1–15.
38. Park JY, Pillinger MH, Abramson SB. Prostaglandin E₂ synthesis and secretion: The role of PGE₂ synthases. *Clin. Immunol.* 2006;119:229–240.
39. Iranshahi M, Chini MG, Masullo M, et al. Can Small Chemical Modifications of Natural Pan-inhibitors Modulate the Biological Selectivity? The Case of Curcumin Prenylated Derivatives Acting as HDAC or mPGES-1 Inhibitors. *J. Nat. Prod.* 2015;78:2867–2879.
40. Ding K, Zhou Z, Hou S, et al. Structure-based discovery of mPGES-1 inhibitors suitable for preclinical testing in wild-type mice as a new generation of anti-inflammatory drugs. *Sci. Rep.* 2018;8:5205.
41. Luz JG, Antonysamy S, Kuklish SL, et al. Crystal Structures of mPGES-1 Inhibitor Complexes Form a Basis for the Rational Design of Potent Analgesic and Anti-Inflammatory Therapeutics. *J. Med. Chem.* 2015;58:4727–4737.
42. Lauro G, Tortorella P, Bertamino A, et al. Structure-Based Design of Microsomal Prostaglandin E₂ Synthase-1 (mPGES-1) Inhibitors using a Virtual Fragment Growing Optimization Scheme. *Chem. Med. Chem.* 2016;11:612–619.
43. Yamada T, Komoto J, Watanabe K, et al. Crystal structure and possible catalytic mechanism of microsomal prostaglandin E synthase type 2 (mPGES-2). *J. Mol. Biol.* 2005;348:1163–1176.
44. Orlando BJ, Malkowski MG. Substrate-selective inhibition of cyclooxygenase-2 by fenamic acid derivatives is dependent on peroxide tone. *J. Biol. Chem.* 2016;291:15069–15081.
45. Blobaum AL, Marnett LJ. Structural and Functional Basis of Cyclooxygenase Inhibition. *J. Med. Chem.* 2007;50:1425–1441.

46. Sherman W, Day T, Jacobson MP, et al. Novel procedure for modeling ligand/receptor induced fit effects. *J. Med. Chem.* 2006;49:534–553.
47. Pergola C, Werz O. 5-Lipoxygenase inhibitors: A review of recent developments and patents. *Expert Opin. Ther. Pat.* 2010;20:355–375.
48. Werz O. Inhibition of 5-Lipoxygenase Product Synthesis by Natural Compounds of Plant Origin. *Planta Med.* 2007;73:1331–1357.
49. Rådmark O, Samuelsson B. Regulation of the activity of 5-lipoxygenase, a key enzyme in leukotriene biosynthesis. *Biochem. Biophys. Res. Commun.* 2010;396:105–110.
50. Tsolaki E, Eleftheriou P, Kartsev V, et al. Application of Docking Analysis in the Prediction and Biological Evaluation of the Lipoxygenase Inhibitory Action of Thiazolyl Derivatives of Mycophenolic Acid. *Molecules.* 2018;23:1621.
51. Chandrasekaran CV, Deepak HB, Thiyagarajan P, et al. Dual inhibitory effect of *Glycyrrhiza glabra* (GutGard™) on COX and LOX products. *Phytomedicine.* 2011;18:278–284.
52. Stamenkovic DM, Laycock H, Karanikolas M, et al. Chronic Pain and Chronic Opioid Use After Intensive Care Discharge—Is It Time to Change Practice? *Front. Pharmacol.* 2019;10:23.
53. Cosmetic Ingredient Review Expert Panel Final report on the safety assessment of Glycyrrhetic Acid, Potassium Glycyrrhetinate, Disodium Succinoyl Glycyrrhetinate, Glyceryl Glycyrrhetinate, Glycyrrhetinyl Stearate, Stearyl Glycyrrhetinate, Glycyrrhizic Acid, Ammonium Glycyrrhizate, Dipotassium Glycyrrhizate, Disodium Glycyrrhizate, Trisodium Glycyrrhizate, Methyl Glycyrrhizate, and Potassium Glycyrrhizinate. *Cosmetic Ingredient Review Expert Panel. Int. J. Toxicol.* 2007;26:79–112.
54. Menegazzi M, Di Paola R, Mazzon E, et al. Glycyrrhizin attenuates the development of carrageenan-induced lung injury in mice. *Pharmacol. Res.* 2008;58:22–31.
55. Feng C, Wang H, Yao C, et al. Diammonium glycyrrhizinate, a component of traditional Chinese medicine Gan-Cao, prevents murine T-cell-mediated fulminant hepatitis in IL-10- and IL-6-dependent manners. *Int. Immunopharmacol.* 2007;7:1292–1298.
56. Yoshida T, Abe K, Ikeda T, et al. Inhibitory effect of glycyrrhizin on lipopolysaccharide and d-galactosamine-induced mouse liver injury. *Eur. J. Pharmacol.* 2007;576:136–142.
57. Ram A, Mabalirajan U, Das M, et al. Glycyrrhizin alleviates experimental allergic asthma in mice. *Int. Immunopharmacol.* 2006;6:1468–1477.
58. Matsui S, Sonoda Y, Sekiya T, et al. Glycyrrhizin derivative inhibits eotaxin 1 production via STAT6 in human lung fibroblasts. *Int. Immunopharmacol.* 2006;6:369–375.
59. Calhoun W, Chang J, Carlson RP. Effect of selected antiinflammatory agents and other drugs on zymosan, arachidonic acid, PAF and carrageenan induced paw edema in the mouse. *Agents Actions.* 1987;21:306–309.

60. Suo J, Linke B, Meyer dos Santos S, et al. Neutrophils mediate edema formation but not mechanical allodynia during zymosan-induced inflammation. *J. Leukoc. Biol.* 2014;96:133–142.
61. Jain N.K., Ishikawa T.O., Spigelman I., et al. COX-2 expression and function in the hyperalgesic response to paw inflammation in mice. *Prostaglandins Leukot. Essent. Fatty Acids.* 2008;79:183–190.
62. Marianecchi C, Rinaldi F, Di Marzio L, et al. Ammonium glycyrrhizinate-loaded niosomes as a potential nanotherapeutic system for anti-inflammatory activity in murine models. *Int. J. Nanomed.* 2014;9:635–651.
63. Cash JL, White GE, Greaves DR. Chapter 17. Zymosan-induced peritonitis as a simple experimental system for the study of inflammation. *Methods Enzymol.* 2009;461:379–396.
64. Bellingan GJ, Caldwell H, Howie SE, et al. *In vivo* fate of the inflammatory macrophage during the resolution of inflammation: Inflammatory macrophages do not die locally, but emigrate to the draining lymph nodes. *J. Immunol.* 1996;157:2577–2585.
65. Schwab JM, Chiang N, Arita M, et al. Resolvin E1 and protectin D1 activate inflammation-resolution programmes. *Nature.* 2007;447:869–874.
66. Leite JA, Alves AK, Galvão JG, et al. Ouabain Modulates Zymosan-Induced Peritonitis in Mice. *Mediat. Inflamm.* 2015;2015:265798.
67. Shi JR, Mao LG, Jiang RA, et al. Monoammonium glycyrrhizinate inhibited the inflammation of LPS-induced acute lung injury in mice. *Int. Immunopharmacol.* 2010;10:1235–1241.
68. Ni YF, Kuai JK, Lu ZF, et al. Glycyrrhizin treatment is associated with attenuation of lipopolysaccharide-induced acute lung injury by inhibiting cyclooxygenase-2 and inducible nitric oxide synthase expression. *J. Surg. Res.* 2011;165:e29–e35.
69. Le Bars D, Gozariu M, Cadden SW. Animal models of nociception. *Pharmacol. Rev.* 2001;53:597–652.
70. Satyanarayana PS, Jain NK, Singh A, et al. Isobolographic analysis of interaction between cyclooxygenase inhibitors and tramadol in acetic acid-induced writhing in mice. *Prog. Neuropsychopharmacol. Biol. Psychiatry.* 2004;28:641–649.
71. Ribeiro RA, Vale ML, Thomazzi SM, et al. Involvement of resident macrophages and mast cells in the writhing nociceptive response induced by zymosan and acetic acid in mice. *Eur. J. Pharmacol.* 2000;387:111–118.
72. Hunskaar S, Hole K. The formalin test in mice: Dissociation between inflammatory and non-inflammatory pain. *Pain.* 1987;30:103–114.
73. Lau GT, Ye L, Leung LK. The licorice flavonoid isoliquiritigenin suppresses phorbol ester-induced cyclooxygenase-2 expression in the non-tumorigenic MCF-10A breast cell line. *Planta Med.* 2010;76:780–785.
74. Song NR, Kim JE, Park JS, et al. Licochalcone A, a polyphenol present in licorice, suppresses UV-induced COX-2 expression by targeting PI3K, MEK1, and B-Raf. *Int. J. Mol. Sci.* 2015;16:4453–4470.

75. Cherng JM, Tsai KD, Yu YW, et al. Molecular mechanisms underlying chemopreventive activities of glycyrrhizic acid against UVB-radiation-induced carcinogenesis in SKH-1 hairless mouse epidermis. *Radiat. Res.* 2011;176:177–186.
76. Hou SZ, Li Y, Zhu XL, Wang ZY, et al. Ameliorative effects of diammonium glycyrrhizinate on inflammation in focal cerebral ischemic-reperfusion injury. *Brain Res.* 2012;1447:20–27.
77. Zhao H, Zhao M, Wang Y, et al. Glycyrrhizic Acid Attenuates Sepsis-Induced Acute Kidney Injury by Inhibiting NF- κ B Signaling Pathway. *Evid. Based Complement. Alternat. Med.* 2016;2016:8219287.
78. Liu W, Huang S, Li Y, et al. Glycyrrhizic acid from licorice down-regulates inflammatory responses via blocking MAPK and PI3K/Akt-dependent NF- κ B signalling pathways in TPA-induced skin inflammation. *MedChemComm.* 2018;9:1502–1510.
79. Afnan Q, Kaiser PJ, Rafiq RA, et al. Glycyrrhizic acid prevents ultraviolet-B-induced photodamage: A role for mitogen-activated protein kinases, nuclear factor kappa B and mitochondrial apoptotic pathway. *Exp. Dermatol.* 2016;25:440–446.
80. Wang XR, Hao HG, Chu L Glycyrrhizin inhibits LPS-induced inflammatory mediator production in endometrial epithelial cells. *Microb. Pathog.* 2017;109:110–113.

CHAPTER 2: Ammonium Glycyrrhizinate Prevents Apoptosis and Mitochondrial Dysfunction Induced by High Glucose in SH-SY5Y Cell Line and Counteracts Neuropathic Pain in Streptozotocin-Induced Diabetic Mice

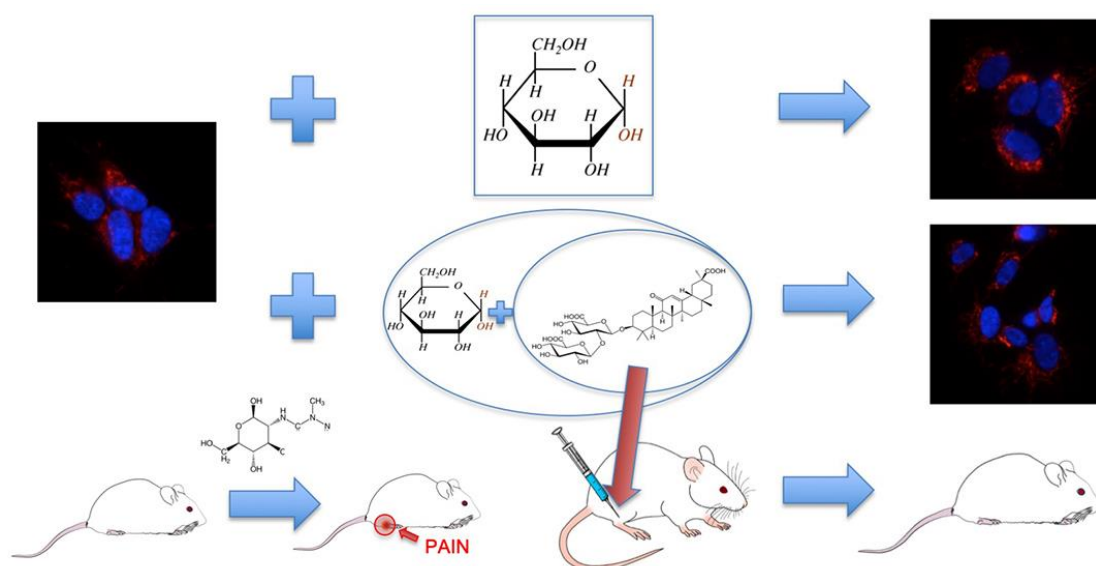
Laura Ciarlo¹, Francesca Marzoli¹, Paola Minosi¹, Paola Matarrese², Stefano Pieretti¹

¹ Istituto Superiore di Sanità, Centro Nazionale Ricerca e Valutazione Preclinica e Clinica dei Farmaci, Viale Regina Elena 299, 00161 Rome, Italy.

² National Center for Gender-Specific Medicine, Istituto Superiore di Sanità, Viale Regina Elena 299, 00161 Rome, Italy

Abstract

Glycyrrhiza glabra, commonly known as liquorice, contains several bioactive compounds such as flavonoids, sterols, triterpene, and saponins; among which, glycyrrhizic acid, an oleanane-type saponin, is the most abundant component in liquorice root. Diabetic peripheral neuropathy is one of the major complications of diabetes mellitus, leading to painful condition as neuropathic pain. The pathogenetic mechanism of diabetic peripheral neuropathy is very complex, and its understanding could lead to a more suitable therapeutic strategy. In this work, we analyzed the effects of ammonium glycyrrhizinate, a derivate salt of glycyrrhizic acid, on an *in vitro* system, neuroblastoma cells line SH-SY5Y, and we observed that ammonium glycyrrhizinate was able to prevent cytotoxic effect and mitochondrial fragmentation after high-glucose administration. In an *in vivo* experiment, we found that a short-repeated treatment with ammonium glycyrrhizinate was able to attenuate neuropathic hyperalgesia in streptozotocin-induced diabetic mice. In conclusion, our results showed that ammonium glycyrrhizinate could ameliorate diabetic peripheral neuropathy, counteracting both *in vitro* and *in vivo* effects induced by high glucose, and might represent a complementary medicine for the clinical management of diabetic peripheral neuropathy.



Introduction

Glycyrrhiza glabra is a perennial plant that has been used in traditional Chinese medicine for thousand years and recently also in Europe [1]. *Glycyrrhiza glabra* was considered in the world as “the grandfather of plants”. Many countries used this plant in medicine for its pharmacological properties. Traditionally, this plant was used for treating asthma, hoarseness of voice, cough, and lung diseases. It was also used as a remedy for diseases of liver, heart palpitation, and angina. Its use has also been suggested in the treatment of bladder and kidney pain, kidney stones, fever, neuralgia, skin, and eye diseases [2].

Glycyrrhizic acid or glycyrrhizin is the main active component extracted from the *glycyrrhiza* root, this compound consisting of a triterpenoid pentacyclic glucoside [3]. Glycyrrhizic acid is an amphiphilic molecule: the hydrophilic part is represented by the glucuronic acid residues, and the hydrophobic part is the glycyrrhetic acid residue [3]. Glycyrrhizin has long been known as a compound with many biological effects: anti-inflammatory, antiulcer, antianaphylaxis, antioxidant, immunoregulatory, membrane stabilization, antiviral, and anticancer activities [4]. In particular, the anti-inflammatory activity of glycyrrhizic acid has been well studied; several *in vitro* studies have shown that glycyrrhizic acid can inhibit the production of the most proinflammatory cytokine such as TNF- α , interleukins IL-1 β , and IL-6 [5]. Sun et al. showed that glycyrrhizic acid inhibits the synthesis of nitric oxide and some inflammatory cytokines in microglial cells treated with LPS [6]. The anti-inflammatory activity lies in its particular conformation, which consists of a pentacyclic triterpenic structure very similar to that of the well-known glucocorticoids.

Two types of drugs can be used to treat pain in the chronic inflammatory diseases: nonsteroidal anti-inflammatory drugs (NSAIDs) and opioids. The treatment with NSAIDs for a long time often leads to several side effects, such as gastrointestinal lesions and nephrotoxicity [7]. In the same vein, the use of opioid induces respiratory depression, tolerance, and physical dependence [8].

Diabetes mellitus is a chronic metabolic disease characterized by a persistent excess of glucose in the blood, known as hyperglycemia. This condition is due to insufficient insulin production that may progress over time, leading to an insulin resistance condition. The major complications due to the onset of chronic diabetes are neuropathy,

retinopathy, and nephropathy [9]. Half of the patients with diabetes suffer from peripheral neuropathy (DPN), leading to painful conditions as neuropathic pain negatively affects the quality of life. The pathogenetic mechanism of DPN is very complex, and its understanding could allow the implementation of a more suitable therapeutic strategy [10].

Chronic hyperglycemia appears to be one of the events responsible for the development of DPN. In fact, hyperglycemia induces an increase in the production of mitochondrial and cytoplasmic reactive oxygen species (ROS) while also inhibiting antioxidant defenses. This generates a vicious cycle in which mitochondrial dysfunction induces more ROS production leading a progressive decline of sensory neuron function and the loss of peripheral innervation that characterizes DPN [11,12]. Neuronal mitochondrial dysfunction and oxidative stress therefore represent key determinants in DPN [13].

The main parameter that influences the ROS generation in mitochondria is represented by the mitochondrial membrane potential (MMP) [14,15], and a significant production of ROS has been observed in mitochondria with more than >140 mV of MMP [16]. On the other hand, the increase in MMP could be the result of ATP synthase inhibition [17]. In fact, it has actually been demonstrated that mitochondria increase ROS production when they are not synthesizing ATP [18]. In the early phase of apoptosis, ROS generation is paralleled by a hyperpolarization of the mitochondrial membrane, followed by mitochondrial membrane depolarization in the execution phase [19]. Maintenance of shape and morphology of mitochondria, required for their normal functions, is regulated by a balance of constitutive fission and fusion dynamic processes. This remodeling has great relevance in both cell life and death, being the mitochondrial network involved in all activities, including proliferation, differentiation, and senescence, as well as cell death [20]. The oxidative stress plays an important role as inductor of mitochondrial fission [21], and several studies seem to indicate that hyperglycemia per se can also stimulate mitochondrial fragmentation [22].

Currently, there are no effective treatments for DPN apart from glycemic control. Saad et al. in their study showed that a new therapeutic strategy, which acts at the level of mitochondrial metabolism, could improve the management of DPN [23].

In this work, we analyzed the effects of ammonium glycyrrhizinate (AG) on a model used for studies on diabetic neuropathy, i.e., neuroblastoma cells line SH-SY5Y [24],

and then, we validated *in vivo* its ability to counteract DPN in streptozotocin-induced diabetic mice.

Materials and Methods

In vitro Experiments

Cells and Treatments

The human neuroblastoma cell line SH-SY5Y was cultured in Dulbecco's modified Eagle's medium (DMEM) (Sigma-Aldrich, St. Louis, MO, USA) containing 4500 mg/L glucose, sodium pyruvate, and sodium bicarbonate; 10% fetal bovine serum, and penicillin and streptomycin at 100 U/mL penicillin and 100 mg/mL streptomycin (Sigma-Aldrich, St. Louis, MO, USA), and kept at 37 °C in a humidified 5% CO₂ incubator. SH-SY5Y cells were obtained from ATCC, and all experiments were carried out up to 12 passages. In total, 80,000 cells/well were seeded on 12-well tissue culture plates. After 24 h, cells were treated with different concentrations of D-Glucose (GLU, Sigma-Aldrich, St. Louis, MO, USA) (75, 100, 150, 200, 250, and 300 mM) for 24, 48, and 72 h to find out the maximum concentration that induce cytotoxicity. At the same time, different concentrations of ammonium glycyrrhizate (AG, Sigma-Aldrich, St. Louis, MO, USA) (200 µg/mL) were used to select the concentration able to counteract the effects of high glucose. As control, we used cells treated with mannitol (MAN, Sigma-Aldrich, St. Louis, MO, USA), an osmotic sugar alcohol that is metabolically inert in humans, at the same concentration as GLU.

Cell Death Assays

Quantitative evaluation of apoptosis was performed by a double-staining flow cytometry method by using fluorescein isothiocyanate (FITC)-conjugated Annexin V/PI apoptosis detection kit according to the manufacturer's protocol (BioVision, Inc. Milpitas, CA, USA). Alternatively, cell death was analyzed after cell staining with Calcein-AM (Molecular Probes, Eugene, OR, USA). All samples were acquired and analyzed with a FACScalibur cytometer (BD Biosciences, San Jose, CA, USA). At least 20,000 events were acquired. Data were recorded and statistically analyzed by a Macintosh computer using CellQuest software (BD Biosciences, San Jose, CA, USA).

Mitochondrial Membrane Potential

The mitochondrial membrane potential of controls and treated cells were studied by using 5-5',6-6'-tetrachloro-1,1',3,3'-tetraethyl benzimidazole-carbocyanine iodide probe (JC-1; Molecular Probes, Eugene, OR, USA), as described [25]. In line with this method, living cells were stained with 10 μ M of JC-1. Tetramethylrhodamine ester 1 μ M (TMRM; Molecular Probes, Eugene, OR, USA) was also used to confirm data obtained by JC-1 (Figure S1).

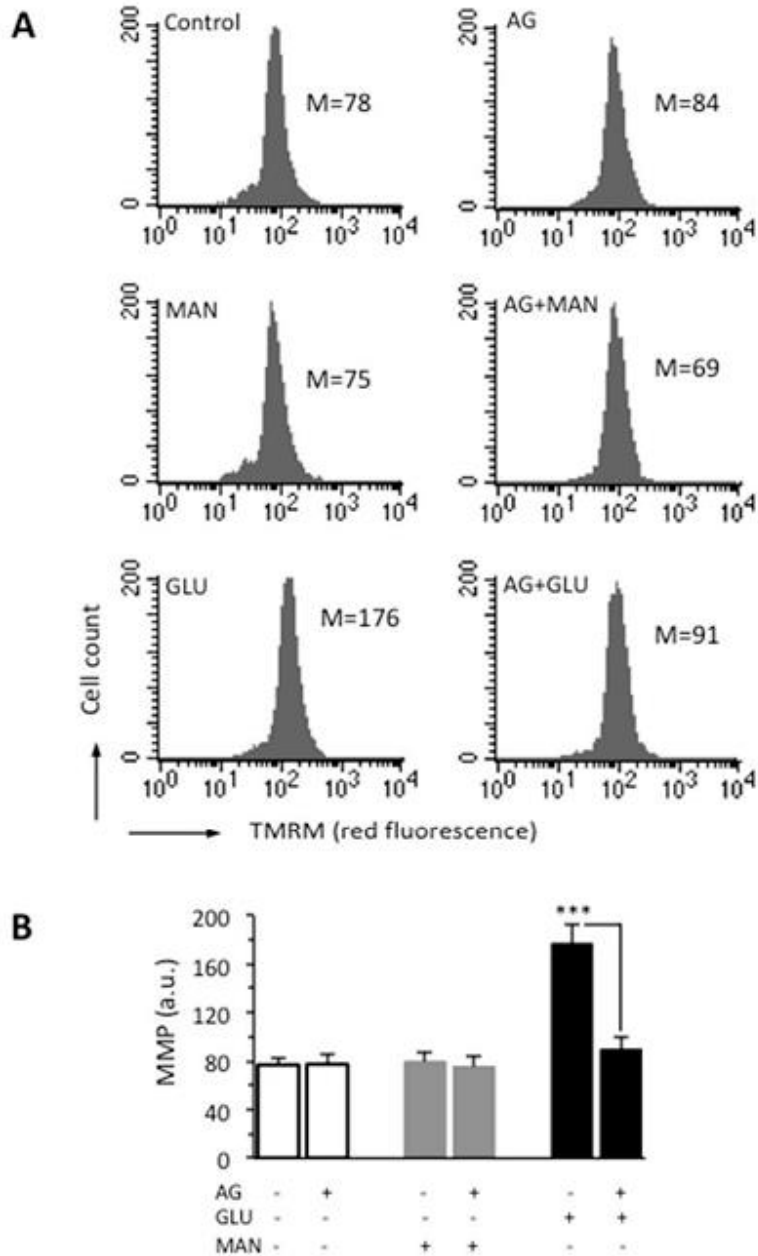


Figure S1

Western Blot Analysis

The samples were subjected to sodium-dodecyl sulphate polyacrilamide gel electrophoresis (SDS-PAGE) under standard protocols. Briefly, each sample was lysed in Ripa buffer (50 μ m Tris-HCL pH 7.4; 1% NP40; 0.5% Na—Deoxycholate; 0.1% SDS; 150 mM NaCl; 2 mM EDTA; 50 mM NAF) with protease and phosphatase inhibitor mixture. Protein content was determined by Bradford assay, and 40 μ g of proteins were loaded. The proteins were electrophoretically transferred to the nitrocellulose membranes (GVS Life Sciences, GVS North America, Sanford, ME, USA) and probed with the following antibodies: MAb anti-DRP1 (BD Biosciences, San Jose, CA, USA), anti-hFis1 polyclonal antibody MAb anti-OPA1 (BD Biosciences, San Jose, CA, USA), PAb anti-MFN2 (Cell Signaling Technology, Inc., Danvers, MA, USA), for mitochondrial investigation; MAb anti-HMGB1 (Sigma-Aldrich, St. Louis, MO, USA), MAb anti-NF κ B p65 (Santa Cruz Biotechnology Inc., Dallas, TX, USA) for inflammation investigation. Bound antibodies were visualized with horseradish peroxidase (HRP)-conjugated antirabbit IgG or antimouse IgG (Jackson Immuno Research Laboratories, Baltimore Pike West Grove, PA, USA) and immunoreactivity assessed by chemiluminescence reaction, using the ECL Western detection system (Millipor, Darmstadt, German). Densitometric scanning analysis was performed by Chemidoc (Bio-Rad, Hercules, CA, USA). To standardize, MAb anti-Tubulin (TUB, Sigma-Aldrich, St. Louis, MO, USA), PAb anti-Actin (Sigma-Aldrich, St. Louis, MO, USA), or anti-GAPDH (Sigma-Aldrich, St. Louis, MO, USA) were used for observations.

Immunofluorescence Analysis

Control and treated cells were fixed with 4% paraformaldehyde (Carlo Erba, Milan, Italy) and then permeabilized by 0.5% Triton X-100 (Sigma-Aldrich, St. Louis, MO, USA). After washings, cells were incubated with PAb to TOM20 (Santa Cruz Biotechnology Inc., Dallas, TX, USA). After washings, cells were incubated with antirabbit AlexaFluor 594-conjugated (Termo Scientific, Rockford, IL, USA) for additional 1 h at 37 °C. All samples were counterstained with Hoechst 33342 (Termo Scientific, Rockford, IL, USA) and mounted with glycerol-PBS (2:1). The images were acquired by intensified video microscopy (IVM) with an Olympus fluorescence microscope (Olympus Corporation of the Americas, Center Valley, PA, USA),

equipped with a Zeiss charge-coupled device (CCD) camera (Carl Zeiss, Oberkochen, Germany).

Morphometric Analysis

Quantitative evaluations of mitochondrial fragmentation were carried out by evaluating at least 50 cells at the same magnification ($\times 1300$). Morphometric analysis was performed by using the ImageJ to measure the average mitochondrial area. To this purpose, red–green–blue (RGB) images were processed using a custom-written ImageJ macro containing plugins that calculate the average area of the mitochondrial particles throughout the cell cytoplasm using the outlines algorithm of the “analyze particles” function. The macroassisted algorithm was set to measure all particle sizes larger than the background pixelation but smaller than the average nuclear size. The average mitochondrial area is expressed as pixel².

In vivo Experiments

Animals

All experiments were performed according to Legislative Decree 26/14, which implements the European Directive 2010/63/UE on laboratory animal protection in Italy, and were approved by the Service for Biotechnology and Animal Welfare of the Istituto Superiore di Sanità and authorized by the Italian Ministry of Health (approval code 198/2013-B). CD-1 mice (Charles River, Sant’Angelo Lodigiano LO, Italy) were housed in colony cages (seven mice per cage) under standard conditions of light, temperature, and relative humidity for at least 1 week before the start of experimental sessions. Food and water were available ad libitum.

Streptozotocin-Induced Diabetes

It was reported that a high dose of streptozotocin (STZ, Sigma Aldrich, St. Louis, MO, USA) is directly toxic to pancreatic β -cells, rapidly causing diabetes, with blood glucose levels of >500 mg/dl within 48 h in mice. Thus, STZ dissolved in saline was administered at 200 mg/kg (1.0 mL/100 g) by a single intraperitoneal (i.p.) injection to induce diabetes [26]. Control mice were injected with vehicle alone. Measures of blood glucose were performed using a One Touch Basic blood glucose monitoring system (LifeScan Italy S.R.L, Milan, Italy) to ensure hyperglycemia. Body weight was also

monitored. Only mice with blood glucose concentration exceeding 500 mg/dL were considered diabetic and used for the study. Notably, 15, 17, and 19 days after the STZ administration, diabetic mice received i.p. injection of saline (10 mL/kg, control mice) or AG in saline (50 mg/kg, 10 mL/kg).

Paw thermal withdrawal latency (PWL) was used to measure thermal hyperalgesia and performed by using an infrared generator (code 7360, Ugo Basile, Gemonio, VA, Italy). Mice were gently restrained using a glove, and after placing the mouse footpad in contact with the radiant heat source paw, withdrawal latency was measured. A timer initiated automatically when the heat source was activated, and a photocell stopped the timer when the mouse withdrew its hind paw. An intensity of 30 and a cut-off time of 15 s were used of the heat source on the plantar apparatus to avoid tissue damage. The PWL, in terms of seconds, of each animal in response to the plantar test was determined [27]. Baseline paw thermal withdrawal latencies were determined before saline or AG administration.

Data Analysis and Statistics

In vitro Data

Collected data analysis was carried out by using 2-way ANOVA test for repeated samples corrected for multiple comparisons by the Bonferroni procedure. All data reported in this paper were verified in at least 3 different experiments performed in triplicate and reported as mean \pm standard deviation (SD). Flow cytometry analyses were performed by using a FACSCalibur flow cytometer (BD Biosciences, San Jose, CA, USA) equipped with a 488 argon laser and with a 635 red diode laser. At least 20,000 events/sample were acquired and analyzed using the Cell Quest Pro software (BD Biosciences, San Jose, CA, USA).

In vivo Data

Statistically significant differences between groups were measured with an analysis of variance (2-way ANOVA) followed by Sidak's or Dunnett's post hoc comparisons test, when the comparison was restricted to two groups. GraphPad Prism 6.0 software (San Diego, CA, USA) was used to analyze the data.

Results

AG Counteracted High Glucose-Induced Cell Death

One of the causes of DPN is death of Schwann cells due to prolonged exposure to high glucose and consequent oxidative stress. On this basis, we investigated the effect of GLU by using SH-SY5Y neuroblastoma as a model cell line. First of all, to determine the effect of high glucose on viability of SH-SY5Y cells, we treated cells with increasing concentrations of GLU or MAN (0–300 mM) for different time points (24, 48 and 72 h). We observed that, starting from 48 h, GLU was able to induce an appreciable cytotoxic effect. The results obtained at this timepoint using Calcein-AM showed that the percentage of dead cells increased along with increasing concentrations of GLU, being about 30% at a concentration of 300 mM (Figure 1A). Importantly, percentage of cell death induced by MAN was significantly lower than that induced by the same concentration of GLU and not significantly different from control untreated cells (Figure 1A). The antiapoptotic and anti-inflammatory effect of AG has been reported in various contexts [28]. Thus, we tested two different concentrations (500 µg/mL and 1000 µg/mL) of AG to verify its ability to inhibit the cytotoxic effects induced by 300 mM GLU (Figure 1B). We observed a protective effect exerted by AG already at 500 µg/mL, which became significantly more marked by increasing the concentration of AG to 1000 µg/mL. On the basis of these preliminary experiments, we selected 300 mM as the concentration of GLU inducing an appreciable cytotoxic effect (also indicated as high glucose through the text, HG) and 1000 µg/mL as the concentration of AG capable of significantly inhibiting it (Figure 1B). Note that both fall within the range of concentrations used, as reported in the literature [29,30].

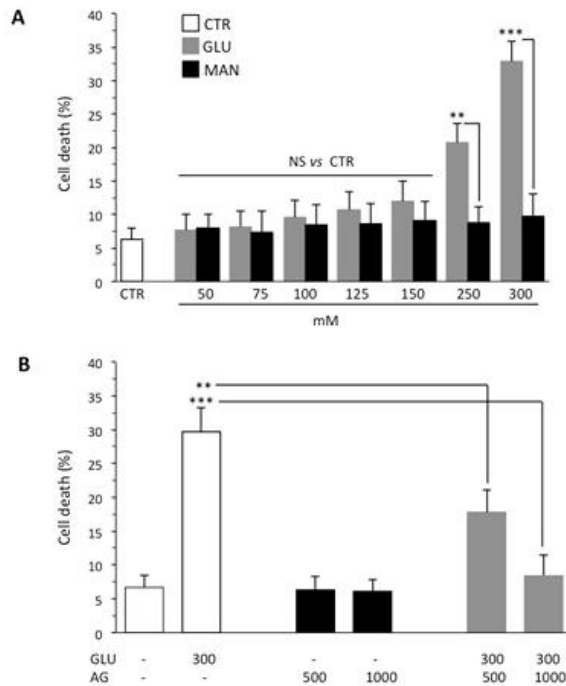


Figure 1. Flow cytometry analysis after staining with Calcein-AM (which is retained in the cytoplasm of live cells). **(A)** SH-SY5Y neuroblastoma cells were analyzed after treatment with increasing concentrations (0–300 mM) of GLU or MAN (used as an osmolarity control) for 48 h. Numbers represent the percentage of Calcein-negative cells (dead cells). Results obtained from three independent experiments are reported as means \pm SD. **(B)** SH-SY5Y cells tested after treatment with 300 mM GLU or MAN alone or in combination with two different concentrations (500 and 1000 μ g/mL) of AG. Results obtained from four independent experiments are reported as means \pm SD. ** is for $p < 0.01$, and *** is for $p < 0.001$.

AG Counteracted HG-Induced Apoptosis and Mitochondrial Alterations

Through flow cytometry analysis after double cell staining with Annexin V (AV)/propidium iodide (PI), we analyzed apoptosis in SH-SY5Y neuroblastoma cells growing in HG conditions for 48 h. We found that HG induced cell death by apoptosis in about 30% of SH-SY5Y cells and that 1000 μ g/mL AG was able to almost completely inhibit HG-induced apoptosis (Figure 2A). Neither MAN (considered as an internal control) nor AG-treated cells showed any significant difference when compared to untreated control cells. It is known that hyperglycemia induces mitochondrial dysfunction [31]. We therefore analyzed the MMP by flow cytometry, after cell staining with JC-1 probe. HG induced a significant increase in the percentage of cells with high MMP, i.e., hyperpolarized mitochondria (boxed area, in Figure 2B). According to apoptosis data, AG was able to significantly ($p < 0.01$) reduce the percentage of cells with high MMP induced by HG, and MAN did not induce any alteration of MMP

(boxed areas in Figure 2B). Overlapping results were obtained using TMRM as a probe for the study of the MMP (Figure S1).

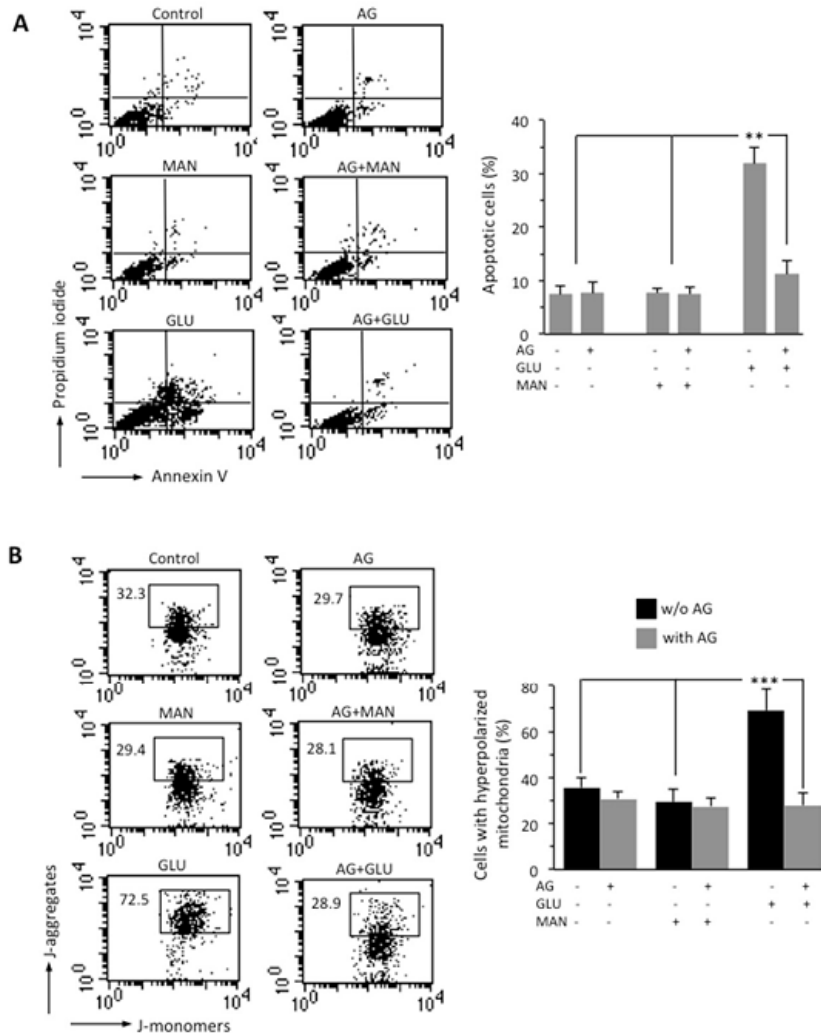


Figure 2. SH-SY5Y neuroblastoma cells were treated with 300 mM GLU or MAN alone or in combination with 1000 µg/mL AG for 48 h. **(A)** FACS analysis after double cell staining with Annexin V/PI. Left panels. Dot plots from a representative experiment are shown. Numbers represent the percentages of Annexin V-positive cells (bottom-right quadrant), Annexin V/PI double-positive cells (upper right quadrant), or PI-positive cells (upper left quadrant). Bar graph shows results obtained from four independent experiments, reported as means ± SD. **(B)** Left panels. Representative dot plots of the FACS analysis of MMP, performed by using JC-1. Numbers in the boxed areas indicate the percentage of cells with high MMP (hyperpolarized mitochondria). Bar graph shows the percentage of cells with hyperpolarized mitochondria obtained from three independent experiments and reported as percentage ± SD. ** is for $p < 0.01$, and *** is for $p < 0.001$.

The accumulation of evidence indicates that the mitochondrial fragmentation and fission represent important contributing factors to alterations of mitochondrial membrane and

ATP production [32,33]. Thus, we also evaluated the mitochondrial network organization by immunofluorescence analysis after cell staining with antimitochondrial import receptor subunit TOM20 (red) and counterstaining with Hoechst (blue) in cells grown under HG conditions. We found that GLU induced mitochondrial fragmentation (Figure 3A), which is normally associated with dysfunctional mitochondria [34]. The administration of AG to cells growing under HG restored normal mitochondrial morphology, as also revealed by morphometric analysis performed by using ImageJ to measure average mitochondrial area in cells stained with an anti-TOM20 antibody (Figure 3B).

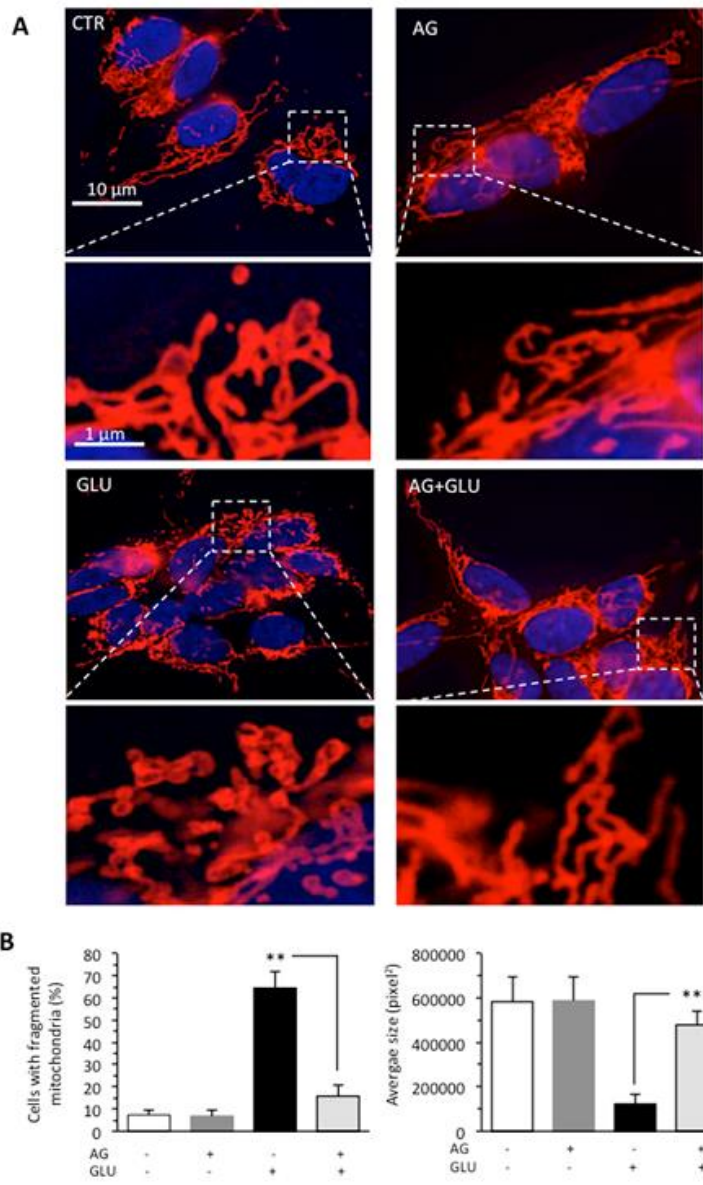


Figure 3. SH-SY5Y neuroblastoma cells were treated with 300 mM GLU or MAN alone or in combination with 1000 µg/mL AG for 48 h. (A) Representative micrographs obtained by IVM showing the mitochondrial network of SH-SY5Y neuroblastoma cells, untreated (CTR) or treated for 48 h with 100 mM GLU with or without AG, after staining with anti-TOM20 (red) and counterstaining with Hoechst (blue). In the bottom pictures, magnification of the boxed areas. (B) Left panel. Bar graph showing the percentage of cells in which fragmented mitochondria were observed. Right panel. Morphometric analysis performed by using the ImageJ software. In ordinate average mitochondrial area is expressed as pixel². Data are reported as mean value ± SD of the results obtained by analyzing at least 50 cells for each sample. ** is for $p < 0.01$, and *** is for $p < 0.001$.

Mitochondria form a highly interconnected and dynamic network and provide necessary ATP for the smooth functioning of cells [35]. Mitochondrial fragmentation due to

fission process is promoted by the activation of dynamin-related protein 1 (DRP1) [36], which, under stress conditions, is recruited in mitochondria [37]. In mammals, at least two proteins, the dynamin-related protein DRP1 and the mitochondrial outer membrane protein hFIS1, participate in mitochondrial fission. The opposite process, mitochondrial fusion, is regulated by various proteins, among which are mitofusin 2 (MFN2) which mediates fusion of outer membrane and the optic atrophy protein 1 (OPA1) which carries out fusion of inner membrane [38]. Since mitochondria fusion and fission are strictly related, the activation of one of these processes leads to the inhibition of the other [39]. Thus, we evaluated DRP1, hFIS1, MFN2, and OPA1 by Western blot analysis. HG induced an increase in the expression levels of both DRP1 and hFIS1 proteins, while in cells subjected to the simultaneous administration of GLU and AG, we did not observe any significant difference from control untreated cells (Figure 4A,B). As far as proteins involved in the fusion process were concerned, HG seemed not to influence significantly the expression of MFN2 but dramatically reduced the expression of OPA1. This reduction was effectively countered by treatment with AG (Figure 4C).

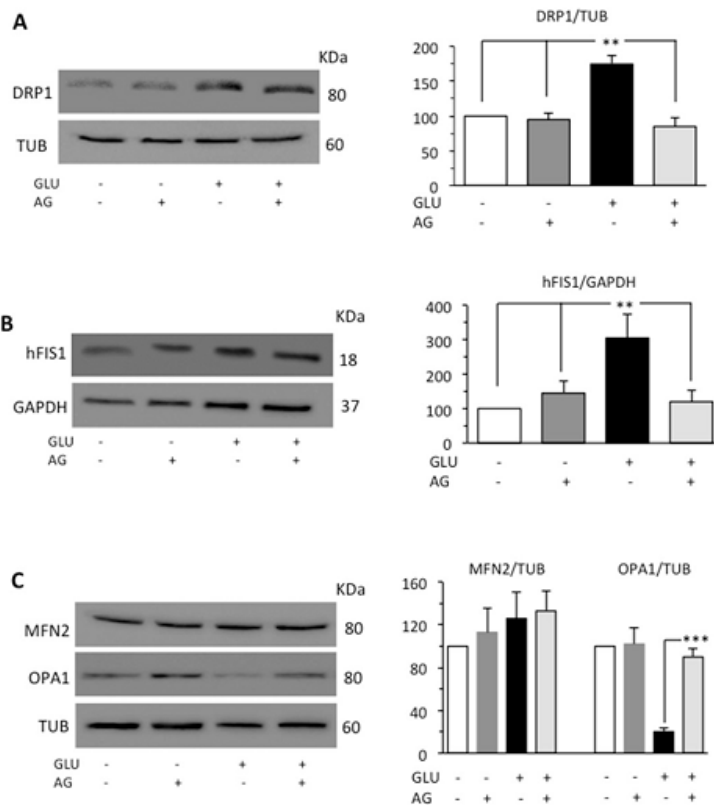


Figure 4. Western blot analysis of (A) DRP1 and (B) hFIS1, and (C) MFN2 and OPA1, involved in fission and fusion processes, respectively. Loading control was evaluated using anti-TUB or anti-GAPDH MAb. A representative experiment among the three is shown. Bar graphs on the right panel show densitometric analysis of the band density ratio of each protein relative to loading control. Mean \pm SD from three independent experiments is shown. ** $p \leq 0.01$ and *** $p \leq 0.001$.

AG Counteracted Inflammation Induced by HG

Diabetic patients have been found to increased HMGB1 and RAGE levels [40,41]. HMGB1 is normally expressed in the nucleus. However, following signals of stress, injury, or tissue damage, the protein was released into the extracellular space. HMGB1 can bind the Toll-like receptor 4 (TLR4) and the receptor for advanced glycation end-products (RAGE), leading to increased inflammation commonly through nuclear factor kappa beta (NF κ B) [42]. On these bases, we investigated the possible anti-inflammatory activity of AG in our cell model analyzing by Western blot HMGB1, which is a ubiquitous nuclear protein that promotes inflammation when extruded from the cell after stress, damage, or death, and p65-nuclear factor kappa-light-chain-enhancer of activated B cells (NF κ B), which is a critical regulator of immune and inflammatory responses. According to the literature's data, HG condition induced a significant increase in the expression levels of both HMGB1 and NF κ B. Administration of AG in

cells subjected to HG effectively decreased the level of both proinflammatory proteins (Figure 5).

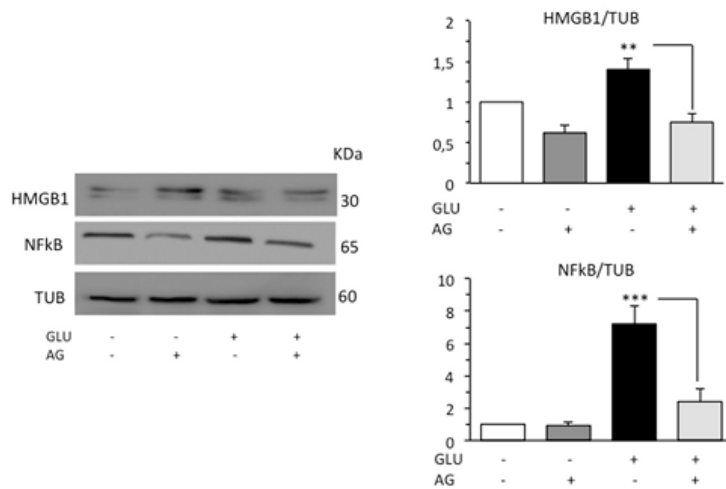


Figure 5. Western blot analysis of the inflammatory proteins HMGB1 and NFκB. Loading control was evaluated using anti-TUB. A representative experiment among the three is shown. Bar graphs on the right panels show densitometric analysis of the band density ratio of each protein relative to loading control. Mean ± SD from three independent experiments is shown. ** $p \leq 0.01$ and *** $p \leq 0.001$.

AG Induced Anti-Hyperalgesic Effect in Diabetic Mice

To test the efficacy of AG in preventing or mitigating diabetic neuropathy induced by hyperglycemia *in vivo*, we used STZ as inducers of diabetes in mice. The results of experiments performed in diabetic mice are reported in Figure 6. STZ resulted in increased thermal hyperalgesia—a reduction in the withdrawal threshold to a noxious stimulus—when compared to baseline recorded before diabetes as observed 13 days after STZ treatment. When AG was first administered 15 days after STZ, a nonsignificant increase in paw withdrawal latencies was observed (Figure 6). AG was administered again at days 17 and 19 after STZ injection, and at this time, a strong increase in paw latency was recorded. Thus, our data demonstrated that a short-repeated treatment with AG is able to induce an anti-hyperalgesic effect in diabetic mice.

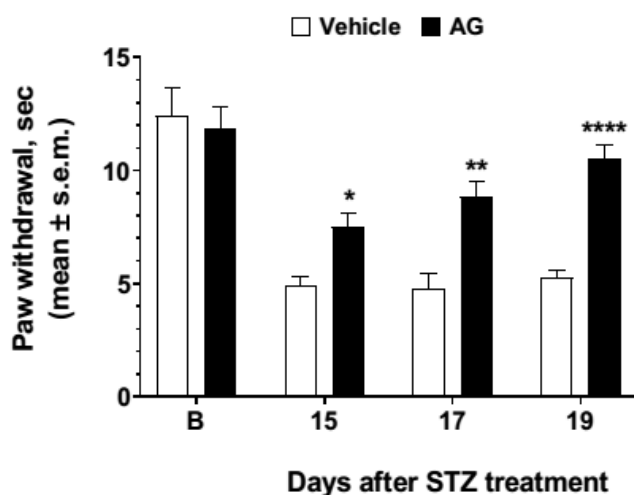


Figure 6. Effects induced by AG in Streptozotocin-induced diabetic mice. Paw withdrawal latency was recorded before STZ treatment (baseline latency, B) and three more times at 15, 17, and 19 thereafter. Vehicle (V, saline 10 mL/kg) and AG (50 mg/kg, 10 mL/kg) were administered three times at day 15, 17, and 19 after STZ injection. * is for $p < 0.05$, ** is for $p < 0.01$, and **** is for $p < 0.001$ vs V. $n = 9$.

Discussion

According to the World Health Organization, diabetes is defined as a chronic metabolic disease characterized by an incorrect glucose metabolism resulting from defects in insulin secretion or insulin action. Diabetic peripheral neuropathy (DPN) is one of the most common complications of diabetes, affecting at least 50% of patients with diabetes during their lifetime [43]. For the treatment of DPN, clinical guidelines recommend symptomatic treatments with different classes of drugs, which include opioids, the γ -aminobutyric acid analogues, and antidepressants [23]. Unfortunately, these drugs induce many adverse effects on the level of several organs; hence, it is necessary to identify new strategies for the management of DPN and DPN-associated pain, both in terms of prevention and treatment. Many clinical studies have been carried out with unsuccessful results, and consequently, the therapeutic advances have not been noteworthy. In fact, as of now, the only recommendation for preventing or slowing the progression of peripheral neuropathy is to maintain close glycemic control. It has also been suggested that pharmacological activation of protective neuronal circuits may be useful for increasing tolerance to the hyperglycemic condition and for promoting neuronal recovery [44].

Although the pathogenic mechanisms of DPN are still not fully understood, the multifactorial nature of the pathological changes induced by the lack of glycemic

control is now clear [45]. One of the mechanisms that lead to the damage of the nervous tissue in DPN is activated in the state of hyperglycemia that triggers the increase in mitochondrial and cytoplasmic ROS/NS production. Mitochondria are particularly abundant at neuronal synapse levels where they play an important role in maintaining calcium homeostasis, and a strong link between neuronal dysfunction and mitochondrial dysfunction has also been observed [46]. The mitochondria constitute a dynamic network that, through fusion and fission processes, maintain their efficiency and distribution within the cell on the basis of energy needs. Furthermore, the mitochondrial transport chain has been shown to contribute significantly to the neuropathic pain, whose pathogenesis would therefore be strongly ATP dependent [47]. The centrality of mitochondrial damage in the etiopathogenesis of DPN was also suggested by the positive correlation between the stage of the disease and the relationship between whole blood and plasma mtDNA levels in patients with diabetes [48]. In mammals, mitochondrial fragmentation due to fission process is promoted by the activation of DRP1 protein [36], which, under stress conditions, is recruited in mitochondria [37] and by the mitochondrial outer membrane protein hFIS1. Various proteins, among which MFN2 and OPA1, regulate mitochondrial fusion [38]. The balance between fission and fusion is crucial for cell fate, and despite the complex etiology of neuropathic pain, a fundamental role has recently been recognized to the excess of mitochondrial fission as a possible early cause of neuronal loss due to apoptotic death [12,49]. In accordance with the central role played by the mitochondrion in the pathogenesis of DPN, we observed in SH-SY5Y neuroblastoma cells subjected to hyperglycemic stress an alteration of the MMP (i.e., hyperpolarization), a mitochondrial fragmentation accompanied by the increase in the expression of DRP1 and hFIS and the decrease in MFN2, and, finally, a significant increase in apoptosis. Moreover, as also reported by numerous recent studies carried out both *in vitro* and *in vivo* [50,51,52,53], we found that SH-SY5Y cells subjected to HG conditions increased the expression of HMGB1 and NFκB. HMGB1, when released by the cell actively or passively due to its death, can interact with the receptor for advanced glycation end products (RAGE) or with Toll-like receptor 4 (TLR4) triggering, by the activation of NFκB, an inflammatory response. Although a strong activation of the inflammatory pathways contributes to diabetic neuropathy, and in the development and maintenance of neuropathic pain, it has nevertheless been shown that normalization of the inflammatory state is per se not

sufficient to revert the neuropathic state. In fact, only the concomitant re-establishment of mitochondrial bioenergetic conditions would seem able to attenuate DPN [54].

Herbs have been used throughout the world in medical practice, for example in traditional Chinese medicine [55] and Ayurvedica [56]. However, due to their complexity, it is very difficult to standardize the composition and production of herbal medicines. On the other hand, the bioactive molecules contained in plants can be isolated and studied by the same methods used for drugs in allopathic medicine. For example, Arauna and coworkers reported that many natural bioactive compounds have the ability to regulate oxidative phosphorylation, production of reactive oxygen species, and mitochondrial dysfunction [57]. Here, we analyzed the effects of AG, a salt derived from the natural triterpene glycoconjugate of the root of licorice, which is the main active compound known to exhibit pharmacological activities—including anti-inflammatory and antioxidative ones [58,59]—in preventing the damage caused by HG in the SH-SY5Y cell line. This cell line is commonly used as an *in vitro* model for the study of diabetic neuropathy, because, when treated with HG, it shows similar alterations to those observed in dorsal root ganglion (DRG) neurons and Schwann cells [24,60]. First of all, we observed that AG was able to attenuate the cytotoxic effect of high glucose (300 mM, 48 h) by inhibiting cell death. Going deeper into the mechanisms underlying this protective effect, we found that cell treatment with AG completely prevented the alterations of the mitochondrial membrane potential and the mitochondrial fragmentation induced by high concentrations of glucose. Although the anti-inflammatory activity of AG has already been documented in experimental models of diabetes [61,62,63], to the best of our knowledge, the effects of this natural compound at the mitochondrial level are reported for the first time in this work.

Too often the encouraging results obtained on simplified *in vitro* models are not matched by more complex *in vivo* models. Although no mouse model exactly reproduces DPN observed in humans, streptozotocin-induced diabetic mice are currently considered an excellent model for preclinical studies [64], as they develop primarily distal axon loss, systemic injury of the peripheral nervous system, and altered interactions with Schwann cells, which are recognized as typical features of DPN [65]. Importantly, in this animal model, we demonstrated that a short-repeated treatment with AG was able to contrast significantly thermal hyperalgesia, known to be associated with increased HMGB1 expression in DRG, as recently reported in Zucker diabetic rat and

ob/ob mice [61]. On the other hand, AG is also able to reduce or suppress nociception in other pain models [66] and the persistent endogenous release of HMGB1 by sensory neurons may be a potent, physiologically relevant modulator of neuronal excitability as observed in tibial nerve injured neuropathic rat [11]. On the other hand, glycyrrhizin bound directly to both HMG boxes of HMGB1 and inhibited its chemoattractant and mitogenic activities [67]. Recently, many studies have investigated the mechanisms of HMGB1 inhibition by AG in a wide number of HMGB1-involved diseases, and it has been demonstrated that AG inhibited extracellular HMGB1 cytokine activity, and protected spinal cord, liver, brain, and myocardium against ischemia–reperfusion (I/R)-induced injury in experimental animals [68].

Considering the absence of cytotoxicity, even at high concentrations, and the good pharmacological tolerability in rodents and humans after acute or subchronic treatment [69], AG may represent a complementary medicine in the clinical management of DPN with the added advantage of providing a multitarget effect on the various etiological factors underlying the pathophysiology of DPN, such as inflammation and mitochondrial damage.

References

1. Selyutina O, Polyakov N. Glycyrrhizic acid as a multifunctional drug carrier – From physicochemical properties to biomedical applications: A modern insight on the ancient drug. *Int. J. Pharm.* 2019, 559, 271–279.
2. Fiore C, Eisenhut M, Ragazzi E, et al. A history of the therapeutic use of liquorice in Europe. *J. Ethnopharmacol.* 2005, 99, 317–324.
3. Pastorino G, Cornara L, Soares S, et al. Liquorice (*Glycyrrhiza glabra*): A phytochemical and pharmacological review. *Phytother. Res.* 2018, 32, 2323–2339.
4. Ming LJ, Yin ACY. Therapeutic Effects of Glycyrrhizic Acid. *Nat. Prod. Commun.* 2013, 8, 415–418.
5. Richard SA. Exploring the Pivotal Immunomodulatory and Anti-Inflammatory Potentials of Glycyrrhizic and Glycyrrhetic Acids. *Mediat. Inflamm.* 2021, 2021, 1–15.
6. Sun X, Zeng H, Wang Q, et al. Glycyrrhizin ameliorates inflammatory pain by inhibiting microglial activation-mediated inflammatory response via blockage of the HMGB1-TLR4-NF- κ B pathway. *Exp. Cell Res.* 2018, 369, 112–119.
7. Musu M, Finco G, Antonucci R, et al. Acute nephrotoxicity of NSAID from the foetus to the adult. *Eur. Rev. Med. Pharmacol. Sci.* 2011, 15, 1461–1472.
8. Benyamin R, Trescot A, Datta S, et al. Opioid complications and side effects. *Pain Physician* 2008, 11, S105–S120.
9. Cole JB, Florez JC. Genetics of diabetes mellitus and diabetes complications. *Nat. Rev. Nephrol.* 2020, 16, 377–390.
10. Callaghan BC, Cheng HT, Stables CL, et al. Diabetic neuropathy: Clinical manifestations and current treatments. *Lancet Neurol.* 2012, 11, 521–534.
11. Feldman P, Due MR, Ripsch MS, et al. The persistent release of HMGB1 contributes to tactile hyperalgesia in a rodent model of neuropathic pain. *J. Neuroinflamm.* 2012, 9, 180.
12. Sifuentes-Franco S, Pacheco-Moisés, FP, Rodríguez-Carrizalez AD, Miranda-Díaz AG. The Role of Oxidative Stress, Mitochondrial Function, and Autophagy in Diabetic Polyneuropathy. *J. Diabetes Res.* 2017, 2017, 1–15.
13. Chowdhury SKR, Smith DR, Fernyhough P. The role of aberrant mitochondrial bioenergetics in diabetic neuropathy. *Neurobiol. Dis.* 2013, 51, 56–65.
14. Turrens JF. Mitochondrial formation of reactive oxygen species. *J. Physiol.* 2003, 552, 335–344.
15. Nicholls DG. Mitochondrial membrane potential and aging. *Aging Cell* 2003, 3, 35–40.
16. Korshunov SS, Skulachev VP, Starkov AA. High protonic potential actuates a mechanism of production of reactive oxygen species in mitochondria. *FEBS Lett.* 1997, 416, 15–18.
17. Wojtczak L, Wie MR. The Mechanisms of Fatty Acid-Induced Proton Permeability of the Inner Mitochondrial Membrane. *J. Bioenerg. Biomembr.* 1999, 31, 447–455.
18. Murphy MP. How mitochondria produce reactive oxygen species. *Biochem. J.* 2009, 417, 1–13.
19. Matarrese P, Straface E, Palumbo G, et al. Mitochondria regulate platelet metamorphosis induced by opsonized zymosan A - activation and long-term commitment to cell death. *FEBS J.* 2009, 276, 845–856.

20. Ciarlo L, Vona R, Manganeli V, et al. Recruitment of mitofusin 2 into “lipid rafts” drives mitochondria fusion induced by Mdivi-1. *Oncotarget* 2018, 9, 18869–18884.
21. Nakagomi S, Barsoum MJ, Bossy-Wetzel E, et al. A Golgi fragmentation pathway in neurodegeneration. *Neurobiol. Dis.* 2008, 29, 221–231.
22. Yu T, Robotham JL, Yoon Y. Increased production of reactive oxygen species in hyperglycemic conditions requires dynamic change of mitochondrial morphology. *Proc. Natl. Acad. Sci. USA* 2006, 103, 2653–2658.
23. Javed S, Alam U, Malik RA. Treating Diabetic Neuropathy: Present Strategies and Emerging Solutions. *Rev. Diabet. Stud.* 2015, 12, 63–83.
24. Hattangady NG, Rajadhyaksha MS. A brief review of *in vitro* models of diabetic neuropathy. *Int. J. Diabetes Dev. Ctries* 2009, 29, 143–149.
25. Matarrese P, Tinari A, Mormone E, et al. Galectin-1 Sensitizes Resting Human T Lymphocytes to Fas (CD95)-mediated Cell Death via Mitochondrial Hyperpolarization, Budding, and Fission. *J. Biol. Chem.* 2005, 280, 6969–6985.
26. Furman BL. Streptozotocin-Induced Diabetic Models in Mice and Rats. *Curr. Protoc. Pharmacol.* 2015, 70, 5.47.1–5.47.20.
27. Dimmito MP, Stefanucci A, Pieretti S, et al. Discovery of Orexant and Anorexant Agents with Indazole Scaffold Endowed with Peripheral Antiedema Activity. *Biomol.* 2019, 9, 492.
28. Tsai J-J, Pan P-J, Hsu F-T et al. Glycyrrhizic Acid Modulates Apoptosis through Extrinsic/Intrinsic Pathways and Inhibits Protein Kinase B- and Extracellular Signal-Regulated Kinase-Mediated Metastatic Potential in Hepatocellular Carcinoma *In vitro* and *In vivo*. *Am. J. Chin. Med.* 2020, 48, 223–244.
29. Chen M, Zheng H, Wei T, et al. High Glucose-Induced PC12 Cell Death by Increasing Glutamate Production and Decreasing Methyl Group Metabolism. *BioMed Res. Int.* 2016, 2016, 1–9.
30. Kao T-C, Shyu M-H, Yen G-C. Neuroprotective Effects of Glycyrrhizic Acid and 18 β -Glycyrrhetic Acid in PC12 Cells via Modulation of the PI3K/Akt Pathway. *J. Agric. Food Chem.* 2009, 57, 754–761.
31. Zochodne DW. The challenges of diabetic polyneuropathy: A brief update. *Curr. Opin. Neurol.* 2019, 32, 666–675.
32. Shenouda SM, Widlansky ME, Chen K, et al. Altered Mitochondrial Dynamics Contributes to Endothelial Dysfunction in Diabetes Mellitus. *Circulation* 2011, 124, 444–453.
33. Yu T, Jhun BS, Yoon Y. High-Glucose Stimulation Increases Reactive Oxygen Species Production through the Calcium and Mitogen-Activated Protein Kinase-Mediated Activation of Mitochondrial Fission. *Antioxid. Redox Signal.* 2011, 14, 425–437.
34. Disatnik M, Ferreira JC, Campos J, et al. Acute Inhibition of Excessive Mitochondrial Fission After Myocardial Infarction Prevents Long-term Cardiac Dysfunction. *J. Am. Heart Assoc.* 2013, 2, e000461.
35. Kuzmicić J, del Campo A, López-Crisosto C, et al. Mitochondrial Dynamics: A Potential New Therapeutic Target for Heart Failure. *Rev. Española Cardiol.* 2011, 64, 916–923.
36. Horbay R, Bilyy R. Mitochondrial dynamics during cell cycling. *Apoptosis* 2016, 21, 1327–1335.
37. Yoon Y, Krueger EW, Oswald BJ, McNiven MA. The Mitochondrial Protein hFis1 Regulates Mitochondrial Fission in Mammalian Cells through an

- Interaction with the Dynamin-Like Protein DLP1. *Mol. Cell. Biol.* 2003, 23, 5409–5420.
38. Tilokani L, Nagashima S, Paupe V, Prudent J. Mitochondrial dynamics: Overview of molecular mechanisms. *Essays Biochem.* 2018, 62, 341–360.
 39. Chan DC. Fusion and Fission: Interlinked Processes Critical for Mitochondrial Health. *Annu. Rev. Genet.* 2012, 46, 265–287.
 40. Škrha J Jr, Kalousova M, Švarcová J, et al. Relationship of Soluble RAGE and RAGE Ligands HMGB1 and EN-RAGE to Endothelial Dysfunction in Type 1 and Type 2 Diabetes Mellitus. *Exp. Clin. Endocrinol. Diabetes* 2012, 120, 277–281.
 41. Dozio E, Vianello E, Briganti S, et al. Expression of the Receptor for Advanced Glycation End Products in Epicardial Fat: Link with Tissue Thickness and Local Insulin Resistance in Coronary Artery Disease. *J. Diabetes Res.* 2015, 2016, 1–8.
 42. Jiang Y, Steinle JJ. HMGB1 inhibits insulin signalling through TLR4 and RAGE in human retinal endothelial cells. *Growth Factors* 2018, 36, 164–171.
 43. Boulton AJ, Vinik AI, Arezzo JC, et al. Diabetic Neuropathies: A statement by the American Diabetes Association. *Diabetes Care* 2005, 28, 956–962.
 44. Emery S, Dobrowsky R. Promoting Neuronal Tolerance of Diabetic Stress. *Int. Rev. Neurobiol.* 2016, 127, 181–210.
 45. Singh R, Kishore L, Kaur N. Diabetic peripheral neuropathy: Current perspective and future directions. *Pharmacol. Res.* 2014, 80, 21–35.
 46. Hoppins S, Lackner L, Nunnari J. The Machines that Divide and Fuse Mitochondria. *Annu. Rev. Biochem.* 2007, 76, 751–780.
 47. Joseph EK, Levine JD. Mitochondrial electron transport in models of neuropathic and inflammatory pain. *Pain* 2006, 121, 105–114.
 48. Rosa HS, Ajaz S, Gnudi L, Malik AN. A case for measuring both cellular and cell-free mitochondrial DNA as a disease biomarker in human blood. *FASEB J.* 2020, 34, 12278–12288.
 49. Dai C-Q, Guo Y, Chu X-Y. Neuropathic Pain: The Dysfunction of Drp1, Mitochondria, and ROS Homeostasis. *Neurotox. Res.* 2020, 38, 553–563.
 50. Wang F-C, Pei J-X, Zhu J, et al. Overexpression of HMGB1 A-box reduced lipopolysaccharide-induced intestinal inflammation via HMGB1/TLR4 signaling *in vitro*. *World J. Gastroenterol.* 2015, 21, 7764–7776.
 51. Wu B, Guo Y, Chen Q, et al. MicroRNA-193a Downregulates HMGB1 to Alleviate Diabetic Neuropathic Pain in a Mouse Model. *Neuroimmunomodulation* 2019, 26, 250–257.
 52. Bestall SM, Hulse RP, Blackley Z, et al. Sensory neuronal sensitisation occurs through HMGB-1/ RAGE and TRPV1 in high glucose conditions. *J. Cell Sci.* 2018, 131, 215939.
 53. Wang X, Feng C, Qiao Y, Zhao X. Sigma 1 receptor mediated HMGB1 expression in spinal cord is involved in the development of diabetic neuropathic pain. *Neurosci. Lett.* 2018, 668, 164–168.
 54. Ma J, Pan P, Anyika M, et al. Modulating Molecular Chaperones Improves Mitochondrial Bioenergetics and Decreases the Inflammatory Transcriptome in Diabetic Sensory Neurons. *ACS Chem. Neurosci.* 2015, 6, 1637–1648.
 55. Tian J, Lian F, Yu X, et al. The Efficacy and Safety of Chinese Herbal Decoction in Type 2 Diabetes: A 5-Year Retrospective Study. *Evid. Based Complement. Altern. Med.* 2016, 2016, 1–8.

56. Gordon A, Buch Z, Baute V, Coeytaux R. Use of Ayurveda in the Treatment of Type 2 Diabetes Mellitus. *Glob. Adv. Health Med.* 2019, 8.
57. Arauna D, Furrianca M, Espinosa-Parrilla Y, et al. Natural Bioactive Compounds As Protectors Of Mitochondrial Dysfunction In Cardiovascular Diseases and Aging. *Molecules* 2019, 24, 4259.
58. Batiha GE-S, Beshbishy AM, El-Mleeh A, et al. Traditional Uses, Bioactive Chemical Constituents, and Pharmacological and Toxicological Activities of *Glycyrrhiza glabra* L. (Fabaceae). *Biomolecules* 2020, 10, 352.
59. Li X, Sun R, Liu R. Natural products in licorice for the therapy of liver diseases: Progress and future opportunities. *Pharmacol. Res.* 2019, 144, 210–226.
60. Shindo H, Thomas TP, Larkin DD, et al. Modulation of basal nitric oxide-dependent cyclic-GMP production by ambient glucose, myo-inositol, and protein kinase C in SH-SY5Y human neuroblastoma cells. *J. Clin. Investig.* 1996, 97, 736–745.
61. Thakur V, Sadanandan J, Chattopadhyay M. High-Mobility Group Box 1 Protein Signaling in Painful Diabetic Neuropathy. *Int. J. Mol. Sci.* 2020, 21, 881.
62. Zheng Y, Yang F, Han L, et al. Efficacy of Chinese Herbal Medicine in the Treatment of Moderate-Severe Painful Diabetic Peripheral Neuropathy: A Retrospective Study. *J. Diabetes Res.* 2019, 2019, 1–10.
63. Biscetti F, Rando MM, Nardella E, et al. High Mobility Group Box-1 and Diabetes Mellitus Complications: State of the Art and Future Perspectives. *Int. J. Mol. Sci.* 2019, 20, 6258.
64. Gao F, Zheng ZM. Animal Models of Diabetic Neuropathic Pain. *Exp. Clin. Endocrinol. Diabetes* 2014, 122, 100–106.
65. O'Brien PD, Sakowski SA, Feldman EL. Mouse Models of Diabetic Neuropathy. *ILAR J.* 2014, 54, 259–272.
66. Maione F, Minosi P, Di Giannuario A, et al. Long-Lasting Anti-Inflammatory and Antinociceptive Effects of Acute Ammonium Glycyrrhizinate Administration: Pharmacological, Biochemical, and Docking Studies. *Molecules* 2019, 24, 2453.
67. Mollica L, De Marchis F, Spitaleri A, et al. Glycyrrhizin Binds to High-Mobility Group Box 1 Protein and Inhibits Its Cytokine Activities. *Chem. Biol.* 2007, 14, 431–441.
68. Musumeci D, Roviello GN, Montesarchio D. An overview on HMGB1 inhibitors as potential therapeutic agents in HMGB1-related pathologies. *Pharmacol. Ther.* 2014, 141, 347–357.
69. Ploeger B, Mensinga T, Sips A, et al. The pharmacokinetics of glycyrrhizic acid evaluated by physiologically based pharmacokinetic modeling. *Drug Metab. Rev.* 2001, 33, 125–147.

CHAPTER 3: Plant-derived peptides rubiscolin-6, soymorphin-6 and their C-terminal amide derivatives: Pharmacokinetic properties and biological activity

Azzurra Stefanucci¹, Marilisa Pia Dimmito¹, Giancarlo Tenore², Stefano Pieretti³, Paola Minosi³, Gokhan Zengin⁴, Chiara Sturaro⁵, Girolamo Calò⁵, Ettore Novellino², Angelo Cichelli⁶, Adriano Mollica¹

¹ Department of Pharmacy, University of Chieti-Pescara "G. d'Annunzio", 66100 Chieti, Italy.

² Department of Pharmacy, University of Naples "Federico II", Via D. Montesano 49, 80131 Naples, Italy.

³ Istituto Superiore di Sanità, Centro Nazionale Ricerca e Valutazione Preclinica e Clinica dei Farmaci, Viale Regina Elena 299, 00161 Rome, Italy.

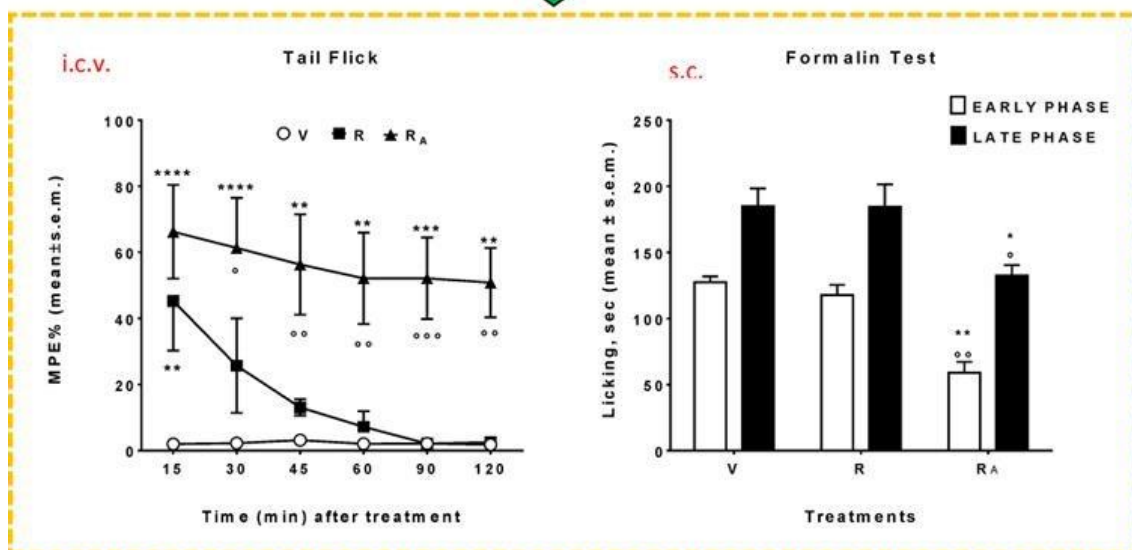
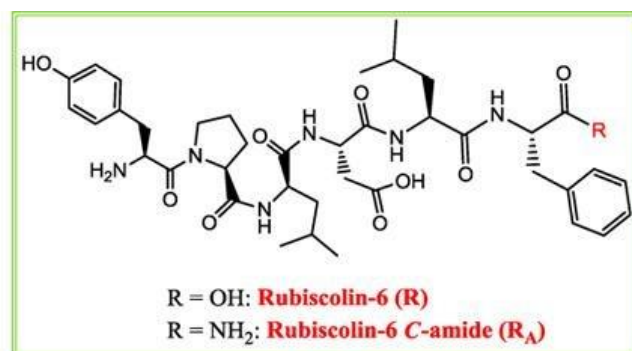
⁴ Department of Biology, Science Faculty, Selcuk University, Konya, Turkey.

⁵ Department of Medical Sciences, Section of Pharmacology, University of Ferrara, Italy.

⁶ Department of Medical, Oral and Biotechnological Sciences, "G. d'Annunzio" University Chieti-Pescara, Via dei Vestini 31, 66100 Chieti, Italy.

Abstract

The aim of this work is to investigate the pharmacokinetic properties, antinociceptive and antioxidant activities of rubiscolin-6, soymorphin-6 and their C-terminal amides; The four peptides were synthesized following FmocSPPS strategy to give the final peptides in excellent overall yields and purity following analytical RP-HPLC analysis. None of them shows antioxidant activity and α -tyrosinase inhibition *in vitro*. All compounds are able to activate G-protein coupled receptor at the δ -opioid receptor (DOR) at 100 μ M concentration however, rubiscolin-6-amide exhibits significant antinociceptive effect after i.c.v. administration in the tail flick test (TF) and s.c. administration in the formalin test (FT). Rubiscolin-6 shows the best *in vitro* intestinal bioavailability in CaCo2 cell monolayer and stability to the brush border exopeptidases in the apical compartment. *In silico* experiments show the interaction of rubiscolin-6 and rubiscolin-6 amide at the binding cavity of DOR compared with the crystallographic ligand TIPP-NH₂.



Introduction

Exogenous peptides endowed with opioid activity deriving from natural proteins, acting on plants and animals are called exorphins [1]. Some peptides derived from plant proteins might show beneficial effect for plant suppressing escape reaction of insects [1,2]. In general, such bioactive peptides may exert several pharmacological activity as receptor's ligands, enzymes inhibitors, peptides modulating transport, anti-microbial peptides and antioxidant and radical scavenger. The affinity of those peptides for opioid receptors are much smaller than the endogenous ones, however some of them exhibit central and peripheral effects after oral administration [3,4].

Accordingly, opioid peptides derived from food through protein digestion, fermentation, or food production processes could produce several benefits against some health problems, such as obesity, cardiovascular diseases, type II-diabetes and immune disorders [5]. Among them, soymorphins and rubiscolins recently received a great attention from researchers due to their potential applications in the development of functional foods and as lead compounds for the design of novel chemical entities.

Soymorphin (SM peptide sequence: Tyr-Pro-Phe-Val-Val-Asn-Ala) is an opioid eptapeptide derived from the enzymatic digestion of soy proteins which are consumed in cereals. Specifically, SM belongs to the enzymatic digestion of soybean β -conglycinin β -subunit by DPP-IV. The shorter sequence YPFVV found in the C-terminal region of β -conglycin β subunit is the homologue of human β -casomorphin-5 (YPFVE) named soymorphin-5 [4].

β -conglycin β subunit releases soymorphin-5 by pancreatic elastase and leucine aminopeptidase, while soymorphin-6 (YPFVVN) is obtained by the action of pepsin and pancreatic elastase. Soymorphin-6 (SM-6) possesses anxiolytic (at a dose of 100 mg/kg in elevated-plus maze experiment in mice) and anorexygenic effects after oral administration in animal models (at a dose of 36 mg/kg in 18-h fasted mice, four hours after administration), together with a selective MOR opioid activity in GPI and MVD assays which is two fold more potent than β -casomorphin (BCM) [4,6-8].

This hexapeptide shares the sequence YPFV with the human β -casomorphin-4, an opioid peptide with morphine-like activity. Endomorphin-1, -2 (EM-1 and EM-2) and hemorphin (YPWT) derived from hemoglobin, containing the sequence Tyr-Pro-aromatic amino acid are also μ -selective opioid peptides of natural origin [9,10]. In

contrast opioid peptides derived from plants such as gluten exorphin and rubiscolin containing the sequence Tyr-Pro-non aromatic amino acids, are selective for the δ -opioid receptors [8].

Rubiscolin-6 (amino acid sequence: YPLDLF) is an opioid peptide derived from the plant enzyme Rubisco, which is responsible for CO₂ fixation in green leaves, but it is also a food source in the biosphere [4,7].

Rubiscolin-6 exhibits memory-enhancing, anxiolytic and orexygenic activities in animal models [11]. Rubiscolin-6 is also able to bind both δ and μ -opioid receptors with a good to moderate affinity respectively (IC₅₀ δ 0.93 μ M vs. IC₅₀ μ >2000 μ M), showing a strong selectivity for DOR. This activity is related to the ability of Rubiscolin-6 to stimulate glucose uptake in L6 and C2C12 cells, in enhancement of GLUT4 expression through the AMPK pathway, and improvement of glucose homeostasis in STZ-induced diabetic rats [11].

Rubiscolin-6 produces antinociceptive effect after i.c.v. administration at a minimum dose of 3 nmol/mouse and 1 nmol/mouse using *in vivo* tail pinch method. It exhibits antinociceptive effect *in vivo* after oral administration at 300 mg/kg, mediated by δ -opioid receptors; in fact, the selective δ -opioid receptor antagonist naltrindole blocks antinociception induced by Rubiscolin-6 [12]. Due to its interesting spectra of biological activities on diverse organic systems, rubiscolin-6 is considered as *lead compound* for building a rational structure-activity relationship study [13].

In order to identify the amino acid residues essential for its opioid activity, Rubiscolin-6 derivatives were synthesized and among them δ -opioid activities of [Ile³]-rubiscolin-6 and [Met³]-rubiscolin-6 were four fold higher than that of rubiscolin [2].

The most potent analogue discovered so far was [Met³,Val⁶]-rubiscolin-6 with 20 fold higher potency than the reference exogenous compound [4,8].

Considering the panel of peripheral and central effects exerted by these natural bioactive peptides [7,11,12,14], we planned to prepare Rubiscolin-6 and Soymorphin-6 as *lead compounds* and their C-terminal amide analogues following solid phase peptide synthesis (SPPS). The antioxidant, α -tyrosinase inhibition activities and G protein stimulation at DOR and MOR with calcium mobilization assay have been evaluated *in vitro*, *in vivo* antinociceptive effects have been also studied through tail flick and

formalin tests after i.c.v. and s.c. administration, respectively. Intestinal bioavailability in CaCo2 cell monolayer was also investigated in order to define their possible oral bioavailability and to assess stability to exopeptidases in the brush border. Furthermore, *in silico* molecular modeling study was performed with the aim to reveal the binding mode at the DOR of rubiscolin-6 and its C-terminal amide.

The aim of this project is to investigate the biological and pharmacokinetic properties of opioid plant-derived peptides soymorphin-6, rubiscolin-6 and their novel C-terminal amides derivatives.

Materials and Methods

Chemistry and reagents

Chemicals and reagents were purchased by VWR (MI, Italy) and Merck (MI, Italy), amino acids from GLS Shanghai (China). Final crude peptides were purified on C18 prep RP-HPLC at 216, 235, 254, and 275 nm (Waters C18 4.6 mm × 150 mm); flow rate of 7 mL/min; gradient eluent of H₂O/ACN-0.1% TFA, from 5% ACN to 90% ACN in 32 min. Pure peptides were identified by ¹H NMR at 25 °C on a 300 MHz Varian Oxford spectrometer, DMSO-d₆ as solvent and chemical shifts in parts per million (δ) downfield from the internal standard TMS. LCQ Finnigan-Mat mass spectrometer (San Jose, CA) equipped with ESI-spray source and ion trap analyzer was used at capillary temperature of 200 °C, spray voltage at 4.00 kV and nitrogen and helium as sheath and auxiliary gas respectively.

Peptides and chemical characterization

Soymorphin-6, Rubiscolin-6 and their C-terminal amide analogues were prepared following the well-established Fmoc-solid phase peptide synthesis (Fmoc-SPPS) and were purified by reverse-phase high-performance liquid chromatography (RP-HPLC) [15,16]. The purity of four peptides was checked by analytical RP-HPLC at 236, 268 and 214 nm (C18-bonded 4.6 mm × 150 mm), flow rate of 1 mL/min, using a gradient of H₂O/ACN-0.1% TFA from 5% to 95% ACN in 26 min, and was found to be ≥95%.

In vitro antioxidant activity

For antioxidant capacity, different test systems, including radical quenching (DPPH and ABTS), reducing power (CUPRAC and FRAP), were used. The methods details were

described in our earlier paper [17,18]. Trolox equivalents were selected as standards and compounds abilities were expressed as equivalents of trolox (mg TE/g). The significance of differences ($p < 0.05$) among the peptides was calculated using the parametric One-way ANOVA test together with Tukey's test (GraphPad Prism 6.0).

α -tyrosinase inhibition assay

For the tyrosinase inhibition assay, we used L-DOPA (as substrate) and mushroom tyrosinase enzyme (E.C. 1.14.18.1) [19]. Kojic acid was used as a standard inhibitor and the results were expressed as kojic acid equivalents (mg KAE/g) the significance of differences ($p < 0.05$) among the peptides was calculated using the parametric One-way ANOVA test together with Tukey's test (GraphPad Prism 6.0).

In vitro calcium mobilization assay

Drugs and reagents

Brilliant black, bovine serum albumin (BSA), 4-(2-hydroxyethyl)-1-piperazineethanesulfonic acid (HEPES), and probenecid were from Sigma Aldrich (St. Louis, MO, USA). Pluronic acid and Fluo-4 AM were from Thermo Fisher Scientific (Waltham, US). All cells culture media and supplements were from Euroclone (Milano, Italy). Rubiscolin-6, rubiscolin-6 C-amide, soymorphin-6, soymorphin-6 C-amide, endomorphin-1 (EM-1) were dissolved in dimethyl sulfoxide (DMSO) at the concentration of 10 mM. The stock solutions were kept at $-20\text{ }^{\circ}\text{C}$ until use.

Cells

CHO cells lines permanently co-expressing μ -receptors with the C-terminally modified $G\alpha_{q15}$ and δ -receptors with the C-terminally modified $G\alpha_{qG66Di5}$, were used. Details regarding the generation of these cells have been previously described [20,21].

Cells were cultured in culture medium consisting of Dulbecco's modified Eagle's medium (DMEM) / HAMS F12 (1:1) supplemented with 10% fetal bovine serum (FBS), penicillin (100 IU/mL), streptomycin (100 mg/mL), geneticin (G418; 200 $\mu\text{g/mL}$) and hygromycin B (100 $\mu\text{g/mL}$). Cell cultures were kept at $37\text{ }^{\circ}\text{C}$ in 5% CO_2 / humidified air. When confluence was reached (3–4 days), cells were sub-cultured as required using trypsin / EDTA and used for experimentation. Cells were seeded at a density of 50,000 cells / well into 96-well black, clear-bottom plates. After 24 h incubation the cells were loaded with Hank's Balanced Salt Solution (HBSS)

supplemented with 2.5 mM probenecid, 3 μ M of the calcium sensitive fluorescent dye Fluo-4 AM, 0.01% pluronic acid and 20 mM HEPES (pH 7.4) for 30 min at 37 °C. Afterwards the loading solution was aspirated and a washing step with 100 μ L/well of HBSS, HEPES (20 mM, pH 7.4), 2.5 mM probenecid and 500 μ M Brilliant Black was carried out. Subsequently 100 μ L/well of the same buffer was added. After placing cell culture and compound plates into the FlexStation II (Molecular Devices, Sunnyvale, CA, USA), changes in fluorescence of the cell-loaded calcium sensitive dye Fluor-4 AM were measured. On-line additions were carried out in a volume of 50 μ L/well.

Data analysis and terminology

All data were analyzed using Graph Pad Prism 6.0 (La Jolla, CA, USA). Data are expressed as mean \pm sem of n experiments performed in duplicate. In calcium mobilization studies, agonist effects were expressed as maximum change in percent over the baseline fluorescence. Baseline fluorescence was measured in wells treated with vehicle. Agonist potency was expressed as pEC₅₀, which is the negative logarithm to base 10 of the agonist molar concentration that produces 50% of the maximal possible effect of that agonist. Concentration response curve to agonists were fitted with the four-parameter logistic non-linear regression model:

$$\text{Effect} = \text{Baseline} + \frac{E_{\max} - \text{Baseline}}{(1 + 10^{\text{LogEC}_{50} \text{Log}_{[\text{compound}]}})^{\text{Hillslope}}}$$

***In vivo* antinociceptive assays**

Animals

CD-1 male mice (Charles River, Italy) weighing 25–30 g were used in all experiments. Before the experimental sessions, the mice were maintained in colony, housed in cages (7 mice per cage) under standard light/dark cycle (from 7:00 AM to 7:00 PM), temperature (21 \pm 1 °C) and relative humidity (60 \pm 10%) for at least 1 week. Food and water were available *ad libitum*. The research protocol was approved by the Service for Biotechnology and Animal Welfare of the Istituto Superiore di Sanità and authorized by the Italian Ministry of Health, according to Legislative Decree 26/14, which

implemented the European Directive 2010/63/UE on the protection of laboratory animals in Italy. Animal welfare was routinely checked by veterinarians from the Service for Biotechnology and Animal Welfare.

Tail flick test

The tail flick test was used to determine antinociceptive response induced by a thermal stimulus and was performed as described earlier [22]. Tail flick apparatus (Ugo Basile, Varese, Italy) consists of an infrared radiant light source (100 W, 15 V bulb) targeted on a photocell utilizing an aluminum parabolic mirror. During the trials, the mice were gently hand restrained with a glove. Radiant heat was targeted 5–6 cm from the tip of the tail, and the latency (s) of the tail withdrawal recorded. The measurement was disconnected if the latency crossed the cutoff time. A cutoff time of 15 s was imposed, and data were expressed as time course of the percentage of maximum effect (% MPE) = (post drug latency/baseline latency)/(cutoff time baseline latency) × 100. In all experiments, the baseline was calculated as the mean of three readings recorded before testing at intervals of 10 min, and the time course of latency was determined 10–120 min after compound treatment. Compounds were freshly diluted in saline containing 0.1% v/v DMSO, and were injected at 10 µg/10 µL for intracerebroventricular (i.c.v.) administrations, as previously reported [23,24].

Formalin test

The method utilized was comparable to the one previously described [25]. Subcutaneous injection of 20 µL of a 1% solution of formalin in saline into the dorsal surface of the mouse hind paw evoked nociceptive behavioural responses, such as licking, biting the injected paw, or both, which are considered indices of nociception. The nociceptive response showed a biphasic trend: an early phase, occurring from 0 to 10 min after formalin injection, produced by the direct stimulation of peripheral nociceptors, and a late prolonged phase, occurring from 15 to 40 min, which reflected the response to inflammatory pain. During the test, the mouse was placed in a Plexiglas observation cage (30 × 14 × 12 cm), 1 h before the formalin administration and allowed to acclimatize to the testing environment. Compounds were solubilized in saline (0.9% NaCl in distilled water) and DMSO in the ratio DMSO:saline 1:3 (v/v) and were administered subcutaneously in the dorsal surface of the right hind paw of the mouse

using a microsyringe with a 27-gauge needle 15 min before formalin injection at the dose of 100 $\mu\text{g}/20 \mu\text{L}$. Then, the total time the animal spent licking or biting its paw in the early and late phase was recorded.

Statistical analysis

Statistically significant differences between groups in the tail flick test and formalin test were measured with a two-way analysis of variance (2-ANOVA) followed by Tukey's or Sidak's post-hoc comparisons. GraphPad Prism 6.0 software (San Diego, CA, USA) was used to analyze the data. Data were considered statistically significant when a value of $p < 0.05$ was performed.

***In vitro* gastrointestinal digestion**

Reagents and standards

All chemicals and reagents used were either analytical-reagent or HPLC grade. The water was treated in a Milli-Q water purification system (Millipore, Bedford, MA, USA) before use. Chemicals and reagents to simulate the GI digestion were: potassium chloride (KCl), potassium thiocyanate (KSCN), monosodium phosphate (NaH_2PO_4), sodium sulphate (Na_2SO_4), sodium chloride (NaCl), sodium bicarbonate (NaHCO_3), urea, α -amylase, hydrochloric acid (HCl), pepsin, pancreatin, bile salts (Sigma Chemical Co., St. Louis, MO, USA). All organic solvents were purchased from Carlo Erba, (Milano, Italy). 2',7'-dichlorofluorescein diacetate (DCFH-DA, Sigma Chemical Co.) was dissolved in dimethylsulfoxide (DMSO) to obtain 100 mM stock solution (aliquoted and stored at -20°C). Work solutions of DCFH-DA were produced by diluting aliquots in 1% phosphate buffer saline (PBS, 10 mM, pH 7.4) at different concentrations. The assay was performed according to the procedure described by Raiola, Meca, Mañes, and Ritieni [26], with slight modification [26].

GI digestion was distinguished into salivary, gastric and duodenal digestive steps. For the salivary digestion, an aliquot of each peptide (1.0 mg) was mixed with 6 mL of artificial saliva composed of: KCl (89.6 g/L), KSCN (20 g/L), NaH_2PO_4 (88.8 g/L), Na_2SO_4 (57.0 g/L), NaCl (175.3 g/L), NaHCO_3 (84.7 g/L), urea (25.0 g/L) and 290 mg of α -amylase. The pH of the solution was adjusted to 6.8 with 0.1 M HCl. The mixture was introduced in a plastic bag containing 10 mL of water and homogenized in a

Stomacher 80 Microbiomaster (Seward, Worthing, UK) for 3 min. Immediately, 0.5 g of pepsin (14,800 U) dissolved in HCl 0.1 N was added, the pH was adjusted to 2.0 with 6 M HCl, and then incubated at 37 °C in a Polymax 1040 orbital shaker (250 rpm) (Heidolph, Schwabach, Germany) for 2 h. After the gastric digestion, the pancreatic digestion was simulated as follows: the pH was increased to 6.5 with 0.5 M NaHCO₃ and then 5 mL of a mixture pancreatin (8.0 mg/mL) and bile salts (50.0 mg/mL) (1:1; v/v), dissolved in 20 mL of water, were added and incubated at 37 °C in an orbital shaker (250 rpm) for 2 h. Intestinal digested sample was freeze-dried and stored at -80 °C until further analysis.

HPLC-DADA analyses

Intestinal digested samples were filtered through a Phenex-PVDF 17 mm Syringe Filter 0.45 µm (Phenomenex, Torrance, CA, USA) and analysed by RP-HPLC. Analyses were run on a Finnigan HPLC system (Thermo Electron Corporation, San Jose, CA, USA) provided with photodiode array detector (DAD). The column selected was a Aeris PEPTIDE 3.6 µm XB-C18 New Column 250 × 4.6 mm (Phenomenex). Elution conditions consisted in 2% acetic acid (solvent A) and 2% acetic acid in methanol (solvent B) gradient at a flow rate of 1.0 mL/min. The gradient conditions were: 0–20 min, 0–100% B; 20–23 min, 100% B; 23–27 min, 0% B, followed by 5 min of maintenance. Chromatograms were recorded at 280 nm.

In vitro intestinal stability and transepithelial transport studies

The assay was performed as previously described by Tenore, Campiglia, Giannetti, and Novellino [27].

Molecular modeling study

Molecular modeling study was performed on rubiscolin-6 and rubiscolin-6 C-amide using Maestro 2017, following the well-established procedure reported by Stefanucci et al. [28].

Results

Antioxidant and tyrosinase inhibition activities of synthetic peptides

The antioxidant abilities of the synthetic peptides were investigated by DPPH, ABTS, FRAP and CUPRAC methods. The results are in Table 1. The highest DPPH radical scavenging ability was found for rubiscolin-6 C-amide, followed by soymorphin, rubiscolin-6 and soymorphin-6 C-amide, while the best ABTS radical ability was recorded by soymorphin-6 C-amide. In FRAP assay, rubiscolin-6 C-amide showed the highest potential with the value of 5.79 mg TE/g. However, there was no significant differences in FRAP values among rubiscolin-6, rubiscolin-6 C-amide and soymorphin-6 C-amide. As shown in Table 1, rubiscolin-6 exhibited the best tyrosinase inhibition ability with a value of 24.51 mg KAE/g, followed by soymorphin-6 C-amide and rubiscolin-6 C-amide. Soymorphin-6 is not active on tyrosinase.

Table 1
Antioxidant properties and tyrosinase inhibitory effects of the tested peptides.*

Peptides	DPPH (mg TE/g)	ABTS (mg TE/g)	CUPRAC (mg TE/g)	FRAP (mg TE/g)	Tyrosinase inhibition (mg KAE/g)
Rubiscolin-6	2.41 ± 0.33 ^a	8.86 ± 0.38 ^b	10.09 ± 0.02 ^a	5.75 ± 0.04 ^a	24.51 ± 1.99 ^a
Soymorphin-6	2.65 ± 0.70 ^a	3.09 ± 0.47 ^c	9.10 ± 0.08 ^b	5.64 ± 0.04 ^b	na
Rubiscolin-6 C-amide	2.72 ± 0.51 ^a	0.77 ± 0.01 ^d	9.55 ± 0.05 ^c	5.79 ± 0.03 ^a	2.81 ± 0.34 ^c
Soymorphin-6 C-amide	1.38 ± 0.21 ^b	11.00 ± 1.96 ^a	9.35 ± 0.13 ^c	5.72 ± 0.08 ^a	9.19 ± 1.43 ^b

* Values are reported as mean ± S.D of three parallel experiments. TE: Trolox equivalents; KAE: Kojic acid equivalents; na: not active. a-d: Different letters indicate significant differences in the peptides ($p < 0.05$).

Calcium mobilization assay

In these experiments we evaluated the capability of the compounds to activate the μ - and δ -human recombinant receptors permanently transfected in CHO cells. In such cells the expression of a chimeric G protein that forces the opioid receptors to couple with the calcium pathway allows measuring receptor activation with an automated calcium mobilization assay. Dermorphin and DPDPE were used as standard ligands for μ - and δ -receptors, respectively. In CHO $_{\mu}$ cells the standard agonist dermorphin evoked a robust concentration-dependent stimulation of calcium release displaying high potency (pEC₅₀ of 8.06) and maximal effects (254 ± 18% over the basal values). EM-1 mimicked the stimulatory effect of dermorphin showing similar maximal effects but 3-fold lower potency (pEC₅₀ of 7.45). Rubiscolin-6 C-amide, Soymorphin-6 and Soymorphin-6 C-amide stimulated calcium mobilization only at micromolar concentrations eliciting incomplete concentration response curves, while Rubiscolin-6 was completely inactive. The pharmacological parameters of the concentration response curves obtained with these ligands in CHO $_{\mu}$ cells are summarized in Table 2. In CHO $_{\delta}$ cells the standard agonist DPDPE evoked a robust concentration-dependent stimulation of calcium release displaying high potency (pEC₅₀ of 7.51) and maximal effects (223 ± 17% over the basal values). All the other compounds showed an

incomplete concentration response curve, being active only at micromolar concentrations.

Table 2
Potencies (pEC₅₀) and maximal effects of standard and novel ligands at μ and δ -opioid receptors.

Compounds	CHO _{μ}		CHO _{δ}	
	pEC ₅₀ (CL _{95%})	E _{max} \pm sem %	pEC ₅₀ (CL _{95%})	E _{max} \pm sem %
Dermorphin	8.06 (7.65–8.46)	254 \pm 18%	6.43 (5.95–6.91) ^a	78 \pm 3% ^a
DPDPE	Inactive ^a		7.51 (7.31–7.70)	223 \pm 17%
EM-1	7.45 (7.08–7.82)	263 \pm 30%	Crc incomplete, at 100 μ M 89 \pm 15%	
Rubiscolin-6	Inactive		Crc incomplete, at 100 μ M 87 \pm 19%	
Rubiscolin-6 C-amide	Crc incomplete, at 100 μ M 131 \pm 29%		Crc incomplete, at 100 μ M 112 \pm 29%	
Soymorphin-6	Crc incomplete, at 100 μ M 110 \pm 13%		Crc incomplete, at 100 μ M 46 \pm 14%	
Soymorphin-6 C-amide	Crc incomplete, at 100 μ M 81 \pm 4%		Crc incomplete, at 100 μ M 79 \pm 14%	

Data are mean of at least 5 separate experiments made in duplicate.

^a Values taken from (Camarda et al., 2009).

Antinociceptive effects of Rubiscolin-6 C-amide and Soymorphin-6 C-amide

The antinociceptive effect of Rubiscolin-6 and Rubiscolin-6 C-amide are reported in Figure 1. In the tail flick test, Rubiscolin-6 induced a significant antinociceptive effect 15 min after administration, followed by a rapid decrease, which becomes similar to that observed in vehicle-treated animals from 60 to 120 min after administration. On the contrary Rubiscolin-6 C-amide induced a robust and significant antinociceptive effect, which is observed 15 min later and which light decreased up to 120 min after administration (Figure 1). In the formalin test, Rubiscolin-6 was not able to change the nociceptive effect of formalin, both in the early and in the late phase of the test. As previously observed in the tail flick test, Rubiscolin-6 C-amide provoked an antinociceptive effect since it reduced formalin-induced nociception in both test phases (Figure 1). In Figure 2 are reported the effects of Soymorphin-6 and Soymorphin-6 C-amide in the tail flick and formalin tests. Soymorphin-6 and Soymorphin-6 C-amide induced similar effects in these tests. Both peptides exerted significant antinociceptive effect 15 and 30 min after the administration, followed by a gradual and similar decrease in the antinociception. In the formalin test, both peptides did not change the nociceptive effects of formalin in the early phase of the test. In the late phase of the formalin test, Soymorphin-6 induced a light increase and Soymorphin-6 C-amide a light decrease of the nociceptive effect provoked by formalin, but both effects were not statistically significant in comparison with vehicle-treated animals.

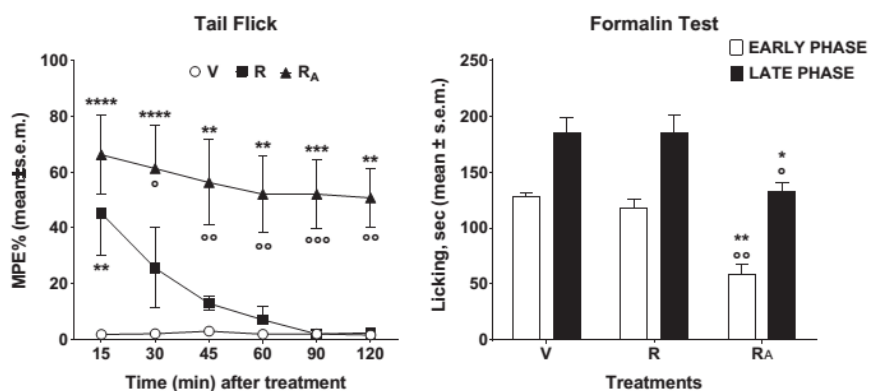


Fig. 1. Effects induced by Rubiscolin-6 (R) and Rubiscolin-6 C-amide (R_A) in the tail flick test (left panel) and in the formalin test (right panel). In the tail flick test, compounds were administered i.c.v. at the dose of 10 µg/10 µL; in the formalin test, compounds were administered s.c., in the dorsal surface of the mouse hind paw, at the dose of 100 µg/20 µL, 15 min before formalin. V is for vehicle-treated animals. ** is for P < 0.01, *** is for P < 0.001, **** is for P < 0.0001 vs V; * is for P < 0.05, ** is for P < 0.01, *** is for P < 0.001 vs R. N = 7.

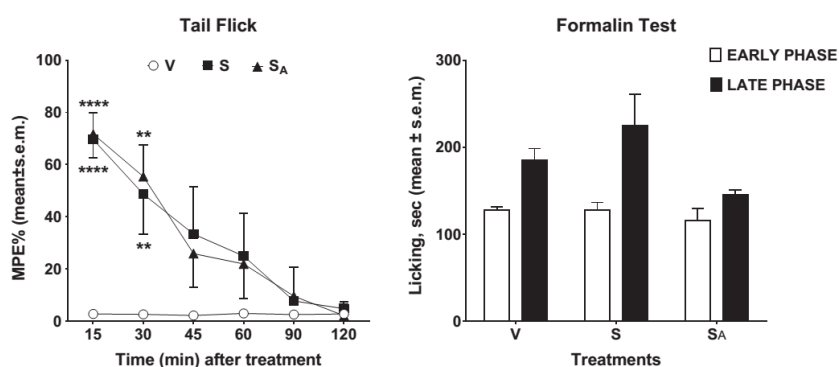


Fig. 2. Effects induced by Soymorphin-6 (S), Soymorphin-6 C-amide (S_A) in the tail flick test (left panel) and in the formalin test (right panel). In the tail flick test, compounds were administered i.c.v. at the dose of 10 µg/10 µL; in the formalin test, compounds were administered s.c., in the dorsal surface of the mouse hind paw, at the dose of 100 µg/20 µL, 15 min before formalin. V is for vehicle-treated animals. ** is for P < 0.01, **** is for P < 0.0001 vs V. N = 7.

***In vitro* intestinal bioaccessibility**

Results shown in Table 3 clearly indicate a quite high susceptibility of the peptides to the *in vitro* gastrointestinal environment. Specifically, their amide derivatives are the least resistant to the chemical and enzymatic conditions of the simulated digestive protocol. The intestinal stability and bioavailability of peptides were evaluated by using single layers of CaCo2 cells as a model of absorption in the small intestine. HPLC analysis highlighted very moderate hydrolysis of Rubiscolin-6 and Soymorphin-6 (less than 10% and 15%, respectively) in the apical solution by the brush border exopeptidases after 120 min incubation and regardless of the peptide concentration. Differently, their respective amide derivatives revealed an important susceptibility to enzymatic degradation, showing average hydrolysis rates of 74% and 65% for Rubiscolin-6 C-amide and Soymorphin-6 C-amide, respectively. HPLC analyses of basolateral solution revealed that all peptides were absorbed intact through CaCo2 monolayer, with a concentration-dependent transport following a saturable pattern

described by a linear curve (Figure 3). Interestingly, the actual amount of Rubiscolin-6 and Soymorphin-6 transepithelially transported was about 10%, thus higher than what generally reported for different size (3–17 aminoacid units) and polarity peptides transported from CaCo2 monolayer apical to basolateral side [29-31].

Table 3

In vitro intestinal bioaccessibility of peptides calculated as area under curve of chromatograms from HPLC-DAD analyses of intestinal digesta.

Peptide	%
Rubiscolin-6	10.2 ± 1.2
Soymorphin-6	7.3 ± 0.8
Rubiscolin-6 C-amide	5.4 ± 0.4
Soymorphin-6 C-amide	3.2 ± 0.3

Values are the means ± SD ($n = 5$; $P < 0.01$).

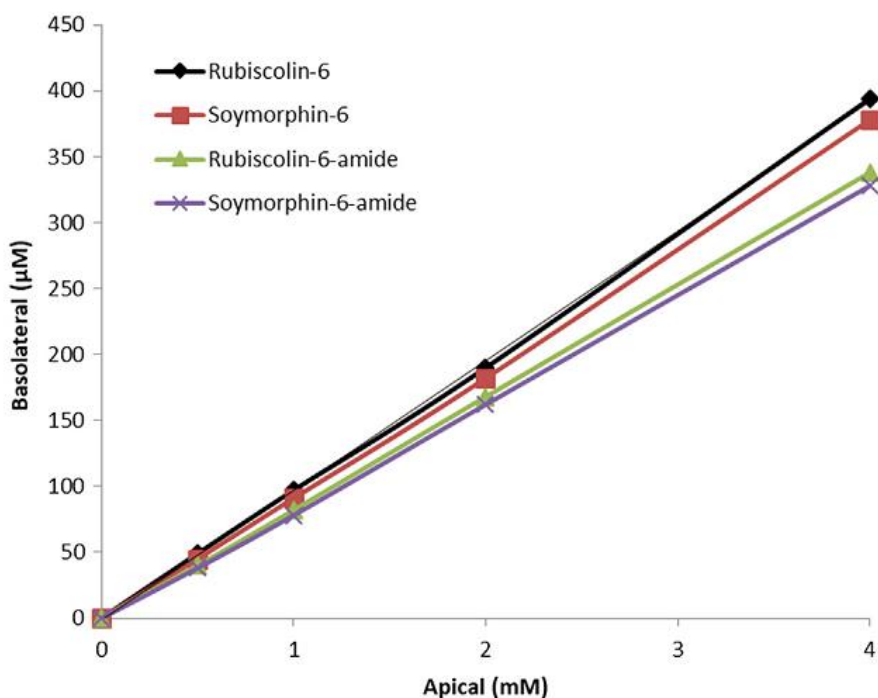


Fig. 3. *In vitro* intestinal bioavailability of peptides. Quantification of peptides in CaCo2 cell monolayer apical and basolateral solutions using a five-point calibration curve of pure peptides as standard analysed by HPLC.

Docking study

In silico molecular modeling approach was applied to investigate the relationship between the bioactivity found *in vitro* and *in vivo* by rubiscolin-6 and its C-terminal amide and their interactions at the δ -opioid receptor (DOR). The docking of the two peptides was performed on the crystal structure of the DOR (4RWD) downloaded from the PDB database and the so obtained poses have been compared with crystallographic ligands. The receptor was prepared for the docking experiments as previously reported [16,28] with the PrepWizard module embedded in Maestro 2017 [32]. The missing side chains were added, and all the co-crystallized molecules were removed except for the opioid ligand TIPP-NH₂ and the water molecules 1303 and 101 which are fundamental for the correct activation of the receptor [33]. These water molecules are necessary for a correct and predictable docking procedure [16,28,33]. Thus in this model is present a water network connecting the ligand to a key residue of Histidine 278.

After the preparation steps, the docking was performed by using the software Gold 6.0 with a docking procedure previously validated by our group [16,28]. The fitness functions GOLDSCORE was employed for these experiments basing on our previous studies [16,28]. The two water molecules were set to “toggle and spin”, in order to allow the program to automatically decide whether the water molecules should be included during the docking and to optimize their orientation. An area of 10 Å around the co-crystallized ligand was defined as the binding site.

The best poses found are reported in Figure 4; At the DOR, both rubiscolin-6 and rubiscolin-6 C-amide showed a similar interaction behavior, by assuming a convergent conformation and by establishing similar interactions to the key residues Asp128, His278 and water network.

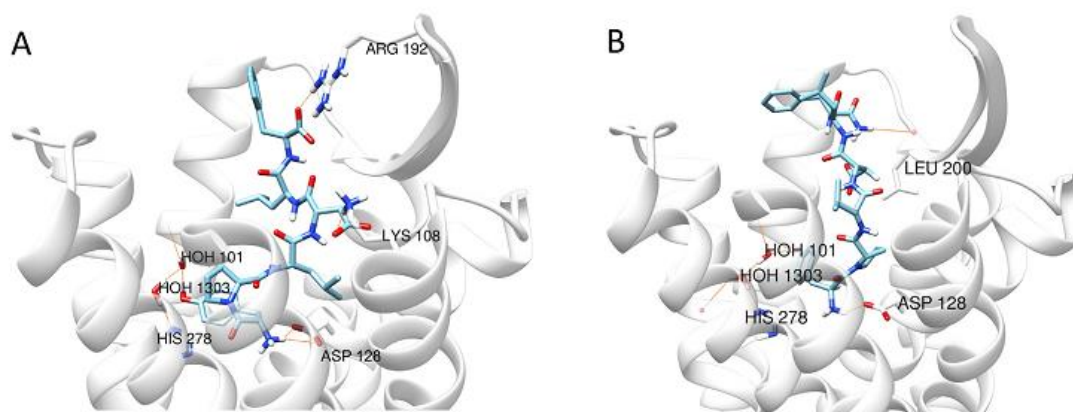


Fig. 4. Best ranked docking poses of Rubiscolin-6 (A) and Rubiscolin-6 C-amide (B) docked at the DOR (4RWD).

TIPP-NH₂ interacts with residues Asp128, His278, Trp284, Leu200 and Arg192, which are partially present in rubiscolin-6 and rubiscolin-6 C-amide poses.

Indeed, rubiscolin-6 is able to bind to the accessory residue Arg192, whereas this interaction is missing in its amide derivative, which preferentially bind the residue Leu200. Both of them lack to interact with Trp284, which is involved in a key interaction present in the crystallographic ligand; on the other hand they show the three main interactions to the water 101, Asp128 and His278 through the water network, which are responsible for the opioid activity found.

However, both peptides weakly bind to DOR in our calcium mobilization assay and are capable of stimulating the activation of G protein coupled to DOR at high doses (Table 2). This binding behavior falling in the micromolar range, could be explained by the lacking of those additional interactions found for TIPP-NH₂ (Trp284) and by the non-simultaneous presence of the interactions to Leu200 and Arg192, which could justify the low potency of rubiscolin-6 and rubiscolin-6 C-amide. The interactions found for both peptides, together with those of the crystallographic ligand have been reported in Table 4.

Table 4

Interactions list found in the best pose of TIPP-NH₂, rubiscolin-6 and rubiscolin-6C-amide to DOR.

DOR interactions					
Compounds	Asp128	His278	Trp284	Leu200	Arg192
TIPP-NH ₂	H bond	H bond through water network	π - π	H bond	Cat- π
Rubiscolin-6	Ionic + H bond	H bond through water network	-	-	H bond
Rubiscolin-6 C-amide	Ionic + H bond	H bond through water network	-	H bond	-

Discussion

Exorphins from plant proteins and their synthetic derivatives could exhibit a plethora of biological activity acting as modulating agents, antioxidants and anti-microbial compounds on diverse human targets such as receptors, cell's membrane and enzymes. Thus, such peptides contain certain desirable functional properties that could make them suitable in several formulated food systems.

In the present paper, we detected antioxidant properties by using different methods (DPPH, ABTS, CUPRAC and FRAP) [34,35]. Generally, the tested peptides exhibit low antioxidant abilities. Rubiscolin-6 C-amide shows the best DPPH scavenging ability while soymorphin-6 C-amide exhibits the best ABTS scavenging ability. Reducing abilities of the tested peptides were evaluated by CUPRAC and FRAP assays, which indicate low electron-donating abilities for all of them. This could be due to the presence of the hydrophobic amino acids such as proline, glycine and methionine in the peptides that can contribute to the reduction abilities because of high electron density [36]. Literature reports that tyrosine and phenylalanine containing oligopeptides and long sequence peptides could present tyrosinase inhibitory activity [37]. Tyrosinase is one key enzyme in the synthesis of melanin, which is an important pigment for protection of the eye and skin from sunlight [38]. Thus novel and safe tyrosinase inhibitors are gaining interest among scientific research topics due to their importance in the prevention of hyperpigmentation problems such as melisma and age spots [39]. Furthermore, recent results indicate that opioids play a key role in skin homeostasis by modulating keratinocyte differentiation, wound healing and inflammation [40,41]; β -

endorphin and MOR are expressed in human epidermal melanocyte (EM) cells and they are closely associated to melanosomes. Kauser and co-workers [42] demonstrated that they up-regulate melanocyte dendricity, proliferation, pigmentation and hair growth [43,44] via melanocortin-1 receptor (MC-1R) independent mechanism, thus the discovery of a peptide with exogenous opioid-like structure able to inhibit tyrosinase enzyme could be useful to better understand the relationship between hyperpigmentation process and opioid peptide system. All our peptides exhibit moderate tyrosinase inhibitory effect with the only exception of soymorphin-6 which is inactive; among them rubiscolin-6 shows the best value. Calcium mobilization assay data reveal that all compounds are able to stimulate the DOR and MOR at 100 μ M concentration, however rubiscolin-6 is inactive at MOR according to literature data [11].

Overall, detailed pharmacological features of rubiscolin-6, soymorphin-6, and their C-amide derivatives could not be investigated due to their low potency in the present calcium mobilization assay. *In vivo* experiments confirm the previously reported antinociceptive effects of rubiscolin-6 in the experimental model of acute pain in laboratory animals [2,13].

Rubiscolin-6 was able to increase the nociceptive threshold to thermal stimuli after supraspinal administration, but was ineffective after subcutaneous administration in an experimental paradigm of chemical-induced nociception as the formalin test. Rubiscolin-6 C-amide centrally administered demonstrates a strong antinociceptive effect higher than the parent compound, and it is effective after subcutaneous administration. To the best of our knowledge no data are available on the *in vivo* effects of Soymorphin-6, thus these results are novel and firstly described. After central administration in the tail flick test, both soymorphin-6 and its derivative soymorphin-6 C-amide induce a robust antinociceptive effect until 30 min after the administration but both peptides are not able to change the behavioral response to chemical-induced nociception in the formalin test. All peptides were absorbed intact through CaCo2 monolayer however, rubiscolin-6 C-amide exhibits the most interesting *in vivo* biological profile, which prompt us to further investigate its effect after oral administration.

The carrier-mediated transport systems involving the H⁺-coupled PepT1 transporter, may be excluded since they are active and saturable symporters specific for intestinal absorption of charged di- and tripeptides [45]. The average polar properties of these peptides would also exclude a possible passive transcellular diffusion since a vesicular-mediated internalization, the main mechanism involved, would imply absorption by apical cell membrane through hydrophobic interactions [46]. The low level of degradation of rubiscolin-6 and soymorphin-6 in transepithelial transfer indicates that passive transcellular diffusion could be partially involved in their transport. In fact, the amino acids ability to join hydrogen bonds with lipid phosphates of cell membranes, has been reported as a key physicochemical feature helping the translocation process via transcytosis route [47].

All together, these data support the possible transport of our peptides via paracellular route. Notheworthy, the passive paracellular transport via tight junctions has been recognized for the absorption of water-soluble low molecular weight and short-chain peptides positively charged due to the average negative charge of tight junctions [48]. Finally, the docking study on rubiscolin-6 and its C-terminal amide into DOR gave an insight on their binding mode and justifies the low potency and efficacy *in vitro*, comparing to the DOR crystallographic ligand TIPP-NH₂. These results are in line with the information previously obtained with CoMFA and CoMSIA models applied to rubiscolin-6 analogues [49], and represent the first tentative to expand our knowledge on the mechanism of action of these natural compounds mediated by DOR contribution.

In conclusion, we found that rubiscolin-6 C-terminal amide is able to exert antinociceptive effect after i.c.v. and s.c. administrations in the formalin test, at 100 μmol to stimulate opioid receptors in calcium mobilization assay. This let us suppose an activity at the central level and periphery [50] by δ-opioid receptor modulation in light of previous studies, our docking prediction and a good pharmacological profile in terms of safety and peripheral use due to a low intestinal absorption. The potential applications of this novel peptide derived from plant involve its use as food supplement, various biotechnological products and processes.

References

1. Zioudrou C, Streaty RA, Klee WA. Opioid peptides derived from food proteins. The exorphins. *Journal of Biological Chemistry*. 1979; 254:2446-2449.
2. Yang S, Yunden J, Sonoda S, et al. Rubiscolin, a delta selective opioid peptide derived from plant Rubisco. *FEBS Letters*. 2001; 509:213-217.
3. Kaneko K, Lazarus M, Miyamoto C, et al. Orally administered rubiscolin-6, a δ opioid peptide derived from Rubisco, stimulates food intake via leptomeningeal lipocallin-type prostaglandin D synthase in mice. *Molecular Nutrition and Food Research*. 2012; 56:1315-1323.
4. Yoshikawa M. Bioactive peptides derived from natural proteins with respect to diversity of their receptors and physiological effects. *Peptides*. 2015; 72:208-225.
5. Stefanucci A, Mollica A, Macedonio G, et al. Exogenous opioid peptides derived from food proteins and their possible uses as dietary supplements: A critical review. *Food Review International*. 2018; 34:8755-9129.
6. Arisoy S, Üstün-Aytekin O. Hydrolysis of food-derived opioids by dipeptidyl peptidase IV from *Lactococcus lactis* spp. *Lactis*. *Food Research International*. 2018; 11:574-581.
7. Kaneko K, Iwasaki M, Yoshikawa M, et al. Orally administered soymorphins, soy-derived opioid peptides, suppress feeding and intestinal transit via gut1-receptor coupled to 5-HT1A, D2, and GABAB systems. *American Journal of Physiology-Gastrointestinal and Liver Physiology*. 2010; 299:799-805.
8. Ohinata K, Agui , Yoshikawa M. Soymorphins, novel mu opioid peptides derived from soy beta-conglycinin beta-subunit, have anxiolytic activities. *Bioscience, Biotechnology and Biochemistry*. 2007; 71:2618-2621.
9. Dvoracsko S, Stefanucci A, Novellino E, et al. The design of multitarget ligands for chronic and neuropathic pain *Future Medicinal Chemistry*. 2017; 7:2469-2483.
10. Torino D, Mollica A, Pinnen F, et al. HrubySynthesis and evaluation of new endomorphin-2 analogues containing (Z)- α , β -didehydrophenylalanine (δ ZPhe) residues. *Journal of Medicinal Chemistry*. 2010; 53:4550.
11. Hirata H, Sonoda S, Agui S, et al. Rubiscolin-6, a δ opioid peptide derived from spinach Rubisco, has anxiolytic effect via activating σ 1 and dopamine D1 receptors. *Peptides*. 2007; 28:1998-2003.
12. Miyazaki Y, Kaneko K, Iguchi S, et al. Orally administered δ opioid agonist peptide rubiscolin-6 stimulates food intake in aged mice with ghrelin resistance. *Molecular Nutrition and Food Research*. 2014; 58:2046-2052.
13. Yang S, Sonoda S, Chen L, et al. Structure-activity relationship of rubiscolins as delta opioid peptides. *Peptides*. 2003; 24:503-508.
14. Perlikowska R, Janecka A. Rubiscolins-highly potent peptides derived from plant proteins. *Mini Reviews in Medicinal Chemistry*. 2018; 18:104-112.
15. Poli G, Dimmito MP, Mollica A, et al. Discovery of novel μ -opioid receptor inverse agonist from a combinatorial library of tetrapeptides through structure-based virtual screening. *Molecules*. 2019; 24:3872.

16. Stefanucci A, Luisi G, Zengin G, et al. Discovery of arginine-containing tripeptides as a new class of pancreatic lipase inhibitors. *Future Medicinal Chemistry*. 2019; 11:5-19.
17. Grochowski DM, Uysal S, Aktumsek A, et al. *In vitro* enzyme inhibitory properties, antioxidant activities, and phytochemical profile of *Potentilla thuringiaca*. *Phytochemistry Letters*. 2017; 20:365-372.
18. Zengin G, Stefanucci A, Rodrigues MJ, et al. *Scrophularia lucida* L. as a valuable source of bioactive compounds for pharmaceutical applications: *In vitro* antioxidant, anti-inflammatory, enzyme inhibitory properties, *in silico* studies, and HPLC profiles. *Journal of Pharmaceutical and Biomedical Analysis*. 2019; 162:225-233.
19. Luisi G, Stefanucci A, Zengin G, et al. Mollica Anti-oxidant and tyrosinase inhibitory *in vitro* activity of amino acids and small peptides: new hints for the multifaceted treatment of neurologic and metabolic dysfunctions. *Antioxidants*. 2018; 8:E7.
20. Camarda V, Fischetti C, Anzellotti N, et al. Pharmacological profile of NOP receptors coupled with calcium signaling via the chimeric protein Gaq15. *Naunyn-Schmiedeberg's Archives of Pharmacology*. 2009; 379:599-607.
21. Lambert DG, Rainbow RD. (eds.), (2013). *Calcium Signaling Protocols, Methods in Molecular Biology*, vol. 937. Springer Science, Business Media, LLC.
22. Dimmito MP, Stefanucci A, Pieretti S, et al. Discovery of orexant and anorexant agents with indazole scaffold endowed with peripheral anti-edema activity. *Biomolecules*. 2019; 9:E492.
23. Mollica A, Costante R, Stefanucci A, et al. Antinociceptive profile of potent opioid peptide AM94, a fluorinated analogue of biphalin with non-hydrazine linker. *Journal of Peptide Science*. 2013; 19:233-239.
24. Piekielna-Ciesielska J, Mollica A, Pieretti, et al. Antinociceptive potency of a fluorinated cyclopeptide Dmt-c[D-Lys-Phe-p-CF₃-Phe-Asp]NH₂. *Journal of Enzyme Inhibition and Medicinal Chemistry*. 2018; 33:560-566.
25. Mollica A, Pinnen F, Feliciani F, et al. New potent biphalin analogues containing p-fluoro-L-phenylalanine at the 4,4' positions and non-hydrazine linkers. *Amino Acids*. 2011; 40:1503-1511.
26. Raiola R, Meca G, Mañes J. Bioaccessibility of deoxynivalenol and its natural co-occurrence with ochratoxin A and aflatoxin B1 in Italian commercial pasta. *Food and Chemical Toxicology*. 2012; 50:280-287.
27. Tenore GC, Campiglia P, Giannetti D, et al. Simulated gastrointestinal digestion, intestinal permeation and plasma protein interaction of white, green, and black tea polyphenols. *Food Chemistry*. 2015; 15:320-326.
28. Stefanucci A, Dimmito MP, Macedonio G, et al. Potent, efficacious, and stable cyclic opioid peptides with long lasting antinociceptive effect after peripheral administration. *Journal of Medicinal Chemistry*. 2020; 63:2673-2687.

29. Okumu FW, Pauletti GM, Vander Velde DG, et al. Effect of restricted conformational flexibility on the permeation of model hexapeptides across Caco-2 cell monolayers. *Pharmaceutical Research*.1997; 14:164-175.
30. Regazzo D, Mollé D, Gabai G, et al. The (193–209) 17-residues peptide of bovine β -casein is transported through Caco-2 monolayer. *Molecular Nutrition and Food Research*. 2010; 54:1428-1435.
31. Satake M, Enjoh M, Nakamura Y, et al. Transepithelial transport of the bioactive tripeptide, Val-Pro-Pro, in human intestinal Caco-2 cell monolayers. *Bioscience, Biotechnology, and Biochemistry*.2002; 66:378-384.
32. Schrödinger Release 2016-4: LigPrep, Schrödinger, LLC, New York, NY (2016).
33. Kaserer T, Lantero A, Schmidhammer H, et al. Opioid receptor: Novel antagonists and structural modelling. *Scientific Reports*. 2016; 6:1-15.
34. Kim D-O, Lee KW, Lee HJ, et al. Vitamin C equivalent antioxidant capacity (VCEAC) of phenolic phytochemicals. *Journal of Agricultural food Chemistry*. 2002; 50:3713-3717.
35. Mareček V, Mikyška A, Hampel D, et al. ABTS and DPPH methods as a tool for studying antioxidant capacity of spring barley and malt *Journal of Cereal Science*.2017; 73:40-45.
36. Nwachukwu ID, Aluko RE. Structural and functional properties of food protein-derived antioxidant peptides. *Journal of Food Biochemistry*.2019; 43:Article e12761.
37. Pillaiyar T, Manickam M, Namasivayam V. Skin whitening agents: Medicinal chemistry perspective of tyrosinase inhibitors. *Journal of Enzyme Inhibition and Medicinal Chemistry*.2017; 32:403-425.
38. Schurink M, van Berkel JW, Wichers HJ, et al. Novel peptides with tyrosinase inhibitory activity. *Peptides*. 2007; 28:485-495.
39. Zolghadri S, Bahrami A, Hassan K, et al. A comprehensive review on tyrosinase inhibitors. *Journal of Enzyme Inhibition and Medicinal Chemistry*.2019; 34:279-309.
40. Bigliardi-Qi M, Gaveriaux-Ruff C, Zhou H, et al. Deletion of delta-opioid receptor in mice alters skin differentiation and delays wound healing. *Differentiation*. 2006; 74:174-185.
41. Schmelz M, Paus R. Opioids and the skin: “Itchy” perspectives beyond analgesia and abuse. *Journal of Investigational Dermatology*.2007; 127:1287–1287.
42. Kauser S, Schallreuter KU, Thody AJ, et al. Regulation of human epidermal melanocyte biology by β -endorphin. *Journal of Investigational Dermatology*. 2003;120:1073-1080.
43. Furkert J, Klug U, Slominski A, et al. Identification and measurement of β -endorphin levels in the skin during induced hair growth in mice. *Biochimica Biophysica Acta*. 1997; 1336:315-322.
44. Tobin DJ, S. Kauser S. Beta-endorphin: The forgotten hair follicle melanotropin. *Journal of Investigative Dermatology Symposium Proceedings*. 2005; 10:212-216.

45. Brandsch M, Knütter I, Bosse-Doenecke E. Pharmaceutical and pharmacological importance of peptide transporters *Journal of Pharmacy and Pharmacology*. 2008; 60:543-585.
46. Knipp GT, Velde DGV, Siahaan TJ, et al. The effect of beta-turn structure on the passive diffusion of peptides across Caco-2 cell monolayers. *Pharmaceutical Research*. 1997; 14:1332-1340.
47. Pauletti GM, Gangwar S, Okumu FW, et al. Esterase-sensitive cyclic prodrugs of peptides: Evaluation of an acyloxyalkoxy promoiety in a model hexapeptide. *Pharmaceutical Research*. 1996; 13:1615-1623.
48. Salamat-Miller N, Johnston TP. Current strategies used to enhance the paracellular transport of therapeutic polypeptides across the intestinal epithelium. *International Journal of Pharmaceutics*. 2005; 294:201-216.
49. Caballero J, Saavedra M, Fernandez M, et al. Quantitative structure-activity relationship of rubiscolin analogues as delta opioid peptides using comparative molecular field analysis (CoMFA) and comparative molecular similarity indices analysis (CoMSIA). *Journal of Agricultural Food Chemistry*. 2007; 55:8101-8104.
50. Cassell RJ, Mores KL, Zerfas Mahmoud AH, et al. Rubiscolins are naturally occurring G protein-biased delta opioid receptor peptides. *European Neuropsychopharmacology*. 2019; 29:450-456.

CHAPTER 4: Selective MOR activity of DAPEA and Endomorphin-2 analogues containing a (R)- γ -Freidinger lactam in position two

Alice Della Valle¹, Azzurra Stefanucci¹, Giuseppe Scioli¹, Edina Szucs², Sandor Benyhe², Stefano Pieretti³, Paola Minosi³, Chiara Sturaro⁴, Girolamo Calò⁵, Gokhan Zengin⁶, Adriano Mollica¹

¹ Department of Pharmacy, University G. d'Annunzio Chieti, Via dei Vestini 31, 66100 Chieti, Italy.

² Institute of Biochemistry, Biological Research Centre, Szeged, Hungary.

³ Istituto Superiore di Sanità, Centro Nazionale Ricerca e Valutazione Preclinica e Clinica dei Farmaci, Viale Regina Elena 299, 00161 Rome, Italy.

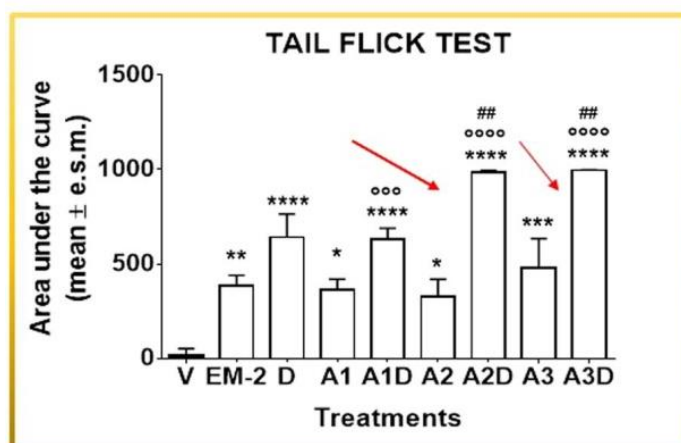
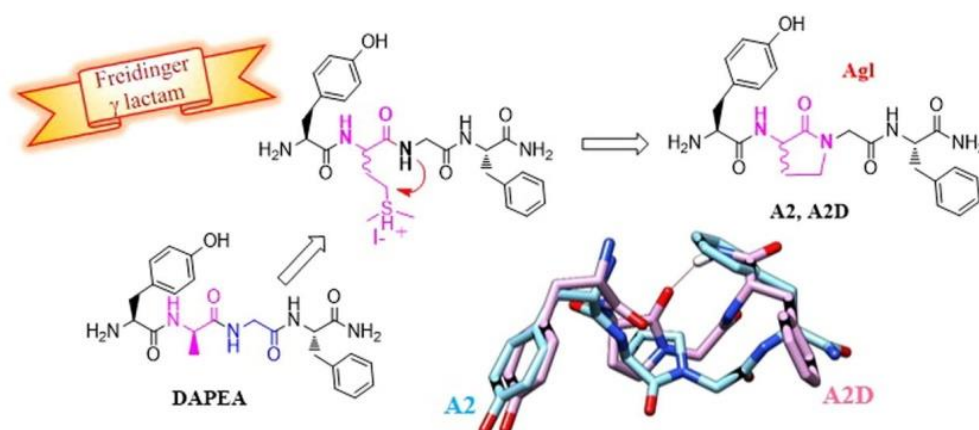
⁴ Department of Neuroscience and Rehabilitation, Section of Pharmacology, University of Ferrara, Ferrara, Italy.

⁵ Department of Pharmaceutical and Pharmacological Sciences, University of Padua, Italy.

⁶ Department of Biology, Science Faculty, Selcuk University, Konya, Turkey.

Abstract

The use of α -amino- γ lactam of Freidinger (Agl) may serve as an impressive method to increase the biological stability of peptides and an appropriate tool to elucidate their structure-activity relationships. The endomorphin-2 (EM-2) and [D-Ala2, des-Leu5] enkephalin amide (DAPEA) are two linear opioid tetrapeptides agonists of MOR and MOR/DOR respectively. Herein, we investigated the influence of the incorporation of (R/S)-Agl in position 2 and 3 on the biological profile of the aforementioned products *in vitro* and *in vivo*. Receptor radiolabeled displacement and functional assays were used to measure *in vitro* the binding affinity and receptors activation of the novel analogues. The mouse tail flick and formalin tests allowed to observe their antinociceptive effect *in vivo*. Data revealed that peptide A2D was able to selectively bind and activate MOR with a potent antinociceptive effect after intracerebroventricular (i.c.v.) administration, performing better than the parent compounds EM-2 and DAPEA. Molecular docking calculations helped us to understand the key role exerted by the Freidinger Agl moiety in A2D for the interaction with the MOR binding pocket.



Introduction

Local constriction in peptide sequences still represents one of the most powerful strategy to modulate the biological activity of a target compound in the rational design of peptidomimetics and peptoids. Note of worthy examples come from the recent literature reporting the modification of peptide's backbone and amino acid's side chain through: (i) N-methylation of amide backbone [1]; (ii) χ -space constriction [2]; (iii) unnatural amino acid incorporation [3]; (iv) intramolecular bond formation [4]; (v) cyclic amino acids and heterocyclic amino acids on the backbone [5,6]; (vi) lactam formation [7]. Among them the incorporation of α -amino- γ -lactam (Agl) residue to create folded peptides permits to identify the bioactive conformation and to improve the therapeutic potential by alleviating some drawbacks such as low metabolic stability and poor oral bioavailability. Pioneering studies by Freidinger and Veber described the key role exerted by Agl residue in forcing the folding of backbone sequence as β -turn inducer in diverse peptides [8,9]. These often show higher metabolic stability than their linear counterparts representing an effective strategy to test biologically active peptides as peptidase and protease inhibitors [10]. Historically the γ -lactam restriction as β -turn inducer was applied to the GHRH to improve the potency, leading to the conclusion that the bioactive conformation was stabilized by the presence of a type-II β -turn, furthermore a bicyclic lactam scaffold was inserted into Gramicidin S with the aim to restrict the β -turn conformation [11,12]. This type of intra-molecular cyclization transforms a secondary amide group [N(2)] of a simple dipeptide backbone in a tertiary amide unit, thus favoring the trans-rotameric form of the amide backbone, also blocking the Ψ 1 rotation, and biasing neighboring ϕ 1 and ϕ 2 torsional angles [13,14]. Conformational and X-ray analyses show Ψ angles of the most stable conformations for 3-amino-2-pyrrolidones in a range of $-130 \pm 15^\circ$ for the (S)-enantiomer and $+130 \pm 15^\circ$ for the corresponding (R)-enantiomer [13]. Native β -turn is composed by four residues at a distance $<7 \text{ \AA}$ between $C\alpha(i)$ and $C\alpha(i+3)$, forming a H-bond between the carbonyl group of the first residue (i) and the NH group of the fourth residue (i+3) (1 \rightarrow 4-type). Small scaffolds able to resemble this behavior are highly desirable in order to develop new peptidomimetic structures that can facilitate or disturb β -turn-mediated recognition's kinetic. Specific dipeptide sequences can promote the formation of a β -turn structure, stabilized by an intramolecular H-bond [15,16]; the sequence Asn-Gly induces a type I β -turn, while Gly-Asn is generally considered a type II β -turn inducer, as well as DPro-LPro, which has been recently employed as facilitator of β -hairpins

formation in the design of peptides-binding DNA [17,18]. X-Ray structures and structural analysis of cyclic and linear analogues of enkephalins endowed with opioid activity revealed that their bioactive conformation is represented by a β -turn [19–23]. The enkephalin-like tetrapeptide H-Tyr-D-Ala-Gly-Phe-NH₂ (DAPEA) was found to be a selective ligand at the μ -opioid receptor (MOR), showing an IC₅₀ of 33.2 nM and 3.48 nM for δ -opioid receptor (DOR) and MOR respectively, resulting in about 10-fold selectivity for MOR [24]. Indeed the importance of β -turn structure in the MOR-ligand interaction has been highlighted by Doi et al., which documented the replacement of the Pro₂ in EM-2 with Homocycloleucine; the so obtained EM-2 derivative embraced a β -turn structure stabilized by an intramolecular H-bond [25]. Other β -turn mimetic heterocyclic scaffolds were also included into EM-2 sequence to yield peptidomimetics retaining bioactivity [26]. However, removing the N(H) group may severely influence the interaction of a lead compound to the target receptor. The design of the Tyr-spiro-(R/S)-Aba-Gly-Phe-NH₂ and Tyr-(R/S)-Aba-Gly-Phe-NH₂ peptides based on the replacement of the sequence [Pro-Phe] in EM-2 with the spiroAba-Gly and Aba-Gly dipeptide mimetics respectively, led to the discovery of a new potent and selective MOR partial agonist Tyr-spiro-(R)-Aba-Gly-Phe-NH₂, bearing preferentially a β -turn structure in the backbone [27]. On the contrary Tyr-(R)-Aba-Gly-Phe-NH₂ showed no detectable affinity and activity for μ and δ -opioid receptors, while Tyr-(S)-Aba-Gly-Phe-NH₂ characterized by an extended conformation of the pseudo dipeptide portion, displayed poor affinity and no apparent bioactivity for both of them. Furthermore Tyr-spiro-(R)-AbaGly-Phe-NH₂ is resistant to proteolytic degradation, while Tyr-(S)-AbaGly-Phe-NH₂ tetrapeptide is totally unstable [27]. Considering the strong demand of peptides able to exert their biological activity with a favorable pharmacokinetic profile in this study we report new tetrapeptide models containing α -amino- γ -lactam of Freidinger in position 2 and 3, as analogues of EM-2 and DAPEA. Opioid binding assay, GTP functional and calcium mobilation assays have been performed to determine the ability of the novel compounds to bind and/or activate opioid receptors. *In vivo* antinociceptive tests finally revealed their capacity to induce analgesia after central and peripheral administrations. Molecular modeling experiments were performed with the aim to predict the best docking pose and to study the conformation of the most promising compound in order to understand its interactions at the binding site on MOR.

Materials and Methods

Chemicals

Chemicals, amino acids and solvents were purchased by SigmaAldrich (Milano, Italy) and VWR International (Pennsylvania, US). HPLC and LRMS solvents are of HPLC grade of purity. All the fullprotected compounds were purified by simple trituration by diethyl ether and the characterization performed by LRMS and ¹H NMR spectroscopy, using a Varian 300 MHz spectrometer, with deuterated DMSO as solvent. Purity of each product as TFA salt was assessed by analytical RP-HPLC (C18-bonded 4.6 × 150 mm), flow: one mL/min; linear gradient: water/ACN (0.1% TFA), from 5% ACN to 95% ACN in 25 min, diode array detection at 216, 235, 254, 270 nm; it was found to be >90% (254 nm) (for experimental data see Supplementary Materials). LRMS were registered on a Finnigan-Mat instrument (San Jose, CA, USA), equipped with ion trap analyzer and an electrospray ionization source, following these parameters: capillary temperature: 290 °C; spray voltage: 4.0 kV; fluid nebulized with N₂ as sheath and auxiliary gas.

Opioid receptor binding and G-protein stimulation assays

Opioid receptor radiolabeled competition assay and G-protein stimulation assay were executed on MOR, DOR and KOR, following the previously described procedures [28-31].

Ca²⁺ mobilization assay

Calcium mobilization test was carried out on CHO cells lines enduringly co-expressing MOR and KOR with mutated carboxylic terminus Gαq_{i5}, and DOR with mutated carboxylic terminus GαqG66Di5 [32,33].

In vivo antinociceptive assays

Tail flick (TF) and formalin tests (FT) were applied to assess the antinociceptive potential of our novel peptides *in vivo* after central (intracerebroventricular) and peripheral (subcutaneous) injection.

Molecular modeling study

Receptor preparation for docking

The crystal structure of MOR in the active state was found in the RCSB database with the PDB ID: 5C1M [34]. 5C1M was submitted to the Protein Preparation Wizard module embedded in Maestro 11.1 by Schrodinger 2017 [35]. Different ionization states were generated by Epik program [36] and water molecules 525 and 546 were selected and kept, due to their essential role in the formation of a water bridge among the crystallographic agonist, His297 and Lys233 residues. PROpKA module was used to assess protonation at the pH = 7.4, then hydrogens were added and the protein was minimized. The water network was optimized through the Interactive optimizer panel embedded in PrepWizard module, in order to correct the orientations of the water molecules by searching the most favorable positioning toward the His297 and the ligand, after re-protonation.

Ligand preparation

The two designed chemical structures, namely A2 and A2D, were prepared by the LigPrep module located in Maestro suite 11.1 [37], neutralized by Ionizer, in order to create different protonation states, and minimized by OPLS3 ff [38].

Docking and ΔG free binding energy calculations

After preparation process, docking experiments have been performed by using the software GOLD 5.0 [39], by the mean of GOLDScore scoring function (GS). The validation of the docking procedure was carried out through the self-docking of the crystallographic ligand BU72 into the active cavity of MOR [40]. The molecular docking of A2 and A2D was performed with Gold 5.0 using the fitness scoring function GOLDScore. The fitness score values obtained for these two compounds docked on MOR were 72.35 for A2D and 70.19 for A2. We also compared the best poses of the docked molecules through MM-GBSA method, embedded in Maestro suite 11.1 [41]. The ΔG free binding energy values were -40.801 kcal/mol and -26.518 kcal/mol for A2D and A2 respectively.

Results and Discussion

Design

This mini-library is composed by six tetrapeptides as C-terminal amides inspired by the amide skeleton of EM-2 (EM-2: Tyr-Pro-PhePheNH₂) and DAPEA (DAPEA: Tyr-D-

Ala-Gly-PheNH₂), which are MOR selective and mixed MOR/DOR agonists respectively (Figure 1) [42]. The N-terminal residue of Tyr1 in opioid endogenous peptides is critical for their receptor's binding, thus we maintained this feature in our novel peptides. The position 3 occupied by Gly residue in enkephalins is generally poorly tolerant versus modifications, accordingly to investigate the influence of Agl of Freidinger on potency and selectivity of DAPEA analogues, it has been retained in the novel analogues A2 and A2D respectively. On the contrary, corresponding analogues namely A1 and A1D incorporating the latter modification in position 3, have been also prepared as comparison. In line with the prospective of Yamazaki et al.[43], the physicochemical properties of amino acid in position 2, the spacer and its position as well as the relative side-chain direction of residue in position 3 impose the selectivity of EMs versus an opioid receptor type. Xiaofeng et al. showed that the substitution of Phe3/Trp3 in the EMs sequences with D-Amino acids more sharply declines the affinity for MOR than that of Pro2 [44]. This is probably due to an attenuation of the interaction between Xaa3 with the receptor and a modification in the conformation of the main-chain, as in the case of [Gly3]EM which can form β -turn. Consequently, we decided to conserve the Phe3 residue in the peptide sequences, while changing the Pro2 residue. [D-Ala2]EMs are less selective for MOR than [D-Pro2]EMs, suggesting that the larger conformational freedom of D-Ala containing peptide, deeply influences the ability of the overall structure to assume the correct positioning on the MOR binding site, compared to D-Pro2 and L-Pro2.

Peptide [D-Pro2]EM-2 exhibited a strong activity and its antinociceptive effect is close to that of the starting compound, owing to the fact that dipeptidyl aminopeptidase IV (DPP IV, EC3.4.14.5) is inactive against D-Pro or D-Ala containing sequences [45]. The replacement of Pro2 with Met/D-Met has been designed to promote the formation of Agl of Freidinger within the two tetrapeptides analogues of EM-2 namely A3 and A3D, with the aim to expand the repertoire of information available on EMs Structure Activity Relationships. Even delicate local constriction on the backbone of the informational portion, could point out relevant variations in their biological profile.

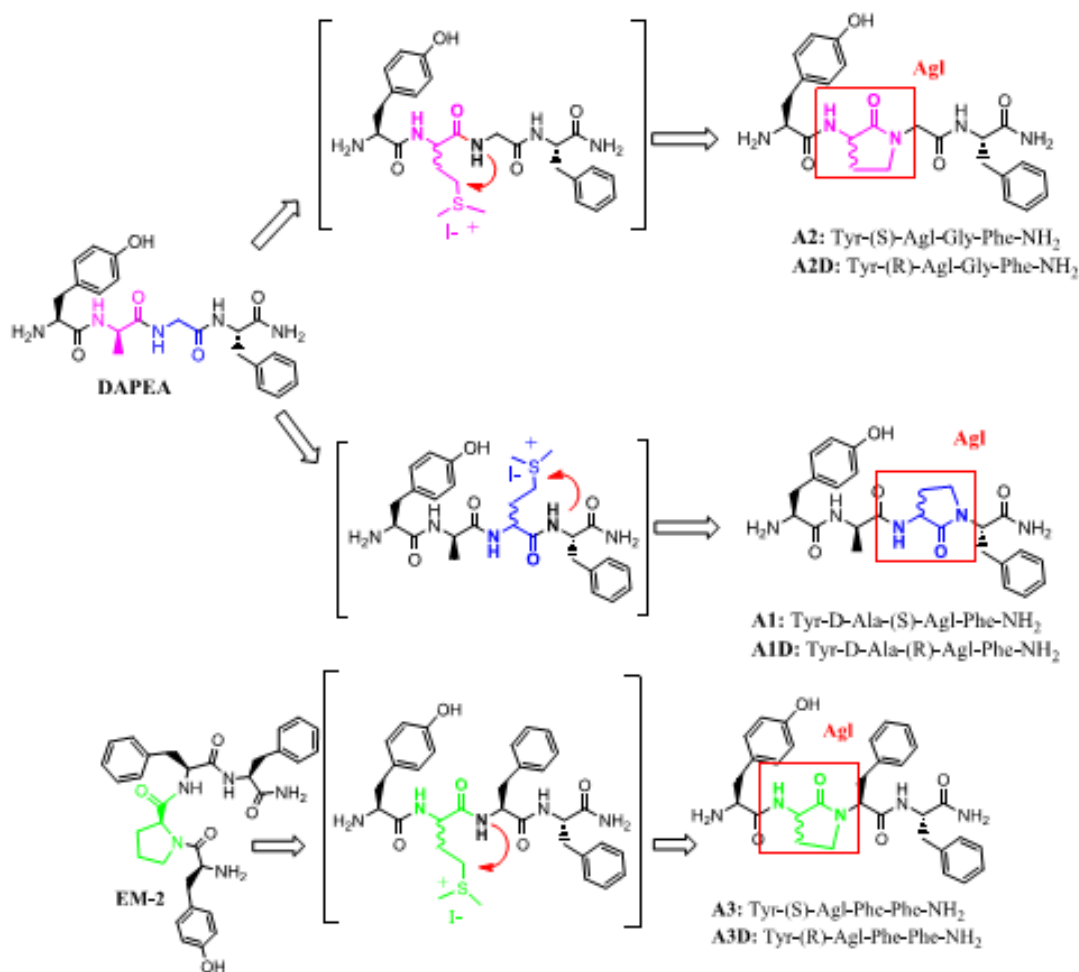
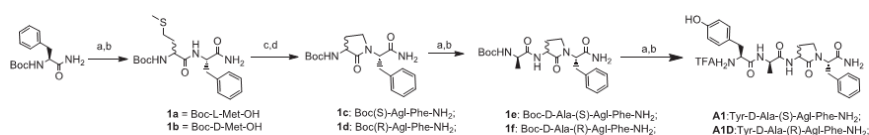


Fig. 1. Design of the novel tetrapeptides containing AgI of Freidinger in position 2 and 3 of EM-2 and DAPEA.

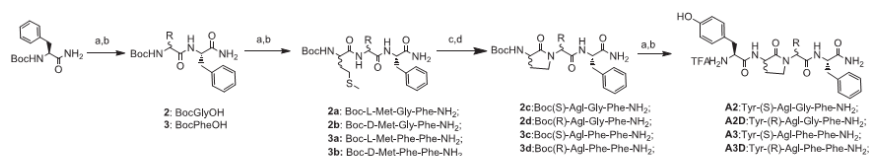
Synthesis

After a careful revision of the synthetic protocols applied for the preparation of γ -lactams containing peptides [46–50], we conceived a classic solution phase peptide synthesis involving the standard γ -lactam formation described by Freidinger [50].

The six novel tetrapeptides have been prepared following Schemes 1, Scheme 2.



Scheme 1. Reagents and Conditions: (a) TFA:DCM = 1:1 at r.t., 1.5 h, quantitative; (b) Boc-L-Met-OH for **1a** and Boc-D-Met-OH for **1b**, Boc-D-Ala-OH for **1e,1f**, Boc-Tyr-OH for **A1,A1D** (1.1 eq.), EDCHCl (1.1 eq.), HOBt (1.1 eq.), DIPEA (3 eq.), DMF, r.t., 12 h (yields **1a,b,e,f**: quantitative; **A1** yield: quantitative; **A1D** yield: 66%); (c) CH₃I (36 eq.), r.t., 72 h, quantitative; (d) NaH (1.1 eq.), DMF, 0 °C to r.t., 2 h (**1c,1d** yields: quantitative).



Scheme 2. Reagents and Conditions: (a) TFA:DCM = 1:1 at r.t., 1.5 h, quantitative; (b) Boc-Gly-OH for **2**, Boc-Phe-OH for **3**, Boc-L-Met-OH for **2a** and **3a**, Boc-D-Met-OH for **2b** and **3b**, Boc-Tyr-OH for **A2-A3D** (1.1 eq.), EDC·HCl (1.1 eq.), HOBT (1.1 eq.), DIPEA (3 eq.), DMF, r.t., 12 h (yields **2**, **3**, **2a,b**, **3a,b**: quantitative; **A2** yield: 58%; **A2D**: 92% yield; **A3** yield: 97%; **A3D** yield: 77%); (c) CH₃I (36 eq.), r.t., 72 h, quantitative; (d) NaH (1.1 eq.), DMF, 0 °C to r.t., 2 h (**2c** yield: quantitative; **2d** yield: 58%; **3c** yield: 60%; **3d** yield: 46%).

Commercially available BocPheOH has been converted in the amide derivative [51], then it was coupled in solution with diverse Boc-protected amino acids to give intermediates 1a,b, **2** and **3** quantitatively. Optically pure 5-membered lactam bridge containing peptides 1- **3c,d** were prepared following the well-established protocol of Freidinger [13,50], in good yields after trituration in diethyl ether. The synthesis of dipeptide γ -lactams was reached by intramolecular alkylation of L/D-methionine side chain, which was converted into a methyl sulfonium salt leaving group in presence of methyl iodide. Sodium hydride promotes the cyclization reaction yielding the γ -lactam after elimination of dimethyl sulfide [52]. Different substituents as side chains could be inserted in the second or third residue of the lactam peptide, preserving the asymmetric centers through the synthesis. Repeated steps of deprotection/coupling (TFA:DCM =1:1) with the Boc- protected amino acids afforded the final peptides as TFA salts in satisfying overall yields and purities, as detected by analytical RP-HPLC and ¹H NMR. Boc-protected intermediates have been obtained after a standard reaction's work-up, checked by ¹H NMR and TLC and used for the next reaction without any further purification.

Opioid receptor affinity

Figure 2 represents the specific binding of the compounds towards MOR, DOR and KOR in [3H]DAMGO, [3H]Ile 5,6-deltorphin II and [3H] HS665 displacement tests in rat (MOR, DOR) and guinea pig (KOR) brain membrane homogenate. Figure 2A, C, D show binding affinity of all analogues in one concentration (10⁻⁵ M), Figure 2B shows DAMGO and the six analogues in increasing concentration (10⁻¹⁰-10⁻⁵ M). Values represent the mean \pm S.E.M. Ligands showed lower equilibrium binding affinity (K_i value) in MOR-opioid system than DAMGO (Figure 2A and B).

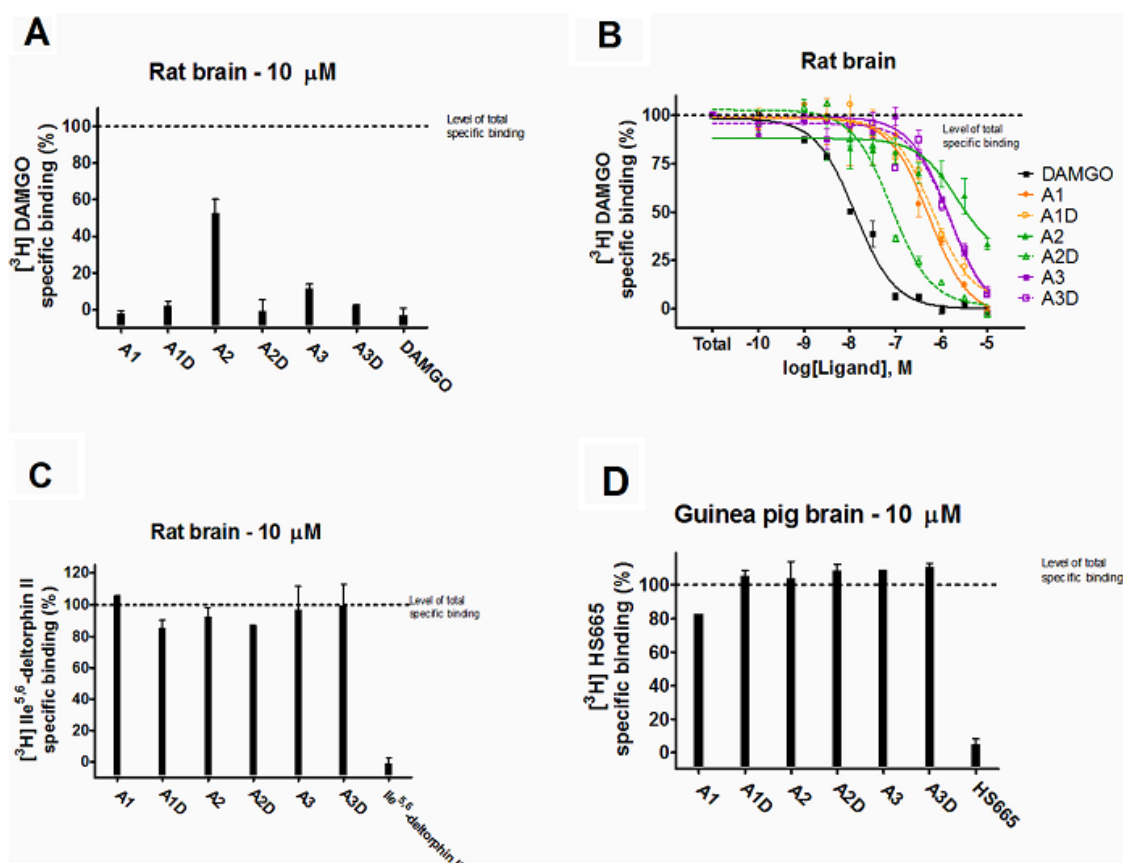


Fig. 2. MOR (A, B), DOR (C) and KOR (D) binding of A1-A3D ligands.

At DOR- and KOR-opioid systems the analogues did not show specific binding (Table1). According to literature, substitution of amino acid in position 3 of enkephalin's branch, induces the loss of binding affinity for MOR and DOR (A1 $K_{i\mu}$: 125.7 nM; A1D $K_{i\mu}$: 144.4 nM), while modifications in position 2 seem to preserve the capability of the analogue to interface with MOR. Indeed among the tested compounds, peptide A2D exhibits the best binding affinity and selectivity for MOR, however about sixth fold smaller binding affinity is observed for A2D ($K_{i\mu}$: 18.9 nM) against the parent compound DAPEA ($IC_{50\mu}$: 3.48 nM) [24,42]. Curiously this peptide lost the ability to bind DOR, which is on the contrary retained by DAPEA ($IC_{50\delta}$: 33.2 nM) [24]. It is worth of noting that the incorporation of AgI of Freidinger in place of D-Ala2 in the MOR- selective opioid ligand TAPP (TAPP: Tyr-D-Ala-Phe-Phe-NH₂), dramatically reduced its ability to bind the receptor (A3D $K_{i\mu}$: 363.1 nM against TAPP $K_{i\mu}$: 5.1 nM) [53]. These data highlight a significative difference in binding affinity values between the two diastereoisomeric peptides A2 and A2D (A2 $K_{i\mu}$: 509.6 nM vs. A2D $K_{i\mu}$: 18.9 nM), suggesting that the chiral center of the AgI in position 2 could be

responsible for the establishment of key interactions and for the overall 3D structural accommodation of the molecule inside the binding cavity of MOR.

Table 1

Displacement of [³H]DAMGO, by DAMGO, DAPEA and EM-2 analogues in brain membranes of rat and guinea pig. The stimulation efficacy (E_{max}) of G-protein by DAMGO and the novel compounds and potency of DAMGO and ligand A2D [³⁵S]GTP γ S binding assays in rat brain membrane homogenates.

Ligand	Ligand affinity			Efficacy	Potency
	K _i + S.E.M. (nM)			E _{max} ± S.E.M. (%)	LogEC ₅₀ ± S.E.M.
	MOR ^a	DOR ^a	KOR ^b	–	–
DAMGO	3.0 ± 0.5	n.d. ^c	n.d. ^c	197.9 ± 0.6	–6.55 ± 0.10
EM-2 ^a	1.3 ± 0.2	5652 ± 202	n.d. ^c	148 ± 5.0	–7.11 ± 0.07
DAPEA ^b	1 ± 0.09	106.8 ± 0.1	368.6 ± 0.16	161 ± 4.08	–7.09 ± 0.22
A1	125.7 ± 0.1	N.B.	N.B.	120.8 ± 2.0	n.d. ^c
A1D	144.4 ± 0.1	N.B.	N.B.	115.8 ± 2.1	n.d. ^c
A2	509.6 ± 0.3	N.B.	N.B.	110.2 ± 1.7	n.d. ^c
A2D	18.9 ± 0.1	N.B.	N.B.	143.3 ± 6.5	–5.63 ± 0.11
A3	347.3 ± 0.1	N.B.	N.B.	115.8 ± 1.0	n.d. ^c
A3D	363.1 ± 1.0	N.B.	N.B.	112.6 ± 1.8	n.d. ^c

^a Data taken from literature [54].

^b Data taken from literature [55].

^c not determined, N.B. no binding.

G-protein stimulation

The ability of the novel peptides to induce the receptor's activation was investigated in functional [³⁵S]GTP γ S binding assays in homogenates of rat brain membranes (Figure 3). The IC₅₀ values calculated accordingly to the displacement curves for the MOR, DOR and KOR have been converted into equilibrium inhibitory constants (K_i), using the Cheng-Prusoff equation [56]. The analogues measured in one concentration (Figure 3A) produce only a weak dose-dependent increase compared to DAMGO, with the convincing exception of ligand A2D. DAMGO and A2D potency was also investigated (Figure 3B, Table 1). The latter is able to stimulate the G-protein coupled receptor with an E_{max} of 143.3% and potency lower than that of the reference ligand DAMGO. However among the designed peptides, this is the only one capable to bind selectively MOR activating the G-protein. The C-amide terminal, the residues Tyr1, Phe4 and the

presence of a R-chiral center in position 2 are common features of peptides A3D, A2D and the reference ligand DAMGO, but only the last two of them retain the ability to bind selectively and to stimulate Gi/o-protein coupled MOR thus the Gly3 residue in A2D as well as the R-configuration of the Ag1 of Freidinger in position 2, could be involved in the recognition event and activation exquisitely observed for it.

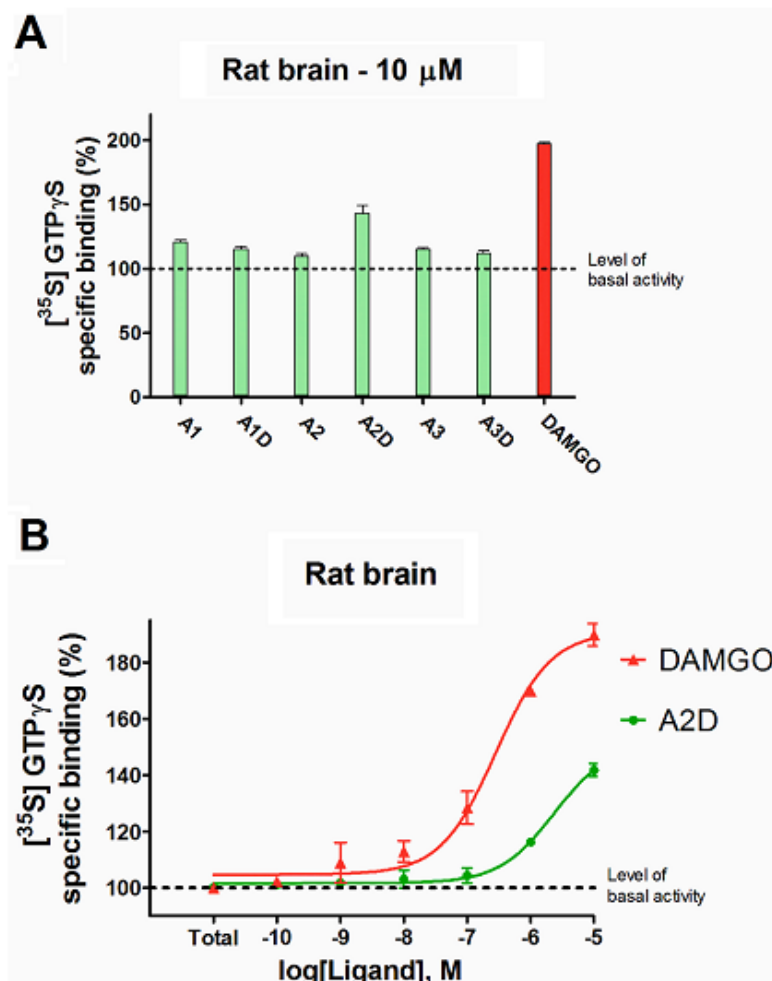


Fig. 3. G-protein activation of DAMGO, DAPEA and EM-2 analogues.

Calcium mobilization assay

In the Ca²⁺ mobilization assay we studied the ability of the novel compounds to stimulate the human recombinant MOR, KOR and DOR, stably transfected in CHO cells expressing the chimeric G proteins. EM-1, DPDPE, and dynorphin A are standard agonists for MOR, DOR, and KOR receptors (Table 2). In CHO-MOR cells EM-1 induced a significant concentration-dependent release of Ca²⁺ resulting in pEC₅₀ = 7.35 and E_{max} = of 202 \pm 30% over the basal values. Peptides A1, A1D, A2D, and A3D displayed an incomplete concentration response curve; assuming a full agonist behavior

of these compounds the following pEC50 values were calculated 5.85, 5.69, 5.84, and 5.80, respectively (Table 2).

Table 2
Potency (pEC₅₀) and maximal effect of standards and new ligands at MOR, DOR, and KOR.

Compounds	MOR		DOR		KOR	
	pEC ₅₀ (CL _{95%})	E _{max} ± sem %	pEC ₅₀ (CL _{95%})	E _{max} ± sem %	pEC ₅₀ (CL _{95%})	E _{max} ± sem %
DYNORPHIN-A	ND		ND		8.38	184 ± 9%
DPDPE	ND		7.70 (7.33–8.06)	283 ± 26%	ND	
EM-1	7.35 (6.82–7.88)	202 ± 30%	ND		ND	
A1	5.85 (5.32–6.38)	168 ± 19%	Inactive		Inactive	
A1D	5.69 (5.27–6.12)	157 ± 30%	Inactive		Inactive	
A2	Inactive		Crc incomplete, at 10 μM 63 ± 16%		Inactive	
A2D	5.84 (5.29–6.38)	185 ± 28%	Crc incomplete, at 10 μM 102 ± 27%		Inactive	
A3	crc incomplete, at 10 mM 95 ± 25%		Crc incomplete, at 10 μM 57 ± 13%		Inactive	
A3D	5.8 (5.54–6.06)	141 ± 17%	Inactive		Inactive	

ND: not determined.

Peptide A3 stimulated calcium mobilization at the higher concentration used while A2 has been found inactive. In CHO-DOR cells DPDPE elicited a strong concentration-dependent calcium release, showing high potency (pEC₅₀ of 7.70) and maximal effects (283 ± 26% over the basal values). Peptides A2, A2D, A3 stimulated calcium mobilization at the higher concentration tested, while A1, A1D and A3D have been found to be inactive. In CHO-KOR cells Dynorphin A provoked a vigorous concentration-dependent calcium release reporting a pEC₅₀ = 8.38 and E_{max} = 184 ± 9% over the basal values. In this assay peptide A2 resulted completely inactive at MOR, while A2D behaved as MOR full agonist. This data corroborates our hypothesis supporting the importance of the R-chiral center in the γ-lactam of Freidinger for the MOR preference and stimulation.

In vivo antinociceptive assays

The antinociceptive potency of the six tetrapeptides was firstly tested after central injection, following a procedure previously reported by our research group (TF test) [57]. The area under curves of antinociceptive effect induced by EM-2 and the new compounds are depicted in Figure 4. In the mouse TF test, compared to vehicle group, intracerebroventricular (i.c.v.) administration of 10 μg EM-2, DAPEA or six novel tetrapeptides produced significant increases in tail withdrawal latencies (Figure 4).

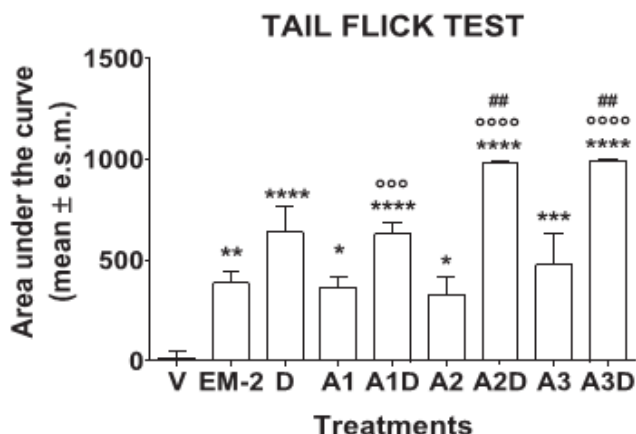


Fig. 4. The effect of EM-2, DAPEA (D) and six novel tetrapeptides in the tail flick test. Administration site: left cerebral ventricle; dose: 10 $\mu\text{g}/10 \mu\text{L}$; time of response to thermal stimuli from 15 to 120 min. Data were expressed as area under the curve of the maximum percentage effect (%MPE). V: Animals treated with vehicle only. Statistical analysis: one-way ANOVA followed by Dunnett's multiple comparisons test. * $p < 0.05$, ** $p < 0.01$, *** $p < 0.001$, and **** $p < 0.0001$ vs. V; ooo $p < 0.001$, oooo $p < 0.0001$ vs EM-2. ## $p < 0.01$ vs D. $n = 7$.

Comparing tetrapeptides with EM-2 or DAPEA, statistical analysis did not reveal significant differences for A1, A2 and A3 in confront to EM2 [$F(3, 24) = 0.4204$; $P = 0.7400$, n.s.] or DAPEA [$F(3, 24) = 1,543$; $P = 0,2291$, n.s.]. Peptides A1D, A2D and A3D induced antinociceptive response higher than that of EM-2 [$F(3, 24) = 52.81$; $P < 0.0001$]. A1D induced the same effects of DAPEA whereas A2D and A3D showed higher antinociceptive effects than DAPEA [$F(3, 24) = 8,815$; $P = 0,0004$].

The antinociceptive effect of our novel peptides was also evaluated in mice after subcutaneous (s.c.) administration in the early (acute) and late (inflammatory) phases of the formalin test. Plantar injections of formalin in rodents provoke a biphasic behavioral effect expressed by an acute phase (0–10 min after the injection) resulting from the specific stimulation of nociceptors and a second phase (10–40 min after injection) involving inflammatory processes [58]. During the acute phase, the treatment with A3D decreased the nociception [$F(8, 57) = 6,434$; $P < 0,0001$], showing a prominent antinociceptive effect compared to EM-2 or DAPEA. In the late inflammatory phase the statistical analysis indicated a significant effect of treatment [$F(8, 57) = 3,778$; $P = 0,0013$], in which A3D exerted a strong antinociceptive effect compared to EM-2 or DAPEA. Peptides A1, A1D, A2, A2D or A3 showed no statistically significant discrepancies from the control group (Figure 5).

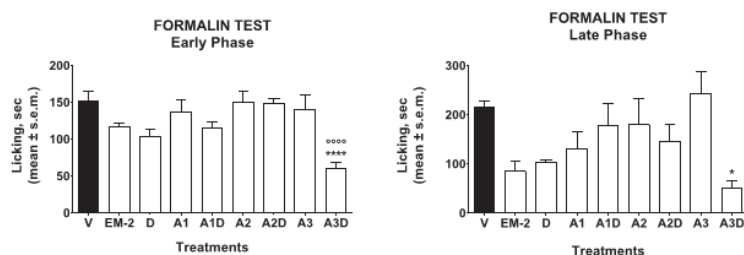


Fig. 5. The effect of EM-2, DAPEA (D) and six novel tetrapeptides in the formalin test. Administration route: subcutaneous (s.c.) in the dorsal face of the mice paw; dose: 100 µg/20 µL; time: 15 min before a s.c. administration of 1% formalin solution (20 µL/paw). V: Animals treated with vehicle only. Statistical analysis: one-way ANOVA followed by Dunnett's multiple comparisons test. * p < 0.05 and **** p < 0.0001 vs. V; °°°° p < 0.0001 vs EM-2. n = 7.

The R-series of Agl-containing tetrapeptides exert a robust antinociceptive activity higher than that of EM-2, after central administration in mice. Among them A2D and A3D exhibit the best antinociception in the TF. If administered subcutaneously, these compounds lost their *in vivo* activity except for peptide A3D, which is also able to produce antinociceptive effect both in the acute and in the inflammatory phase of the FT. This could be due to an improved metabolic plasma stability of A3D against A2D following peripheral administration, as well as to possible interactions of A3D with other receptors in the periphery involved in the mediation of the nociceptive stimuli [58,59].

Molecular modeling study

The designed molecule A2D binds to MOR by establishing two key interactions with Asp147, one H-bond and one salt bridge with the protonated amine group at the N-terminus, and forming the water network between water 546 and His297 (Figure 6A). Peptide A2D and crystallographic ligand basically share the same interactions (Table 3) and this is due to the position of some group of key atoms; in particular, by overlapping their structures we can observe the same orientation of:

- a) the phenolic moiety of both compounds;
- b) the nitrogen atoms, which belong to lactam moiety of A2D and to the condensed pyrrolidine moiety of BU72;
- c) the protonated nitrogen atoms, belonging to the primary amine group of A2D Tyr moiety and to the tertiary amine of crystallographic ligand (Figure 6B).

Table 3
Interactions found for the best docked poses of **A2** and **A2D** (Distance in Å)
compared to those of the crystallographic ligand Bu72 on MOR.

Compounds	Interactions of the crystallographic ligand, A2 , and A2D				
	Asp147	H ₂ O	Tyr148	Asn127	Asp216
BU72*	Salt bridge (1.90)	H-bond (1.72)	Cation- π (5.96)	-	-
A2	Salt bridge (3.28) H-bond (1.31)	H-bond (2.22)	Cation- π (4.35)	H-bond (2.04)	H-bond (1.50)
A2D	Salt bridge (3.26) H-bond (2.18)	H-bond (1.80)	Cation- π (5.45)	-	-

* Data already published by our research group [40].

Nicely peptide A2D is able to establish an intramolecular H-bond among the carbonyl group of the AgI moiety and the amide nitrogen of the Phe4 thus forming a β -turn structure comprising ten atoms (Figure 6B).

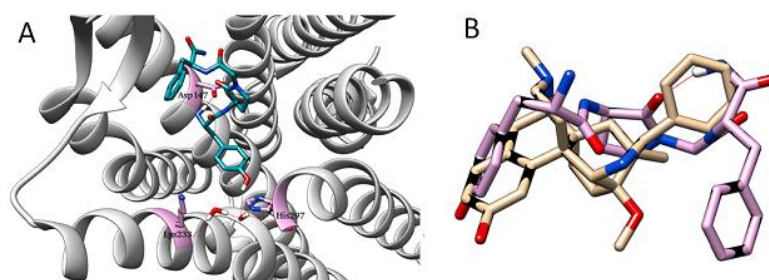


Fig. 6. (A) Interactions between **A2D** and key residues at the active site of MOR (PDB ID: 5C1M) [34] (B) Superimposition of **A2D** (pink) and crystallographic ligand BU72 (brown). (For interpretation of the references to colour in this figure legend, the reader is referred to the web version of this article.)

Peptides A2D and A2 have the same chemical formula, but they differ for the configuration of the stereogenic center in the AgI moiety, which brings about the stereo-isomer A2D with configuration R and stereo-isomer A2 (S). This change in stereochemistry leads to several differences among the preferred conformation, e.g. the folding that the two molecules may assume in the interaction with the MOR. The compound A2 is stabilized inside the orthosteric site of MOR through the key interactions with Asp147 (H-bond and salt bridge), π -cation interaction with Tyr148 and H-bond with the water molecule 546, which connects A2 to His297, as displayed in Figure 7A. The superimposition of BU72 and A2 shows that phenolic moiety N-terminus and phenyl moiety C-terminus of both compounds almost match (Figure 7B).

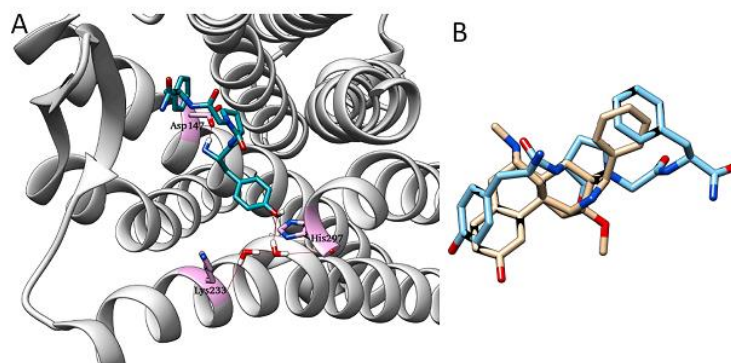


Fig. 7. (A) Interactions between A2 and key residues at the active site of MOR (PDB ID: 5C1M) [34]. (B) Superimposition of crystallographic ligand BU72 (brown) and A2 (pale blue). (For interpretation of the references to colour in this figure legend, the reader is referred to the web version of this article.)

The RMSD found for this pose was 3.823 Å, which is not really high considering the peptidic structure of A2 and the crystallographic ligand which is a morphinan. However, the stereogenic center in the Agl confers a specific linear conformation to this ligand which push the C-amide terminus toward the residues Asn127 and Asp216. This behavior is not observed neither for the crystallographic ligand Bu72 or peptide A2D (Figure 9a-b).

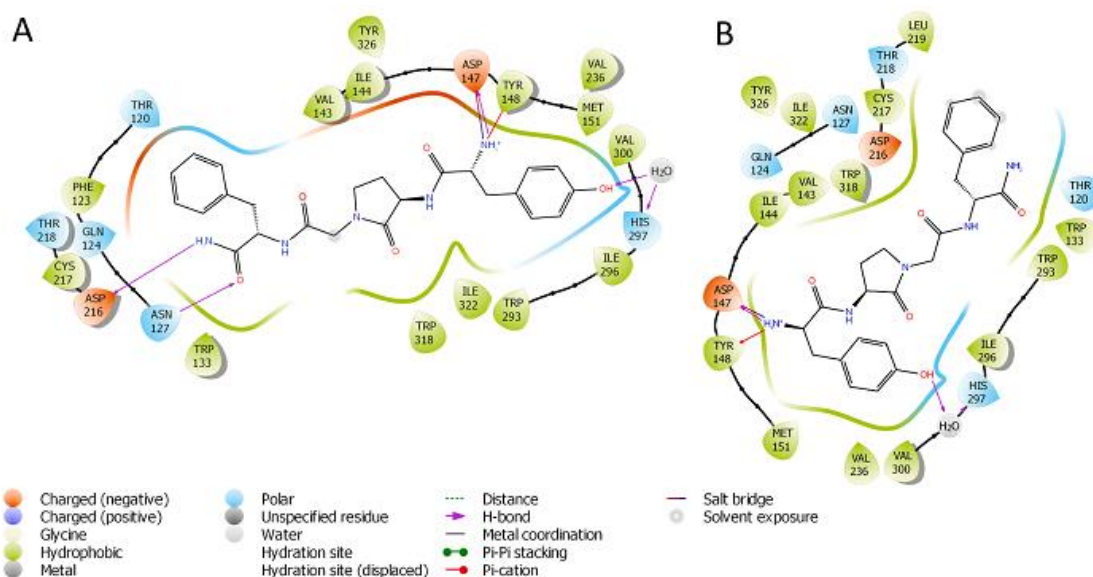


Fig. 9. Best docking pose interactions of A2 (A) and A2D (B) docked to 5C1M.

Thus, the novel designed molecules A2 and A2D display interesting features. Through the RMSD of these compounds, (3.823 Å for A2 and 4.676 Å for A2D) calculated in the docking process by Gold 5.0 vs the crystallographic ligand Bu72, it is possible to observe in detail how the different stereochemistry affects the conformation of the two peptides; more specifically the A2D best pose exhibits a folded β -turn like structure

whereas the ligand A2 assumes a linear conformation which could affect its binding affinity and efficacy (Figure 8). Both structures have in common the interaction of the phenolic rings and the N-terminus, as well as the orientation of hydroxyl group bound to the same water molecule in the orthosteric cavity; while phenyl moieties and the C-terminus amides are located on opposite sides (Figure 8). Peptide A2 shows an extended conformation in comparison to A2D, for this reason the intramolecular H-bond does not take place.

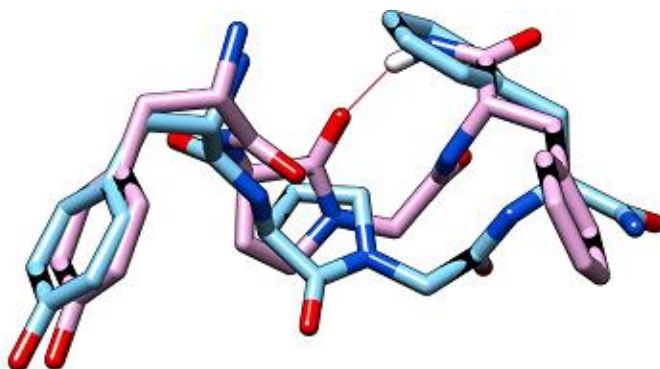


Fig. 8. Superimposition of the best docking poses of A2D (pink) and A2 (pale blue). (For interpretation of the references to colour in this figure legend, the reader is referred to the web version of this article.)

Consequently, the deviating structures lead to different binding modes, precisely A2D shows the best value of fitness score and MM-GBSA outcome, displaying an efficient and strong pattern of interactions inside the active pocket of MOR. Instead peptide A2 exhibits weaker interactions than A2D according to lower values of gold score and MM-GBSA results. The only structural discrimination between the two ligands is represented by the chiral center of the Agl2 moiety, which is fundamental in the determination of the overall 3D structure at the MOR binding pocket and in combination with Gly3 force the folding of peptide A2D in a stable β -turn conformation. This feature could be largely responsible of the strong selectivity for MOR and its biological properties.

A small library of new γ -lactam containing peptides was designed and synthesized in solution in good yields and purity following a well-established procedure [50,60]. All the prepared compounds were tested for their binding ability and functional activity on MOR, DOR and KOR. One of them (peptide A2D) exhibited a strong selectivity and capacity to stimulate G-coupled MOR in two different functional assays. An interesting *in vivo* antinociceptive effect was registered after central (i.c.v.) injection in mouse,

which is stronger than the reference ligand DAMGO. Finally, docking studies confirmed the ability of compound A2D to interact with the binding site of MOR, assuming a β -turn conformation, while its diastereomeric partner A2 is not able to resemble the same behavior *in silico*. This difference could stand at the basis of peptide A2D-MOR selectivity/activation paving the way to more potent analogues than EM-2 and DAPEA *in vivo*.

References

1. Sharma A, Kumar A, Abdel Monaim SAH, et al. N-methylation in amino acids and peptides: Scope and limitations. *Biopolymers* 109, 2018, e23110.
2. Stefanucci A, Pinnen F, Feliciani F, et al. Conformationally constrained histidines in the design of peptidomimetics: Strategies for the χ -space control. *Int. J. Mol. Sci.* 12, 2011, 2853–2890.
3. Ding Y, Ting JP, Liu J, et al. Impact of non- proteinogenic amino acids in the discovery and development of peptide therapeutics. *Amino Acids* 52, 2020, 1207–1226.
4. Vu QN, Young R, Krishna SH, et al. Cyclisation strategies for stabilising peptides with irregular conformations. *RSC Med. Chem*, 2021.
5. White C, Yudin A. Contemporary strategies for peptide macrocyclization. *Nature Chem* 3, 2011, 509–524.
6. Liu J, Han J, Izawa K, et al. Cyclic tailor-made amino acids in the design of modern pharmaceuticals. *Eur. J. Med. Chem.* 208, 2020, 112736.
7. Liskamp RM, Rijkers DT, Kruijtz JA, Kemmink J. Peptides and proteins as a continuing exciting source of inspiration for peptidomimetics. *Chembiochem* 12, 2011, 1626–1653.
8. Freidinger RM, Perlow DS, Veber F. Protected lactam-bridged dipeptides for use as conformational constraints in peptides. *J. Org. Chem.* 47, 1982, 104–109.
9. Freidinger RM, Veber DF, Perlow DS, et al. Bioactive conformation of luteinizing hormone-releasing hormone: evidence from a conformationally constrained analog. *Science* 210, 1980, 656–658.
10. Lubell WD, Blankenship JW, Fridkin G, Kaul R. “Peptides,” in: S.M. Weinreb (Ed.), *Science of Synthesis*, Thieme, Stuttgart, 2005, 713–809.
11. Nagai U, Sato K. Synthesis of a bicyclic dipeptide with the shape of β -turn central part. *Tetrahedron Lett.* 26, 1985, 647–650.
12. Sato K, Nagai U. Synthesis and antibiotic activity of a gramicidin S analogue containing bicyclic β -turn dipeptides. *J. Chem. Soc. Perkin Trans. I*, 1986, 1231–1234.
13. LeTiran A, Stables JP, Kohn H. Functionalized amino acid anticonvulsants: synthesis and pharmacological evaluation of conformationally restricted analogues. *Bioorg. Med. Chem.* 9, 2001, 2693–2708.
14. Wolfe MS, Dutta D, Aube J. Stereoselective synthesis of Freidinger lactams using oxaziridines derived from amino acids. *J. Org. Chem.* 62, 1997, 654–663.
15. Wu L, Mcelheny D, Setnicka V, et al. Role of different β -turns in β -hairpin conformation and stability studied by optical spectroscopy, *Proteins Struct. Funct. Bioinforma.* 80, 2012, 44–60.
16. Tyndall JD, Pfeiffer B, Abbenante G, Fairlie DP. Over one hundred peptide-activated G protein-coupled receptors recognize ligands with turn structure. *Chem Rev.* 105, 2005, 793–826.
17. Stefanucci A, Amato J, Brancaccio D, et al. A novel β -hairpin peptide derived from the ARC repressor selectively interacts with the major groove of B-DNA. *Bioorganic Chem.* 112, 2021, 112:10483.
18. Stefanucci A, Mosquera J, Vazquez E, et al. Synthesis, Characterization, and DNA Binding Profile of a Macrocyclic β -Sheet Analogue of ARC Protein. *ACS Medicinal Chem. Lett.* 6, 2015, 1220–1224.
19. Sanfelice D, Temussi PA. The conformation of enkephalin bound to its receptor: an “elusive goal” becoming reality. *Front. Mol. Biosci.* 1 2014, 1–8.

20. Blomberg D, Hedenstrom M, Kreye P, et al. Synthesis and Conformational Studies of a β -Turn Mimetic Incorporated in Leu-encephalin. *J. Org. Chem.* 69 2004, 3500–3508.
21. Blomberg D, Kreye P, Fowler C, et al. Synthesis and biological evaluation of leucine enkephalin turn mimetics. *Org. Biomol. Chem.* 4 2006, 416–423.
22. Blundell TL, Hearn L, Tickle IJ, et al. Crystal structure of [Leu5]encephalin. *Science* 205 1979, 220.
23. Aubry A, Birlirakis N, Sakarellos-Daitsiotis M, et al. A crystal molecular conformation of leucine-enkephalin related to the morphine molecule. *Biopolymers* 28 1989, 27–40.
24. Shimohigashi Y, Costa T, Chen HC, Rodbard D. Dimeric tetrapeptide enkephalins display extraordinary selectivity for the opiate receptor. *Nature* 297 1982, 333–335.
25. Doi M, Asano A, Komura E, Ueda Y. The structure of an endomorphinanalogue incorporating 1-aminocyclohexane-1-carboxylic acid for proline is similar to the β -turn of Leu-enkephalin. *Biochem. Biophys. Res. Commun.* 297 2002, 138–142.
26. Eguchi M, Shen RY, Shea JP, et al. Design, synthesis, and evaluation of opioid analogues with non-peptidic β -turn scaffold: Enkephalin and endomorphin mimetics. *J. Med. Chem.* 45 2002, 1395–1398.
27. Tomboly C, Ballet S, Feytens D, et al. Endomorphin-2 with a β -Turn Backbone Constraint Retains the Potent μ -Opioid Receptor Agonist Properties. *J. Med. Chem.* 51 2008, 173–177.
28. Oktem HA, Moitra J, Benyhe S, et al. Opioid receptor labeling with the chloromethyl ketone derivative of [3H]Tyr-D-Ala-Gly-(Me)Phe-Gly-ol (DAMGO) II: Covalent labeling of mu opioid binding site by 3H-Tyr-D-Ala-Gly-(Me)Phe chloromethyl ketone. *Life Sci.* 48 1991, 1763–1768.
29. Guerrieri E, Mallareddy JR, Toth G, et al. Synthesis and pharmacological evaluation of [(3)H]HS665, a novel, highly selective radioligand for the kappa opioid receptor. *ACS Chem. Neurosci.* 6 2015, 456–463.
30. Sim LJ, Selley DE, Childers SR. *In vitro* autoradiography of receptor-activated G proteins in rat brain by agonist-stimulated guanylyl 5'-[gamma-[35S]thio]-triphosphate binding. *Proc. Natl. Acad. Sci. USA* 92 1995, 7242–7246.
31. Traynor JR, Nahorski SR Modulation by mu-opioid agonists of guanosine-5'-O-(3-[35S]thio)triphosphate binding to membranes from human neuroblastoma SH-SY5Y cells. *Mol. Pharmacol.* 47 1995, 848–854.
32. Camarda V, Fischetti C, Anzellotti N, et al. Pharmacological profile of NOP receptors coupled with calcium signaling via the chimeric protein G alpha q15. *Naunyn Schmiedebergs Arch Pharmacol.* 379 2009, 599–607.
33. Camarda V, G. Calò. Chimeric G proteins in fluorimetric calcium assays: experience with opioid receptors. *Methods Mol. Biol.* 937 2013, 293–306.
34. Huang W, Manglik A, Venkatakrisnan AJ, et al. Structural insights into μ -opioid receptor activation. *Nature* 524 2015, 315–321.
35. Schrodinger Release 2017-3: Protein Preparation Wizard, Schrödinger, LLC, New York, NY, 2017.
36. Schrodinger Release 2017-3: Epik, Schrödinger, LLC, New York, NY, 2017.
37. Schrodinger Release 2017-3: LigPrep, Schrödinger, LLC, New York, NY, 2017.

38. Harder E, Damm W, Maple J, et al. OPLS3: A Force Field Providing Broad Coverage of Drug-like Small Molecules and Proteins. *J. Chem. Theory Comput.* 12 2015, 281–296.
39. Jones G, Willett P, Glen RC, et al. Development and Validation of a Genetic Algorithm for Flexible Docking. *J. Mol. Biol.* 267 1997, 727–748.
40. Stefanucci A, Dimmito MP, Macedonio G, et al. Potent, efficacious, and stable cyclic opioid peptides with long lasting antinociceptive effect after peripheral administration. *J. Med. Chem.* 63 2020, 2673–2687.
41. Schrodinger Release 2017-3: Prime, Schrödinger, LLC, New York, NY, 2017.
42. Feliciani F, Pinnen F, Stefanucci A, et al. Structure-activity relationships of biphalin analogs and their biological evaluation on opioid receptors. *Mini-Rev. Med. Chem.* 13 2013, 11–33.
43. Yamazaki M, Suzuki T, Narita M, Lipkowski AW. The opioid peptide biphalin induces less physical dependence than morphine. *Life Sci.* 69 2001, 1023–1028.
44. Xiaofeng H, Ning W, Weihua R, et al. Structure-activity relationship of endomorphins and their analogs. *Chin. Sci. Bull.* 46 2001, 1096–1099.
45. Shane R, Wilk S, Bondar RJ. Modulation of endomorphin-2-induced analgesia by dipeptidyl peptides IV. *Brain Res.* 815 1999, 278.
46. Geranurimi A, Cheng CWH, Quiniou C, et al. Probing Anti-inflammatory Properties Independent of NF- κ B Through Conformational Constraint of Peptide-Based Interleukin-1 Receptor Biased Ligands. *Front Chem.* 7 2019, 23.
47. Kumar S, Wang Q, Sasaki NA. Synthesis of conformationally constrained analogues of RGD tripeptide. *Tetrahedron* 63 2007, 2084–2092.
48. Lee PJ, Dunlap B, Rich DH. Synthesis and immunosuppressive activities of conformationally restricted cyclosporin lactam analogues. *Int. J. Pept. Prot. Res.* 35 1990, 481–494.
49. Lama T, Campiglia P, Carotenuto A, et al. A novel route to synthesize Freidinger lactams by microwave irradiation. *J. Pept. Res.* 66 2005, 231–235.
50. Freidinger RM. Design and Synthesis of Novel Bioactive Peptides and Peptidomimetics. *J. Med. Chem.* 46 2003, 5553–5566.
51. Mollica A, Pinnen F, Stefanucci A, et al. The cis-4- amino-1-proline residue as a scaffold for the synthesis of cyclic and linear endomorphin-2 analogues. *J. Med. Chem.* 55 2012, 3027–3035.
52. Bondebjerg J, Fuglsang H, Rosendal Valeur K, et al. Dipeptidyl nitriles as human dipeptidyl peptidase I inhibitors. *Bioorg. Med. Chem. Lett.* 16 2006, 3614–3617.
53. Tymecka D, Lipinski PFJ, Kosson P, Misicka A. β 2-Homo-Amino acid scan of μ -selective opioid tetrapeptide TAPP. *Molecules* 25 2020, 2461.
54. Keresztes A, Szucs M, Borics A, et al. New endomorphin analogues containing alicyclic β -amino acids: Influence on bioactive conformation and pharmacological profile. *J. Med. Chem.* 51 2008, 4270–4279.
55. Mollica A, Pelliccia S, Famiglini V, et al. Exploring the first rimonabant analog-opioid peptide hybrid compounds, as bivalent ligand for CB1 and opioid receptors. *J. Enz. Inhib. Med. Chem.* 32 2017, 444–451.
56. Cheng Y-C, Prusoff WH. Relationship between the inhibition constant (K_1) and the concentration of inhibitor which causes 50 per cent inhibition (I_{50}) of an enzymatic reaction. *Biochem. Pharmacol.* 22 1973, 3099–3108.
57. Szucs E, Stefanucci A, Dimmito MP, et al. Discovery of kynurenines containing oligopeptides as potent opioid receptor agonists. *Biomolecules* 10 2020, 284.

58. Sufka KJ, Watson GS, Nothdurft RE, Mogil JS. Scoring the mouse formalin test: validation study. *Eur. J. Pain* 2 1998, 351–358.
59. Gentilucci L, De Marco R, Cerisoli L. Chemical modifications designed to improve peptide stability: incorporation of non-natural amino acids, pseudo-peptide bonds, and cyclization. *Curr. Pharmaceutical des.* 16 2010, 3185–3203.
60. Mollica A, Pinnen F, Stefanucci A, Costante R. The evolution of peptide synthesis: From early days to small molecular machines. *Curr. Bioact. Comp.* 9 2013, 184–202.

CHAPTER 5: *In silico* identification of Tripeptides as Lead Compound for the design of KOR

Azzurra Stefanucci¹, Valeria Iobbi², Alice Della Valle¹, Giuseppe Scioli¹, Stefano Pieretti³, Paola Minosi³, Sako Mirzaie⁴, Ettore Novellino⁵, Adriano Mollica¹

¹ Department of Pharmacy, University G. d'Annunzio Chieti, Via dei Vestini 31, 66100 Chieti, Italy.

² Department of Pharmacy (DIFAR), University of Genova, 16128 Genova, Italy.

³ Centro Nazionale Ricerca e Valutazione Preclinica e Clinica dei Farmaci, Istituto Superiore di Sanità, Viale Regina Elena 299, 00161 Rome, Italy.

⁴ Advanced Pharmaceutics and Drug Delivery Laboratory, Leslie L. Dan Faculty of Pharmacy, University of Toronto, 27 King's College Circle, Toronto, ON M5S 1A1, Canada.

⁵ NGN Healthcare, Via Nazionale Torrette, 207, 83013 Mercogliano, Italy.

Abstract

The kappa opioid receptor (KOR) represents an attractive target for the development of drugs as potential antidepressants, anxiolytics and analgesics. A robust computational approach may guarantee a reduction in costs in the initial stages of drug discovery, novelty and accurate results. In this work, a virtual screening workflow of a library consisting of ~6 million molecules was set up, with the aim to find potential lead compounds that could manifest activity on the KOR. This *in silico* study provides a significant contribution in the identification of compounds capable of interacting with a specific molecular target. The main computational techniques adopted in this experimental work include: (i) virtual screening; (ii) drug design and leads optimization; (iii) molecular dynamics. The best hits are tripeptides prepared via solution phase peptide synthesis. These were tested *in vivo*, revealing a good antinociceptive effect after subcutaneous administration. However, further work is due to delineate their full pharmacological profile, in order to verify the features predicted by the *in silico* outcomes.

Introduction

Opioids represent the most effective and widely used analgesics to treat acute and intense pain since ancient times. Most of them are selective agonists of G-coupled opioid receptors μ -, δ -, and κ -opioid receptors (MOR, DOR and KOR respectively) [1]. Although opioid receptors are the best-known therapeutic targets for the treatment of acute and chronic diseases, their clinical use is limited by adverse side effects such as tolerance and dependence; thus, the development of analgesics with reduced side effects and lack of tolerance remains a main target in the field of medicinal chemistry [2]. KORs are considered an attractive target for the discovery of safe analgesics avoiding side effects including respiratory depression, tolerance, dependence, and constipation. They are widely expressed throughout the central and peripheral nervous system; among them dynorphins (encoded by the *Pdyn* gene) primarily activate the KORs with very low affinity for MOR and DOR [3]. In contrast to MOR and DOR receptor agonists, KOR agonists have been recognized as analgesics without addiction and tolerance insurgence, despite their tendency to induce dysphoria, anhedonia and hallucinations [4,5]. The crystal structure of human KOR in complex with the selective antagonist JD1c has been resolved in 2012 [6]. Che et al. provided the crystal structure of human KOR in complex with the agonist MP1104 in the active-state [7,8]. These clarify the conformational differences between inactive and active states, providing details on ligand–receptor interactions [7,8,9,10]. The activation of KOR by endogenous peptide or exogenous synthetic agonists is associated with behavioral and mood effects, including analgesia, sedation, and perceptual distortions [11,12,13], while antagonists binding at the same site block the activation of KOR; thus, they may be used for treatment of depression, anxiety, addictive disorders, and other psychiatric conditions [14,15].

KOR is the main subtype of opioid receptors responsible for mediating dynorphin-related actions and dynorphin-related peptides, such as stress, addiction, emotion, and perception. KOR agonists have also been shown to inhibit hyperalgesia induced by the μ agonist receptor [9,16]. Recent studies have uncovered further potential therapeutic areas for KOR ligands, such as affective disorders and addiction-related behaviors. As recently demonstrated for other GPCRs, structural insights from active and inactive receptors can be exploited in virtual ligand screening protocols providing new compounds as promising analgesics [17,18]. Several groups have shown that, unlike

other opioid receptors, KOR agonists inhibit dopamine efflux in the mesolimbic system and block the gratifying effects of abuse drugs such as heroin and cocaine [19,20,21]. Most KOR agonists belong to five chemical classes: endogenous peptides (dynorphins), benzodiazepines (diazepam, tifludom), benzazocines (bremazocine, pentazocine), arilacetamides (enadoline, U50488), and diterpenes (salvinorin A). Benzazocins, such as bremazocine, are not strictly selective KOR agonists, but they show strong analgesic effects. However, these molecules were discarded during clinical development due to psychotomimetic and dysphoric effects, although they had low tolerance potential and drug dependence [22,23]. KOR agonists were generally thought to exhibit adverse effects due to off-target action; thus, new κ -selective agonists such as aryl-acetamide derivatives (enadolines, U69593, U50488) were developed to avoid psychotomimetic and dysphoric effects; however, they also produce hallucinations and aversion [24,25].

Salvinorin A, a very potent and selective KOR agonist is known for its psychedelic effects [26]. Despite such a different chemical structure, κ receptor agonists have more or less psychotomimetic effects, and, therefore, clinical development has failed. Not surprisingly, the simultaneous inhibition of multiple neurotransmitter systems by KOR agonists causes complex multidimensional effects, such as hallucination, dysphoria and analgesia [27].

In addition, agonists induce phosphorylation of protein kinase 3 (GRK3) receptors of the κ receptor in the C-terminal region and the subsequent recruitment of β -arrestins, which are scaffolding proteins leading to the phosphorylation of P38 MAPK [28,29]. The identification of G proteins not dependent from the activation of P38 MAPK in the serotonergic neurons of the dorsal Rafe by the KOR agonist U50488 was a step forward into the elucidation of the mechanisms by which the receptor κ averages adverse effects. Interference on this signaling pathway in mice through receptor mutation (KORS369A), the deletion of GRK3 or the conditional cancellation of P38-MAPK blocks the adverse effects of κ agonists without reducing their analgesic effects [30,31,32,33]. These studies have important therapeutic implications because a selective partial κ receptor agonist that does not efficiently activate arrestin-dependent reporting could produce analgesia without significant dysphoria. In addition, the κ -receptor-mediated activation of the P38 MAPK in glia seems to be important for the development of hyperalgesia following peripheral neuropathy [34,35,36].

Roth and colleagues performed systematic pharmacological studies to discover a partial G receptor agonist, RB-64 (22-thiocyanatosalvinorin A) [26]. This study, using KO wild type and β -arrestin-2 mice, showed that RB-64-mediated G protein signaling induces analgesia and aversion, while β -arrestin-2 signaling averages sedation, anhedonia, and motor incoordination. This is a clear example of how the characterization of signaling pathways, which mediate specific behaviors, can ultimately be used for drug development. So far, almost all studies to determine the biased agonism of GPCR have investigated the partiality of a ligand for both protein G and β -arrestin, dependent only on downstream signaling.

Thus, diverse signals (e.g., phosphorylation of the PKC or GRK-dependent receptor) are a prerequisite. Over the years, several opioid ligands have been identified with the deconvolution of mixture-based combinatorial libraries at the Torrey Pines Institute of Molecular Studies (TPIMS) [37,38]. Computational studies through molecular scaffolds, molecular properties, and structural fingerprints show the diversity of these libraries and their uniqueness, based on: (a) the partial overlap with the structural space of drugs; (b) the presence of scaffolds not contained in other collections of compounds; (c) the increased molecular complexity compared to libraries of compounds commonly used in high-throughput screening (HTS) programs [39]. Structure-based drug design employs methods of receptor-based virtual screening (VS) and molecular docking for binding pose prediction, hit identification, and lead optimization. As part of our ongoing effort to discover new κ modulators with novel structures [40], the study herein is focused on the crystal structure of the KOR active-state for the discovery of novel KOR ligands using VS (Figure 1).

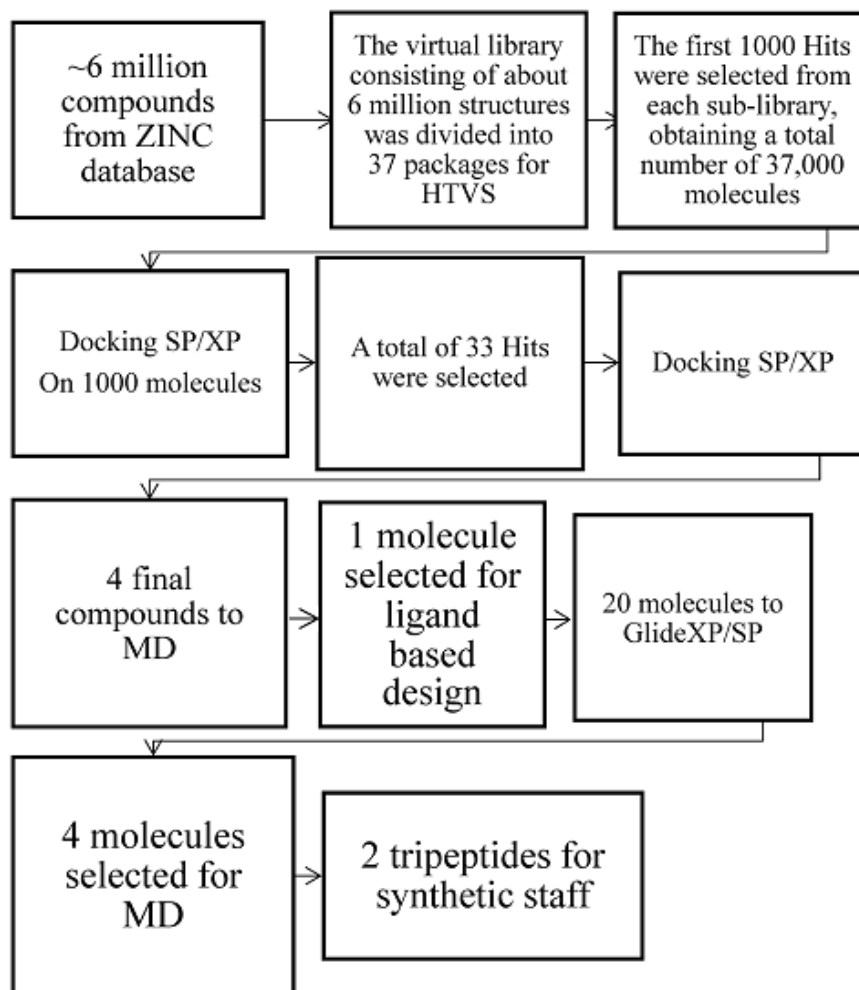


Figure 1. Computational workflow for the identification of the best two hits via Glide XP/SP and MD simulations.

Our computational protocol allowed us to identify two best hits as tripeptides that were synthesized in solution following standard peptide protocol synthesis [41,42]. The two compounds obtained in modest yields and excellent purity were also tested *in vivo*. A comparison with other opioid receptor structures identifies residues critical for KOR activation and highlights the key molecular characteristics of subtype selectivity and signal bias.

The basic scaffolds JDtic and MP1104 take distinctive poses, although with common characteristics typical of opioid ligands: (1) anchoring in the receptor binding pocket through a saline bridge with D138 in TM3; (2) interaction with TM5 through a phenolic group; (3) forming interactions with TM2/3 through chemically different portions [43,44]. The JDtic antagonist and the MP1104 agonist both form a saline bridge between their respective amino and D138 receptor patterns as observed in many GPCR-

ligand complexes. The greater distance of this saline bridge (3.0 Å) compared to similar interactions in KOR-JDtic (2.6 Å) and MOR-BU-72-Nb39 (2.7 Å) involves a weaker ionic interaction between MP1104 and KOR. D138 also forms a hydrogen bonding network with T1112.56 and Y3207.43 in KOR-MP1104-Nb, which is probably critical for full KOR activation; additionally, the mutation of these residues strongly attenuate or delete β arrestin2-recruitment mediated by MP1104 or Dynorphin A 1–17, respectively. The phenolic groups MP1104 and JDtic extend towards TM5, forming hydrogen bonds mediated by water with the backbone of the K227 carbonyl oxygen. This interaction was proposed to simulate the N-terminal tyrosine found in endogenous opioid peptides [45,46,47].

Directing the orientation of a rigid and hindered structure inside the binding pocket is fundamental to determine the effectiveness/strength of the ligand by minor changes in contact forces or tensions generated by substituents [48]. The orientation within the pocket probably depends (i) on the hybridization of the intramolecular bonds that determine the angles between the functional modules of the compound and (ii) specific interactions of the receptor subtype. Consequently, even small changes to identical scaffolds can subtly affect the compound binding pose, its potency, and/or effectiveness, as observed for other GPCR ligands [49].

Results and Discussion

Structure Based Design

The dipeptide H-D-Tyr-Val-NH₂ (ZINC71788314) obtained from virtual screening, presents interesting features: (a) a favorable docking score, with a value of –8.592; (b) structural simplicity, which allows an easy *in silico* optimization process and a feasible synthetic process; (c) amino-terminal tyrosine residue, essential for an optimal interaction with the opioid receptor [50]. Thus it was considered as the lead compound for the further development of KOR ligands. In the first attempt, a lipophilic portion was inserted, represented by a benzyl group bonded to the carboxy-terminal, in order to stabilize the ligand at the orthosteric site of the receptor through the formation of hydrophobic interactions [51]. The different combinations of the D and L amino acids in the dipeptide tyrosyl-valine benzyl ester were considered for the calculations with Glide SP and XP docking methods. Then the elongation of the dipeptide's carboxy-terminal was taken in consideration, through the insertion of valine (Table 1) or

tryptophan (Table 2) in the third position. The latter were considered by virtue of their chemical-physical properties, with the aim of creating a hydrophobic cluster [52]. The amino acid sequences of the two tripeptides, Tyr-Val-Val-OBz and Tyr-Val-Trp-OBz, were modified by D and L amino acids, and a docking score was calculated for each of them. The best result in terms of docking score values was obtained for the sequence D-Tyr-L-Val-L-Val-OBz, which was assumed as lead compound for further modification. The third approach consisted in the insertion of a bromine in meta position on the C-terminal aromatic ring. This modification was carried out with the aim of increasing the lipophilicity of the molecule intensifying the hydrophobic interactions between the C-terminal portion and the receptor pocket [53]. Both D and L series were considered in the docking prediction (Table 3).

Table 1. Docking score values for the designed peptides based on the insertion of valine in third position (second approach).

Peptides Sequences	Docking Score
D-Tyr-L-Val-L-Val-OBz	-11.789
D-Tyr-D-Val-L-Val-OBz	-11.467
L-Tyr-L-Val-D-Val-OBz	-11.189
D-Tyr-D-Val-D-Val-OBz	-11.154
D-Tyr-L-Val-D-Val-OBz	-9.975
L-Tyr-D-Val-D-Val-OBz	-9.598
L-Tyr-L-Val-L-Val-OBz	-8.510
L-Tyr-D-Val-L-Val-OBz	-8.188

Table 2. Docking score values for the designed peptides based on the insertion of tryptophan in third position (second approach).

Peptides Sequences	Docking Score
D-Tyr-L-Val-L-Trp-OBz	-11.582
L-Tyr-D-Val-L-Trp-OBz	-11.075
D-Tyr-D-Val-L-Trp-OBz	-8.174
L-Tyr-L-Val-L-Val-OBz	-7.523

Table 3. Docking score values for the designed peptides based on the third approach.

Peptides Sequences	Docking Score
D-Tyr-L-Val-L-Val-O-(3-Br)-OBz	-11.288
D-Tyr-D-Val-L-Val-(3-Br)-OBz	-10.728
D-Tyr-L-Val-D-Val-O-(3-Br)-OBz	-9.849
L-Tyr-L-Val-D-Val-O-(3-Br)-OBz	-9.451
D-Tyr-D-Val-D-Val-O-(3-Br)-OBz	-9.150
L-Tyr-L-Val-L-Val-O-(3-Br)-OBz	-9.087
L-Tyr-D-Val-D-Val-O-(3-Br)-OBz	-8.792
L-Tyr-D-Val-L-Val-O-(3-Br)-OBz	-7.774

The peptides with the best docking score values were selected for the next phase of molecular dynamics (MD), which allows one to simulate and analyze the physical movements of atoms and groups of atoms within a molecular system. The final poses of the best tripeptides obtained by the Glide/XP docking method are reported below (Figure 2).

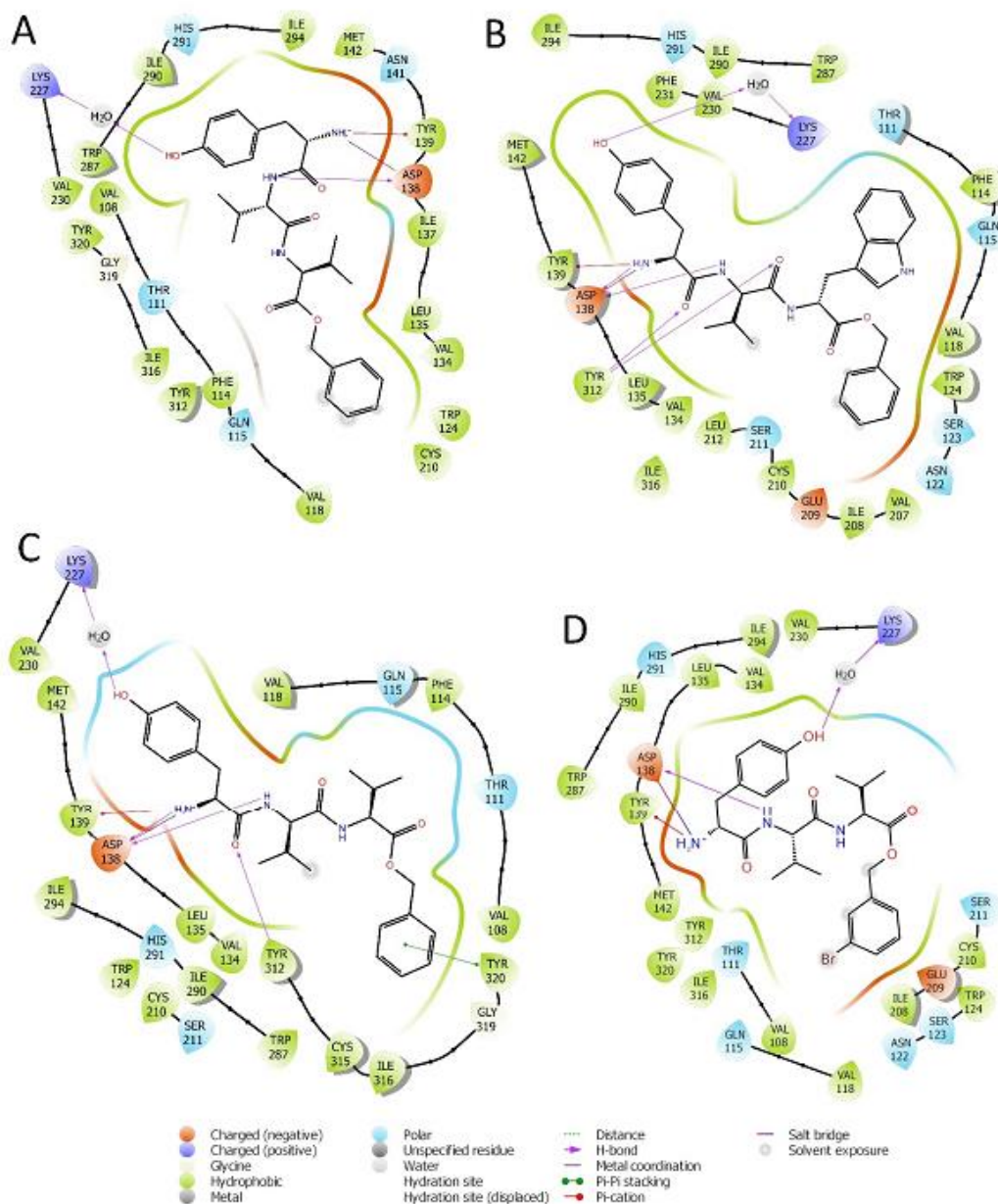


Figure 2. Interactions of peptides H-D-Tyr-Val-Val-OBz (A), H-D-Tyr-Val-Trp-OBz (B), H-D-Tyr-D-Val-Val-OBz (C), and H-D-Tyr-Val-Val-O-(3-Br)-Bz (D) with the amino acids residues of KOR binding site.

Molecular Dynamics Simulation

The simulation was conducted on the four peptides selected in the design phase: H-D-Tyr-Val-Val-OBz, H-D-Tyr-Val-Trp-OBz, H-D-Tyr-D-Val-Val-OBz, and H-D-Tyr-

Val-Val-O-(3-Br)-Bz, which were submitted to the Desmond Molecular Dynamic System [54] feature and incorporated into Maestro 2017. RMSD analysis provides information on the stability of the ligand within the active site of the receptor (Figure 3 and Figure 4). The P-RMSF allows one to visualize the areas of the protein chain that fluctuate the most during the simulation, while the L-RMSF shows how the ligand fragments interact with the protein and determine its entropic role during the binding process. The bonds established between receptor and ligand have been evaluated and classified into four categories: (a) hydrogen bonds, (b) hydrophobic interactions, (c) ionic bonds, and (d) aqueous bridges, which mediate the interactions between the ligand and amino acid residues of the receptor. Below are the RMSD values of the four designed tripeptides and the crystallographic ligand (Figure 3).

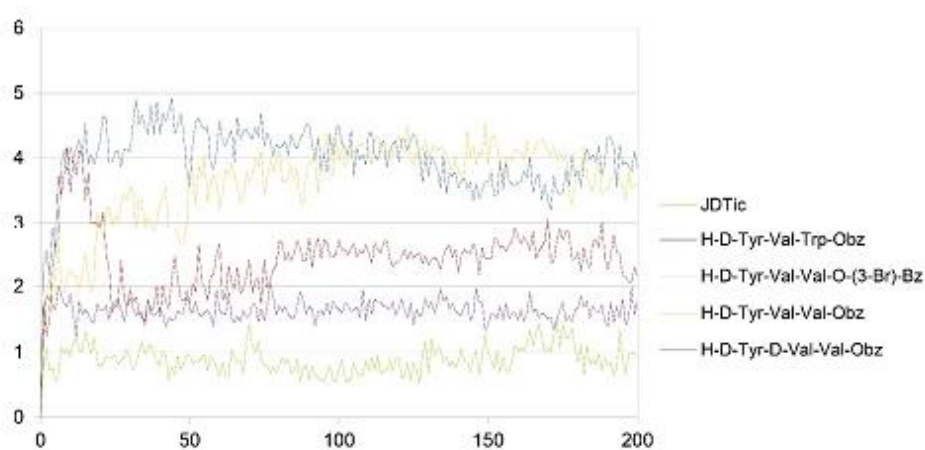


Figure 3. RMSD values of JDtic and the designed peptides (x axis: RMSD in Angstrom; y axis: time in ns).

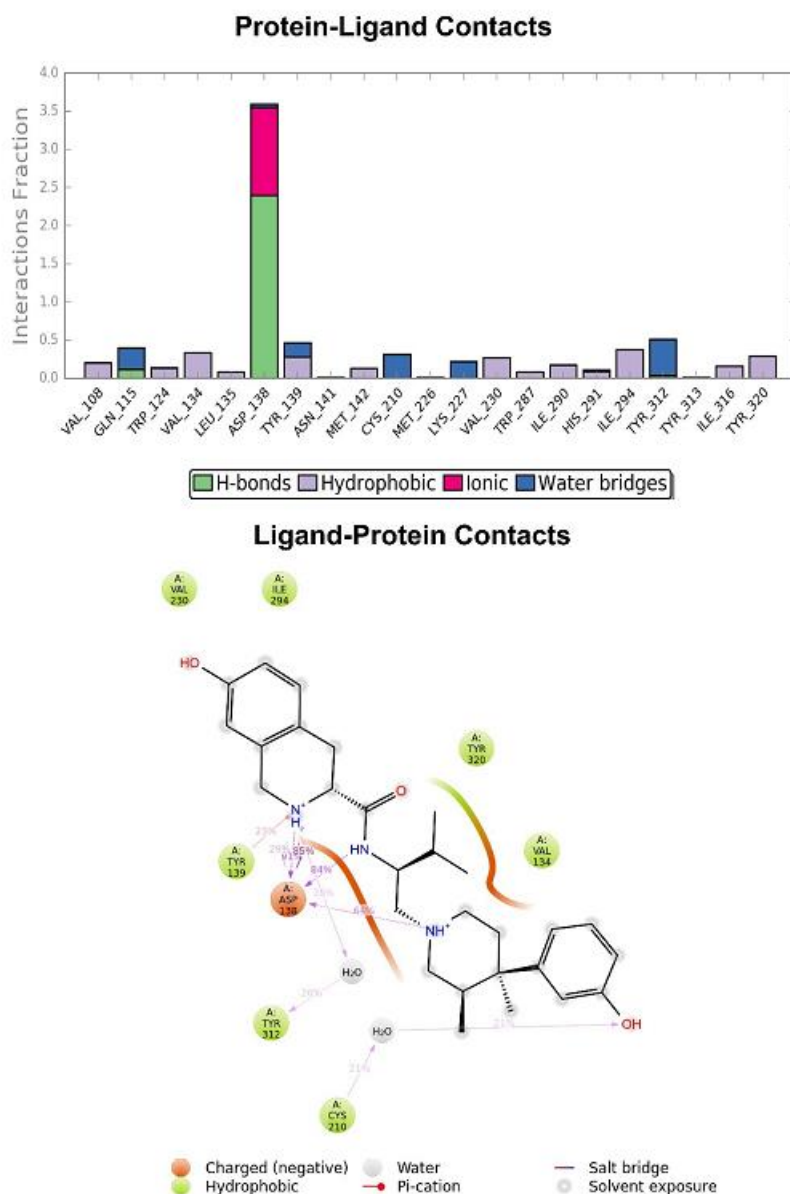


Figure 4. Graphic representation of the interactions between the JD_{Tic} and KOR binding site, expressed in %. Hydrogen bonds are in violet lines.

The crystallographic ligand has a stable pose inside the receptor pocket, as can be seen from the RMSD in Figure 3. The protein–ligand interactions are mainly represented by hydrogen bonds and the ionic nature with the residue of Asp138. The water bridge with the residue of Lys227, present both in the original pose and in the docked pose, was lost during the simulation (Figure 4). In the P-RMSF are reported the areas of the protein most affected by fluctuations, which exceed the value of 4.5 Å (Figure 5). JD_{Tic} does not show fluctuations greater than 1.0 Å, except for one of the two methyl groups linked to the isopropyl fragment (fragment 16), which reaches values greater than 1.5 Å (Figure 5).

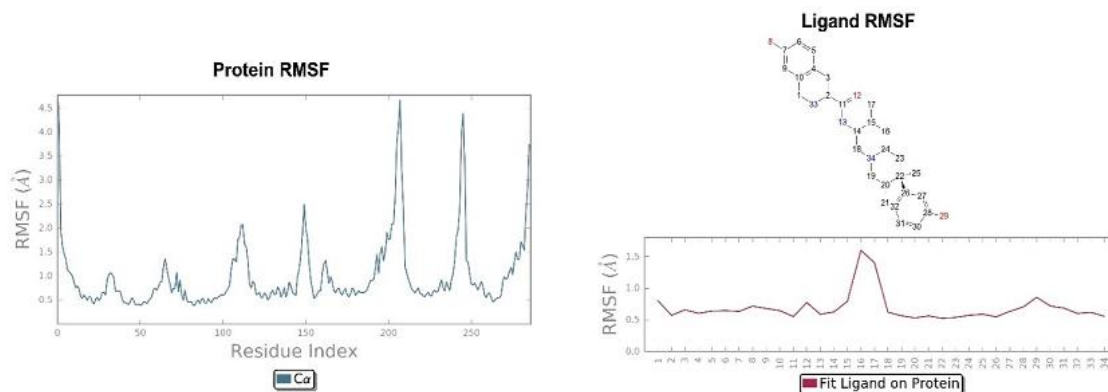


Figure 5. On the left: P-RMSF for KOR; on the right: L-RMSF of JDtic.

The RMSD of the H-D-Tyr-Val-Val-OBz tripeptide located in the receptor active site appears to stabilize after 4 ns (Figure 3). The interactions with the KOR are better than in JDtic. In addition to the numerous hydrogen bonds and ionic interactions involving the Asp138 residue, there are further stabilizations of the ligand through different hydrophobic interactions with Tyr139 and Trp287 (Figure 6). Interestingly the water bridge is established between the phenolic hydroxyl group of D-Tyr and the Hys291 residue of the protein. The P-RMSF illustrates the fluctuations of the protein at slightly higher values (5.6 Å) than that found in JDtic (Figure 7). In the L-RMSF graph the best fluctuations are recorded for the side chain of the valine at the C-terminal end (fragment 24) (Figure 7).

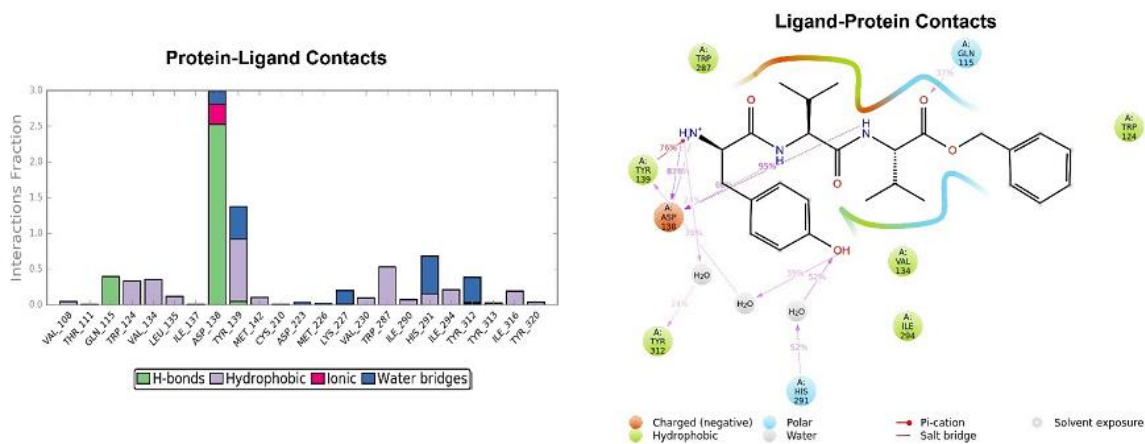


Figure 6. Representation of the main interactions found for H-D-Tyr-Val-Val-OBz in the KOR binding site, expressed in %. Hydrogen bonds are in violet lines.

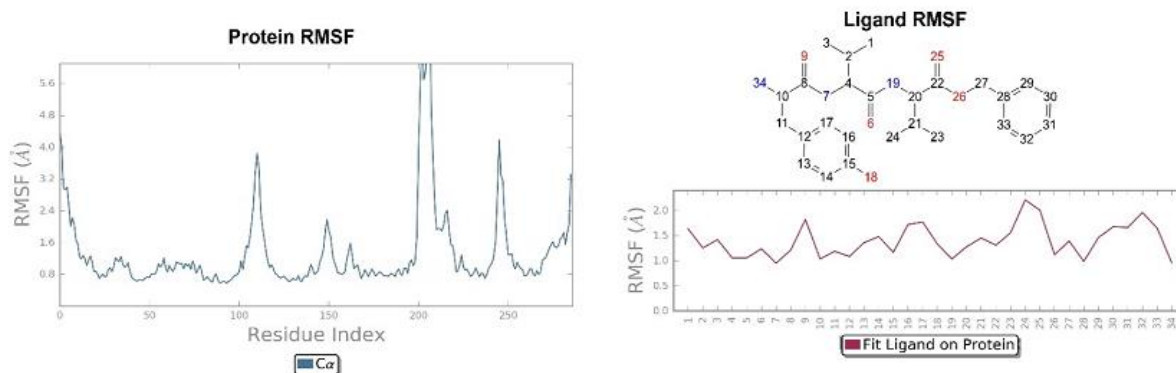


Figure 7. On the left: P-RMSF, receptor kappa; on the right: L-RMSF di H-D-Tyr-Val-Val-OBz.

Looking at Figure 8, the tripeptide H-D-Tyr-Val-Val-O-(3-Br)-Bz (6) turns out to be the ligand with the most stable profile during the simulation time. The receptor–ligand interactions are mainly characterized by hydrogen bonds with Asp138 and Gln115, with multiple hydrophobic interactions involving non-polar amino acid residues, such as Ile294 and Val118. Similarly to the tripeptide analyzed previously, there is interaction with the Hys291 residue assisted by a water molecule (Figure 8). The P-RMSF graph is comparable to the previous one (Figure 9); while the highest fluctuations are in correspondence with the aromatic ring replaced with the bromine atom (fragments 28–33 and 34).

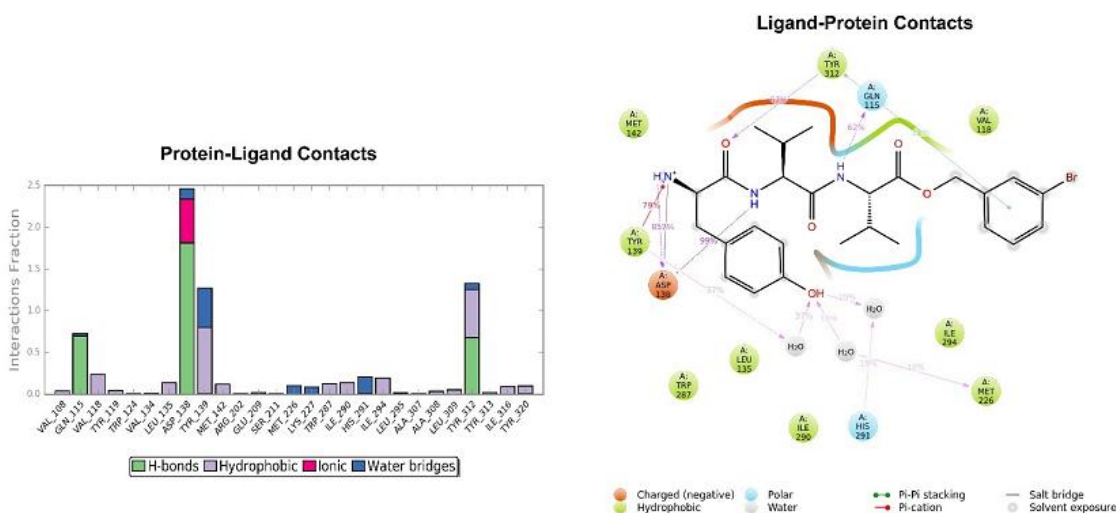


Figure 8. Key interactions of H-D-Tyr-Val-Val-O-(3-Br)-Bz (6) with KOR binding pocket expressed in %. Hydrogen bonds are in violet lines.

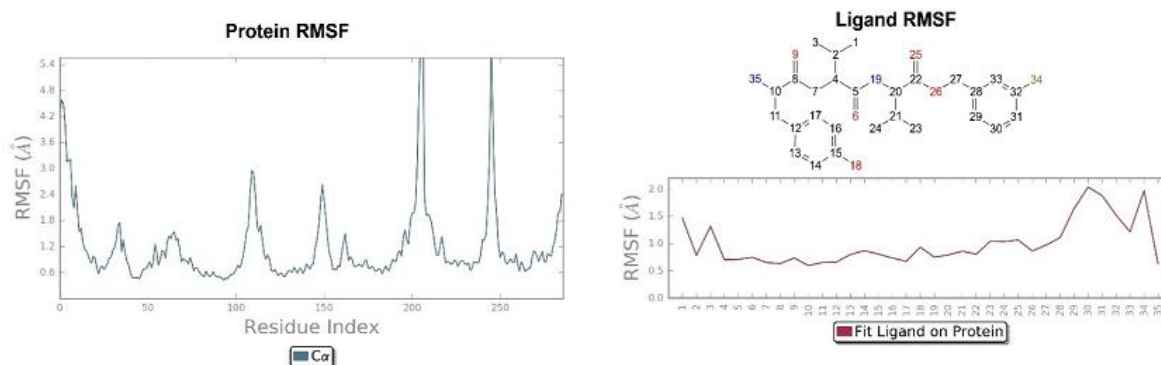


Figure 9. On the left: P-RMSF, KOR; on the right: L-RMSF of H-D-Tyr-Val-Val-O-(3-Br)-Bz (6).

The pose of H-D-Tyr-Val-Trp-OBz (11) is generally stable during molecular dynamics, and the binding with the KOR mainly focuses on hydrogen interactions with Asp138. The additional interactions of a hydrophobic nature allow for a good stabilization of the molecule within the receptor site; however, the hydrogen bond with the catalytic water molecule that acts as a bridge with the Lys227 residue is lost (Figure 10). The P-RMSF graph is comparable to the previous ones, and, in the L-RMSF, the main fluctuations are observed for fragments 25–31, due to the C-terminal benzyl group (Figure 11).

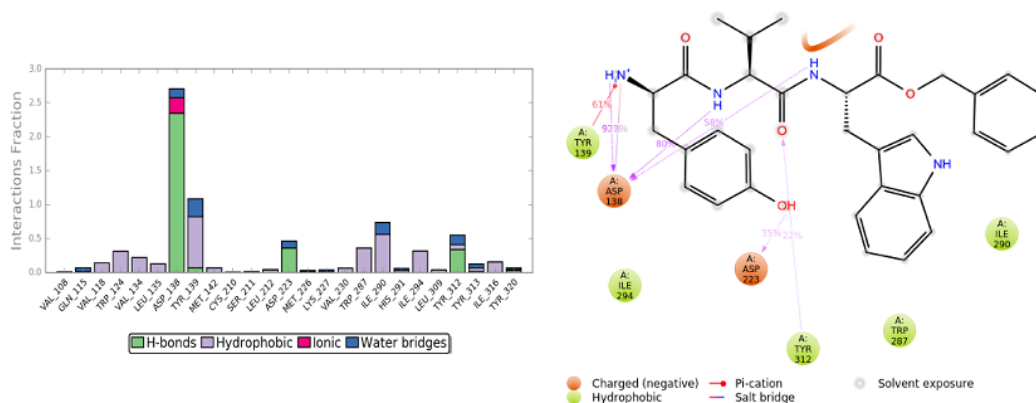


Figure 10. Interactions of H-D-Tyr-Val-Trp-OBz (11) within the KOR binding pocket, expressed in %. Hydrogen bonds are in violet lines.

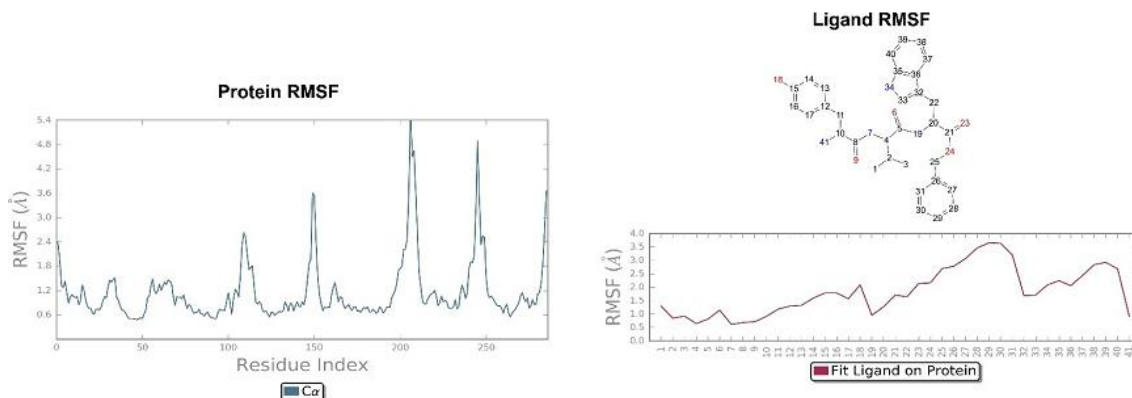


Figure 11. On the left: P-RMSF of KOR; on the right: L-RMSF of H-D-Tyr-Val-Trp-OBz (11).

The pose of the tripeptide H-D-Tyr-D-Val-Val-OBz is stable and characterized by the prevalence of a hydrogen bond between the NH group of the backbone and the Asp138 residue. Interestingly the N-terminal group of tyrosine is involved in the hydrogen bond with Asp138 and a water molecule (Figure 12); the benzyl ring established a π - π stack interaction with Tyr320 and hydrophobic contacts with Val108, Trp287. The key interaction between the hydroxyl group of Tyr and His291 is also present. The highest fluctuations occur at the valine-O-benzyl portion (fragments 25–34) of the peptide (Figure 13).

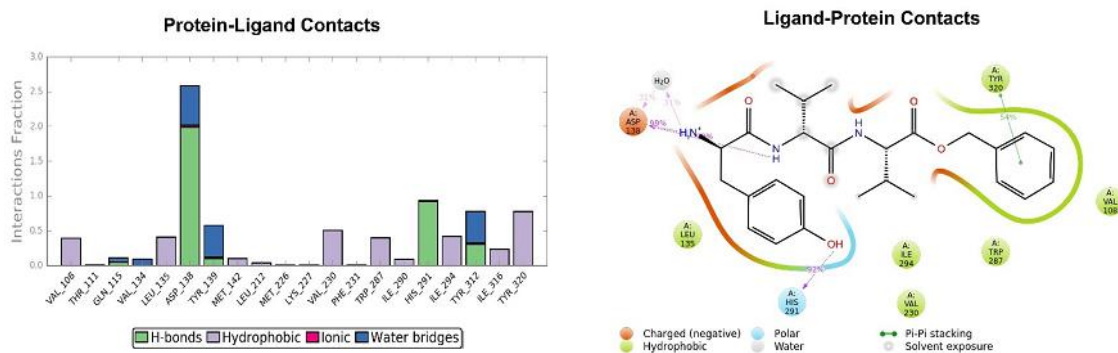


Figure 12. Interactions of H-D-Tyr-D-Val-Val-OBz within the KOR binding pocket, expressed in %. Hydrogen bonds are in violet lines.

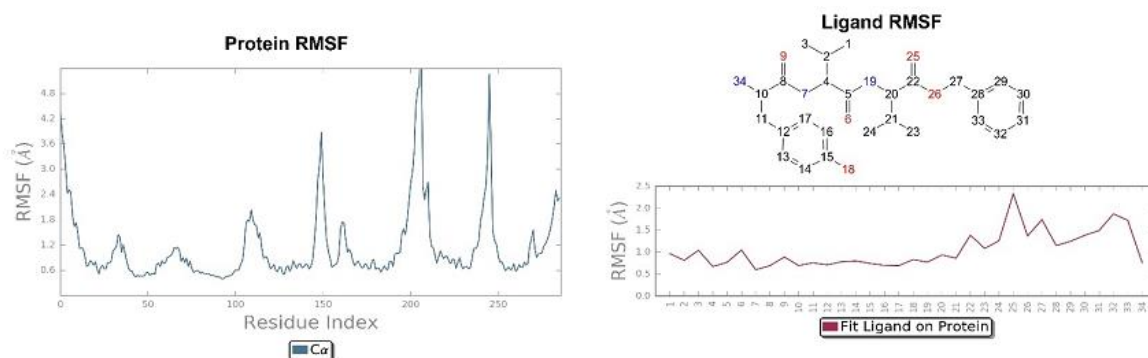


Figure 13. On the left: P-RMSF for KOR; on the right: L-RMSF of H-D-Tyr-D-Val-Val-OBz.

To conclude tripeptides H-D-Tyr-Val-Val-O-(3-Br)-Bz (6) and H-D-Tyr-Val-Trp-OBz (11) are of great interest because they exhibit enhanced docking score values compared to the original dipeptide H-D-Tyr-Val-NH₂ (−11.288 and −11.582 respectively, Table 2 and Table 3), higher than that of the crystallographic ligand (−11.176 with Glide/XP). The tripeptides designed *in silico* show strong stability, preserve the key interaction with the Asp138 residue, and are stabilized by efficient additional hydrophobic interactions. Thus, they were selected for solution phase peptide synthesis and further tested *in vivo* by means of tail flick and formalin tests.

Antinociceptive Effect In vivo

The results obtained in the tail flick and in the formalin tests are reported in Figure 14. In the tail flick test, the administration of tripeptides 6 and 11 induced antinociceptive effects that peaked 30 min after the administration (Figure 14, left panel). After the peak time, compound 6 induced significant antinociceptive effect at 45 min after the administration, then its effect declined to MPE values similar to those observed in vehicle-treated animals 90–120 min thereafter. On the contrary, peptide 11 induced antinociceptive effects that were still significant at 45, 60, and 90 min after administration. The results obtained in the formalin test are reported in Figure 14, right panel. In the early phase of the formalin test, both 6 and 11 were able to reduce the nociceptive behavior induced by aldehyde. When the late phase was recorded, only compound 11 was able to reduce the licking nociceptive behavior induced by formalin, whereas compound 6 was ineffective. All together these data highlight a better antinociceptive effect for peptide 11 compared to 6 in both tests. The inflammation process contributes to the second phase of the test, during which compound 11 is still active, indicating an acute response to a model of ongoing acute pain involving

inflammation and aspects of central sensitization. This could be due either to a good penetration of the blood–brain barrier ,as well as to the ability of this tripeptide to interact with opioid receptors at the periphery. With the aim of shedding some light on the possible pharmacokinetic profiles of these two compounds, an ADME study was performed *in silico* by means of SwissADME free web tool (<http://www.swissadme.ch/index.php>, accessed on 8 February 2021) [52].

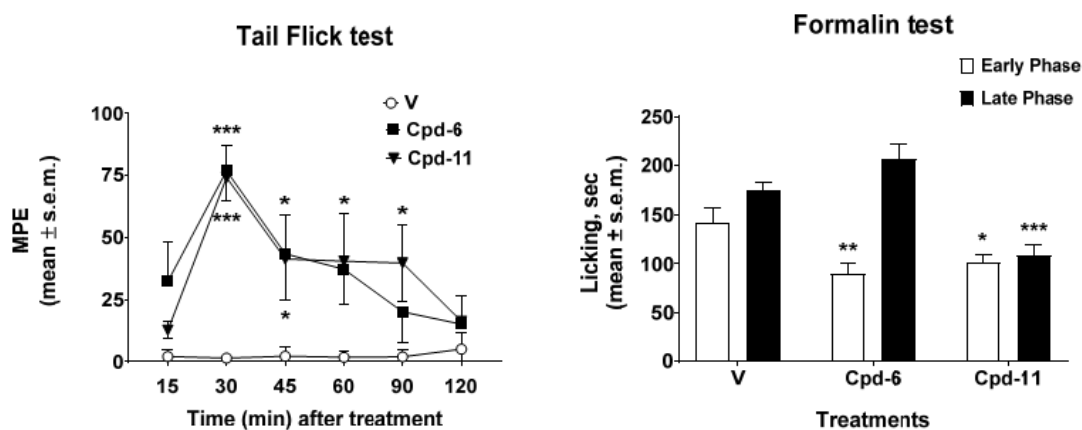


Figure 14. Effects induced by compounds 6 and 11 in the tail flick (left panel) and in the formalin (right test) tests. In the tail flick test, compounds were injected i.c.v. at a dose of 0.6 nmol/10 μ L. In the formalin test, compounds were injected s.c. in the dorsal surface of the hind paw, 15 min before formalin. V is for vehicle-treated animals. * is for $p < 0.05$; ** is for $p < 0.01$; *** is for $p < 0.001$. $N = 7$.

In silico ADME and Drug-Likeness Evaluation

The best two tripeptides 6 and 11 were submitted to an *in silico* evaluation of ADME (adsorption, distribution, metabolism, excretion) properties to estimate their pharmacokinetics and drug-likeness (Table 4). Prediction of GIA is based on the brain or intestinal estimated permeation (BOILED-egg) model, which calculates the passive gastrointestinal absorption and blood–brain barrier penetration. This was high for peptide 6 and low for 11; however, both of them show the same bioavailability score (0.55); this could be due to the fact that they turn out to be good substrates for P-glycoprotein, which is a cell membrane transport protein responsible for pumping drugs out [54,55,56]. Moreover, peptide 11 showed inhibition of CYP3A4, an enzyme involved in the metabolism of drugs [54], while peptide 6 lacks this interaction, which could prevent the accumulation of drugs. Peptides 6 and 11 have more than 10 rotatable bonds and a TPSA value $> 130 \text{ \AA}$ (Table 4), indicating a low oral bioavailability [56]; in fact, both values of POLAR (TPSA) and FLEX for 6 and 11 are outside the desired

range for improved bioavailability. Overall, this *in silico* study indicates slightly better pharmacokinetic properties for 6 compared to 11 but similar lipophilicity, which reflects their poor predicted bioavailability.

Table 4. *in silico* ADME study for peptides 6 and 11.

Peptides	Lipophilicity		Drug-Likeness		Pharmacokinetics		
	TPSA (Å)	CLogP (o/w)	Bioavailability Score	Lipinski Filter	GIA	P-gp Substrate	CYP3A4 Inhibitor
6	132.37	2.59	0.55	Yes (1)	high	yes	no
11	148.16	2.46	0.55	Yes (1)	low	yes	yes

Abbreviations: CLogP (o/w), logarithm of compound partition coefficient between n-octanol and water; CYP3A4, cytochrome P450 3A4; GIA, gastrointestinal absorption; Lipinski filter (with number of violations in bracket); TPSA, topological polar surface area.

Methods and Materials

Library Preparation

The virtual library of compounds was retrieved from the ZINC database [57], from which a subset of ~6 million commercially available molecules were selected using the following filtering criteria: (i) molecules with molecular weight between 150 and 500; (ii) log P less than or equal to 5; (iii) hydrogen binding donor groups less than or equal to 5; (iv) hydrogen binding acceptor groups lower than or equal to 10; (v) PSA (molecular polar surface area) less than 150 and rotatable bonds less than or equal to 7. Compounds containing extremely reactive functional groups were discarded, e.g., thiol groups, Michael acceptors, and aldehyde groups. The selected molecules in MOL2 format were submitted to LigPrep tool [58], incorporated in Maestro Schrödinger 2017-1 [59]. LigPrep allows one to generate accurate and energetically minimized 3D structures, following these parameters: (i) the addition of any absent hydrogen atoms; (ii) the removal of unwanted molecules (water, salts); (iii) the neutralization of all groups, before generating the states of ionization with the Epik [60] function, setting a pH range of 7.4 +/- 0.0, with the aim of replicating physiological conditions. The final steps of this process consist in the generation of a series of tautomers for each structure, preserving the stereochemistry of the chiral centers of the ligands.

Protein Preparation

The human KOR (PDB code 4DJH) was retrieved from PDB in complex with a selective antagonist JD_{Tic} ((3R)-7-hydroxy-N-[(2S)-1-[(3R,4R)-4-(3-hydroxyphenyl)-3,4-dimethylpiperidin-1-yl]-3-methylbutan-2-yl]-1,2,3,4-tetrahydroisoquinoline-3-carboxamide) [6]. The Protein Preparation Wizard tool embedded in Maestro 2017-1 [61] allows for the accurate conversion of the raw PDB file into a fully prepared protein structure. During this phase, hydrogen atoms were added to all protein residues, and three of the four chains were removed from the crystallized structure, retaining only the A chain containing the binding cavity. Then, hydrogen bonds and residue protonation states were refined by setting the pH to 7.4 with the PropKa function [62]. The minimization was carried out using the force field OPLS3 [63].

Receptor Grid Generation

The Receptor Grid Generation tool embedded in the Maestro 2017 suite was applied to form the grid that delimits the area of possible interactions between the ligand and the amino acid residues of the receptor. The kappa receptor and the crystallographic ligand (JD_{Tic}) are displayed in the Workspace, and an orthorhombic box is generated by exclusively centering the ligand, within which the virtual library of molecules will be anchored. A scaling factor of 1.00 on the Van der Waals radii of the non-polar atoms of the receptor was preserved, and the cutoff of the partial atomic charge was set at 0.25. A grid of 20 Å allows one to carry out the docking with ligands having dimensions comparable to the reference crystallographic ligand.

Glide Docking of the Co-Crystallized Ligand

The crystallographic ligand was prepared with LigPrep, following the steps previously illustrated in paragraph 2.1. The JD_{Tic} antagonist was anchored to the active site of the kappa receptor through the Glide SP method, suitable for screening ligands with undefined quality, and subsequently with Glide XP [64]. The default parameters have been maintained and flexible docking has been opted for. The validation criterion of the docking method was the RMSD (root mean square deviation) value, i.e., the root of the mean square deviation, useful for calculating the average distance of structurally equivalent atoms. The calculated RMSD value, resulting from the overlap between the crystallographic ligand and the ligand prepared and repositioned in the active site by

GlideXP, was found to be 0.119 Å. The JDtic crystallographic ligand was also subjected to HTVS with the aim to evaluate the interactions within the receptor pocket. Two key interactions were present, e.g., ionic interactions with the residue of Asp138 and the hydrogen bond between water molecule 1303 and Lys227 (Figure 15).

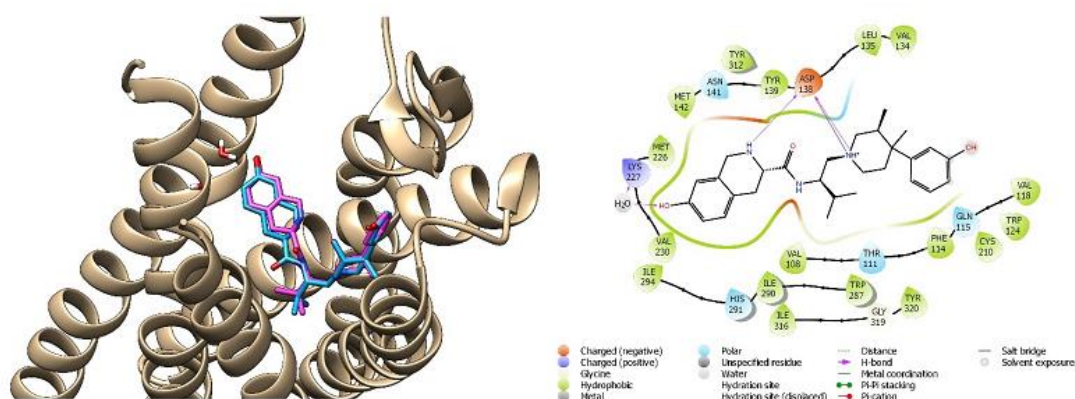


Figure 15. On the left: superimposition of the crystallographic ligand's pose JDtic (pink) on the crystallized complex and its binding pose obtained with GLIDE/XP (blue); on the right: interactions of the HTVS binding pose of JDtic in the KOR binding cavity.

Virtual Screening Workflow

The virtual library consisting of about 6 million structures was divided into 37 packages or sub-libraries. The HTVS docking method was applied to each packet, designed to perform rapid screening operations on a large number of ligands. The first 1000 hits were selected from each sub-library, obtaining a total number of 37,000 molecules; among them, a first set was selected manually based on (i) the key interactions with the receptor: an ionic bond with Asp138 and a hydrogen bond with Lys227 assisted by a water molecule, (ii) docking score value, (iii) additional interactions with the kappa receptor: possible additional bonds, in addition to key interactions, were evaluated to favor a better pattern of interactions between the ligand and the active site of the receptor. (iv) RMSD value; (v) biological activity: the possible presence of biologically active molecular structures has been investigated in the literature. A total of 33 hits were selected, of which 10 with the best docking score values, 10 with interesting additional interactions, 10 with the best degree of overlap with JDtic and 3 with biological activity previously reported in literature [65,66,67]. Further docking optimization was done using Glide, which allows the ligand to be anchored to the active site of the receptor, providing for its binding mode. The previously created grid was selected, and

two scoring functions with increasing precision were adopted: SP and XP Glidescore. We opted for a flexible docking model, leaving unchanged the standard Scaling factor parameters equal to 0.80 on the Van der Waals radii of the non-polar atoms of the receptor, defined as the atoms whose absolute value of the partial atomic charge (δ^- or δ^+) is positive and with a maximum value of 0.15. The ZINC04632302 outcome is a benzoimidazole that was characterized *in vitro* on MOR and DOR [68] and the compound ZINC06697859, which expressed antagonist activity with a high affinity for KOR ($K_i = 0.09 \mu\text{M}$) [69]. The ZINC71788314 is a D-tyrosyl-valinamide (H-D-Tyr-Val-NH₂), a dipeptide obtained from the α -amidation process of the synthetic peptide D-tyrosyl-valyl-glycine (H-D-Tyr-Val-Gly-OH) in the brain [70].

Molecular Dynamics

The simulation was conducted on the four peptides H-D-Tyr-Val-Val-OBz, H-D-Tyr-Val-Trp-OBz, H-D-Tyr-D-Val-Val-OBz, and H-D-Tyr-Val-Val-O-(3-Br)-Bz through the Desmond Molecular Dynamic System [60,61,62,63,64,65,66,67,68,69,70,71] feature incorporated into Maestro 2017-1. The system builder instrument in Desmond was used for the preparation of receptor–ligand complexes; the lipid bilayer membrane DPPC was set at 325 K, through which the various complexes to be examined were inserted. The entire system was centered by an orthorhombic box of 302,956 Å³ after minimization, which was saturated with water molecules by setting the TIP3P aqueous solvent model, in order to recreate physiological conditions. In the “Ions” section, the NaCl salt at a concentration of 0.15 M was added and the OPLS3 force field set. The resulting system, displayed in the Workspace, was loaded in the “Molecular Dynamics” panel, belonging to the Desmond package. For each protein–ligand system, the overall simulation time was 20 ns, with an approximate number of frames equal to 200. For the ensemble option, which represents the macroscopic conditions of the system, the statistical set NPT (ensemble isothermal-isobaric), characterized by constant values of the number of particles, pressure, and temperature. In each molecular dynamics, the following parameters have been set: (a) temperature at 309.15 K and (b) pressure at 1.01325 bar. Newton’s equations of motion in the molecular dynamics trajectory were integrated with the r-RESPA method. Constraints have been placed on atoms capable of participating in hydrogen interactions, as they determine higher frequency vibrations, causing a restriction of the integration step (time-step) to about 0.5fs in an MD. Therefore the SHAKE method was used, reaching an integration step of 2 fs [70]. The

contribution of the short range electrostatic interactions and the Lennard-Jones potential was evaluated by applying a spherical cut-off of 10 Å. Instead, the contribution of long-range electrostatic interactions, represented by the summation of the pairs of unbound atoms of the system, was estimated using the particle mesh Ewald method [71,72].

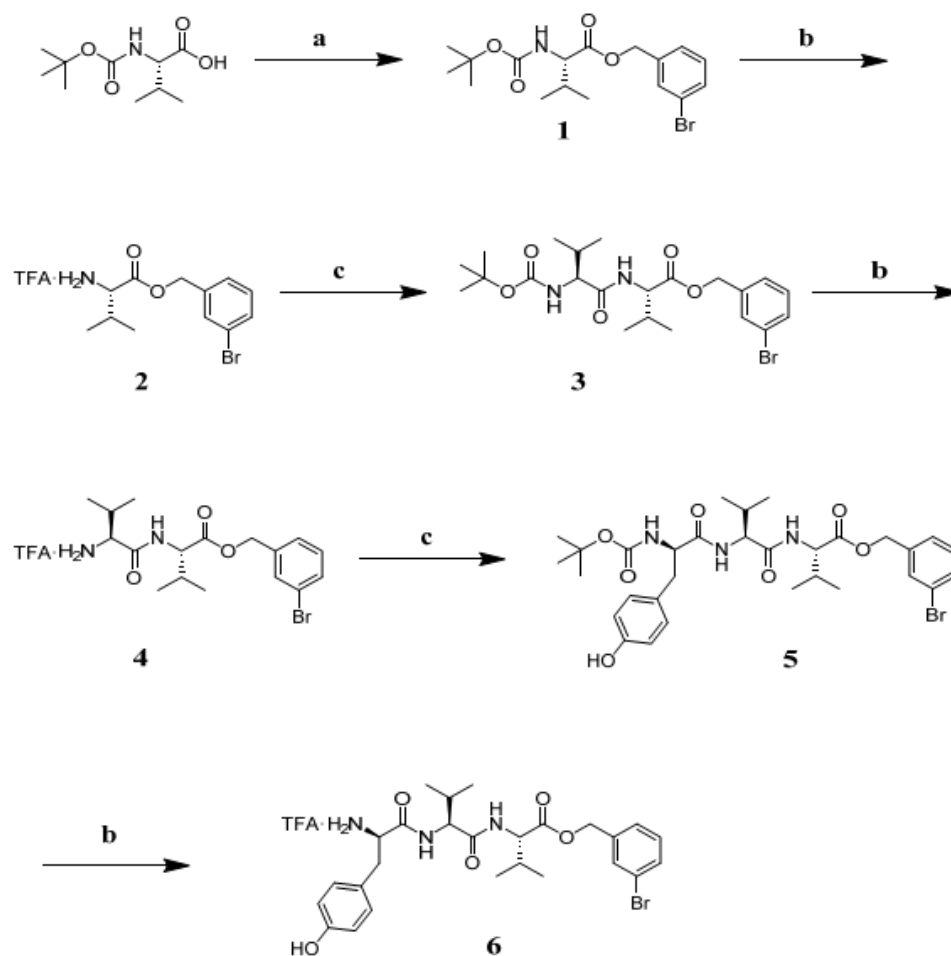
Chemistry

General

All the reagents and amino acids for the synthesis were purchased from Sigma Aldrich (Milan, Italy). Final products were purified in RP-HPLC using a Waters XBridge™ Prep BEH130 C18 column, 5.0 µm, 250 mm × 10 mm at a flow of 4 mL/min, and a Waters 600 binary pump (Milford, MA, USA), using as eluent a linear gradient of H₂O/ACN 0.1% TFA, starting from 5% ACN to 90% ACN in 35 min. The nature of the protected N α -Boc(D)Tyr-Val-Val-O-(3-Br)-Bz and N α -Boc(D)Tyr-Val-Trp-OBz was confirmed by NMR with a Varian Inova 300 MHz instrument and ESI-LRMS Thermo Finnigan mass spectrometry (Somerset, NJ, USA). The purity of all final products as TFA salts was confirmed by NMR analysis, ESI-LRMS, and analytical RP-HPLC (C18-bonded 4.6 × 150 mm; 1 mL/min; 0.1% H₂O/ACN gradient TFA from 5% to 95% ACN in 30 min), and the results were $\geq 95\%$.

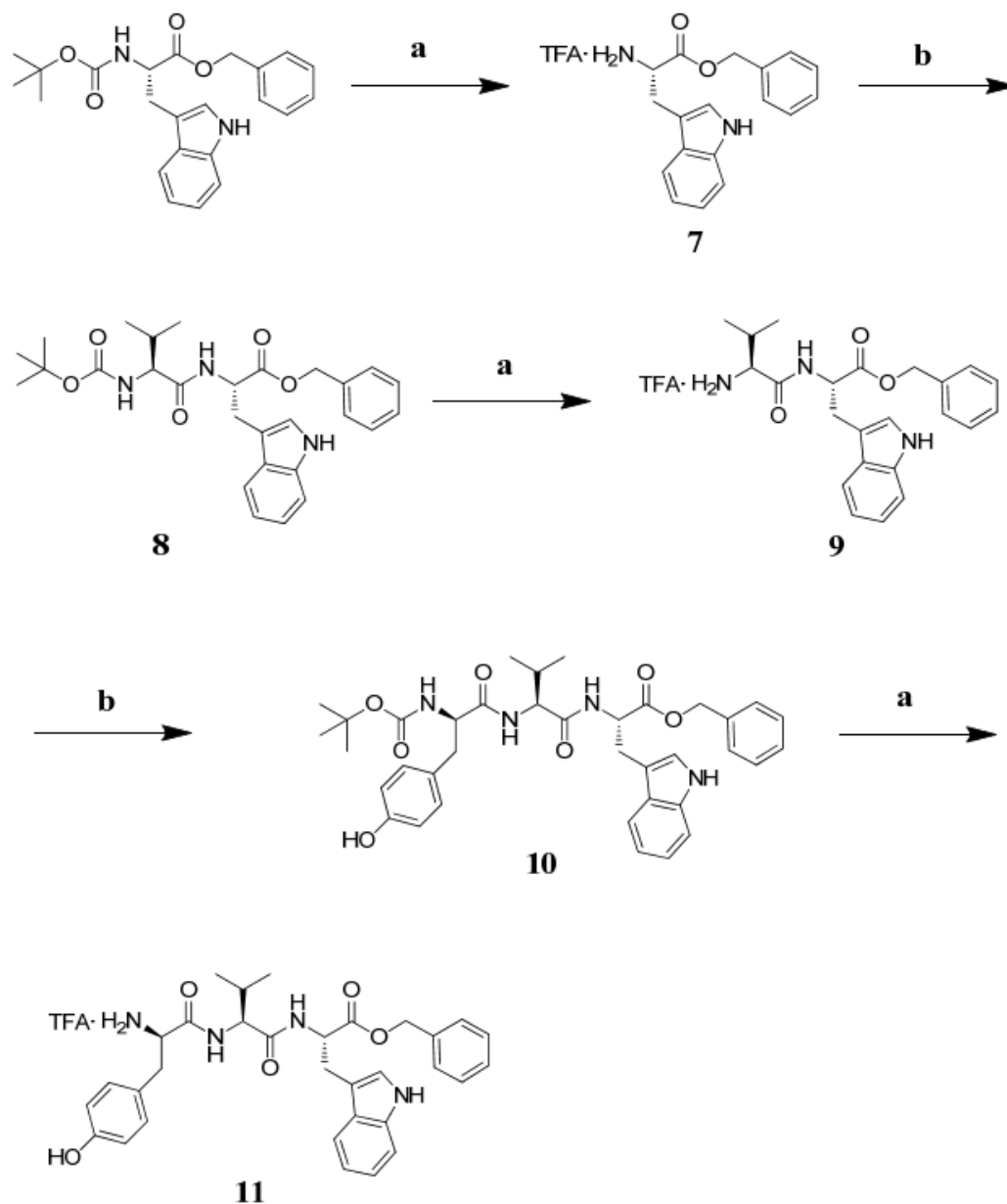
Synthesis

The tripeptide TFA.NH₂-(D)Tyr-Val-Val-O-(3-Br)-Bz (6) was obtained starting from Boc-Val-OH, which was involved in a benzylation reaction with 3-bromo-benzyl, K₂CO₃ at reflux in ACN for 4 h. Intermediate 1 was deprotected with a mixture TFA:DCM = 1:1 at r.t. under stirring for 1 h. Intermediate 2 was reacted with Boc-Val-OH, EDC.HCl, HOBt and DIPEA in DMF at r.t. for 2 h. Repeated deprotection and coupling steps afforded Boc-protected intermediate 5 [73]. This peptide was treated with the TFA/DCM mixture so as to obtain the desired final product 6 as a TFA salt (Scheme 1).



Scheme 1. Reagents and conditions: (a) K₂CO₃ (1.2 eq), 3-bromo-benzyl (1 eq), ACN (5 mL), reflux, 4 h; (b) TFA:DCM = 1:1, r.t., 1 h; (c) EDC·HCl (1.1 eq), HOBT (1.1 eq), Boc-Val-OH for **2** or Boc-Tyr-OH for **5** (1 eq), DIPEA (3 eq), in DMF r.t. 12 h.

The tripeptide TFA·NH₂-D-Tyr-Val-Trp-OBz (**11**) was prepared in solution starting from Boc-Trp-OBz. The amino acid was deprotected with a mixture of TFA: DCM = 1: 1 at r.t. for 1 h and subsequently reacted with Boc-Val-OH in DMF, EDC.HCl, HOBT, and DIPEA at r.t. for 12 h. Intermediate **8** was deprotected and reacted with Boc-D-Tyr-OH under the aforementioned conditions. The final product **11** was obtained following the removal of the tert-butyloxycarbonyl group with an overall yield of 5.86% (Scheme 2).



Scheme 2. Reagents and conditions: (a) TFA:DCM = 1:1, r.t. 1 h; (b) EDC·HCl (1.1 eq), HOBT (1.1 eq), Boc-Val-OH or **9**, or Boc-D-Tyr-OH (1 eq) for **10**, DIPEA (3 eq), in DMF, r.t. 12 h.

Characterization of Peptides and Intermediates

Boc-Val-O-(3-Br)-Bz (**1**). Boc-Val-OH (100 mg, 0.46 mmol) was dissolved in ACN (5 mL) with K₂CO₃ (69.65 mg, 1.2 eq) and 3-bromo-benzyl (104.97 mg, 1 eq). The mixture was left to reflux for 4 h., checking the completeness of the reaction with TLC (100% DCM). The solvent was removed in vacuum giving a raw material pure in TLC (100% DCM, R_f = 0.3) in 92% yield. ¹H NMR (CDCl₃) δ: 7.45 (m, 2H, aromatics); 7.25–7.20 (m, 2H, aromatics); 5.17–4.98 (m, 3H, NHα + CH₂ benzyl), 4.27 (m, 1H, CHα), 2.13 (m, 1H, CHβ), 1.43 (s, 9H, Boc), 0.94 (d, 3H, CH₃), 0.84 (d, 3H, CH₃).

TFA.NH₂Val-O-(3-Br)-Bz (2). Intermediate 1 was treated with a mixture of TFA:DCM = 1:1 stirring for 1 h at r.t. then the solvent was removed in a rotary evaporator, washed with DCM (5 times), dried in high vacuum, and used as such in the next step without further purification.

Boc-Val-Val-O-(3-Br)-Bz (3). Boc-Val-OH (90.81 mg, 1.1 eq) was dissolved in DMF (15 mL) at 0 °C, stirring for 5 min, then EDC·HCl (80.51 mg, 1.1 eq) and HOBt (56.75 mg, 1.1 eq) were added. After 10 min, intermediate 2 (149.10 mg, 0.38 mmol) and DIPEA (0.2 mL, 3 eq) were added, stirring at 0 °C for 10 min., then at r.t. for 12 hs. After a standard work-up, the desired peptide was obtained in 68% yield, pure in TLC (DCM:AcOEt = 1:1; R_f = 0.2).

TFA.NH₂-Val-Val-O-(3-Br)-Bz (4). Intermediate 3 was deprotected following the same procedure reported for intermediate 2, and used as is without further purification.

Boc-D-Tyr-Val-Val-O-(3-Br)-Bz (5). Dipeptide 4 as a TFA salt was coupled with Boc-D-Tyr-OH (84.39 mg, 1.1 eq), following the procedure previously reported for peptide 3. The Boc-protected peptide was purified on silica gel column (mobile phase AcOEt:DCM = 1:1). The desired product was obtained with 39.7% yield. LRMS for C₃₁H₄₂BrN₃O₇: calcd m/z: 647.2; found: 670.1 [M + Na]⁺.

TFA·NH₂-D-Tyr-Val-Val-O-(3-Br)-Bz (6): Peptide 5 was treated with a TFA/DCM mixture following the procedure previously described, so as to give final peptide 6 as a TFA salt, the identity of which was confirmed through ¹H-NMR. ¹H-NMR (CDCl₃) δ: 7.45 (m, 2H, aromatics); 7.25–7.20 (m, 9H, aromatics + NH₃⁺); 6.86 (d, 2H, aromatics); 6.61 (dd, 2H, 2*NH_α); 5.17–4.98 (m, 3H, NH_α + CH₂ benzyl), 4.57 (m, 1H, CH_α Val); 4.35 (m, 1H, CH_α Tyr); 4.27 (m, 1H, CH_α Val), 2.93 (m, 2H, CH₂β Tyr); 2.13 (m, 1H, CH_β Val), 2.02 (m, 1H, CH_β Val); 0.94 (d, 6H, CH₃), 0.84 (d, 6H, CH₃).

TFA·NH₂-Trp-OBz (7). Boc-Trp-OBz was treated with a mixture of TFA:DCM = 1:1 at r.t. for 1 h and used as such for the next reaction.

Boc-Val-Trp-OBz (8). Boc-Val-OH (40.6 mg, 1.1 eq) was dissolved in DMF (7 mL) in an ice bath, stirring for 5 min. EDC·HCl (36.42 mg, 1.1 eq) and HOBt (25.68 mg, 1.1eq) were added; after 10 min, intermediate 7 (1.1 mg, 1 eq) and DIPEA (3 eq) were transferred into the reaction round bottom flask left at 0 °C for 10 min and at r.t. overnight. The desired product was obtained after a standard reaction work-up in 85% yield, pure in TLC (AcOEt:DCM = 1:9, Rf = 0.3).

TFA·NH₂-Val-Trp-OBz (9). The Boc-protecting group was removed from 8 following the same procedure adopted for 7.

Boc-D-Tyr-Val-Trp-OBz (10). The coupling reaction among intermediate 9 (66 mg, 0.13 mmol) and Boc-Tyr-OH (39.38 mg, 1.1 eq) was setup following the procedure previously described. The so obtained crude peptide was purified on silica gel column (mobile phase 1:1 AcOEt:DCM) affording the pure peptide in 19.93% yield (AcOEt:DCM =1:1; Rf = 0.3). The identity was confirmed by LRMS and ¹H-NMR. LRMS for C₃₇H₄₄N₄O₇: calcd m/z: 656.3; found m/z: 679.2 [M + Na]⁺. ¹H-NMR (CDCl₃) δ: 8.27 (s, 1H, NH indolic); 7.51 (d, 1H, Trp indolic); 7.32–7.07 (m, 6H, aromatics Trp + NH α Trp + NH α Val); 6.68 (d, 2H, Tyr aromatics); 6.48 (d, 2H, Tyr aromatics); 6.32 (d, 1H, Boc NH); 4.92 (s, 1H, CH₂ benzyl); 4.94–4.90 (m, 1H, CH α Tyr); 4.19–4.17 (m, 2H, CH α Trp, Val); 2.95–2.88 (m, 4H, CH β Tyr, Trp); 1.96 (m, 1H, CH β Val); 1.39 (s, 9H, 3*CH₃); 0.79–0.65 (dd, 6H, 2*CH₃ Val).

TFA·NH₂-D-Tyr-Val-Trp-OBz (11). Boc-D-Tyr-Val-Trp-OBz 10 was treated with a mixture of TFA/DCM = 1:1 at r.t. for 1 h. The so-obtained product as a TFA salt was purified on RP-HPLC, and the structure was confirmed with ¹H-NMR. ¹H-NMR (CDCl₃) δ: 10.96 (s, 1H, OH Tyr); 8.27 (s, 1H, NH indolic); 7.99 (s, 3H, NH₃⁺ Tyr); 7.51 (d, 1H, Trp indolic); 7.32–7.07 (m, 6H, aromatics Trp + NH α Trp + NH α Val); 6.68 (d, 2H, Tyr aromatics); 6.48 (d, 2H, Tyr aromatics); 4.92 (q, 1H, CH₂ benzyl); 4.94–4.90 (m, 1H, CH α Tyr); 4.19–4.17 (m, 2H, CH α Trp, Val); 2.95-.88(m,4H, H β Tyr, Trp); 1.96 (m, 1H, CH β Val); 0.79–0.65 (dd, 6H, 2*CH₃ Val).

In vivo Assays

Animals

In our experiments, we used CD-1 male mice (Charles River, Italy, Sant'Angelo Lodigiano, 25–30 g) maintained in colony, housed in cages (7 mice per cage) under

standard light/dark cycle (from 7:00 a.m. to 7:00 p.m.), temperature (21 ± 1 °C) and relative humidity ($60\% \pm 10\%$) for at least 1 week. Food and water were available ad libitum. The Service for Biotechnology and Animal Welfare of the Istituto Superiore di Sanità and the Italian Ministry of Health authorized the experimental protocol according to Legislative Decree 26/14.

Treatment Procedure

DMSO was purchased from Merck (Rome, Italy). Peptide solutions were freshly prepared using saline containing 0.9% NaCl and DMSO in the ratio DMSO/saline 1:5 v/v every experimental day. These solutions were injected at a volume of 10 μ L/mouse for intracerebroventricular (i.c.v.) administrations or at a volume of 20 μ L/mouse for subcutaneous (s.c.) administrations.

Surgery for Intracerebroventricular Injection

For i.c.v. injections, mice were lightly anesthetized with isoflurane, and an incision was made in the scalp, and the bregma was located. Injections were performed using a 10 μ L Hamilton microsyringe equipped with a 26-gauge needle, 2 mm caudal and 2 mm lateral from the bregma at a depth of 3 mm.

Tail Flick Test

The tail flick latency was obtained using a commercial unit (Ugo Basile, Gemonio, Italy), consisting of an infrared radiant light source (100 W, 15 V bulb) focused onto a photocell utilizing an aluminum parabolic mirror. During the trials, the mice were gently hand-restrained using leather gloves. Radiant heat was focused 3–4 cm from the tip of the tail, and the latency (s) of the tail withdrawal to the thermal stimulus was recorded. The measurement was interrupted if the latency exceeded the cut off time (15 s). The baseline latency was calculated as mean of three readings recorded before testing at intervals of 15 min and the time course of latency determined at 15, 30, 45, 60, 90, and 120 min after treatment. Data were expressed as the area under the curve of the maximum percentage effect (%MPE) = $(\text{post-drug latency} - \text{baseline latency}) / (\text{cut-off time} - \text{baseline latency}) \times 100$.

Formalin Test

In the formalin test, the injection of a dilute solution of formalin (1%, 20 μ L/paw) into the dorsal surface of the mouse hind paw evoked biphasic nociceptive behavioral responses, such as licking, biting the injected paw, or both, occurring from 0 to 10 min after formalin injection (the early phase) and a prolonged phase, occurring from 10 to 40 min (the late phase). Before the test, mice were individually placed in a Plexiglas observation cage (30 \times 14 \times 12 cm) for one hour, to acclimatize to the testing environment. The total time the animal spent licking or biting its paw during the early and late phase of formalin-induced nociception was recorded.

Data Analysis and Statistics

Experimental *in vivo* data were expressed as mean \pm s.e.m. Significant differences among the groups were evaluated with one-way ANOVA followed by Dunnett's multiple comparisons test. GraphPad Prism 6.03 software was used for all the analyses. Statistical significance was set at $p < 0.05$. The data and statistical analysis comply with the recommendations on experimental design and analysis in pharmacology.

In conclusion, KORs play a crucial role in the pathogenesis of various disorders affecting the central nervous system, such as depression, anxiety, and pain. The stimulation of KOR leads to rather complex effects that reflect the structural complexity of this class of G protein coupled receptors. *In silico* experiments play an important role in the early stages of drug discovery, allowing one to reduce the time and costs associated with the identification of new molecules. In this experimental project, we used the computational technique of virtual screening to identify molecular structures that could show affinity for the KOR through significant interactions. In this phase, the virtual library, consisting of ~6 million molecules, was submitted to the HTVS rapid docking method. Among the 33 selected molecules, the H-D-Tyr-Val-NH₂ dipeptide turned out to be of particular interest due to its structural requirements; therefore, it was considered for the next rational design step. In the drug design phase, we exploited knowledge about the KOR structure, designing tripeptides with higher docking score values than the JDTic crystallographic ligand and a more marked lipophilicity, with the aim of improving the pattern of hydrophobic interactions within the orthosteric receptor site. The most promising tripeptides were further analyzed through molecular dynamics simulations, which provided a more detailed picture of the evolution of tripeptide-KOR

complexes. The entire *in silico* process furnished the necessary data to identify and estimate the most suitable compounds for synthesis and pharmacological tests. The two tripeptides H-D-Tyr-Val-Val-O-(3-Br)-Bz and H-D-Tyr-Val-Trp-OBz contain Tyr as the first amino acid, which is essential for the interaction with the receptor, while leaving the stereochemistry of the initial dipeptide unchanged because it showed a greater affinity for KOR. The H-D-Tyr-Val-Val-O-(3-Br)-Bz structure was found to be the most stable within the receptor's active site and recorded the highest docking score; these results are probably due to improved hydrophobic interactions involving important amino acid residues, such as Ile294, Val118, and Tyr312. The HD-Tyr-Val-Trp-OBz tripeptide does not show significant values in MD simulation analyses; however, it exhibits favorable stabilization in the receptor pocket due to additional hydrophobic interactions with Tyr139, Ile290, and Trp287, as well as a docking value score higher than JD_{Tic}. This shows structural similarities with the endogenous opioid tetrapeptide EM-2 (H-Tyr-Pro-Trp-Phe-NH₂) selective on MOR. *In vivo* tests revealed their ability to induce an antinociceptive effect after i.c.v. and s.c. administrations in the tail flick and formalin tests, respectively. Among them, peptide 11 is active also in the second phase of the last test. This is somewhat in agreement with the ADME prediction, which indicates a possible inhibition of the drug-metabolizing cytochrome CYP3A4 and a low GIA absorption. However both of them show poor bioavailability, prompting us to further investigate their structural modifications with the aim of improving the pharmacokinetic properties and drug-likeness. Overall this experimental work allowed us to find interesting lead compounds for the next steps of structure optimization and pharmaceutical characterization.

References

1. Brownstein MJ. A brief History of opiates, opioid peptides, and opioid receptors. *Proc. Natl. Acad. Sci. USA*. 1993;90:5391–5393.
2. Williams JT, Ingram SL, Henderson G, et al. Regulation of μ -Opioid Receptors: Desensitization, Phosphorylation, Internalization, and Tolerance. *Pharmacol. Rev.* 2013;65:223–254.
3. Chavkin C, James IF, Goldstein A. Dynorphin is a specific endogenous ligand of the κ opioid receptor. *Science*. 1982;215:413–415.
4. Carlezon WA, Thome J, Olson VG, et al. Regulation of Cocaine Reward by CREB. *Science*. 1998;282:2272–2275.
5. Pfeiffer A, Brantl V, Herz A, Emrich HM. Psychotomimesis mediated by kappa opiate receptors. *Science*. 1986;233:774–776.
6. Goldstein A, Tachibana S, Lowney LI, et al. Dynorphin-(1-13), an extraordinary potent opioid peptide. *Proc. Natl. Acad. Sci. USA*. 1979;76:6666–6670.
7. Wu H, Wacker D, Mileni M, et al. Structure of the human kappa-opioid receptor in complex with JDTC. *Nature*. 2012;485:327–332.
8. Che T, Majumdar S, Zaidi SA, et al. Structure of the Nanobody-Stabilized Active State of the Kappa Opioid Receptor. *Cell*. 2018;172:55–67.
9. Bruchas MR, Roth BL. New Technologies for Elucidating Opioid Receptor Function. *Trends Pharmacol. Sci.* 2016;37:279–289.
10. Thomas JB, Atkinson RN, Rothman RB, et al. Identification of the first trans-(3R,4R)-dimethyl-4-(3-hydroxyphenyl)piperidine derivative to possess highly potent and selective opioid kappa receptor antagonist activity. *J. Med. Chem.* 2001;44:2687–2690.
11. Fredriksson R, Lagerstrom MC, Lundin LG, Schioth HB. The G-Protein-Coupled Receptors in the Human Genome Form Five Main Families. Phylogenetic Analysis, Paralogon Groups, and Fingerprints. *Mol. Pharmacol.* 2003;63:1256–1272.
12. Bruijnzeel AW. Kappa-Opioid receptor signaling and brain reward function. *Brain Res. Rev.* 2009;62:127–146.
13. Waldhoer M., Bartlett S.E., Whistler J.L. Opioid receptors. *Annu. Rev. Biochem.* 2004;73:953–990.
14. Urbano M, Guerrero M, Rosen H, Roberts E. Antagonists of the kappa opioid receptor. *Bioorg. Med. Chem. Lett.* 2014;24:2021–2032.
15. Martin WR, Eades CG, Thompson JA, et al. The effects of morphine- and nalorphine- like drugs in the nondependent and morphine-dependent chronic spinal dog. *J. Pharmacol. Exp. Ther.* 1976;197:517–532.
16. Meng ID, Johansen JP, Harasawa I, Fields HL. Kappa Opioids Inhibit Physiologically Identified Medullary Pain Modulating Neurons and Reduce Morphine Antinociception. *J. Neurophysiol.* 2005;93:1138–1144.
17. Kenakin T, Christopoulos A. Signalling bias in new drug discovery: Detection, quantification and therapeutic impact. *Nat Rev. Drug Discov.* 2013;12:205–216.

18. Wang S, Wacker D, Levit A, et al. D4 dopamine receptor high-resolution structures enable the discovery of selective agonists. *Science*. 2017;358:381–386.
19. Di Chiara G, Imperato A. Opposite effects of mu and kappa opiate agonists on dopamine release in the nucleus accumbens and in the dorsal caudate of freely moving rats. *J. Pharmacol. Exp. Ther.* 1988;244:1067–1080.
20. Narita M, Funada M, Suzuki T. Regulations of opioid dependence by opioid receptor types. *Pharmacol. Ther.* 2001;89:1–15.
21. Spanagel R, Herz A, Shippenberg TS. The Effects of opioid peptides on dopamine release in the nucleus accumbens: An *in vivo* microdialysis study. *J. Neurochem.* 1990;55:1734–1740.
22. Dortch-Carnes J, Potter DE. Bremazocine: A κ -opioid agonist with potent analgesic and other pharmacologic properties. *CNS Drug Rev.* 2005;11:195–212.
23. Land BB, Bruchas MR, Schattauer S, et al. Activation of the kappa opioid receptor in the dorsal raphe nucleus mediates the aversive effects of stress and reinstates drug seeking. *Proc. Natl. Acad. Sci. USA.* 2009;106:19168–19173.
24. Robles CF, McMackin MZ, Campi KL, et al. Effects of kappa opioid receptors on conditioned place aversion and social interaction in males and females. *Behav. Brain Res.* 2014;262:84–93.
25. Roth BL, Baner K, Westkaemper R, et al. Salvinorin A: A potent naturally occurring nonnitrogenous κ opioid selective agonist. *Proc. Natl. Acad. Sci. USA.* 2002;99:11934–11939.
26. Bruchas MR, Land BB, Chavkin C. The dynorphin/kappa opioid system as a modulator of stress-induced and pro-addictive behaviors. *Brain Res.* 2010;1314:44–55.
27. Bruchas MR, Macey TA, Lowe JD, Chavkin C. Kappa Opioid Receptor Activation of p38 MAPK Is GRK3- and Arrestin-dependent in Neurons and Astrocytes. *J. Biol. Chem.* 2006;281:18081–18089.
28. McLaughlin JP, Xu M, Mackie K, Chavkin C. Phosphorylation of a carboxyl-terminal serine within the kappa-opioid receptor produces desensitization and internalization. *J. Biol. Chem.* 2003;278:34631–34640.
29. Bruchas MR, Land BB, Aita M, et al. Stress-induced p38 mitogen-activated protein kinase activation mediates kappa opioid-dependent dysphoria. *J. Neurosci.* 2007;27:11614–11623.
30. El Rawas R, Amaral IM, Hofer A. Is p38 MAPK Associated to Drugs of Abuse-Induced Abnormal Behaviors? *Int. J. Mol. Sci.* 2020;21:4833.
31. Bruchas MR, Schindler AG, Shankar H, et al. Selective p38 α MAPK deletion in serotonergic neurons produces stress resilience in models of depression and addiction. *Neuron.* 2011;71:498–511.
32. Pradhan AA, Smith ML, Kieffer BL, Evans CJ. Ligand-directed signalling within the opioid receptor family. *Br. J. Pharmacol.* 2012;167:960–969.

33. Schattauer SS, Miyatake M, Shankar H, et al. Ligand directed signaling differences between rodent and human κ -opioid receptors. *J. Biol. Chem.* 2012;287:41595–41607.
34. Xu M, Bruchas MR, Ippolito DL, et al. Sciatic Nerve ligation-induced proliferation of spinal cord astrocytes is mediated by κ opioid activation of p38 mitogen-activated protein kinase. *J. Neurosci.* 2007;27:2570–2581.
35. White KL, Robinson JE, Zhu H, et al. The G protein-biased kappa-opioid receptor agonist RB-64 is analgesic with a unique spectrum of activities *in vivo*. *J. Pharmacol. Exp. Ther.* 2015;352:98–109.
36. White KL, Scopton AP, Rives ML, et al. Identification of novel functionally selective kappa-opioid receptor scaffolds. *Mol. Pharmacol.* 2014;85:83–90.
37. Yan F, Bikbulatov RV, Mocanu V, et al. Structure-based design, synthesis, and biochemical and pharmacological characterization of novel Salvinorin A analogues as active state probes of the κ -opioid receptor. *Biochemistry.* 2009;48:6898–6908.
38. Yongye AB, Pinilla C, Medina-Franco JL, et al. Integrating computational and mixture-based screening of combinatorial libraries. *J. Mol. Model.* 2011;17:1473–1482.
39. Lopez-Vallejo F, Giulianotti MA, Houghten RA, Medina-Franco JL. Expanding the medicinally relevant chemical space with compound libraries. *Drug Discov. Today.* 2012;17:718–726.
40. Poli G, Dimmito MP, Mollica A, et al. Discovery of novel μ -opioid receptor inverse agonist from a combinatorial library of tetrapeptides through structure-based virtual screening. *Molecules.* 2019;24:3872.
41. Torino D, Mollica A, Pinnen F, et al. Synthesis and evaluation of new endomorphin-2 analogues containing (Z)-alpha,beta-didehydrophenylalanine (Delta(Z)Phe) residues. *J. Med. Chem.* 2010;53:4550–4554.
42. Giordano C, Sansone A, Masi A, et al. Synthesis and activity of endomorphin-2 and morphiceptin analogues with proline surrogates in position 2. *Eur. J. Med. Chem.* 2010;45:4594–4600.
43. Vardy E, Robinson JE, Li C, et al. A new DREADD facilitates the multiplexed chemogenetic interrogation of behavior. *Neuron.* 2015;86:936–946.
44. Fenalti G, Giguere PM, Katritch V, et al. Molecular control of δ -opioid receptor signalling. *Nature.* 2014;506:191–196.
45. Fenalti G, Zatsopin NA, Betti C, et al. Structural basis for bifunctional peptide recognition at human δ -opioid receptor. *Nat. Struct. Mol. Biol.* 2015;22:265–268.
46. Stefanucci A, Pinnen F, Feliciani F, et al. Conformationally constrained histidines in the design of peptidomimetics: Strategies for the χ -Space control. *Int. J. Mol. Sci.* 2011;12:2853–2890.
47. Wacker D, Wang S, McCorvy JD, et al. Crystal structure of an LSD-bound human serotonin receptor. *Cell.* 2017;168:377–389.

48. Feliciani F, Pinnen F, Stefanucci A, et al. Structure-activity relationships of biphalin analogs and their biological evaluation on opioid receptors. *Mini Rev Med Chem.* 2013;13:11–33.
49. Johnson TW, Gallego RA, Edwards MP. Lipophilic efficiency as an important metric in drug design. *J. Med. Chem.* 2018;61:6401–6420.
50. Saha S, Das R, Divyanshi D, et al. Ratio of hydrophobic-hydrophilic and positive-negative residues at lipid-water-interface influences surface expression and channel-gating of TRPV1. *BioRxiv.* 2020;4:272484.
51. Ferreira de Freitas R, Schapira M. A systematic analysis of atomic protein–ligand interactions in the PDB. *Med. Chem. Commun.* 2017;8:1970–1981.
52. Daina A, Michielin O, Zoete V. SwissADME: A free web tool to evaluate pharmacokinetics, drug-likeness and medicinal chemistry friendliness of small molecules. *Sci. Rep.* 2017;7:42717.
53. Wolking S, Schaeffeler E, Lerche H, et al. Impact of genetic polymorphisms of ABCB1 (MDR1, P-glycoprotein) on drug disposition and potential clinical implications: Update of the literature. *Clin. Pharmacokinet.* 2015;54:709–735.
54. Guengerich FP. Cytochrome P450 and chemical toxicology. *Chem. Res. Toxicol.* 2008;21:70–83.
55. Mbarik M, Poirier SJ, Doiron J, et al. Phenolic acid phenylesters and their corresponding ketones: Inhibition of 5-lipoxygenases and stability in human blood and HepaRG cells. *Pharmacol. Res. Pers.* 2019;7:e00524.
56. Veber DF, Johnson SR, Cheng HY, et al. Molecular properties that influence the oral bioavailability of drug candidates. *J. Med. Chem.* 2002;45:2615–2623.
57. Irwin JJ, Shoichet BK. ZINC—a free database of commercially available compounds for virtual screening. *J. Chem. Inf. Model.* 2005;45:177–182.
58. Schrödinger Release 2017-1: LigPrep. Schrödinger, LLC; New York, NY, USA: 2017.
59. Schrödinger Release 2017-1: Maestro. Schrödinger, LLC; New York, NY, USA: 2017.
60. Schrödinger Release 2017-1: Epik. Schrödinger, LLC; New York, NY, USA: 2017.
61. Schrödinger Release 2017-1: Protein Preparation Wizard. Schrödinger, LLC; New York, NY, USA: 2017. Epik.
62. Impact, Schrödinger, LLC, New York, NY. Schrödinger, LLC; New York, NY, USA: 2017. Prime.
63. Olsson MHM, Søndergaard CR, Rostkowski M, Jensen J.H. PROPKA3: Consistent treatment of internal and surface residues in empirical pKa predictions. *J. Chem. Theory Comput.* 2011;7:525–537.
64. Harder E, Damm W, Maple J, et al. OPLS3: A Force Field Providing Broad Coverage of Drug-like Small Molecules and Proteins. *J. Chem. Theory Comput.* 2016;12:281–296.
65. Schrödinger Release 2017-1: Glide. Schrödinger, LLC; New York, NY, USA: 2017.

66. Balboni G, Salvadori S, Guerrini R, et al. Opioid pseudopeptides containing heteroaromatic or heteroaliphatic nuclei. *Peptides*. 2000;21:1663–1671.
67. Zheng Z, Huang XP, Mangano TJ, et al. Structure-based discovery of new antagonist and biased agonist chemotypes for the kappa opioid receptor. *J. Med. Chem.* 2017;60:3070–3081.
68. Wand GS, Ney RL, Baylin S, et al. Characterization of a peptide alpha-amidation activity in human plasma and tissues. *Metabolism*. 1985;34:1044–1052.
69. Schrödinger Release 2017-1: Desmond Molecular Dynamics System, D.E. Shaw Research, New York, NY, 2017. Maestro-Desmond Interoperability Tools. Schrödinger, LLC; New York, NY, USA: 2017.
70. Kräutler V, Van Gunsteren WF, Hünenberger PH. A fast SHAKE algorithm to solve distance constraint equations for small molecules in molecular dynamics simulations. *J. Comput. Chem.* 2001;22:501–508.
71. Petersen HG. Accuracy and efficiency of the particle mesh Ewald method. *J. Chem. Phys.* 1995;103:3668–3679. Mollica A., Costante R., Stefanucci A., Pinnen F., Lucente G., Fidanza S., Pieretti S. Antinociceptive profile of potent opioid peptide AM94, a fluorinated analogue of biphalin with non-hydrazine linker. *J. Pept. Sci.* 2013;19:233–239.
72. Mollica A, Carotenuto A, Novellino E, et al. Novel Cyclic Biphalin Analogue with Improved Antinociceptive Properties. *ACS Med. Chem. Lett.* 2014;5:1032–1036.

CHAPTER 6: Discovery of Orexant and Anorexant Agents With Indazole Scaffold Endowed With Peripheral Antiedema Activity

Marilisa P Dimmito¹, Azzurra Stefanucci¹, Stefano Pieretti², Paola Minosi², Szabolcs Dvorácskó³, Csaba Tömböly³, Gokhan Zengin⁴, Adriano Mollica¹

¹ Department of Pharmacy, University of Chieti-Pescara "G. d'Annunzio", 66100 Chieti, Italy.

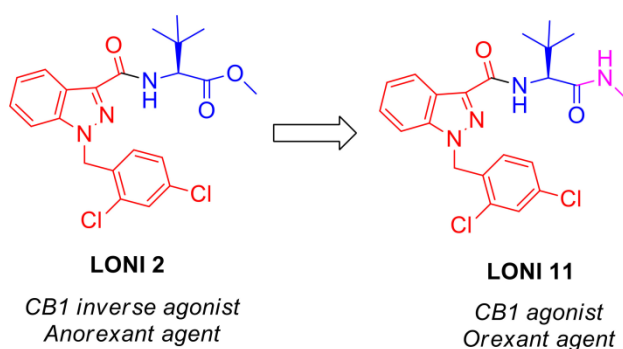
² National Center for Drug Research and Evaluation, Italian National Institute of Health, 00161 Rome, Italy.

³ Institute of Biochemistry, Biological Research Centre of the Hungarian Academy of Sciences, Temesvári krt. 62, 6726 Szeged, Hungary.

⁴ Department of Biology, Science Faculty, Selcuk University, 42005 Konya, Turkey.

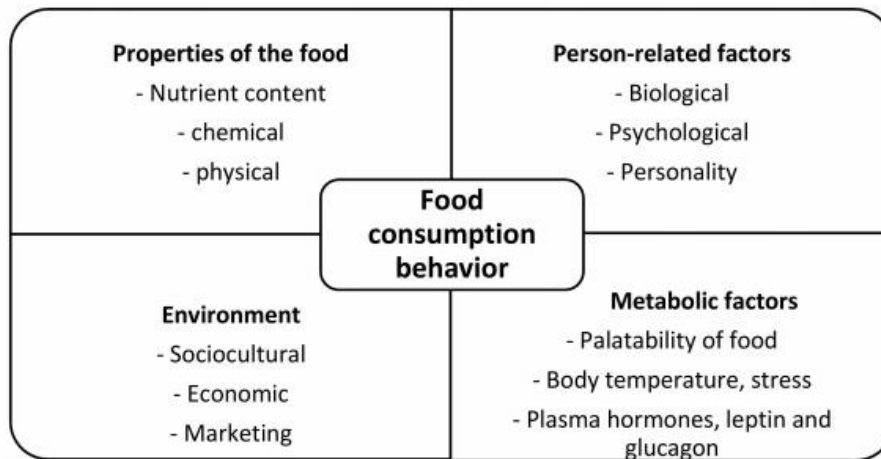
Abstract

The endocannabinoid system represents an integrated neuronal network involved in the control of several organisms' functions, such as feeding behavior. A series of hybrids of 5-(4-chlorophenyl)-1-(2,4-dichloro-phenyl)-4-methyl-*N*-(piperidin-1-yl)-1*H*-pyrazole-3-carboxamide (mimonabant), a well-known inverse agonist of the type-1 cannabinoid receptor (CB1), once used as an antiobesity drug, and the *N*-(2*S*)-substitutes of 1-[(4-fluorophenyl)methyl]indazole-3-carboxamide with 1-amino-3-methyl-1-oxobutane (AB-Fubinaca), 1-amino-3,3-dimethyl-1-oxobutane (ADB-Fubinaca), and 3-methylbutanoate (AMB-Fubinaca), endowed with potent agonistic activity towards cannabinoid receptors CB1 and CB2 were in solution as *C*-terminal amides, acids, methyl esters and *N*-methyl amides. These compounds have been studied by binding assays to cannabinoid receptors and by functional receptor assays, using rat brain membranes *in vitro*. The most active among them as an agonist, (S)-1-(2,4-dichlorobenzyl)-*N*-(3,3-dimethyl-1-(methylamino)-1-oxobutan-2-yl)-1*H*-indazole-3-carboxamide (LONI11), and an antagonist, (S)-2-(1-(2,4-dichlorobenzyl)-1*H*-indazole-3-carboxamido)-3-methylbutanoic acid (LONI4), were tested *in vivo* in mic, to evaluate their ability to stimulate or suppress feeding behavior after intraperitoneal (i.p.) administration. For a LONI11 formalin test and a tail flick test after an administration by the subcutaneous (s.c.) and intracerebroventricular (i.c.v.) routes, respectively, were also carried out *in vivo* in mice to investigate the antinociceptive property at the central and peripheral levels. We observed a significant orexant effect for LONI11 and an intense anorexant effect for (S)-methyl 2-(1-(2,4-dichlorobenzyl)-1*H*-indazole-3-carboxamido)-3,3-dimethylbutanoate (LONI2) and LONI4. In zymosan-induced edema and hyperalgesia, LONI11 reduced the percent of paw volume increase and paw latency after s.c. administration, also suggesting a possible peripheral anti-inflammatory activity.



Introduction

Metabolic syndrome is the result of a group of multifactorial conditions, characterized by the loss of balance between energy income and caloric needs. An efficacious equilibrium between orexigenic and anorexigenic signals ensures a mild feeding behavior, whereas a delicate and growing interference in neurochemistry is enough to provoke its alteration. Motivational feeding behavior is the base of human beings' underlying food intake to obtain energy from food. This is strongly associated with the concept of "food grabbing," which is influenced by parents' food-choice strategies, behavioral contexts, and dietary quality. Metabolic and cultural factors involved in the regulation of food consumption and food intake are reported below (Scheme 1).



Scheme 1. Metabolic and cultural factors involved in the regulation of food intake.

Type 1 endocannabinoid receptors and endogenous cannabinoids are both involved in the management of appetite stimuli and food intake in the central region of the hypothalamus [1]. In the autonomic nervous system, the hypothalamus is deputed to the control of metabolism's functions, fat storage and weight. The hypothalamus constantly receives feedback signals depending on metabolic requests in terms of energy needs to balance energy demand in order to regulate the food intake [2]. This process is modulated by two inputs: (i) The short and medium-term hunger signals of orexigenic input and satiety as anorexygenic inputs modify feeding behavior, and (ii) based on adiposity, the amount of the energy stored as fats produces a neurohormone called leptin [3]. The endogenous cannabinoid system (ECS) has been related to the

modulation of the reward mechanism, which is a well-defined neural network deputed to motivation, desire, craving, learning, and positive emotions associated with pleasure, such as joy in specific mesencephalic zones mostly related to reinforcing mechanisms. In rats, orexigenic stimuli have been observed after the administration of endogenous cannabinoids in the hypothalamus, which indicates the role of the ECS located in the limbic forebrain zone in the activation of the motivational feeding mechanism [4]. According to some other works, endocannabinoids, namely anandamide and arachidonic ester of glycerol (2-AG), stimulate the type-1 cannabinoid receptor (CB1) and simultaneously induce the reduction of energy consumption, activating food grabbing behavior. In laboratory animals, cannabinoid agonists have demonstrated orexigenic effects; the administration of Δ^9 -tetrahydrocannabinol (THC) or anandamide into the hypothalamus also induced food intake [5]. Indeed, CB1^{-/-} mice or animals previously injected with CB1 antagonists have been found to assume an anorexigenic behavior [6]; when administered to drug naive animals, CB1 antagonists such as 5-(4-chlorophenyl)-1-(2,4-dichloro-phenyl)-4-methyl-*N*-(piperidin-1-yl)-1*H*-pyrazole-3-carboxamide (rimonabant) are able to evoke anorexigenic effects in rodents [7]. Furthermore, the ECS might be involved in the secretion of neuropeptides which play a pivotal role in the feeding mechanism at the hypothalamus, such as dynorphin A, endomorphin-2, met-enkephalin and leu-enkephalin. These endogenous peptides increase food grabbing behavior through an interaction with opioid receptors. Through motivational and rewarding mechanisms, the opioid system may activate feeding intake alone or by cross-talking with other systems present at the striatum level [8,9]. Other interactions have been found between the endocannabinoid and the orexin systems. Sub-effective doses of rimonabant are able to prevent the orexigenic effect of orexin A by increasing food intake in starving conditions in the short term. The physical dimerization between CB1 and orexin A receptors could be due to their co-expression in several areas of the hypothalamus, as observed in experiments with co-transfected cells [10,11]. Recently, some bioactive substances such as sibutramine and rimonabant have been used to reduce body weight due to their modulation of several neuroendocrine mediators, despite their serious side effects [12]. Sibutramine is one of the most frequently hidden drug ingredients in products claimed to be food supplements. The Food and Drug Administration (FDA) has recently highlighted an adulteration of a supplement-like weight loss, which was marketed in the United States by Abbott Laboratories as a prescription weight loss aid under the brand name Meridia [13]. The

drug was retrieved from the market due to increased blood pressure and heart rate, which are risk factors in patients with coronary heart disease (CHD), arrhythmia and stroke. An early clinical trial was done on the CB1 antagonist rimonabant, during which the patients were treated with 20 mg of this drug. The results showed an amelioration of metabolic and cardiac parameters related to type 2 diabetes and heart diseases [14], a decrease of triglyceride, and an increase in high-density lipoprotein (HDL) cholesterol levels. Other effects have been also observed, including a reduction of waist circumference and body fat, as well as an improvement of tolerance to glucose and blood pressure [15]. However, in 2008, Sanofi-Aventis and Pfizer suspended research activity on rimonabant and its related chemical analogues with similar pharmacological profiles due to their serious side effects on the central nervous system [16]. Thus, the development of CB1 antagonists that act selectively in peripheral tissues represents an important task to overcome these drawbacks in the treatment of obesity or related diseases (Figure 1) [17].

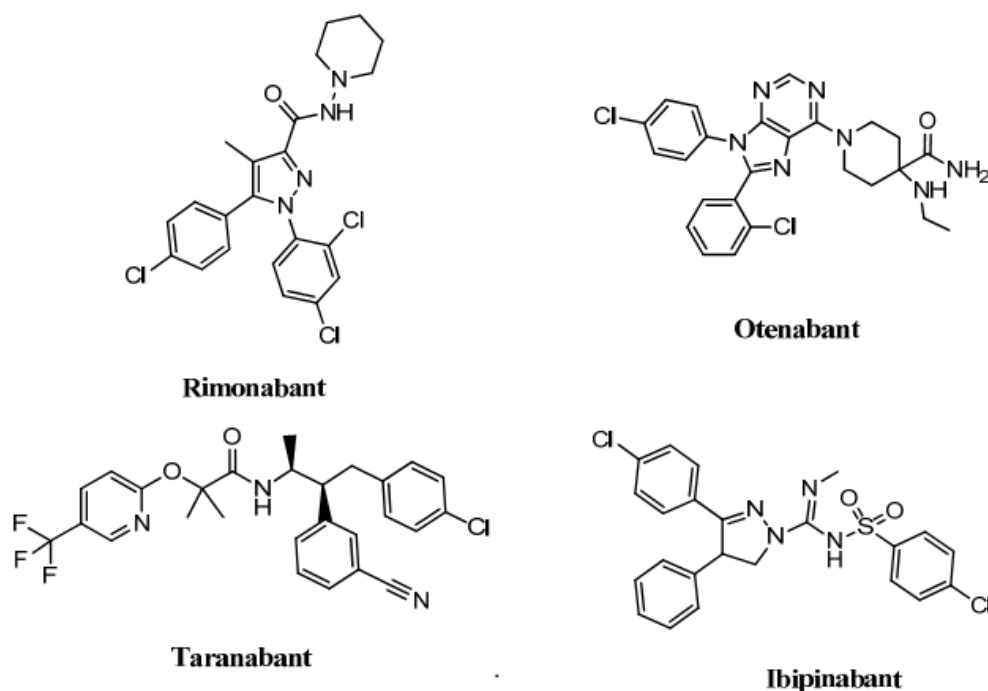
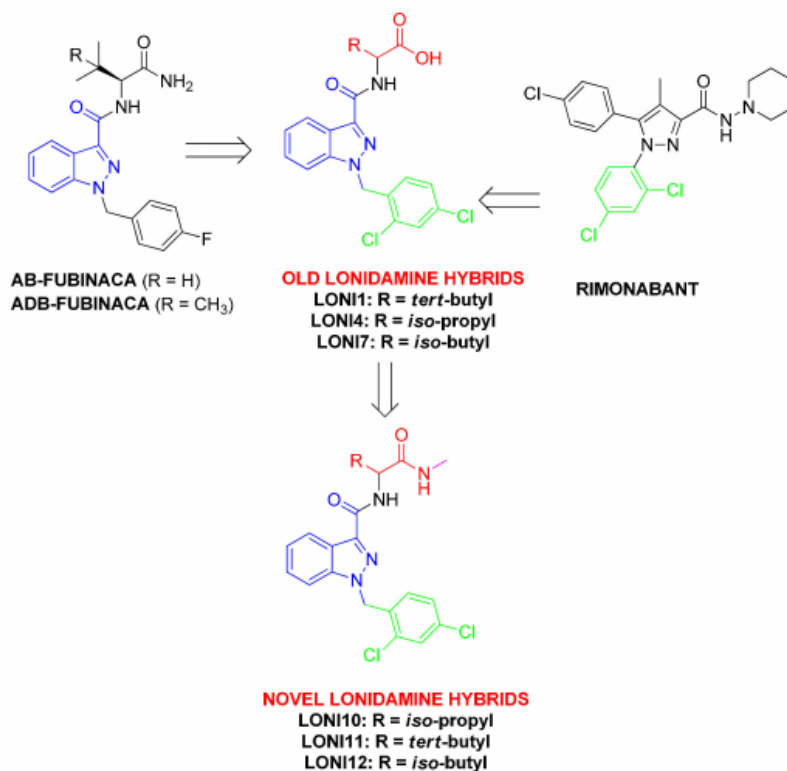


Figure 1. The type-1 cannabinoid receptor (CB1) antagonists: Rimonabant, taranabant, otenabant and ibipinabant.

Taranabant and otenabant have different structures than rimonabant, but they share similar side effects, which resulted in the early end of their clinical studies [17,18]. In this context, the concept of “biased signaling” provides an exciting new direction for developing therapeutics with less adverse effects. The CB1 and CB2 receptors interact

with several pathways by different signaling cascades; thus, they possibly bias other effects by the fine-tuning of the receptors conformations, allowing them to address specific symptoms or pathologies without side effects [19,20]. Given their importance as potential therapeutics for overweight and other dysmetabolisms, psychiatric symptoms, liver dysfunction, and addiction to nicotine [21,22,23,24,25,26,27], our research group developed hybrids of rimonabant and the *N*-(2*S*)-substitutes of 1-[(4-fluorophenyl)methyl]indazole-3-carboxamide with 1-amino-3-methyl-1-oxobutane (AB-Fubinaca), 1-amino-3,3-dimethyl-1-oxobutane (ADB-Fubinaca), and 3-methylbutanoate (AMB-Fubinaca), endowed with potent agonistic activity towards cannabinoid receptors CB1 and CB2 (Scheme 2). Synthetic cannabinoids (SCs) AB-FUBINACA and ADB-FUBINACA (Scheme 2) have been identified in illicit drugs in the Japanese market. The administration of Fubinaca family compounds is associated with serious side effects, neurotoxicity and cardiotoxicity. They exert potent psychotropic adverse effects, including delirium and drug seizures, which have reportedly led, on some occasions, to hospitalization and death. Coronary arterial thrombosis in combination with SC use was ascertained as one of the major causes of death [28,29,30]. Numerous cases of fatal intoxication have led to the withdrawal of these products from the market in the US, Germany and China [31,32].



Scheme 2. Chemical modifications applied to lonidamine structure in the design of novel compounds LONI10-12.

Our novel compounds have high CB1 receptor affinity and selectivity with different biological activity depending on the C-terminal substitution and amino acid residues; given their close structural similarity with rimonabant, we hypothesized a similar biological activity *in vivo* in the feeding behavior modulation. It was found that compounds containing the C-terminal methyl ester of *tert*-Leu (S)-methyl 2-(1-(2,4-dichlorobenzyl)-1H-indazole-3-carboxamido)-3,3-dimethylbutanoate (LONI2) and Val as the free acid ((S)-2-(1-(2,4-dichlorobenzyl)-1H-indazole-3-carboxamido)-3-methylbutanoic acid (LONI4)) are able to decrease food intake at 10 mg/Kg, acting as inverse agonists/antagonists at the CB1. Thus, it has been supposed that the C-terminal methyl ester group could be easily cleavable *in vivo* to give the free C-terminal acid derivative.

With the aim to stabilize the agonist activity of this series of compounds [33], we designed N-methyl amide derivatives of 1-(2,4-dichlorobenzyl)-1H-indazole-3-carboxylic acid (lonidamine) joined to Leu, Val and *tert*-Leu amino acids. In this study, we were able to demonstrate that compound (S)-1-(2,4-dichlorobenzyl)-N-(3,3-dimethyl-1-(methylamino)-1-oxobutan-2-yl)-1H-indazole-3-carboxamide (LONI11) is a

full agonist of the CB1 receptor endowed with an orexant effect, while the previously published C-terminal methyl ester and the compounds of lonidamine with *tert*-Leu (LONI1) and Val (LONI4) as free acids showed an anorexic profile *in vivo*. Furthermore, several antinociception models were also studied to characterize the analgesic potential of this novel compound (LONI11).

Materials and Methods

Chemistry

Lonidamine, solvents, reagents and amino acids Boc-*tert*-Leu-OH, Boc-Val-OH, and Boc-Leu-OH, are commercially available and were acquired from Sigma-Aldrich (Milano, Italy). The intermediate compounds LONI1-4,7 were synthesized, as previously published by Stefanucci et al. [33]. The structures of the intermediates and the final compounds were confirmed by ¹H-NMR and ¹³C-NMR spectra recorded on a 300 MHz Varian Inova spectrometer (Varian Inc., Palo Alto, CA). Chemical shifts were reported in parts per million (δ) downfield from the internal standard tetramethylsilane (Me₄Si). The purity of each final product was established by analytical reverse phase-high performance liquid chromatography (RP-HPLC) (C18-bonded 4.6 \times 150 mm) at a flow rate of 1 mL/min by using (as an eluent) a gradient of H₂O/ACN 0.1% TFA ranging from 10% ACN to 90% ACN for 30 min; it was found to be >95% (see Supplementary Materials). UV detection at 254 nm was chosen for analytical HPLC. Mass spectra were performed on an LCQ (Finnigan–Mat) ion trap mass spectrometer (San Jose, CA, USA) equipped with an electrospray ionization (Supplementary Materials) source. The capillary temperature was set at 300 °C, and the spray voltage was set at 3.5 kV. The fluid was nebulized using nitrogen as both the sheath gas and the auxiliary gas [34,35,36].

General Procedure for the N-Methyl Amide Formation

HOBt anhydrous (1.1 eq.) in DMF (3 mL), EDC·HCl (1.1 eq.) and NMM (1 eq.) were added to a stirred solution of lonidamine-amino acid compound (200 mg) at 0 °C; this was followed by the addition of a solution of methylamine 40% in water (2 eq.) and NMM (2 eq.) in DMF (3 mL). After 10 min at 0 °C, the reaction was stirred at room temperature (r.t.) overnight. Later, the reaction mixture was evaporated to dryness, and

the residue taken up in ethyl acetate (EtOAc). The organic phase was washed with 5% citric acid, NaHCO₃ saturated solution (s.s.) and NaCl s.s., dried and evaporated in a high vacuum. The crude compound was triturated in Et₂O two times to give the desired white solid product. The characterization of the final LONI10-12 compound is reported in the Supplementary Materials.

(S)-2-(1-(2,4-dichlorobenzyl)-1H-indazole-3-carboxamido)-3,3-dimethylbutanoic acid (LONI1). Boc-*tert*-Leu-OH was coupled to lonidamine according to Stefanucci et al. [33].

(S)-methyl-2-(1-(2,4-dichlorobenzyl)-1H-indazole-3-carboxamido)-3,3-dimethylbutanoate (LONI2). Boc-*tert*-Leu-OH was transformed in its methyl ester derivative and coupled to lonidamine according to Stefanucci et al. [33].

(S)-*N*-(1-amino-3,3-dimethyl-1-oxobutan-2-yl)-1-(2,4-dichlorobenzyl)-1H-indazole-3-carboxamide (LONI3). Boc-*L-tert*-Leu-OH was converted into the amide derivative and coupled to lonidamine according to Stefanucci et al. [33].

(S)-2-(1-(2,4-dichlorobenzyl)-1H-indazole-3-carboxamido)-3-methylbutanoic acid (LONI4). Boc-Val-OH was coupled to lonidamine according to Stefanucci et al. [33].

(S)-1-(2,4-dichlorobenzyl)-*N*-(3-methyl-1-(methylamino)-1-oxobutan-2-yl)-1H-indazole-3-carboxamide (LONI10). The LONI4 compound was transformed in the *N*-methyl amide derivative LONI 10 following the general procedure. The desired compound was obtained in a 96% yield after reaction work up.

(S)-1-(2,4-dichlorobenzyl)-*N*-(3,3-dimethyl-1-(methylamino)-1-oxobutan-2-yl)-1H-indazole-3-carboxamide (LONI11). The LONI1 compound was transformed in the *N*-methyl amide derivative LONI 11 following the general procedure. The desired compound was obtained in a 97% yield after reaction work up.

(S)-1-(2,4-dichlorobenzyl)-*N*-(4-methyl-1-(methylamino)-1-oxopentan-2-yl)-1H-indazole-3-carboxamide (LONI12). The LONI7 compound was transformed in the *N*-methyl amide derivative LONI12 following the general procedure. The desired compound was obtained in a quantitative yield after reaction work up.

In vitro Biological Assays

Preparation of Brain Membrane Homogenates

Wistar rats were locally bred and handled according to the EU Directive 2010/63/EU and to the Regulations on Animal Protection (40/2013. (II. 14.) Korm. r.) of Hungary. Crude membrane fractions were prepared from the brain. Brains were quickly removed from the euthanized rats and directly put in an ice-cold 50 mM Tris–HCl buffer (pH 7.4). The collected tissue was then homogenized in 30 volumes (v/w) of an ice-cold buffer with a Braun Teflon-glass homogenizer at the highest rpm. The homogenate was centrifuged at 20,000× *g* for 25 min, and the resulting pellet was suspended in the same volume of a cold buffer followed by incubation at 37 °C for 30 min to remove endogenous ligands. Centrifugation was then repeated. The final pellets were taken up in five volumes of a 50 mM Tris–HCl (pH 7.4) buffer containing 0.32 M sucrose and stored at –80 °C. Prior to the experiment, aliquots were thawed and centrifuged at 20,000× *g* for 25 min and then they were resuspended in 50 mM Tris–HCl (pH 7.4), homogenized with a Douncer, followed by the determination of the protein concentration by the method of Bradford. The membrane suspensions were immediately used either in radioligand binding experiments or in [³⁵S]GTPγS functional assays.

Radioligand Competition Binding Assay

Binding experiments were performed at 30 °C for 60 min in a 50 mM Tris–HCl binding buffer (pH 7.4) containing 2.5 mM of EGTA, 5 mM of MgCl₂ and 0.5 mg/mL of fatty acid-free BSA in plastic tubes in a total assay volume of 1 mL that contained 0.3–0.5 mg/mL of a membrane protein [33,37]. Competition binding experiments were carried out by incubating rat brain membranes with 5 nM of [³H]WIN55212-2 (*K*_d: 10.1 nM) in the presence of increasing concentrations (10⁻¹¹–10⁻⁵ M) of various competing unlabeled ligands. Non-specific binding was determined in the presence of 10 μM of WIN 55212-2. The incubation was terminated by diluting the samples with an ice-cold wash buffer (50 mM of Tris–HCl, 2.5 mM of EGTA, 5 mM of MgCl₂, 0.5% fatty acid free BSA, pH 7.4), followed by repeated washing and rapid filtration through Whatman GF/B glass fiber filters (Whatman Ltd., Maidstone, UK) presoaked with 0.1% polyethyleneimine (30 min before the filtration). Filtration was performed with a 24-well Brandel Cell Harvester (Gaithersburg, MD, USA). Filters were air-dried and immersed into Ultima Gold MV scintillation cocktail, and then radioactivity was

measured with a TRI-CARB 2100TR liquid scintillation analyzer (Packard, Perkin Elmer, Waltham, MA, USA).

Ligand Stimulated [³⁵S]GTP γ S Binding Assay

Rat brain membranes (30 μ g protein/tube), prepared as described above, were incubated with 0.05 nM of [³⁵S]GTP γ S (PerkinElmer) and 10^{-10} – 10^{-5} M unlabeled ligands in the presence of 30 μ M of GDP, 100 mM of NaCl, 3 mM of MgCl₂ and 1 mM of EGTA in a 50 mM Tris–HCl buffer (pH 7.4) for 60 min at 30 °C. Basal [³⁵S]GTP γ S binding was measured in the absence of ligands and set as 100%. Nonspecific binding was determined by the addition of 10 μ M unlabeled GTP γ S and subtracted from total binding. Incubation, filtration and radioactivity measurements of the samples were carried out as described above.

Data Analysis

The results of the competition binding studies are reported as means \pm S.E.M. of at least three independent experiments each performed in duplicate. In competition binding studies, the inhibitory constants (K_i) were calculated from the inflection points of the displacement curves using non-linear least-square curve fitting and the Cheng–Prusoff equation, $K_i = EC_{50}/(1 + [\text{ligand}]/K_d)$.

In [³⁵S]GTP γ S binding studies, data were expressed as the percentage stimulation of the specific [³⁵S]GTP γ S binding over the basal activity and are given as means \pm S.E.M. Each experiment was performed in triplicate and analyzed with sigmoid dose–response curve fitting to obtain potency (EC_{50}) and efficacy (E_{max}) values. All data and curves were analyzed by GraphPad Prism 5.0 (San Diego, CA, USA).

In vivo Biological Assays

Animals

The international and national law and policies approved by Italian Ministry of Health were used to comply with all animal care and experimental procedures. Animal studies were advised in compliance with the ARRIVE guidelines and with the recommendations made by EU Directive 2010/63/EU for animal experiments and the Basel declaration including the 3Rs concept [38,39]. CD-1 male mice (10–14 weeks of age, 25–30 g of weight) were bought from Charles River (Milan, Italy). Shortly after

their arrival and for at least one week, they were kept in an animal care facility under controlled standard conditions of temperature (21 ± 1 °C), light (from 7:00 AM to 7:00 PM), and relative humidity ($60 \pm 10\%$). Access to drinking water and food was assured. All procedures were performed to decrease the number of animals used ($n = 6$ per group) and their distress.

Feeding Test

The test was carried out as previously described [40]. At 24 h before the start of a feeding test, all food was removed from the home cages of mice to be tested. The next day and at least 1 h before the feeding test began, the mice were transported to the laboratory. On test days, the animals were placed in the home cages for 30 min of drug assimilation, during which food was not available. Then compounds were intraperitoneally administered (10 mg/kg). Mice were transferred into transparent and individual plastic cages with thick white paper lining the bottom and access to a pre-measured amount of their regular lab chow (2 gr) for the 1-h test. At the end of 1 h, mice were repositioned into their home cage. The amount of food left in the trial cage, including crumbs, was measured, and the amount consumed was calculated. Feeding trials normally happened on Tuesdays and Fridays between 12:00 and 14:00 h.

Tail Flick Test

The tail flick test was used to determinate antinociceptive responses [41]. Tail flick latency (Ugo Basile, Varese, Italy) consists of an infrared radiant light source (100 W, 15 V bulb) targeted on a photocell utilizing an aluminum parabolic mirror. During the trials, the mice were gently hand restrained with a glove. Radiant heat was targeted 5–6 cm from the tip of the tail, and the latency (s) of the tail withdrawal recorded. The measurement was disconnected if the latency crossed the cutoff time. A cutoff time of 15 s was imposed, and data were expressed as time course of the percentage of maximum effect (% MPE) = (post drug latency/baseline latency)/(cutoff time baseline latency) \times 100. In all experiments, the baseline was calculated as the mean of three readings recorded before testing at intervals of 10 min, and the time course of latency was determined 10–120 min after compound treatment. Compounds were freshly diluted in saline 0.1% v/v DMSO and were injected at 10 μ g/10 μ L for intracerebroventricular (i.c.v.) administrations, as previously reported [42,43].

Formalin Test

The method utilized was comparable to the one previously described by Pieretti et al. [44]. Mice were located to adapt into the transparent cages individually (30 × 14 × 12 cm) for at least an hour before testing. They were injected with 20 µL of a 1% solution of formalin in saline. Then, the compounds were administered subcutaneously in the dorsal surface of the right hind paw of the mouse using a microsyringe with a 27-gauge needle for 15 min before. Compounds were prepared by freshly diluting saline containing 0.9% NaCl in the ratio DMSO:saline 1:3 (v/v). Then, these solutions were injected for subcutaneous (s.c.) administrations in doses of 30–100 µg/20 µL. The total time the animal spent licking or biting its paw was calculated.

Edema Induced by Zymosan

In this test, 100 µg of the compounds were administered subcutaneously in a volume of 20 µL in the dorsal surface of mice hind paw; this was done 15 min before a subcutaneous injection (20 µL/paw) of zymosan A (2.5% w/v in saline) into the same paw. Then, paw edema was calculated as formerly described [45]. The percentage difference between the paw volume at each time point and the basal paw volume was used as an index of the increase in paw volume. Paw volume was quantified using a hydroplethysmometer modified for small volumes (Ugo Basile, Varese, Italy) three times before the injections and at 1, 2, 3, 4 and 24 h thereafter.

Zymosan-Induced Hyperalgesia

The compounds (100 µg) were administered subcutaneously in a volume of 20 µL in the dorsal surface of mice hind paw; this was done 15 min before a subcutaneous injection (20 µL/paw) of zymosan A (2.5% w/v in saline) into the same paw before the measurement of hyperalgesia [45]. The sensitivity to a noxious heat stimulus was measured by the plantar test (Ugo Basile, Italy), in order to evaluate thermal hyperalgesia after the zymosan-induced inflammation of the mouse hind paw. Mice were allocated in clear plastic boxes with a glass floor and acclimatized for at least 1 h in a temperature-controlled (21 °C) experimental room for three consecutive days prior to testing. Furthermore, on the test day, the animals were acclimatized to the experimental room 1 h before paw withdrawal latency (PWL) was calculated. Using a timer and in term of seconds, the paw withdrawal latency was measured automatically

after placing the mouse footpad in contact with a radiant heat source. A timer initiated automatically when the heat source was activated, and a photocell stopped the timer when the mouse withdrew its hind paw. An intensity of 30 and a cut-off time of 15 s were used for the heat source on the plantar apparatus to avoid tissue damage. Animals were first tested to define their baseline PWL in terms of seconds against 1, 2, 3, 4, 5 and 24 h after zymosan A injection.

Data Analysis and Statistics

The mean \pm S.E.M. was used to explain the results obtained. Statistically significant differences between groups were measured with an analysis of variance (ANOVA) followed by Tukey's post-hoc comparisons or the Mann-Whitney test when the comparison was restricted to two groups. GraphPad Prism 6.0 software (San Diego, CA, USA) was used to analyze the data. Data were considered statistically significant when a value of $p < 0.05$ was performed. The data and statistical analyses respected the recommendations on experimental design and analysis [46].

In silico Experiments

Receptor Preparation

The crystal structure of the human CB1 receptor co-crystallized with an MDMB-Fubinaca agonist was downloaded from the RSCB database (pdb id: 6N4B) [47]. The raw file was prepared for the docking experiment by the PrepWizard module of Maestro 10.2 [48]. Briefly, the missing chains were added automatically by Prime [49], and the protonation state was calculated by PropKa at pH = 7.4 [48]. Finally the receptor-ligand complex was minimized by OPLS-3 force field following a well-established protocol reported by our research group [42,50].

Docking Grid Generation

The docking grid was generated by the Glide module of Maestro [51]. The grid was centered on the MDMB-Fubinaca ligand present in the crystal structure and extended to a space of $20 \times 20 \times 20$ Angstrom. The generated grid was used for the docking experiments.

Self-Docking and Validation Procedure

In order to validate the docking procedure, a self-docking experiment was conducted. The crystallographic ligand MDMB-Fubinaca was removed from the receptor, prepared, and minimized by the LigPrep module [52] of Maestro using EpiK at pH = 7.4 [48]. The software generated 32 minimized structures, and the best ranked structure was used for the self-docking procedure. The obtained ligand was submitted to a first round of docking by using Glide at Standard Precision (Glide-SP) accuracy. The best ranked pose was subjected to a second round of docking by using Glide in eXtra Precision (Glide-XP) mode. Then, the RMSD of the best ranked pose was measured as 0.5 Å below the original crystallographic pose. This procedure was applied to the docking experiments of the novel compounds.

Ligands Preparation

LONI4 and LONI11 were drawn by the 2D editor embedded in Maestro and prepared by the LigPrep module following the same procedure applied to MDMB-Fubinaca. Then, the minimized structures were submitted to the docking experiments without further modifications.

Ligand Docking Experiments

The prepared molecules LONI4 and LONI11 were docked to the CB1 receptor. The first round of docking was performed by Glide in Standard Precision mode. The best pose generated from the first step was then submitted to the second round of docking by using Glide in eXtra Precision accuracy.

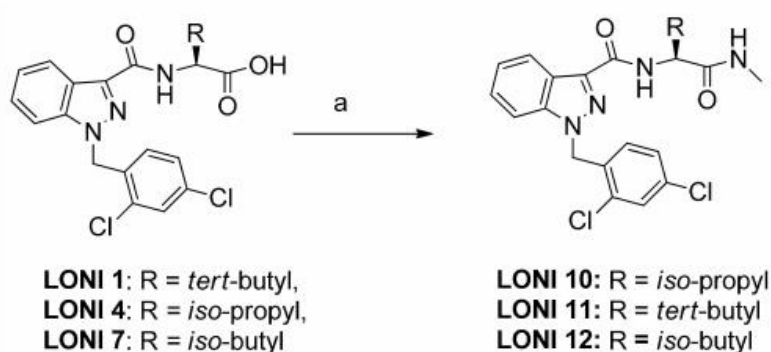
Molecular Dynamic

The LONI4-CB1, LONI11-CB1 and MDMB-Fubinaca-CB1 complexes obtained from self-docking were also submitted to molecular dynamic (MD) experiments by the Desmond module embedded in Maestro 12.0 [53]. The MD simulation system was composed of the receptor–ligand complex embedded into a dipalmitoylphosphatidylcholine (DPPC) membrane-bilayer surrounded by water. Firstly, each complex was positioned in the membrane bilayer of DPPC lipids and then inserted into a water box to simulate a model of cellular bilayer system. The water box had a minimum size as to contain the receptor complex embedded in the membrane, ensuring a distance of 10 Å from the edge of the box and the protein. In order to neutralize the system, 0.15 M of NaCl was added. The OPLS-3 force field was used for

all the experiments, and the TIP4P model was used for the water [54]. The system was minimized up to 2000 steps, holding all the protein and ligand atoms. Then, the minimized system was subjected to MD simulations, using the NPT ensemble and periodic boundary conditions for 20 ns. The Martyna–Tobias–Klein algorithm [55] was used to keep the pressure of the system at 1.01 bar by using the isotropic coupling method. The Nose–Hoover thermostat was applied to control the temperature at 310K [56]. The trajectories and other parameters were saved every 20 and 1.2 ps, respectively, to return 1000 frames. The simulation analysis was done by the simulation interactive diagram (Supplementary Materials, to visualize the RMSD fluctuations of the ligand and the receptor, the hydrogen bonds stability, the water network formation and the overall stability of the secondary structure of the enzyme.

Results

The LONI1-4,7 compounds were prepared by a well-established procedure previously reported by Stefanucci et al. [33]. The LONI10-12 novel chemical entities were efficiently recovered in excellent yields by standard solution phase peptide synthesis using EDC/HOBt coupling reagents, NMM as a base, and a solution of methylamine 40% in water (Scheme 3). All the final compounds were triturated in diethyl ether two times and then characterized by low resolution mass spectroscopy (LRMS), ¹H- and ¹³C-NMR; the purity of the final products was determined by analytical RP-HPLC and found to be >95% (see Supplementary Materials).



Scheme 3. Reagents and Conditions: (a) EDC·HCl (1.1 eq.), HOBT an. (1.1 eq.), NMM (3 eq.), methylamine 40% in water (2 eq.), DMF (6 mL), r.t. 12 h (LONI10: 96% yield; LONI11: 97% yield; LONI12: Quantitative).

The novel compounds were tested for their property to bind to cannabinoid receptors and for their ability to activate the G protein-coupled receptors (Figure 2). Efficacy (E_{max}) and potency (EC_{50}) of lonidamine-based compounds are reported in Table 1.

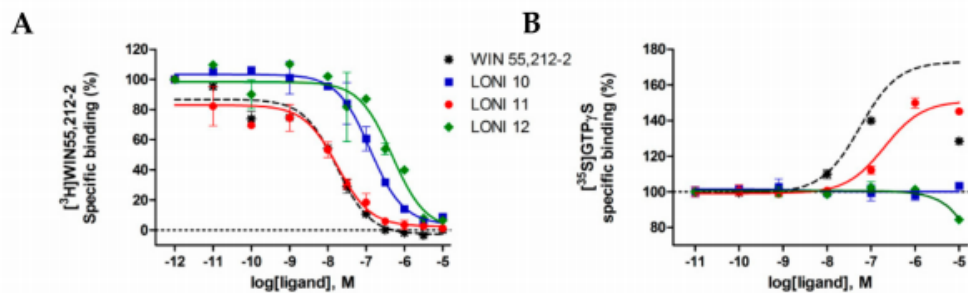


Figure 2. (A) CB₁ receptor binding affinity of LONI 10-12 in [³H]WIN55,212-2 competition binding assays to rat whole brain membrane homogenates. Figures represent the specific binding of the radioligand in percentage in the presence of increasing concentrations (10⁻¹⁰–10⁻⁵ M) of the indicated ligands. Data are expressed as percentage of mean specific binding ± S.E.M. (*n* ≥ 3). (B) G protein activation effects of the novel ligands in [³⁵S]GTPγS binding assays in rat brain membrane homogenates. Figures represent the relative specific binding of [³⁵S]GTPγS in the presence of increasing concentrations (10⁻¹⁰–10⁻⁵ M) of the indicated compounds. Data are expressed as percentage of mean specific binding ± S.E.M. (*n* ≥ 3).

Table 1. Binding affinity (*K_i*) and signal properties efficacy (*E_{max}*) and potency (*EC₅₀*) of lonidamine-based compounds.

Compounds	Sequence	<i>K_i</i> (nM)	[³⁵ S]GTPγS Binding	
			<i>E_{max}</i> (%)	<i>EC₅₀</i> (nM)
WIN55,212-2		10 ± 1	173 ± 11	56 ± 3.8
JWH-018 [33]		3.5 ± 1	163 ± 5.2	16 ± 3
LONI1 [33]	Lonidamine- <i>tert</i> -Leu-OH	0.08 *	84 ± 6.6	>1 μM
LONI2 [33]	Lonidamine- <i>tert</i> -Leu-OCH ₃	3.1 *	143 ± 5.7	8.4
LONI3 [33]	Lonidamine- <i>tert</i> -Leu-NH ₂	17 *	139 ± 4.5	126
LONI4 [33]	Lonidamine-Val-OH	2.6 *	82 ± 10.6	>1 μM
LONI10	Lonidamine-Val-NHMe	84 ± 3.4	100 ± 1.7	n.r.
LONI11	Lonidamine- <i>tert</i> -Leu-NHMe	11 ± 1.2	151 ± 3	200 ± 13
LONI12	Lonidamine-Leu-NHMe	320 ± 16	101 ± 1	n.r.

K_i values were calculated from the corresponding displacement curves of Figure 2A. The *E_{max}* and *EC₅₀* were extrapolated from the dose–response curves of Figure 2B. Data represent the mean ± S.E.M. from least three independent experiments. n.r.: Not relevant. * Mean of three independent experiments (S.D. values are in the range of 5%–10%).

The biological *in vitro* assay revealed that LONI11 was able to bind CB₁ with a *K_i* value (11 nM) very close to that of WIN55,212 (10 nM), and it was also able to stimulate the GTP-binding protein with an *E_{max}* of 151% but with three-fold less potency than WIN55,212. The other compounds bind the CB₁ with less affinity and show antagonist properties. These results suggest that LONI11 binds CB₁ and stimulates the GTP coupled to the CB₁ receptor, showing a biological profile very similar to that of the full CB₁ agonist WIN55,212. Encouraged by these data, we planned to study the potential orexant effect of LONI 1 in the *in vivo* model of food intake in comparison to the previously described compounds LONI1-4 which exhibit agonist and partial agonist profiles (Figure 3) [33].

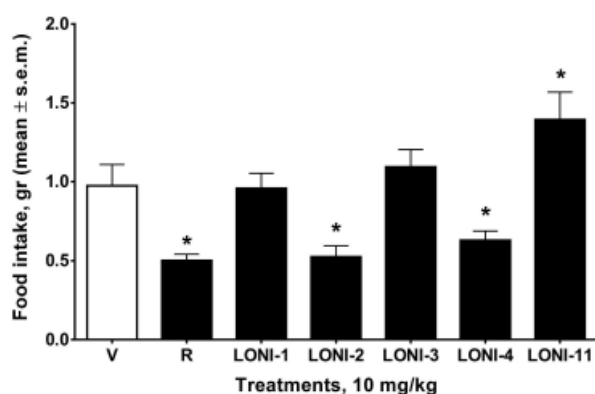


Figure 3. Activities of rimonabant, LONI1-4, LONI11 and vehicle (V, 1:1:18 mix of DMSO: Tween 80: sterile saline) on food intake. The compounds were injected intraperitoneally (10 mg/kg), and, after 30 min drug assimilation, mice were placed into individual cages and with access to a pre-defined amount of their regular lab chow (2 gr) for the 1-h test. Bars represent the mean \pm s.e.m. of data from the same six mice at each dose for food intake. * is for $p < 0.05$ vs. V (vehicle-treated animals). N = 6.

The LONI1-4 reference compounds were ineffective for food intake at 3 mg/Kg per dose after i.p. administration, while LONI2 and 4 were able to reduce food intake at 10 mg/Kg per dose as the positive control rimonabant. Interestingly, as suggested by its agonist activity, the novel compound LONI11 increased the food intake at 10 mg/Kg per dose after i.p. administration, revealing a potential orexant effect. To better understand the pharmacological properties of this novel compound and to verify if LONI11 is able to exert a significant biological effect at the central level and periphery, we also performed tail flick and formalin tests *in vivo*. LONI11 at 10 μ g/10 μ L and 100 μ g/20 μ L produced a slight antinociceptive effect after i.c.v. and s.c. injections, respectively, in tail flick (Figure 4) and formalin tests (Figure 5).

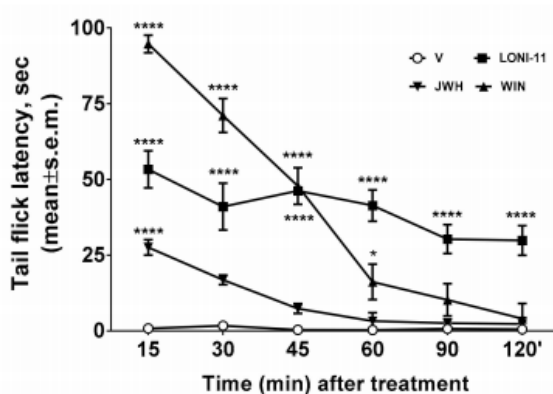


Figure 4. Antinociceptive effect of JWH-018 (JWH), WIN 55,212-2 (WIN), LONI11 and vehicle (V, saline 0.1% *v/v* DMSO) at the dose of 10 μ g/10 μ L after intracerebroventricular (i.c.v.) administration in the tail flick test. The antinociceptive activity is expressed as percentage of the maximum possible effect (%MPE \pm s.e.m.). * is for $p < 0.05$ and **** is for $p < 0.0001$ vs. V (vehicle-treated animals). N = 6.

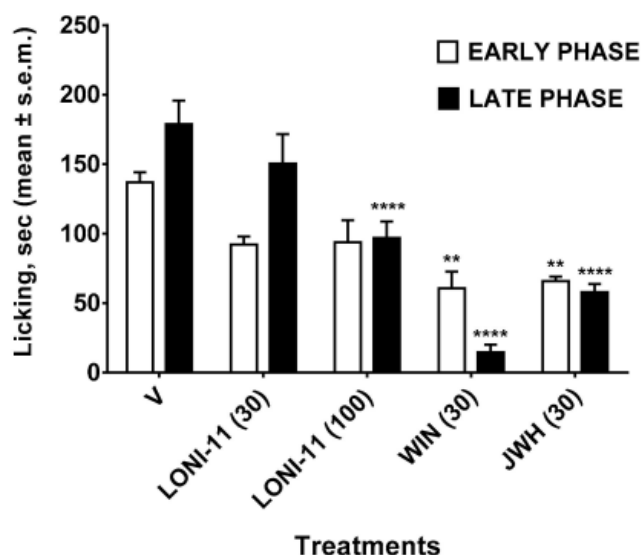


Figure 5. Effects induced in the early (white bars) and in the late (black bars) phase of the formalin test by vehicle (V, saline containing 0.9% NaCl in the ratio DMSO:saline 1:3 (*v/v*)), LONI11, WIN 55,212-2 and JWH-018 (JWH). The compounds were injected subcutaneously (s.c.) at a single dose (30–100 μ g in 20 μ L) 15 min before formalin injection (20 μ L; s.c.). Early: Licking activity recorded from 0 to 10 min after formalin administration. Late: Licking activity recorded from 15 to 40 min after formalin administration. The results obtained are expressed as the mean \pm S.E.M.; ** is for $p < 0.01$ and **** is for $p < 0.0001$ vs. V (vehicle-treated animals). N = 6.

Zymosan-induced edema and hyperalgesia assays were also performed to estimate the anti-inflammatory activity of our novel compound (Figure 6 and Figure 7). LONI11 at 100 μ g/20 μ L after s.c. route maintained the percent of paw volume at 100% for 24 h before zymosan administration (Figure 6), and it was also able to reduce the percent of paw latency to about 50% after 3 h following the s.c. administration at the same dose (Figure 7).

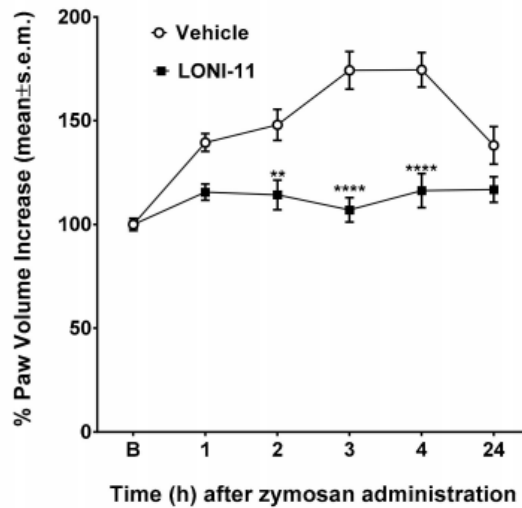


Figure 6. Effects of vehicle (V, saline containing 0.9% NaCl in the ratio DMSO:saline 1:3 (*v/v*)), and LONI11 on zymosan-induced edema. Zymosan (2.5% *w/v* in saline, 20 μ L) was subcutaneously administered in the dorsal surface of the right hind paw. Drugs were administered subcutaneously in the dorsal surface of the right hind paw at the dose of 100 μ g/20 μ L, 15 min before zymosan. Paw volume was measured 1 h before zymosan and 1, 2, 3, 4 and 24 h thereafter. The paw volume increase was evaluated as the percentage between the paw volume at each time-point and the basal paw volume. The results obtained are expressed as the mean \pm S.E.M.; ** is for $p < 0.01$ and **** is for $p < 0.0001$ vs. V. N = 6.

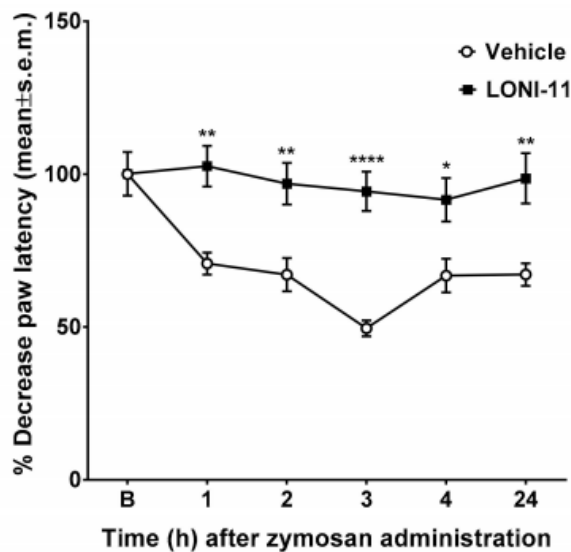


Figure 7. Effects of vehicle (V, saline containing 0.9% NaCl in the ratio DMSO:saline 1:3 (*v/v*)), and LONI11 on zymosan-induced paw hyperalgesia. Zymosan (2.5% *w/v* in saline, 20 μ L) was subcutaneously administered in the dorsal surface of the right hind paw. Drugs were administered subcutaneously in the dorsal surface of the right hind paw at the dose of 100 μ g/20 μ L, 15 min before zymosan. Paw latency was measured 1 h before zymosan and 1, 2, 3, 4 and 24 h thereafter. The paw latency decrease was evaluated as the percentage between the paw latency at each time-point and the basal paw latency. The results obtained are expressed as the mean \pm S.E.M.; * is for $p < 0.05$, ** is for $p < 0.01$ and **** is for $p < 0.0001$ vs. V. N = 6.

Discussion

Compounds LONI2 and LONI4, namely lonidamine-*tert*-LeuOCH₃ and lonidamine-Val-OH, respectively, were found to inhibit food intake, consistent with an inverse agonism at CB1 receptors (Table 1) [33].

The C-terminal methyl ester LONI2, which has been shown to possess CB1 agonist activity *in vitro*, should be expected to enhance food intake in normal animals. LONI2 exerts an activity very similar to that of C-terminal acid (LONI4) and amide (LONI3) derivatives at 10 and 3 mg/Kg, respectively, probably due to its fast hydrolysis *in vivo*, which promptly converts LONI2 into LONI1 [57]. Then, we synthesized further analogues with the *N*-methyl amide terminus. Among them, LONI11 was the most potent agonist CB1 receptor. We tested this compound for food intake *in vivo* and revealed orexant activity, unlike the less chemically stable methyl ester analogue LONI2. We observed a significant orexant effect for LONI11 and an intense anorexant effect for LONI2 and LONI4 comparable to that of rimonabant (10 mg/Kg). Considering the well-established analgesic effect of the synthetic CB1 agonist THC on pain [58], the full agonist LONI11 was further tested to study the antinociceptive effect at the central and periphery levels. This compound was able to exert a good antinociceptive effect in tail flick and formalin tests *in vivo* following different administration routes. Furthermore, the subcutaneous administration of LONI11 at 100 mg/20 μ L in zymosan induced edema and hyperalgesia rat models, decreased the percent of paw latency, and counteracted the percent of paw volume increase, suggesting potential activity at peripheral tissues. Though these interesting data prompted us to further investigate their effects upon chronic use, the toxicological study of these rimonabant/Fubinaca hybrids should be a primary issue. Documented side effects of Fubinaca series compounds are impaired driving, acute psychiatric distress, aggressiveness and polysubstance abuse with several SCs and alcohol [59,60,61,62,63,64]. These effects are also correlated to populations' changes in consuming SCs, such as incarcerated persons, homeless, and their cultural heritage [65,66,67]. In order to better understand the molecular bases of LONI11 activity as an agonist and LONI4 activity as a partial inverse agonist, *in silico* docking experiments and molecular dynamic (MD) simulations were carried out. The best pose of LONI11 generated by Glide is depicted in Figure 8B. The key interactions observed in the crystal complex 6N4B were well represented in the docking pose of LONI11, namely the π - π

interactions with Phe268, Trp279, Phe200 and the hydrogen bond formed with His178. The best docking pose of LONI11 was very close to that of the crystallographic ligand MDMB-Fubinaca (Figure 8A).

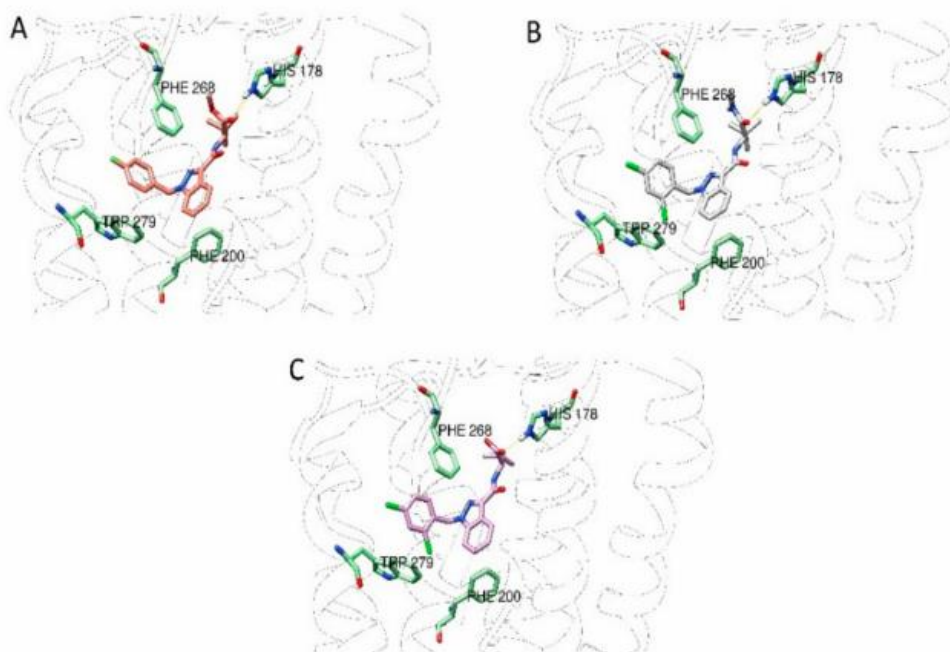


Figure 8. Best ranked pose of MDMB-Fubinaca (A), LONI11 (B) and LONI4 (C) docked to the CB1 receptor.

LONI4, which has been demonstrated to have partial inverse agonist activity, was also able to interact with the binding pocket of the CB1 receptor by forming the same key interactions found for LONI11 (see Figure 8B,C). The docking score of the best pose found was -11.7 Kcal/mol for LONI11, similar to that of MDMB-Fubinaca (-11.1 kcal/mol) and lower than that of LONI4 (-10.5 Kcal/mol). Thus, the difference of activity could have been only due to the C-terminal group. At physiological pH (7.4), the carboxylic moiety was largely deprotonated and the C-terminus of LONI4 bore a stable negative charge. However, the molecular docking experiments alone are not able to explain its different activity. Indeed, all the starting poses were similar each other, as highlighted in the docking experiments, bearing all the same interactions to His178, Phe200, Phe268 and Trp279. We further submitted the best pose of each compound to molecular dynamic simulation over 20 ns. The RMSD of the reference ligand MDMB-Fubinaca was found to be very low, fluctuating from 0.8 to 2.4 Å, which revealed a good and stable pose. The MD simulation showed significant differences from the

starting pose: The Fubinaca analogue was able to form several hydrogen bonds to the water molecules present in the environment and to establish a water network with Ser383 and His178. Thus, these two residues should have been highly involved in the stabilization of Fubinaca ligand pose together with the previously observed Trp279, Phe200 and Phe268. This water network was also predicted by Kumar et al. and Michel et al. [47,68].

During the MD simulation, LONI11 maintained the π - π stack with the aromatic residues Phe268, Trp279 and Phe379. However, the polar portion of the molecule largely lost the initial hydrogen bond to His178, and a water network between one water and the residue Ser383 was formed, as in the case of Fubinaca ligand. The presence of the free carboxylic group in LONI4 deeply influenced the stabilization of the starting docked pose during the MD simulation. Indeed, the RMSD plot of LONI4 ranged from 0.8 to 4.5 Å, demonstrating that the starting pose was scarcely stable. During the MD simulation, several novel interactions were formed, along with a strong hydration of the free carboxylic terminus, higher than that found for the methyl ester group of Fubinaca and for the *N*-methylamide group of LONI11.

The water permanency of LONI4 was more than 10% of the time, whereas for MDMB-Fubinaca and LONI11, it reached only 5%. The authors Michel et al. and Kumar et al. previously predicted the possible involvement of a water network formed by a water molecule strongly bound to the receptor, mediating the interactions among the ligand, His178 and Ser383 [47,68]. The capacity of the ligand to activate or deactivate the receptor could be largely due to its ability to form a specific water network. However, in the case of LONI4, the MD experiments demonstrated that the presence of a permanent negative charge allowed the carboxylic group to form strong polar interactions with three positive centers in the binding pocket represented by Arg182, Lys192 and Lys376 residues. This binding mode seemed to be preferred over the water network and the related interactions with Ser383 and His178. This difference is fundamental to explain the inverse agonist activity of LONI4. Moreover, the aromatic portion of the molecule seems to prefer a different accommodation in the receptor pocket. Thus, the novel compound LONI11 bearing the *N*-methyl-amide *C*-terminus and the 2,4-dichlorobenzyl ring largely interacted with the CB1 binding cavity, as in the case of MDMB-Fubinaca. On the contrary, LONI4 (bearing a free carboxylic acid) was not able to strongly interact with the polar key residues His178 and Ser383 either directly or

through a water network; instead, it may have been able to establish a whole new set of polar interactions with the positive residues present at the receptor binding cavity (Lys376, Lys192 and Arg182), leading to the inactivation of the CB1 receptor.

Conclusions

In the last two decades, obesity has assumed the form of a pandemic, often related to the development of cardiovascular diseases (CVD) and strokes. There is a worldwide emergency that requires the development of novel and safer anti-obesity treatments. Rimonabant and sibutramine associated with lifestyle modifications were successfully engaged in the control of obesity by reducing appetite and weight gain. Their complex action mechanism promotes monoamine reuptake in the central nervous system (CNS), the secretion of neuropeptides with anorexigenic activity and the lowering of those with orexigenic properties, the elevation of metabolism, and the improvement of the peripheral sympathetic activity. Though those drugs have shown to be effective to control body weight and to manage obesity, they have been withdrawn from the market due to their important side effects. Thus, a novel drug able to provide the same therapeutic efficacy without the dangerous side effects is an urgent need. An agonist able to bind a specific receptor that preferentially drives a single downstream signaling cascade could represent a possible solution. However, the broad distribution of cannabinoid receptors in different areas of the body allows them to interact with a variety of system networks. The CB1 receptors are connected with different receptor-activity modulatory proteins, and the possibility to assume a selectively targetable ligand-binding conformation is still uncertain; currently, there are few process and site-specific CB1 targeted drugs.

Our study identified a series of lonidamine joined Leu, *tert*-Leu and Val amino acids with different C-terminal functional groups (LONI1-4,11) as novel compounds endowed with orexant/anorexant activity. They are structurally related to the Fubinaca series and follow the same general structure reported by Schoeder et al. [30]. However, in this study, novel features were identified. In particular, the four structural features described by Huffman et al. [69,70] were well defined in our compounds, namely: (i) An heterocyclic scaffold represented by an indole, indazole or imidazole ring with several substitutions; (ii) a dipolar linker such as an amide or ester; (iii) a lipophilic moiety such as the side chain of an amino acid or a lipophilic chain; and (iv) a

hydrophobic side chain bound to the heterocyclic scaffold. This general structure was only able to establish the structural requirements for CB1 receptor affinity without taking intrinsic activity into consideration. In this work, we have demonstrated the importance of the C-terminus group, which is shown in the general structure depicted in Figure 9. Polar and uncharged C-terminus groups such as methyl ester and methyl amide moiety are able to act as H bond donors and are required for agonist activity, while a more polar C-terminal amide group is detrimental, giving weak agonists [33]. The free carboxylic group at C-terminus is able to shift agonist to antagonist activity. However, a large structure-activity relationships (SAR) study should be designed in order to verify our hypothesis.

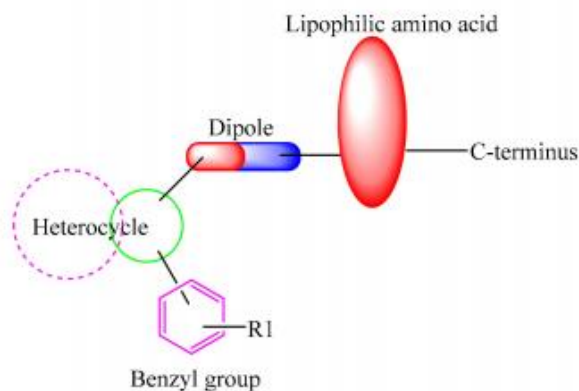


Figure 9. Structural features of the synthetic cannabinoids reported in this study.

Since one of them (LONI11) exhibited a potent agonist activity at CB1, the antinociceptive activity was also analyzed and revealed a good analgesic effect after sub-cutaneous and intracerebroventricular administration *in vivo* and a significant anti-inflammatory effect after s.c. administration, suggesting potential activity at the periphery. Even if the preliminary biological data *in vivo* and *in vitro* of these novel compounds were promising, a deep investigation on animal models is necessary to assess their selectivity, potency and long-term effects upon chronic and acute administration. These results could be useful as a starting point to optimize the pharmacological properties of rimonabant/Fubinaca hybrids and to better understand the molecular mechanism below their biological profile. An understanding of all the neuroendocrine networks and their roles in the hypothalamus to regulate the feeding behavior could lead to the development of novel and safer approaches to manage the main nutritional disorders.

References

1. Carella AM, Conte M, Melfitano A, et al. Neuroendocrine Mediators, Food Intake and Obesity: A Narrative Review. *Int. J. Cardiol. Lipidol. Res.* 2014;1:18–32.
2. Thomas BF. Neuroanatomical basis for the therapeutic applications of cannabinoid receptor 1 antagonists. *Drug Dev. Res.* 2009;70:527–554.
3. Foster-Schubert KE, Cummings DE. Emerging Therapeutic Strategies for Obesity. *Endocr. Rev.* 2006;27:779–793.
4. Soria-Gomez E, Matias I, Rueda-Orozco PE, et al. Pharmacological enhancement of the endocannabinoid system in the nucleus accumbens shell stimulates food intake and increases c-Fos expression in the hypothalamus. *Br. J. Pharmacol.* 2007;151:1109–1116.
5. Kirkham TC, Williams CM, Fezza F, et al. Endocannabinoid levels in rat limbic forebrain and hypothalamus in relation to fasting, feeding and satiation: Stimulation of eating by 2-arachidonoyl glycerol. *Br. J. Pharmacol.* 2002;136:550–557.
6. Di Marzo V, Matias I. Endocannabinoid control of food intake and energy balance. *Nat. Neurosci.* 2005;8:585–589.
7. Colombo G, Agabio R, Diaz G, et al. Appetite suppression and weight loss after the cannabinoid antagonist SR141716. *Life Sci.* 1998;63:PL113–PL117.
8. Lambert P, Wilding J, Al-Dokhayel A, et al. The effect of central blockade of kappa-opioid receptors on neuropeptide Y-induced feeding in the rat. *Brain Res.* 1993;629:146–148.
9. Brunetti L, Ferrante C, Orlando G, et al. Orexigenic effects of endomorphin-2 (EM-2) related to decreased CRH gene expression and increased dopamine and norepinephrine activity in the hypothalamus. *Peptides.* 2013;48:83–88.
10. Crespo I, De Heras RG, de Fonseca FR, et al. Pretreatment with subeffective doses of Rimonabant attenuates orexigenic actions of orexin A-hypocretin 1. *Neuropharmacology.* 2008;54:219–225.
11. Hilairt S, Bouaboula M, Carrière D, et al. Hypersensitization of the Orexin 1 Receptor by the CB1 Receptor: Evidence For Cross-Talk Blocked by the Specific Cb1 Antagonist, SR141716. *J. Biol. Chem.* 2003;278:23731–23737.
12. Scheen AJ. Sibutramine on Cardiovascular Outcome. *Diabetes Care.* 2001;34:114–119.
13. Zhang W, Roederer MW, Chen WQ, et al. Pharmacogenetics of drugs withdrawn from the market. *Pharmacogenomics.* 2012;13:223–231.
14. Després JP, Golay A, Sjöström L. Effects of Rimonabant on Metabolic Risk Factors in Overweight Patients with Dyslipidemia. *N. Engl. J. Med.* 2005;353:2121–2134.

15. Després JP, Ross R, Boka G, et al. Effect of rimonabant on the high-triglyceride/low-HDL-cholesterol dyslipidemia, intra-abdominal adiposity, and liver fat: The ADAGIO-Lipids trial. *Arterioscler. Thromb. Vasc. Biol.* 2009;29:416–423.
16. Sam AH, Salem V, Ghatei MA. Rimonabant: From RIO to Ban. *J. Obes.* 2011;2011:432607.
17. Erkekoglu P, Giray B, Sahin G. Toxicological evaluation of Rimonabant, Taranabant, Surinabant and Otenabant in the treatment of obesity: Why the trials on endocannabinoid receptor antagonists and inverse agonists are suspended? *FABAD J. Pharm. Sci.* 2008;33:95–108.
18. Janero DR, Makriyannis A. Cannabinoid receptor antagonists: Pharmacological opportunities, clinical experience, and translational prognosis. *Expert Opin. Emerg. Drugs.* 2009;14:43–65.
19. Ibsen MS, Connor M, Glass M. Cannabinoid CB1 and CB2 Receptor Signaling and Bias. *Cannabis Cannabinoid Res.* 2017;2:48–60.
20. Al-Zoubi R, Morales P, Reggio PH. Structural Insights into CB1 Receptor Biased Signaling. *Int. J. Mol. Sci.* 2019;20:1837.
21. Al-Zoubi W, Salih AA, Duraid SA, et al. Synthesis, characterization, and antioxidant activities of imine compounds. *J. Phys. Org. Chem.* 2019;32:3916.
22. Ibsen DB, Laursen ASD, Lauritzen L, et al. Substitutions between dairy product subgroups and risk of type 2 diabetes: The Danish Diet, Cancer and Health cohort. *Br. J. Nutr.* 2017;118:989–997.
23. Mazier W, Saucisse N, Gatta-Cherifi B, et al. The Endocannabinoid System: Pivotal Orchestrator of Obesity and Metabolic Disease. *Trends Endocrinol. Metab.* 2015;26:524–537.
24. Black AD, Car J, Pagliari C, et al. The Impact of eHealth on the Quality and Safety of Health Care: A Systematic Overview. *PLoS Med.* 2011;8:e1000387.
25. Rubino F, Nathan DM, Eckel RH, et al. Metabolic Surgery in the Treatment Algorithm for Type 2 Diabetes: A Joint Statement by International Diabetes Organizations. *Diabetes Care.* 2016;39:861–877.
26. Mallat SG, Abu Samra S, Younes F, et al. Identifying predictors of blood pressure control in the Lebanese population—A national, multicentric survey—I-PREDICT. *BMC Public Health.* 2014;14:1142.
27. Schindler K, Themessl-Huber M, Hiesmayr M, et al. To eat or not to eat? Indicators for reduced food intake in 91,245 patients hospitalized on nutritionDays 2006–2014 in 56 countries worldwide: A descriptive analysis. *Am. J. Clin. Nutr.* 2016;104:1393–1402.
28. Banister SD, Longworth M, Kevin R, et al. Pharmacology of Valinate and tert-Leucinate synthetic cannabinoids 5F-AMBICA, 5F-AMB, 5F-ADB, AMB-FUBINACA, MDMB-FUBINACA, MDMB-CHMICA, and their analogues. *ACS Chem. Neurosci.* 2016;7:1241–1254.
29. Shanks KG, Clark W, Behonick G. Death Associated With the Use of the Synthetic Cannabinoid ADB-FUBINACA. *J. Anal. Toxicol.* 2016;40:236–239.

30. Schoeder CT, Hess C, Madea B, et al. Pharmacological evaluation of new constituents of “Spice”: Synthetic cannabinoids based on indole, indazole, benzimidazole and carbazole scaffolds. *Forensic Toxicol.* 2018;36:385–403.
31. Adamowicz P, Meissner E, Maślanka M. Fatal intoxication with new synthetic cannabinoids AMB-FUBINACA and EMB-FUBINACA. *Clin. Toxicol.* 2019;26:1–6.
32. Scourfield A, Flick C, Ross J, et al. Synthetic cannabinoid availability on darknet drug markets—Changes during 2016–2017. *Toxicol. Commun.* 2019;3:7–15.
33. Stefanucci A, Macedonio G, Dvorácskó S, et al. Novel Fubinaca/Rimonabant hybrids as endocannabinoid system modulators. *Amino Acids.* 2018;50:1595–1605.
34. Mollica A, Costante R, Akdemir A, et al. Exploring new Probenecid-based carbonic anhydrase inhibitors: Synthesis, biological evaluation and docking studies. *Bioorganic Med. Chem.* 2015;23:5311–5318.
35. Mollica A, Pelliccia S, Famigliani V, et al. Exploring the first Rimonabant analog-opioid peptide hybrid compound, as bivalent ligand for CB1 and opioid receptors. *J. Enzym. Inhib. Med. Chem.* 2017;32:444–451.
36. Mollica A, Pinnen F, Stefanucci A, et al. The evolution of peptide synthesis: From early days to small molecular machines. *Curr. Bioact. Comp.* 2013;9:184–202.
37. Dvorácskó S, Keresztes A, Mollica A, et al. Preparation of bivalent agonists for targeting the mu opioid and cannabinoid receptors. *Eur. J. Med. Chem.* 2019;178:571–588.
38. Kilkeny C, Browne W, Cuthill IC, et al. Animal research: Reporting *in vivo* experiments: The ARRIVE guidelines. *Br. J. Pharmacol.* 2010;160:1577–1579.
39. McGrath JC, Lilley E. Implementing guidelines on reporting research using animals (ARRIVE etc.): New requirements for publication in *BJP*. *Br. J. Pharmacol.* 2015;172:3189–3193.
40. Wiley JL, Burston JJ, Leggett DC, et al. CB1 cannabinoid receptor-mediated modulation of food intake in mice. *Br. J. Pharmacol.* 2005;145:293–300.
41. Pieretti S, di Giannuario A, de Felice M, et al. Stimulus-dependent specificity for annexin 1 inhibition of the inflammatory nociceptive response: The involvement of the receptor for formylated peptides. *Pain.* 2004;109:52–63.
42. Stefanucci A, Lei W, Pieretti S, et al. On resin click-chemistry-mediated synthesis of novel enkephalin analogues with potent anti-nociceptive activity. *Sci. Rep.* 2019;9:5771.
43. Maione F, Minosi P, di Giannuario A, et al. Long-Lasting Anti-Inflammatory and Antinociceptive Effects of Acute Ammonium Glycyrrhizinate Administration: Pharmacological, Biochemical, and Docking Studies. *Molecules.* 2019;24:2453.
44. Pieretti S, Dominici L, di Giannuario A, et al. Local anti-inflammatory effect and behavioral studies on new PDE4 inhibitors. *Life Sci.* 2006;79:791–800.

45. Niederberger E, Schmidtko A, Gao W, et al. Impaired acute and inflammatory nociception in mice lacking the p50 subunit of NF-kappaB. *Eur. J. Pharmacol.* 2007;559:55–60.
46. Curtis MJ, Bond RA, Spina D, et al. Experimental design and analysis and their reporting: New guidance for publication in *BJP. Br. J. Pharmacol.* 2015;172:3461–3471.
47. Kumar KK, Shalev-Benami M, Robertson MJ, et al. Structure of a Signaling Cannabinoid Receptor 1-G Protein Complex. *Cell.* 2019;176:448–458.e12.
48. Schrödinger Release 2019-3: Schrödinger Suite 2019-2 Protein Preparation Wizard. Epik, Schrödinger, LLC; New York, NY, USA: Impact, Schrödinger, LLC; New York, NY, USA: Prime, Schrödinger, LLC; New York, NY, USA: 2019.
49. Jacobson MP, Pincus DL, Rapp CS, et al. A hierarchical approach to all-atom protein loop prediction. *Proteins Struct. Funct. Bioinform.* 2004;55:351–367.
50. Stefanucci A, Novellino E, Mirzaie S, et al. Opioid Receptor Activity and Analgesic Potency of DPDPE Peptide Analogues Containing a Xylene Bridge. *ACS Med. Chem. Lett.* 2017;8:449–454.
51. Schrödinger Release 2019-3: Glide. Schrödinger, LLC; New York, NY, USA: 2019.
52. Schrödinger Release 2019-3: LigPrep. Schrödinger, LLC; New York, NY, USA: 2019.
53. Schrödinger Release 2019-3: Desmond Molecular Dynamics System. D. E. Shaw Research; New York, NY, USA: Maestro-Desmond Interoperability Tools, Schrödinger; New York, NY, USA: 2019.
54. Chandrasekhar J, Impey RW, Jorgensen WL, et al. Comparison of simple potential functions for simulating liquid water. *J. Chem. Phys.* 1983;79:926.
55. Martyna GJ, Tobias DJ, Klein ML. Constant pressure molecular dynamics algorithms. *J. Chem. Phys.* 1994;101:4177–4189.
56. Hünenberger PH. Thermostat Algorithms for Molecular Dynamics Simulations. *Adv. Polym. Sci.* 2005;173:105–149.
57. Matsubara K, Kagawa M, Fukui Y. *In vivo* and *in vitro* studies on cocaine metabolism: Ecgonine methyl ester as a major metabolite of cocaine. *Forensic Sci. Int.* 1984;26:169–180.
58. Slomski A. THC for Chronic Pain. *JAMA.* 2018;320:1631.
59. Kaneko S. Motor vehicle collisions caused by the ‘super-strength’ synthetic cannabinoids, MAM-2201, 5F-PB-22, 5F-AB-PINACA, 5F-AMB and 5F-ADB in Japan experienced from 2012 to 2014. *Forensic Toxicol.* 2017;35:244–251.
60. Castaneto MS, Gorelick DA, Desrosiers NA, et al. Synthetic cannabinoids: Epidemiology, pharmacodynamics, and clinical implications. *Drug Alcohol Depend.* 2014;144:12–41.
61. Deng H, Verrico CD, Kosten TR, et al. Psychosis and synthetic cannabinoids. *Psychiatry Res.* 2018;268:400–412.

62. Abouchedid R, Ho JH, Hudson S, et al. Acute Toxicity Associated with Use of 5F-Derivations of Synthetic Cannabinoid Receptor Agonists with Analytical Confirmation. *J. Med. Toxicol.* 2016;12:396–401.
63. Langford AM, Bolton JR. Synthetic cannabinoids: Variety is definitely not the spice of life. *J. Forensic Leg. Med.* 2018;59:36–38.
64. European Monitoring Centre for Drugs and Drug Addiction . EMCDDA–Europol Joint Report on a New Psychoactive Substance: 1-(4-Cyanobutyl)-N-(2-Phenylpropan-2-yl)Indazole-3-Carboxamide (CUMYL-4CN-BINACA) Publications Office of the European Union; Luxembourg: 2017. Joint Reports.
65. Van Hout MC, Benschop A, Bujalski M, et al. Health and social problems associated with recent novel psychoactive substance (NPS) use amongst marginalised, nightlife and online users in six European countries. *Int. J. Ment. Health Addict.* 2018;16:480–495.
66. European Monitoring Centre for Drugs and Drug Addiction . Report on the Risk Assessment of 1-(4-Cyanobutyl)-N-(2-Phenylpropan-2-yl)-1H-Indazole-3-Carboxamide (CUMYL-4CN-BINACA) in the Framework of the Council Decision on New Psychoactive Substances. Publications Office of the European Union; Luxembourg: 2018. Risk Assessments.
67. Drug Enforcement Administration, Department of Justice Schedules of controlled substances: Temporary placement of six synthetic cannabinoids (5F-ADB, 5F-AMB, 5F-APINACA, ADB-FUBINACA, MDMB-CHMICA and MDMB-FUBINACA) into Schedule I. *Fed. Regist.* 2017;82:17119–17124.
68. Michel J, Tirado-Rives J, Jorgensen WL. Prediction of the Water Content in Protein Binding Sites. *J. Phys. Chem. B.* 2009;113:13337–13346.
69. Huffman JW, Dai D, Martin BR, et al. Design, Synthesis and Pharmacology of Cannabimimetic Indoles. *Bioorganic Med. Chem. Lett.* 1994;4:563–566.
70. Huffman JW, Zengin G, Wu MJ, et al. Structure-activity relationships for 1-alkyl-3-(1-naphthoyl)indoles at the cannabinoid CB(1) and CB(2) receptors: Steric and electronic effects of naphthoyl substituents. New highly selective CB(2) receptor agonists. *Bioorg. Med. Chem.* 2005;13:89–112.

CHAPTER 7: Long-Lasting, Antinociceptive Effects of pH-Sensitive Niosomes Loaded With Ibuprofen in Acute and Chronic Models of Pain

Francesca Marzoli¹, Carlotta Marianecchi², Federica Rinaldi³, Daniele Passeri⁴, Marco Rossi^{4,5}, Paola Minosi¹, Maria Carafa², Stefano Pieretti¹

¹ National Center for Drug Research and Evaluation, Italian National Institute of Health, 00161 Rome, Italy.

² Department of Drug Chemistry and Technology, Sapienza University of Rome, 00185 Rome, Italy.

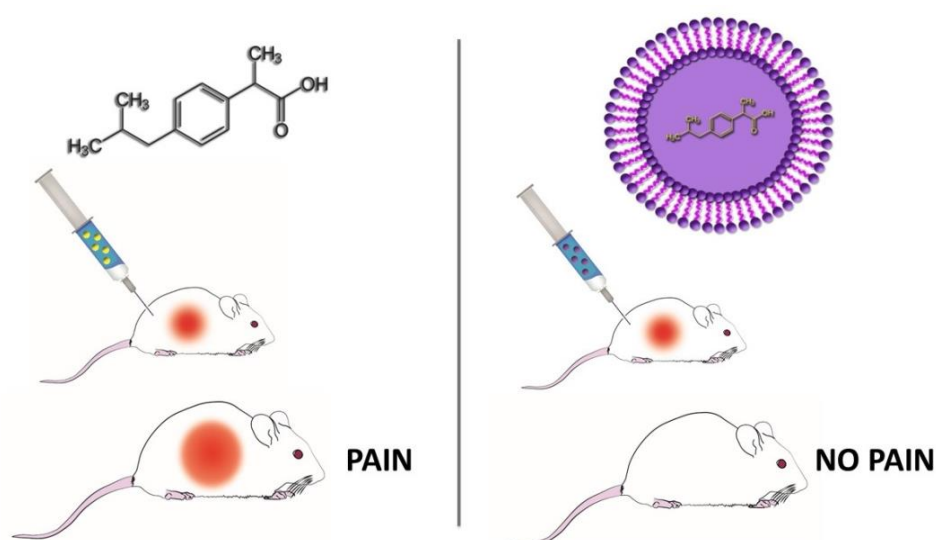
³ Center for Life Nano Science@Sapienza, Istituto Italiano di Tecnologia (ITT), 00161 Rome, Italy.

⁴ Department of Basic and Applied Sciences for Engineering, Sapienza University of Rome, 00161 Rome, Italy.

⁵ Research Center for Nanotechnology Applied to Engineering, Sapienza University of Rome (CNIS), 00185 Rome, Italy.

Abstract

Ibuprofen is one of the non-steroidal anti-inflammatory drugs (NSAIDs) widely used to treat pain conditions. NSAIDs encounter several obstacles to passing across biological membranes. To overcome these constraints, we decided to study the effects of a new pH-sensitive formulation of niosomes containing Polysorbate 20 derivatized by Glycine and loaded with ibuprofen (NioIbu) in several animal models of pain in mice. We performed two tests commonly used to study acute antinociceptive activity, namely the writhing test and the capsaicin test. Our results demonstrated that NioIbu, administered 2 h before testing, reduced nociception, whereas the free form of ibuprofen was ineffective. In a model of inflammatory pain, hyperalgesia induced by zymosan, NioIbu induced a long-lasting reduction in hyperalgesia in treated mice. In a model of neuropathic pain induced by sciatic nerve chronic constriction, NioIbu reduced both neuropathy-induced allodynia and hyperalgesia. The results obtained in our experiments suggest that pH-sensitive niosomes containing Polysorbate 20 derivatized by Glycine is an effective model for NSAIDs delivery, providing durable antinociceptive effects and reducing the incidence of side effects.



Introduction

The non-steroidal anti-inflammatory drug (NSAID) Ibuprofen (-methyl-4-(2-methylpropyl) benzeneacetic acid, IBU) is commonly used in the treatment of pain, fever, and inflammatory diseases. Ibuprofen was discovered in 1960 for the treatment of some pain conditions and inflammatory autoimmune diseases, such as rheumatoid arthritis [1]. In 1961, Ibuprofen became available in tablet form, and in 1983 was launched as a topical formulation. Ibuprofen is an analgesic drug that inhibits the production of cyclooxygenase (Cox-2) pathway-derived prostaglandins, which increase in inflamed tissues and control inflammatory disorder [2,3]. As is well-known, prostanoids mediate the sensation of peripheral and central pain, increasing membrane excitability and reducing the threshold of nociceptor stimulation [4]. While ibuprofen is completely absorbed after oral administration [5], the plasma level is still low several hours after topical application [6]. Various studies have reported different techniques to increase the permeability of cell membranes and the transdermal transport of ibuprofen and other drugs: preparing colloidal microstructures with lysinate and lecithin [7,8], nanoscaled emulsion with palm olein esters [9], iontophoresis [10], and using surfactants and various vehicles, such as the niosomes [11,12]. Niosomes are unilamellar or multilamellar non-ionic surfactant vesicles similar to liposomes that can be used as therapeutic nanocarriers. The main characteristic of these vesicles is their capability to encapsulate both hydrophilic and lipophilic drugs. Hydrophilic drugs are encapsulated in the inner core where the aqueous compartment is located, while lipophilic drugs are encapsulated into the lipophilic domain of the bilayer [13–15]. The basic components of niosomes are non-ionic surfactants in addition to cholesterol (Chol). The surfactants are mainly composed of two distinct regions and are classified as anionic, cationic, amphoteric, and non-ionic according to the feature of the hydrophilic head, which contains sulfonate or ammonium salts of fatty and zwitterionic acids. Non-ionic surfactants have no charge groups in their hydrophilic heads and are able to form niosomal vesicles that represent an innovative system with better performance compared to conventional drug delivery systems. Indeed, niosomes are more stable than liposomes. They show greater bioavailability compared with conventional dosage forms because they are able to increase the permeation of drugs through the skin [16]. Furthermore, they can be employed for oral and parenteral administration, protecting drugs from biological enzymes and the environment. Moreover, the surfactants employed in the preparation of niosomes are less expensive

and more versatile than the phospholipids used for liposomal formulations [17]. To obtain a site-specific drug release, pH-sensitive molecules can be added to the formulation or used to derivatize the surfactants employed. It is well known that some pathological states are associated with pH profiles different from that of normal tissues. Examples include ischemia, infection, inflammation, and cancer, which are often associated with acidosis. Extracellular pH values ranging from 5.5 to 7.0 have been detected in inflamed tissues associated with bacterial infections [18], atherosclerotic plaque, [19], and cancers [20]. This pH gradient is of particular importance since several drugs and drug carriers are taken up by endocytosis and found and/or trapped within endosomes and lysosomes. In this context, niosomes with increased affinity for an acidic pH microenvironment can take advantage of pathological conditions of inflammation for selective targeting. Recently, Rinaldi et al. [21,22] have described the formulation of pH-sensitive niosomes containing Polysorbate 20/Chems (Tween 20, Tw20) or Polysorbate 20 derivatized by Glycine (Tw20-Gly) as an effective strategy for the delivery of anaesthetics and anti-inflammatory drugs. In particular, the preparation steps (panel A) and mechanism of bilayer destabilization (panel B) are shown in Figure 1.

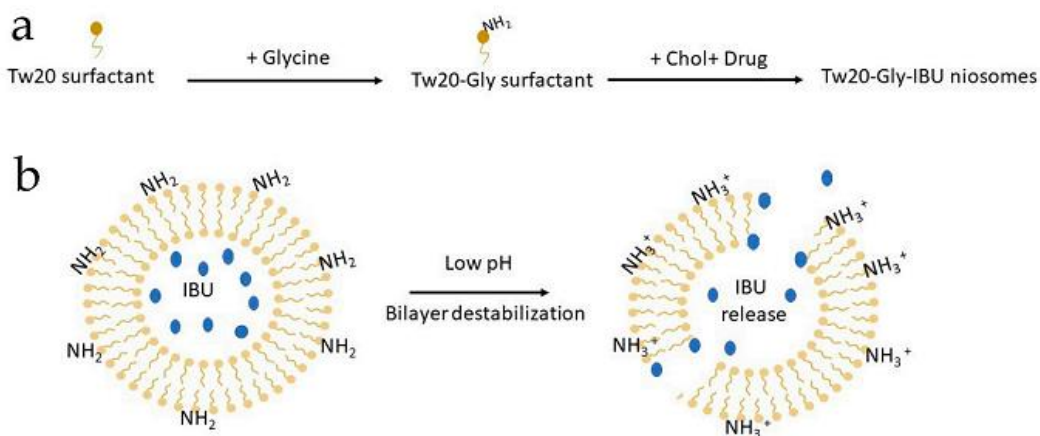


Figure 1. Cartoon describing: (a) niosomal preparation by a derivatized surfactant; and (b) bilayer destabilization at an acidic pH and consequent drug release. IBU is for Ibuprofen.

In this paper, the well-characterized and selected samples of the previous research study [16,17] were newly prepared to compare the analgesic activity of pH-Tw20Gly niosomes loaded with ibuprofen (NioIbu) to that of free ibuprofen in animal models of acute and chronic pain. We showed that NioIbu strongly increases Ibuprofen's analgesic activity, promoting a longer duration of action of this drug. We suggest that NioIbu is a

new and more effective strategy to treat pain arising from chronic inflammatory conditions.

Materials and Methods

Materials

Tween 20 (Tw20), Cholesterol >99% (Chol), N-(2-Hydroxyethyl)piperazine-N'-(2-ethanesulfonic acid) (HEPES) >99.5%, Sephadex G75, Glycine (Gly), and all other chemicals and solvents of the highest purity and of spectroscopic grade were purchased from Sigma-Aldrich (Sigma-Aldrich S.r.l., Milan, Italy). Water was purified through a Millipore Milli-Q system (Merck S.p.a., Milan, Italy).

Nanovesicle Formulation and Characterization

Niosomes based on a polysorbate-20 glycine derivative (Tw20Gly) were prepared by the thin film evaporation method at different Ibuprofen loading concentrations (Table 1) and purified by glass chromatography, as previously described [21,22]. A Nano ZS90 Dynamic light scattering LS (Malvern Instruments Ltd., Malvern, UK) at a scattering angle of 90.0 and a LS50B spectrofluorometer (PerkinElmer, MA, USA), were both employed for the physico-chemical characterization of vesicles (hydrodynamic diameter, size distribution, zeta potential, bilayer properties, stability, and *in vitro* release studies) [21]. Drug entrapment within non-ionic surfactant vesicles was determined using high-performance liquid chromatography (HPLC). HPLC analyses were carried out with a Perkin-Elmer 250 liquid chromatography apparatus (PerkinElmer, MA, USA), equipped with a Perkin-Elmer 235 photo-diode array detector, a 20-l-loop Rheodyne injector and a computer hardware, as previously described, on purified niosomes after disruption with isopropanol (vesicle dispersion/isopropanol 1:1 v/v final ratio) [23].

Table 1. Sample composition (NioIbu 5% has been the analyzed formulation). Nio, pH-Tw20Gly niosomes; NioIbu, pH-Tw20Gly niosomes loaded with different percentages of Ibuprofen Hepes solutions. Tw 20, is for Tween 20; Chol, is for Cholesterol; IBU, is for Ibuprofen.

Sample	Tw20 (mM)	Tw20-Gly (mM)	Chol (mM)	IBU (% p/v)
Nio	3.75	11.25	7.5	=
NioIbu 1%	3.75	11.25	7.5	1
NioIbu 3%	3.75	11.25	7.5	3
NioIbu 5%	3.75	11.25	7.5	5
NioIbu 7%	3.75	11.25	7.5	7

Atomic force microscopy (AFM) topographical characterization has been carried out using a standard AFM setup (Dimension Icon, Bruker Inc. in ‘soft tapping’ mode, Billerica, MA, USA) equipped with standard silicon cantilevers (OTESPA, Bruker Inc., Billerica, MA, USA). Analysis of niosomal dimensions was carried out by means of atomic force microscopy (AFM) by imaging the samples in tapping mode after deposition on a Si substrate. A diameter and height of nine isolated niosomes were measured. These allowed us to determine the surface of the niosomes deposited on the substrate (which obviously lost their original spherical shape) given by the sum of areas of the surface of the spherical cap and of the base circle. Assuming that the flattening of niosomes resulted in the modification of shape and volume without significantly affecting the surface area, the diameter of niosomes in solution was evaluated as that of a sphere having the same surface area.

Animals and Treatments

We used male CD-1 mice (Harlan, Italy) weighing 25 g in all of the experiments. Mice were housed in colony cages under standard conditions of light, temperature, and relative humidity for at least 1 week before the start of experimental sessions. All experiments were performed according to Legislative Decree 26/14, which implements the European Directive 2010/63/UE on laboratory animal protection in Italy, and were approved by the local ethics committee. Animal studies are reported in accordance with the ARRIVE (Animal Research: Reporting of *In vivo* Experiments) guidelines [24]. In all experiments, NioIbu 5%, diluted to obtain the same drug concentration, was compared to: (i) HEPES buffer (HB), (ii) an “unstructured” surfactant formulation (TG), composed of surfactant and cholesterol, and (iii) an “unstructured” surfactant formulation (TG-Ibu), composed of surfactant, cholesterol, and ibuprofen at the same concentrations as the ones present in NioIbu, but not organized in vesicular systems.

Writhing Test

The procedure was similar to the one previously described [25]. After 1 h of adaptation to transparent cages, mice received a subcutaneous (s.c.) injection of 1500 μ L of HB, TG, TG-Ibu, and NioIbu into the loose skin over the interscapular area. One hundred and twenty minutes after sample injection, mice received an intraperitoneal (i.p.) injection (10 mL/kg) of 0.6% acetic acid solution. A writhing is characterized by a wave of abdominal muscle contractions accompanied by body elongation and the extension of

one or both hind limbs. The number of writhes in a 20-min period was counted, starting 5 min after acetic acid injection.

Capsaicin-Induced Paw Licking

The method used was similar to the one previously described [26]. Mice were allowed to adapt to transparent cages individually for 1 h before testing. Then, s.c. injections of samples (HB, TG, TG-Ibu, and NioIbu, 40 μ L) were performed in the dorsal surface of mice hind paw for 120 min before 1.6 μ g of capsaicin (20 μ L). A micro syringe with a 26-gauge needle was used to inject capsaicin and samples. The time (in seconds) the animals spent licking the injected paw, for a total period of 5 min, was registered and considered as indicative of pain. Capsaicin was dissolved in DMSO as a stock solution and stored at -20 °C. On the test day, this solution was diluted in order to obtain the final concentration of 1.6 μ g/20 μ L in DMSO:saline (1:3 v:v).

Zymosan-Induced Hyperalgesia

In these experiments, 20 μ L of zymosan A (2.5% w/v in saline) were administered s.c. into the dorsal surface of one hind paw. Then, thermal thresholds were determined, as previously reported [27]. Briefly, mice were placed in clear plastic boxes with a glass floor and allowed to acclimatize to their surroundings for at least 1 h in a temperature-controlled (21 °C) experimental room for three consecutive days prior to testing. On the test day, the animals were acclimatized to the experimental room 1 h before paw withdrawal latency (PWL) was measured. Attention was taken to start the test when the animal was not walking, with its hind paw in contact with the glass floor of the apparatus. A radiant heat source was directed at the mouse footpad until an aversive action was observed, such as paw withdrawal, foot drumming, or licking. A timer automatically measured in seconds the paw withdrawal latency. The heat source was set to an intensity of 30 and a cutoff time of 15 s was used to prevent tissue damage. Animals were first tested to determine their baseline PWL; after zymosan injection, the PWL (s) of each animal in response to the plantar test was determined again at 1, 2, 3, 4, 5, 24, and 48 h. In these experiments, HB, TG, TG-Ibu, and NioIbu were injected s.c. in a volume of 40 μ L in the dorsal surface of mice hind paw, 15 min before zymosan injection.

Neuropathy-Induced Allodynia and Hyperalgesia

The chronic constriction injury (CCI) model was carried out as previously described [28], with slight modifications [23]. Briefly, mice were anesthetized with chloralium hydrate-xylazine (400 + 10 mg/kg, i.p.). The right sciatic nerve was exposed at the mid-thigh level and, in the vicinity of the sciatic nerve trifurcation, was loosely tied with two ligatures of nylon black monofilament (9-0 non-absorbable, S&T, Neuhausen, Switzerland). Ligatures spaced 1.5–2 mm apart. Then, the muscles and the skin were closed with sutures. These animals were used in two nociceptive tests in the following order: mechanical allodynia followed by thermal hyperalgesia. The threshold for mechanical allodynia was assessed with the dynamic plantar aesthesiometer (Ugo Basile, Italy). Animals were trained on the apparatus, consisting of clear cages with a wire mesh floor, for 3 days before experimental sessions to allow for acclimatization. When the animal was at rest, a straight metal filament exerting an increasing upward force at a constant rate (5 g/s) with a maximum cutoff force of 50 g was placed under the plantar surface of the hind paw. Measurement was stopped when the paw was withdrawn and the results were expressed in grams. The measurement was repeated three times for each paw and averaged.

The development of thermal hyperalgesia was measured by subjecting the injured animals to the plantar test, as described in the “Zymosan-induced hyperalgesia” section.

Behavioural assessments of CCI-induced allodynia and thermal hyperalgesia were carried out 10 days after nerve injury, and behavioural responses compared with the ones measured before surgery. In these experiments, s.c. injection volumes of 40 μ L of HB, TG, TG-Ibu, and NioIbu were performed in the dorsal surface of mice hind paw.

Data Analysis and Statistics

Experimental data are presented as mean \pm standard error of the mean (s.e.m.). Statistically significant differences between groups were calculated with an analysis of variance (ANOVA) followed by Tukey’s post-hoc comparisons. Data were analyzed using the GraphPad Prism 6.03 software. The criterion for significance was set at $P < 0.05$. The data and statistical analysis conformed to the recommendations on experimental design and analysis in pharmacology [29].

Results

Nanovesicle Formulation and Characterization

All *in vivo* tests were performed by administration of well-characterized (Table 2) and stable (at least 3 months when stored at 4 °C) pH-sensitive vesicles (Nio, NioIbu). AFM characterization indicates that niosomes have a spherical shape (Figure 2). In agreement with DLS, AFM images indicate that NioIbu nanovesicles are smaller and have a less-uniform size than the Nio ones. Sizes deduced from AFM images seem underestimated with respect to the DLS results. In particular, for both the samples, the diameter evaluated by AFM is 70% of that evaluated by DLS, probably due to the approximations assumed in the model. In particular, Ibuprofen-loaded vesicles show the appropriate dimensions and zeta potential to be tested in animal studies. Drug entrapment efficiency is useful to perform *in vivo* studies, and the bilayer fluidity is quite high to ensure drug release, as reported in Rinaldi et al. [21]. This selection was carried out based on the best in-vitro performance of the sample, in particular in terms of the percentage of released drug [21]; in this previous study, sample characterization in the presence of different pH conditions was carried out, and the pH sensitivity of the selected formulation was confirmed.

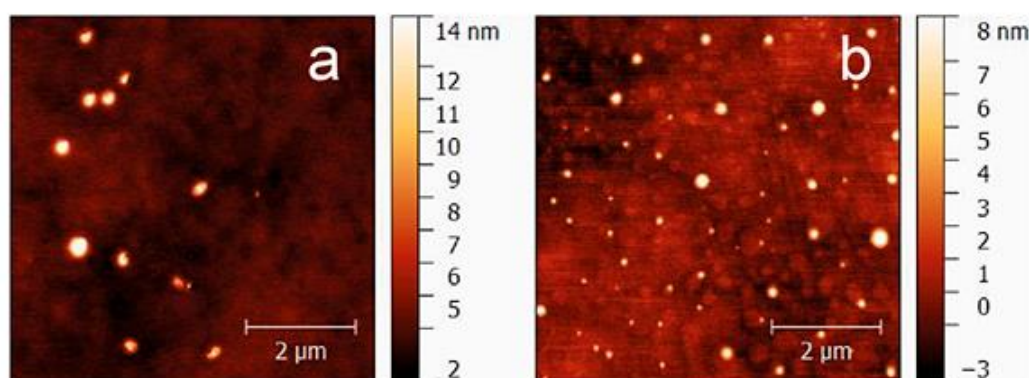


Figure 2. AFM images of Nio (a) and NioIbu (b) samples.

Table 2. Vesicle characterization. Nio, pH-Tw20Gly niosomes; NioIbu, pH-Tw20Gly niosomes loaded with a 5% Ibuprofen Hepes solution.

Niosomes	Diameter (nm)	AFM Diameter (nm)	ζ Potential (mV)	Polydispersity Index	Fluorescence Anisotropy (AU)	Loaded Drug Conc. (mg/mL)
Nio	215.0 ± 3.0	152 ± 18	-41.0 ± 1.2	0.160 ± 0.08	0.17 ± 0.01	-
NioIbu 5%	122.1 ± 19.6	89 ± 24	-40.2 ± 0.1	0.404 ± 0.05	0.20 ± 0.04	0.37 ± 0.05

Writhing Test

The *in vivo* antinociceptive activity of NioIbu was first assessed through a writhing test (Figure 2). As detailed in the experimental procedure section, acetic acid was used to induce peripheral pain. Analgesic activity was determined by recording the decrease in the number of writhes after acetic acid injection. The acetic-acid-induced writhing test in mice is the most commonly used method for measuring preliminary antinociceptive activity, since, in this test, both central and peripheral analgesics are detected. In these experiments, tested mice were injected with acetic acid 120 min after drug treatment. Statistical analysis revealed significant differences between treatments [$F_{(3, 28)} = 5.545, P = 0.0041$]. In this test, the administration of TG or TG-Ibu did not change the response to acetic acid in mice (Figure 3). Strong inhibition of the number of writhes was instead observed when NioIbu was administered 120 min before the acetic acid (Figure 3). In comparison with the TG group, NioIbu significantly reduced the number of writhes ($P < 0.05$), and the inhibition ratio was 52.5.

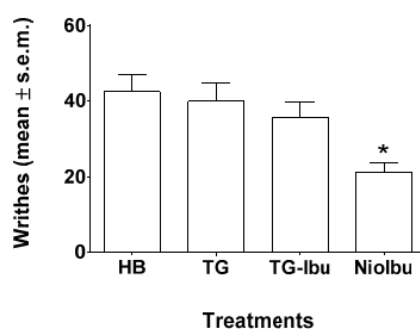


Figure 3. Effects of Hapes buffer (HB), the unstructured surfactant formulation (TG), the unstructured surfactant formulation with the same Ibuprofen (IBU) concentration (TG-Ibu), and TW20-Gly loaded with IBU (NioIbu) on the number of writhes induced by acetic acid. Samples were subcutaneously injected 120 min before acid acetic injection. * is for $P < 0.05$ versus TG. $N = 8$.

Capsaicin Test

In order to better evaluate the antinociceptive activity of ibuprofen-loaded vesicles, we also performed the capsaicin test (Figure 4). This test reflects acute pain responses related to neurogenic inflammation. In sensory neurons, capsaicin is an activator of the TRPV1 channels present in C-fibers and, to a lesser extent, $A\delta$. After injection, capsaicin shows a biphasic effect, i.e., it stimulates TRPV1 located in sensory neurons, producing a rapid phase of burning sensation, and local vascular and extravascular

responses, followed by a persistent desensitization with concomitant long-lasting analgesia. Statistical analysis revealed significant differences between treatments, as revealed by ANOVA ($F_{(3, 36)} = 10.22, P < 0.0001$). In this test, neither TG nor TG-Ibu reduced the duration of the licking response as compared with the HB-treated mice (Figure 4). A statistically significant antinociceptive effect was shown for NioIbu (inhibition ratio, 55.4%, $P < 0.001$) versus TG-treated mice.

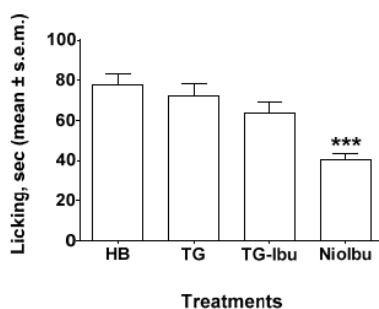


Figure 4. Effects of HEPES buffer (HB), the unstructured surfactant formulation (TG), the unstructured surfactant formulation with the same Ibuprofen (IBU) concentration (TG-Ibu), and TW20-Gly loaded with IBU (NioIbu) on the time spent licking the capsaicin-injected paw. Samples were injected subcutaneously in the dorsal surface of the hind paw 120 min before capsaicin injection. *** is for $P < 0.001$ versus TG. $N = 10$.

Zymosan-Induced Hyperalgesia

A s.c. injection of zymosan into mice footpad induces persistent dose- and time-dependent thermal and mechanical hyperalgesia associated with inflammation up to 24 h after treatment (Figure 5). Primary hyperalgesia in the hind paw inflammation model is thought to result from a release of pro-inflammatory mediators that include bradykinin, cytokines, and prostaglandins [30,31]. The reduction in latency response to a thermal stimulus applied to a paw and induced by zymosan was measured as a percentage. In these experiments, samples were injected into the dorsal surface of the right hind paw 15 min before zymosan injection. As observed in the writhing and capsaicin test, TG and TG-Ibu did not affect the decrease in nociceptive threshold induced by zymosan. On the contrary, the highest increase in pain threshold was observed in NioIbu-treated mice. (Figure 5). Furthermore, the increase in the nociceptive threshold induced by NioIbu was long-lasting, since two-way ANOVA revealed significant differences from 3 to 24 h after NioIbu treatment ($F_{(10, 135)} = 3.44, P = 0.0005$).

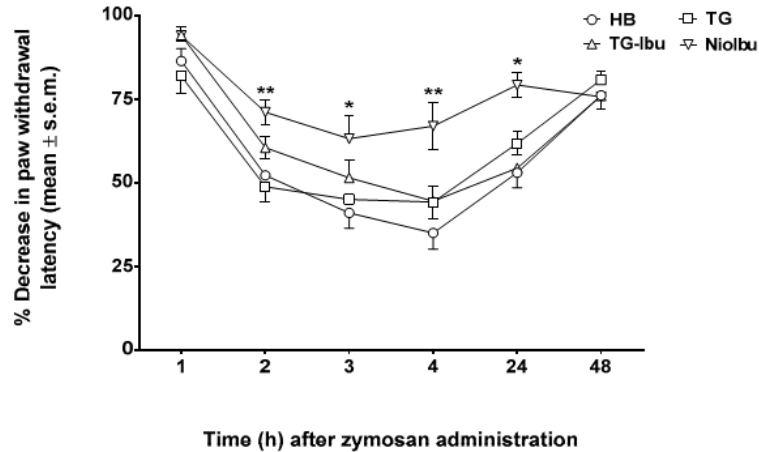


Figure 5. Effects of Hepes buffer (HB), the unstructured surfactant formulation (TG), the unstructured surfactant formulation with the same Ibuprofen (IBU) concentration (TG-Ibu), and TW20-Gly loaded with IBU (NioIbu) on zymosan-induced hyperalgesia. * is for $P < 0.05$ and ** is for $P < 0.01$ versus TG. $N = 10$.

Neuropathy-Induced Allodynia and Hyperalgesia

Neuropathic pain is a chronic condition caused by injury to the nervous system. This condition is characterized by spontaneous pain, as well as by exaggerated pain responses to painful stimuli (hyperalgesia) and to normally non-painful stimuli (allodynia). In our experiments, allodynia and hyperalgesia were measured 10 days after nerve injury, because this is when the pain threshold reaches the minimum value. The results obtained in these experiments are shown in Figure 6 and Figure 7. When allodynia was measured (Figure 6), two-way ANOVA showed a significant difference between treatments ($F_{(12, 126)} = 4.453$; $P < 0.0001$). A Tukey's multiple comparison test demonstrated that NioIbu significantly increased paw withdrawal latency from 1 to 3 h after treatment, whereas TG-Ibu induced a transient, not significant increase in the nociceptive threshold (Figure 6).

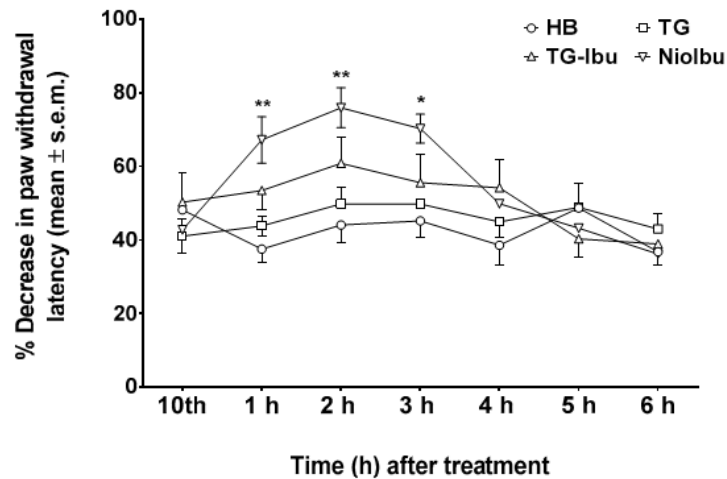


Figure 6. Effects of HEPES buffer (HB), the unstructured surfactant formulation (TG), the unstructured surfactant formulation with the same Ibuprofen (IBU) concentration (TG-Ibu), and TW20-Gly loaded with IBU (NioIbu) on allodynia induced by a chronic constriction injury of the right sciatic nerve. * is for $P < 0.05$ and ** is for $P < 0.01$ versus TG. $N = 8$.

In the same way, two-way ANOVA revealed significant differences in pain threshold when hyperalgesia was measured ($F_{(12, 126)} = 6.811$; $P < 0.0001$) (Figure 7). NioIbu increased the pain threshold from 2 h up to 4 h after treatment, whereas the increase in the pain threshold observed 1 h after TG-Ibu administration was not statistically significant.

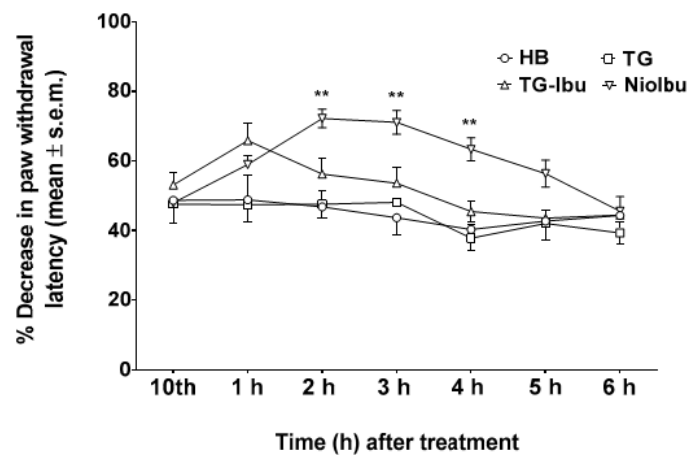


Figure 7. Effects of HEPES buffer (HB), the unstructured surfactant formulation (TG), the unstructured surfactant formulation with the same Ibuprofen (IBU) concentration (TG-Ibu), and TW20-Gly loaded with IBU (NioIbu) on hyperalgesia induced by a chronic constriction injury of the right sciatic nerve. * is for $P < 0.05$ and ** is for $P < 0.01$ versus TG. $N = 8$.

Discussion

Several researchers have focused on alternative drug delivery systems to overcome the difficulties associated with the distribution and effectiveness of analgesic drugs. This is

mainly due to the low capability of analgesic drugs to pass across biological membranes [32]. One of the strategies adopted to overcome these limitations was loading the drugs into liposomes, which are spherical vesicles composed of phospholipids, such as phosphatidylcholine and phosphatidyl-serine, and possibly other lipids as well [33]. However, liposomes have high production costs due to the phospholipids employed and tend to fuse or aggregate, resulting in an early release of the vesicle payload. Moreover, phospholipids are prone to oxidative degradation. Finally, liposomes have low solubility and stability, and their applicability is limited because they have short half-lives in blood circulation [13,34,35]. To overcome these constraints, we decided to use a new non-toxic drug delivery system, the niosomes. These carriers offer several advantages compared to liposomes: a higher capability to entrap lipophilic, hydrophilic, and amphiphilic drugs; an ability to reach the site of action via oral, parenteral, and topical routes of administration; and a lower cost. [36]. Recently, Di Marzio et al. [13] described specific pH-sensitive, non-ionic surfactant vesicles with polysorbate-20 (Tween-20)/Chems as a good delivery system for analgesic drugs, which increase the stability and affinity in the tissue pH alterations that occur during inflammatory pathologic conditions [37]. These vesicles showed the ability to control and sustain release as well as to protect drugs from catalytic enzymes, thereby increasing drug stability.

Niosomes containing pH-sensitive components, such as TW20Gly, that protonate at lower pH [35] showed bilayer destabilization, leading to localized drug release. This approach could be useful in targeting inflamed tissues. In this study, we evaluated the antinociceptive effects of s.c. injections of Ibuprofen-loaded, pH-sensitive niosomes in comparison with the free form of the drug. To address this issue, we utilized mice under different pain stimuli. This work demonstrates that the use of these nanocarriers enhances the therapeutic efficacy of Ibuprofen, since Ibuprofen-loaded niosomes were effective in reducing pain in laboratory mice. The use of nanovesicles as delivery systems has already been successfully exploited to supply compounds topically and orally. In fact, some studies showed that NSAID-loaded vesicles have better performance in terms of prolonged drug release [38] and improved therapeutic effects [39] compared with the free form of the same compound. Considering that niosomes are a very promising system to administer compounds of different features topically or orally [40,41,42], we evaluated the capability of niosomes to increase antinociceptive

effects of Ibuprofen also in terms of lasting effects after s.c injection. Writhing and capsaicin tests are screening assays commonly used to study peripheral and central antinociceptive activity. Our results showed that, when Ibuprofen-loaded niosomes were administered, there was an increase in the positive response time. In fact, when Ibuprofen was given 120 min earlier, the antinociceptive activity was maintained only in the niosomal form and not in the free form. The capsaicin test confirmed the long-lasting effects of Ibuprofen-loaded niosomes. Similar results were obtained with diclofenac-loaded liposomes administered orally, as reported by Goh et al. [43]. Consistently, in a formalin test, Ibuprofen-loaded niosomes displayed a peripheral antinociceptive activity and were more effective than free Ibuprofen in suppressing inflammatory pain. The niosomal form also had a long-lasting action, while the free form was probably rapidly catabolized [16]. Therefore, the encapsulation of the drug into niosomes significantly enhances drug efficacy and increases the durability of antinociceptive effects. This allows for a reduction in doses and, consequently, might also reduce the drug's side effects.

Some studies reported that nano-formulations reduce hyperalgesic responses to thermal stimuli more efficiently than free drugs [44,45]. Our results on zymosan-induced hyperalgesia are in line with these studies and demonstrate that Ibuprofen-loaded, pH-sensitive niosomes were able to reduce nociception up to 24 h after administration. These results confirm that niosomes release the encapsulated drug efficiently when behavioural experiments were performed. Similarly, Ibuprofen-loaded niosomes decrease neuropathic pain, since the treatment reduced both hyperalgesia and allodynia induced by chronic sciatic nerve constriction.

The increase in drug activity when released by niosomes could be explained by the capability of niosomes to transport lipophilic drugs, in this case Ibuprofen, across tissue membranes. This facilitates drug diffusion around the site of application and consequently improves efficacy [13,22]. In conclusion, the present study reveals that Ibuprofen-loaded, pH-sensitive niosomes are able to produce consistent and long-lasting antinociceptive effects. The antinociceptive effects of Ibuprofen-loaded niosomes were observed both in acute and chronic animal models of pain and these results, together with those reported in our previous study [21], suggest that an Ibuprofen pH-sensitive nanocarrier formulation could be further developed and used to treat different pain conditions in humans.

References

1. Patel A, Bell M, O'Connor C, et al. Delivery of ibuprofen to the skin. *Int. J. Pharm.* 2013;457:9–13.
2. Vane JR, Botting RM. Anti-inflammatory drugs and their mechanism of action. *Inflamm. Res.* 1998;47:78–87.
3. Doherty NS, Beaver TH, Chan KY, et al. The role of prostaglandins in the nociceptive response induced by intraperitoneal injection of zymosan in mice. *Br. J. Pharmacol.* 1987;91:39–47.
4. Brunton LL, Chabner BA, Knollman BC Goodman & Gilman's the Pharmacological Basis of Therapeutics. 12th ed. McGraw-Hill Medical; New York, NY, USA: 2011.
5. Moffat AC, Osselton MD, Widdop B. Clarke's Analysis of Drugs and Poisons: In Pharmaceuticals, Body Fluids and Postmortem Material, 2. Pharmaceutical Press and American Pharmacists' Association; London, UK: 2004. p. 1125.
6. Berner G, Engels B, Vögtle-Junkert U. Percutaneous ibuprofen therapy with Trauma-Dolgit gel: Bioequivalence studies. *Drugs Exp. Clin. Res.* 2004;XV:559–564.
7. Pereira-Leite C, Nunes C, Reis S. Interaction of nonsteroidal anti-inflammatory drugs with membranes: *In vitro* assessment and relevance for their biological actions. *Prog. Lipid Res.* 2013;52:571–584.
8. Stoye I, SchrDer K., Müller-Goymann C.C. Transformation of a liposomal dispersion containing ibuprofen lysinate and phospholipids into mixed micelles—Physico-chemical characterization and influence on drug permeation through excised human stratum corneum. *Eur. J. Pharm. Biopharm.* 1998;46:191–200.
9. Abdullah GZ, Abdulkarim MF, Salman IM, et al. *In vitro* permeation and *in vivo* anti-inflammatory and analgesic properties of nanoscaled emulsions containing ibuprofen for topical delivery. *Int. J. Nanomed.* 2011;6:387–396.
10. Santi P, Nicoli S, Colombo G, et al. Post-iontophoresis transport of ibuprofen lysine across rabbit ear skin. *Int. J. Pharm.* 2003;266:69–75.
11. Park ES, Chang SY, Hahn M, et al. Enhancing effect of polyoxyethylene alkyl ethers on the skin permeation of ibuprofen. *Int. J. Pharm.* 2000;209:109–119.
12. Brown MB, Hanpanitcharoen M, Martin GP. An *in vitro* investigation into the effect of glycosaminoglycans on the skin partitioning and deposition of NSAIDs. *Int. J. Pharm.* 2001;225:113–121.
13. Di Marzio L, Marianecchi C, Petrone M, et al. Novel pH-sensitive non-ionic surfactant vesicles: Comparison between Tween 21 and Tween 20. *Colloids Surf. B Biointerfaces.* 2011;82:18–24.
14. Dalmoro A, Bochicchio S, Nasibullin SF, et al. Polymer-lipid hybrid nanoparticles as enhanced indomethacin delivery systems. *Eur. J. Pharm. Sci.* 2018;121:16–28.
15. Rinaldi F, Hanieh PN, Chan LKN, et al. Chitosan Glutamate-Coated Niosomes: A Proposal for Nose-to-Brain Delivery. *Pharmaceutics.* 2018;10:38.
16. Marianecchi C, Di Marzio L, Rinaldi F, et al. Niosomes from 80s to present: The state of the art. *Adv. Colloid Interface.* 2014;205:187–206.
17. Rajera R, Nagpal K, Singh SK, et al. Niosomes: A controlled and novel drug delivery system. *Biol. Pharm. Bull.* 2011;34:945–953.
18. Edlow DW, Sheldon WH. The pH of inflammatory exudates. *Proc. Soc. Exp. Biol. Med.* 1971;137:1328–1332.

19. Naghavi M, John R, Naguib S, et al. pH Heterogeneity of human and rabbit atherosclerotic plaques: A new insight into detection of vulnerable plaque. *Atherosclerosis*. 2002;164:27–35.
20. Gatenby RA, Gillies RJ. Why do cancers have high aerobic glycolysis? *Nat. Rev. Cancer*. 2004;4:891–899.
21. Rinaldi F, Del Favero E, Rondelli V, et al. pH-sensitive niosomes: Effects on cytotoxicity and on inflammation and pain in murine models. *J. Enzym. Inhib. Med. Chem*. 2017;32:538–546.
22. Marianecchi C, Rinaldi F, Di Marzio L, et al. Ammonium glycyrrhizinate-loaded niosomes as a potential nanotherapeutic system for anti-inflammatory activity in murine models. *Int. J. Nanomed*. 2014;9:635–651.
23. Carafa M, Marianecchi C, Rinaldi F, et al. Span and Tween neutral and pH-sensitive vesicles: Characterization and *in vitro* skin permeation. *J. Liposome Res*. 2009;19:332–334.
24. Kilkeny C, Browne WJ, Cuthill IC, et al. Improving bioscience research reporting: The ARRIVE guidelines for reporting animal research. *PLoS Biol*. 2010;8:1000412.
25. Pieretti S, Di Giannuario A, Capasso A, et al. Effects induced by cysteamine on chemically-induced nociception in mice. *Life Sci*. 1994;54:1091–1099.
26. Sakurada T, Katsumata K, Tan-No K, et al. The capsaicin test in mice for evaluating tachykinin antagonists in the spinal cord. *Neuropharmacology*. 1992;31:1279–1285.
27. Colucci M, Maione F, Bonito MC, et al. New insights of dimethyl sulphoxide effects (DMSO) on experimental *in vivo* models of nociception and inflammation. *Pharmacol. Res*. 2008;57:419–425.
28. Bennett GJ, Xie YK. A peripheral mononeuropathy in rat that produces disorders of pain sensation like those seen in man. *Pain*. 1988;33:87–107.
29. Curtis MJ, Bond RA, Spina D, et al. Experimental design and analysis and their reporting: New guidance for publication in *BJP. Br. J. Pharmacol*. 2015;172:3461–3471.
30. Bélichard P, Landry M, Faye P, et al. Inflammatory hyperalgesia induced by zymosan in the plantar tissue of the rat: Effect of kinin receptor antagonists. *Immunopharmacology*. 2000;46:139–147.
31. Ren K, Dubner R. Inflammatory Models of Pain and Hyperalgesia. *ILAR J*. 1999;40:111–118.
32. Lucio M, Lima JL, Reis S. Drug-membrane interactions: Significance for medicinal chemistry. *Curr. Med. Chem*. 2010;17:1795–1809.
33. Gaur PK, Bajpai M, Mishra S, et al. Development of ibuprofen nanoliposome for transdermal delivery: Physical characterization, *in vitro/in vivo* studies, and anti-inflammatory activity. *Artif. Cells Nanomed. Biotechnol*. 2016;44:370–375.
34. Bozzuto G, Molinari A. Liposomes as nanomedical devices. *Int. J. Nanomed*. 2015;10:975–999.
35. Masotti A, Vicennati P, Alisi A, et al. Novel Tween 20 derivatives enable the formation of efficient pH-sensitive drug delivery vehicles for human hepatoblastoma. *Bioorg. Med. Chem. Lett*. 2010;20:3021–3025.
36. Verma S, Singh SK, Syan N, et al. Nanoparticle vesicular system: A versatile tool for drug delivery. *J. Chem. Pharm. Res*. 2010;2:496–509.
37. Lehner R, Wang X, Wolf M, et al. Designing switchable nanosystems for medical application. *J. Control. Release*. 2012;161:307–316.

38. Das MK, Palei NN. Sorbitan ester niosomes for topical delivery of rofecoxib. *Indian J. Exp. Biol.* 2011;49:438–445.
39. Naresh RA, Raja GK, Pillai N, et al. Anti-inflammatory activity of niosome encapsulated diclofenac sodium in arthritic rats. *Indian J. Pharmacol.* 1994;26:46–48.
40. Shahiwala A, Misra A. Studies in topical application of niosomally entrapped Nimesulide. *J. Pharm. Pharm. Sci.* 2002;5:220–225.
41. Goh JZ, Tang SN, Zuraini A, et al. Enhanced anti-inflammatory effects of nanoencapsulated diclofenac. *Eur. J. Inflamm.* 2013;11:855–861.
42. Sankhyan A, Pawar P. Recent Trends in Niosome as Vesicular Drug Delivery System. *J. Appl. Pharm. Sci.* 2012;2:20–32.
43. Goh JZ, Tang SN, Chiong HS, et al. Evaluation of antinociceptive activity of nanoliposome-encapsulated and free-form diclofenac in rats and mice. *Nanomedicine.* 2014;10:297–303.
44. Narasimha Reddy D, Udupa N. Formulation and Evaluation of Oral and Transdermal Preparations of Flurbiprofen and Piroxicam Incorporated with Different Carriers. *Drug Dev. Ind. Pharm.* 2008;19:843–852.
45. Joshi SK, Hernandez G, Mikusa JP, et al. Comparison of antinociceptive actions of standard analgesics in attenuating capsaicin and nerve-injury-induced mechanical hypersensitivity. *Neuroscience.* 2006;143:587–596.

GENERAL DISCUSSION

Two types of treatments can be used to treat inflammatory and chronic pain: nonsteroidal anti-inflammatory drugs (NSAIDs) and opioids. Very often there are several side effects, such as gastrointestinal lesions [1] and nephrotoxicity [2], in the case of treatment with NSAIDs, when they are used for a long time, and respiratory depression, tolerance, and physical dependence for opioids [3]. Thus, the identification of new potential targets which may affect pain and inflammatory processes is becoming an urgent clinical and therapeutic need.

In recent years, in close collaboration with various national and foreign research groups, we have established an efficient and highly multidisciplinary approach to investigate the pharmacological profile of new compounds and herbal derivatives with significant antinociceptive and antiinflammatory effects. In particular, my colleagues and I have conducted *in vivo* studies at National Center for Drug Research and Evaluation of Istituto Superiore di Sanità in Rome, using murine models of pain and nociception. So the research approach involves the *in vivo* studies of natural and non-natural compounds, which have been produced by our colleagues through the use of molecular modelling and/or new synthetic methods for their synthesis.

The use of natural components in the pharmaceutical field is receiving growing attention from the scientific world. In fact, there is a greater interest in natural compounds, such as dietary supplement and herbal remedies, which have been used for centuries to reduce pain and inflammation [4]. Many of these natural compounds also work by inhibiting the inflammatory pathways in a similar manner as NSAIDs. In addition to the COX pathway, many natural compounds act to inhibit nuclear factor- κ B (NF- κ B) inflammatory pathways [4].

Based on these considerations we first investigated, in Chapter 1, the long-lasting effects induced by ammonium glycyrrhizinate (AG), an endemic natural compound derived from *Glycyrrhiza glabra*, after a single administration in mice using animal models of pain and inflammation [5].

It has been previously demonstrated that AG is able to induce antinociceptive effects in the writhing test, formalin test, and thermal hyperalgesia [6,7] and these effects were observed from 1 to 5 h after AG administration. Our data demonstrated, for the first time, that AG exerts long-lasting antinociceptive effects, since AG-induced

antinociception was observed until 24–48h after a single administration. In particular, our *in vivo* results clearly indicate that a single intraperitoneal injection of AG was able to produce anti-inflammatory effects in zymosan-induced paw edema and peritonitis. Moreover, in several animal models of pain (writhing test, formalin test and hyperalgesia induced by zymosan), AG administered 24h before the tests was able to induce a strong antinociceptive effect [5].

Driven by the curiosity to investigate the role of AG in diabetic peripheral neuropathy (DPN), one of the major complication of chronic diabetes [8], we analyzed the *in vivo* effects of AG in preventing or mitigating neuropathic hyperalgesia induced by streptozotocin (STZ) injection [9]. The results are reported in the Chapter 2. We found that a short-repeated treatment with AG was able to contrast significantly thermal hyperalgesia. In fact, when AG was first administered 15 days after STZ, a nonsignificant increase in paw withdrawal latencies was observed. AG was administered again at days 17 and 19 after STZ injection, and at this time, a strong increase in paw latency was recorded. This is believed to be primarily due to reduce the HMGB1 expression, a protein which plays an important role in the pathogenesis of inflammatory and autoimmune disease [10], as recently reported in Zucker diabetic rat and ob/ob mice [11]. In fact, it is known that glycyrrhizin binds directly to both HMG boxes of HMGB1 [12] and inhibits extracellular HMGB1 cytokine activities, and protected spinal cord, liver, brain, and myocardium against ischemia–reperfusion (I/R)-induced injury in experimental animals [13].

Taken together these findings reported in Chapter 1 and in Chapter 2 suggest the potential use of AG for clinical treatment of pain and/or inflammatory-related diseases, included diabetic peripheral neuropathy.

As mentioned at the beginning of this section, the research approach involves the *in vivo* studies of natural and non-natural compounds, which have been produced through the use of molecular modelling and/or new synthetic methods for their synthesis. Notably, there has been a growing interest for discovering novel natural product-derived potential modulators of nociception, a hot research topic worldwide. In fact, natural products have an important role in the discovery of analgesic and antiinflammatory drugs along with the determining of the complex mechanisms involved in pain transmission and pain relief. Lately, several substances with antinociceptive actions have been purified

from natural sources and further identified, resulting in novel structural classes and more understanding of the underlying pharmacological mechanisms of actions. Yet, natural products still hold great potential for the discovery of novel agents for treatment of pain disorders and potentially drug addictions with exciting pharmacological profiles [14].

Based on that, our research was focused on the evaluation of the antinociceptive and anti-inflammatory effects of two natural compounds, rubiscolin-6 and soymorphin-6, and their C-terminal amides derivatives [15]. The results are reported in the Chapter 3. Soymorphin (SM peptide sequence: Tyr-Pro-Phe-Val-Val-Asn-Ala) is an opioid eptapeptide derived from the enzymatic digestion of soy proteins, which are consumed in cereals. Rubiscolin-6 (amino acid sequence: YPLDLF) is an opioid peptide derived from the plant enzyme *Rubisco*. In order to investigate the antinociceptive activities of these natural and non-natural compounds my colleagues and I conducted *in vivo* studies using murine models of pain and inflammation. *In vivo* experiments of rubiscolin-6 were mostly in line with those obtained in Yang's experimental model of acute pain in laboratory animals [16,17]. In fact, rubiscolin-6 was able to increase the nociceptive threshold to thermal stimuli after supraspinal administration, but was ineffective after subcutaneous administration in an experimental paradigm of chemical-induced nociception as the formalin test. On the other hand, instead, its non-natural derivatives, rubiscolin-6 C-amide, centrally administered demonstrates a strong antinociceptive effect higher than rubiscolin-6, and it is effective after subcutaneous administration. This might be explained by the fact that, as reported by Cassel et al, rubiscolin peptides bind to and activate G protein signaling at DOR opioid receptors [18]. On the other hand, there is no records of the antinociceptive effects of soymorphine-6 in the literature. Based on the results of our experiments, we observed that both soymorphin-6 and its derivative soymorphin-6 C-amide induced a robust antinociceptive effect until 30 min after central administration in tail flick test but both peptides have not been able to change the behavioral response to chemical-induced nociception in the formalin test [15]. Starting from these results, we can say that rubiscolin-6 C-amide could have huge potential as food supplement with antinociceptive and anti-inflammatory property.

In addition to natural products also endogenous opioid peptides, such as β -endorphin, endomorphin, enkephalins, and dynorphins, could also be valid candidates for the treatment of pain and inflammation. In fact, these opioids act as neurotransmitters and

neuromodulators at three major classes of receptors, termed MOR, DOR and KOR, and produce analgesia [19]. In particular, dynorphin A and B, which are derived from PDYN, have relatively high affinity for KOR, but also some affinity for MOR and DOR. ENK and leu-enkephalin are endogenous ligands derived from PENK that display preferential binding to DOR, lower affinity for MOR, and negligible binding to KOR [20]. Endomorphin-1 and endomorphin-2 (EM-1 and EM-2) are MOR-selective endogenous peptides of so far unknown origin that have been found in distinct regions of rat brain as well as primary neurons and the spinal cord [21]. Like their endogenous counterparts, the opioid drugs, or opiates, act at these same receptors to produce both analgesia and undesirable side effects [22]. In particular, the discovery of the EM-1 and EM-2 raises the possibility that EMs might be a good alternative to the exogenous opioid morphine. The results of *in vitro* and *in vivo* studies have revealed that EM-1 and EM-2 exerted a more potent analgesia in acute and neuropathic pain than other opiates, such as morphine [23,24]. Compared with other opiates, EMs had remarkably fewer side effects [25]. However, EMs are associated with undesirable effects in certain animal experiments, such as tolerance and addiction, which restricted their development as therapeutic analgesics [26,27], and their low membrane permeability and susceptibility to enzymatic degradation also prohibit their direct clinical application [28].

Therefore, many attempts have been made to remodel the EMs and the other endogenous opioid to identify possible solutions, indicating their potential value in clinical application. Building on these premises, in the Chapter 4 of this thesis we report the *in vivo* biological profile of new six tetrapeptide models containing α -amino- γ -lactam of Freidinger in position 2 and 3, as analogues of EM-2 and DAPEA [D-Ala², des-Leu⁵], an enkephalin amide agonist of MOR/DOR [29].

Data collected by our colleagues revealed that one of them (peptide A2D) exhibited a strong selectivity and capacity to stimulate G-coupled MOR in two different functional assays. These results have been confirmed by us, through the mouse tail flick and formalin tests allowed to observe their antinociceptive effect *in vivo*. In fact, our results show that peptide A2D was able to selectively bind and activate MOR with a potent antinociceptive effect after intracerebroventricular administration, performing better than the parent compounds EM-2 and DAPEA. On the other hand, peptide A2D if administered subcutaneously lost its *in vivo* activity. Instead, peptide A3D is also able to

produce antinociceptive effect both in the acute and in the inflammatory phase of the formalin test. The explanation could lie in the fact that A3D has greater metabolic plasma stability than A2D after peripheral administration or it might be possible that A3D binds to other receptors involved in the mediation of the nociceptive stimuli in the periphery [30,31].

Another promising method of development of analgesics with reduced side effects and lack of tolerance is *in silico* studies, which allows to have a significant contribution in the identification of compounds capable of interacting with a specific molecular target [32]. These computational methods are relevant in limiting the use of animal models in pharmacological research, for aiding the rational design of novel and safe drug candidates, and for repositioning marketed drugs, supporting medicinal chemists and pharmacologists during the drug discovery trajectory [32]. KORs play a crucial role in the pathogenesis of various disorders affecting the central nervous system, such as depression, anxiety, and pain. They are widely expressed throughout the central and peripheral nervous system; among them dinorphins primarily activate the KORs with very low affinity for MOR and DOR [33]. In contrast to MOR and DOR receptor agonists, KOR agonists have been recognized as analgesics without addiction and tolerance insurgence, despite their tendency to induce dysphoria, anhedonia and hallucinations [34,35]. In the Chapter 5, a virtual screening workflow of a library consisting of ~6 million molecules was set up with the aim to find potential lead compounds that could manifest activity on the KOR. The entire *in silico* process furnished the necessary data to identify and estimate the most suitable compounds for synthesis and pharmacological tests, such as tripeptides 6 and 11. So we tested *in vivo* this two compounds, H-D-Tyr-Val-Val-O-(3-Br)-Bz (tripeptide 6) and H-D-Tyr-Val-Trp-OBz (tripeptide 11) [36]. *In vivo* tests revealed their ability to induce an antinociceptive effect after intracerebroventricular and subcutaneous administrations in the tail flick and formalin tests, respectively. Among them, peptide 11 is active also in the second phase of the last test. Although the results are not yet complete, this experimental approach allowed us to find interesting lead compounds for the next steps of structure optimization and pharmaceutical characterization.

The endogenous cannabinoid system plays a major role in the control of pain as well as in mood regulation, reward processing and the development of addiction along with opioid system [37]. The endogenous cannabinoid system comprises lipid

neuromodulators (endocannabinoids), enzymes for their synthesis and their degradation and two well-characterized receptors, cannabinoid receptors CB1 and CB2. Distribution of the two receptors in the central and peripheral system is rather different [38]. Indeed, CB1 is highly abundant in the central nervous system in areas involved in reward, regulation of appetite and nociception while CB2 was initially described as a peripheral receptor [39]. Both opioid and cannabinoid receptors are coupled to G proteins and are expressed throughout the brain reinforcement circuitry. In addition to their specific ligands, both systems have also been implicated in the action mechanism of several other addictive drugs, like ethanol, nicotine, or psychostimulants [37]. Endogenous and synthetic agonists of CB1 and CB2 receptors were subsequently reported to be effective in alleviating hyperalgesia in models of pain associated with nerve injury and inflammation [40]. In addition, CB1 receptor and endogenous cannabinoids are both involved in the management of appetite stimuli and food intake in the central region of the hypothalamus [41].

On this basis, we tested a series of lonidamine joined Leu-, tertLeu- and Val-amino acids with different C-terminal functional groups (LONI 1-4,11) as novel compounds with high CB1 receptor affinity and selectivity with different biological activity depending on the C-terminal substitution and amino acid residues and endowed with orexant/anorexant and antinociceptive activities [42]. The most *in vitro* active among them as an agonist towards cannabinoid receptors CB1 and CB2, (S)-1-(2,4-dichlorobenzyl)-N-(3,3-dimethyl-1-(methylamino)-1-oxobutan-2-yl)-1H-indazole-3-carboxamide (LONI11), and an antagonist (S)-2-(1-(2,4-dichlorobenzyl)-1H-indazole-3-carboxamido)-3-methylbutanoic acid (LONI4), were tested *in vivo* to evaluate their ability to stimulate or suppress feeding behavior after intraperitoneal administration as we can observe from the reported results in Chapter 6. Compounds LONI2 and LONI4 were found to inhibit food intake (anorexant effect) consistent with an inverse agonism at CB1 receptors. On the other hand, we observed a significant orexant effect for LONI11 consistent with a potent agonism at CB1 receptors. Considering the well-established analgesic effect of the synthetic CB1 agonist THC on pain [43], the full agonist LONI11 was further tested *in vivo* to study the antinociceptive effect at the central and periphery levels. Particularly, we found that LONI11 revealed a good analgesic effect after subcutaneous and intracerebroventricular administration *in vivo*

and a significant anti-inflammatory effect after subcutaneous injection, suggesting potential activity at the periphery [42].

Finally, our work has focused on alternative drug delivery systems to overcome the difficulties associated with the distribution and effectiveness of analgesic and anti-inflammatory drugs. An example is ibuprofen, that is completely absorbed after oral administration [44], the plasma level is still low several hours after topical application [45]. For these reasons, various studies have reported different techniques to increase the permeability of cell membranes and the transdermal transport of ibuprofen and other drugs [46-49].

In this thesis, we evaluated the analgesic activity of a new pH-sensitive formulation of niosomes containing Polysorbate 20 derivatized by Glycine and loaded with ibuprofen (NioIbu) in several animal models of pain and inflammation [50]. The results reported in Chapter 7 highlight the role of NioIbu that strongly increases Ibuprofen's analgesic activity, promoting a longer duration of action of this drug. In fact our results demonstrated that NioIbu, administered 2h before testing, reduced nociception, whereas the free form of ibuprofen was ineffective. In a model of inflammatory pain (hyperalgesia induced by zymosan) NioIbu induced a long-lasting reduction in hyperalgesia in treated mice. In a model of neuropathic pain induced by sciatic nerve chronic constriction, NioIbu reduced both neuropathy-induced allodynia and hyperalgesia [50].

FINAL CONCLUSION

As we have observed in the various chapters of this thesis, our compounds that we tested *in vivo* are of a different nature: natural components; sample produced by molecular modelling, such as *in silico* studies, and/or new synthetic methods for their synthesis from natural or endogenous compounds; agonist compounds of other receptor classes, such as CB1 and CB2 receptors; drugs conveyed by delivery systems, such as pH-sensitive niosomes. In conclusion, these findings create prospects for conducting clinical studies with the compounds presented, which show in fact their effectiveness for chronic pain and inflammation control.

References

1. Sinha M, Gautam L, Shukla PK, et al. Current perspectives in NSAID-induced gastropathy. *Mediat. Inflamm.* 2013;2013:258209.
2. Musu M, Finco G, Antonucci R, et al. Acute nephrotoxicity of NSAID from the foetus to the adult. *Eur. Rev. Med. Pharmacol. Sci.* 2011;15:1461–1472.
3. Benyamin R, Trescot AM, Datta S, et al. Opioid complications and side effects. *Pain Physician.* 2008;11:S105–S120.
4. Maroon JC, Bost JW, Maroon A. Natural anti-inflammatory agents for pain relief. *Surg Neurol Int.* 2010;1:80.
5. Maione F, Minosi P, Di Giannuario A, et al. Long-Lasting Anti-Inflammatory and Antinociceptive Effects of Acute Ammonium Glycyrrhizinate Administration: Pharmacological, Biochemical, and Docking Studies. *Molecules.* 2019 Jul 4;24(13):2453.
6. Khaksa G, Zolfaghari ME, Dehpour AR, Samadian T. Anti-inflammatory and anti-nociceptive activity of disodium glycyrrhethinic acid hemiphthalate. *Planta Med.* 1996;62:326–328.
7. Wang HL, Li YX, Niu YT, et al. Observing Anti-inflammatory and Antinociceptive Activities of Glycyrrhizin Through Regulating COX-2 and Pro-inflammatory Cytokines Expressions in Mice. *Inflammation.* 2015;38:2269–2278.
8. Cole JB, Florez JC. Genetics of diabetes mellitus and diabetes complications. *Nat. Rev. Nephrol.* 2020, 16, 377–390.
9. Ciarlo L, Marzoli F, Minosi P, et al. Ammonium Glycyrrhizinate Prevents Apoptosis and Mitochondrial Dysfunction Induced by High Glucose in SH-SY5Y Cell Line and Counteracts Neuropathic Pain in Streptozotocin-Induced Diabetic Mice. *Biomedicines.* 2021 May 26;9(6):608.
10. Magna M, Pisetsky DS. The role of HMGB1 in the pathogenesis of inflammatory and autoimmune diseases. *Mol Med.* 2014;20(1):138-146.
11. Thakur V, Sadanandan J, Chattopadhyay M. High-Mobility Group Box 1 Protein Signaling in Painful Diabetic Neuropathy. *Int. J. Mol. Sci.* 2020;21:881.
12. Mollica L, De Marchis F, Spitaleri A, et al. Glycyrrhizin Binds to High-Mobility Group Box 1 Protein and Inhibits Its Cytokine Activities. *Chem. Biol.* 2007;14:431–441.
13. Musumeci D, Roviello GN, Montesarchio D. An overview on HMGB1 inhibitors as potential therapeutic agents in HMGB1-related pathologies. *Pharmacol. Ther.* 2014;141:347–357.
14. Abdel-Rahman RF. Natural Products as a Source for Novel Analgesic Compounds. *Pain Relief - From Analgesics to Alternative Therapies*, Chapter 14. 2017.
15. Stefanucci A, Dimmito MP, Tenore G, et al. Plant-derived peptides rubiscolin-6, soymorphin-6 and their c-terminal amide derivatives: Pharmacokinetic properties and biological activity. *Journal of Functional Foods.* 2020; 73, 104154.
16. Yang S, Yunden J, Sonoda S, et al. Rubiscolin, a delta selective opioid peptide derived from plant Rubisco. *FEBS Letters.* 2001; 509:213-217.
17. Yang S, Sonoda S, Chen L, et al. Structure-activity relationship of rubiscolins as delta opioid peptides. *Peptides.* 2003;24:503-508.

18. Cassell RJ, Mores KL, Zerfas BL, et al. Rubiscolins are naturally occurring G protein-biased delta opioid receptor peptides. *European Neuropsychopharmacology*. 2019; 29(3):450-456.
19. Holden JE, Jeong Y, Forrest JM. The endogenous opioid system and clinical pain management. *AACN Clin Issues*. 2005 Jul-Sep;16(3):291-301.
20. Przewlocki R, Hassan AH, Lason W, et al. Gene expression and localization of opioid peptides in immune cells of inflamed tissue: functional role in antinociception. *Neuroscience*. 1992;48:491–500.
21. Zadina JE, Hackler L, Ge LJ, et al. A potent and selective endogenous agonist for the mu-opiate receptor. *Nature*. 1997;386:499–502.
22. Holden JE, Jeong Y, Forrest JM. The endogenous opioid system and clinical pain management. *AACN Clin Issues*. 2005 Jul-Sep;16(3):291-301.
23. Stone LS, Fairbanks CA, Laughlin TM, et al. Spinal analgesic actions of the new endogenous opioid peptides endomorphin-1 and -2. *Neuroreport*. 1997; 8: 3131-3135.
24. Tseng LF, Narita M, Suganuma C, et al. Differential antinociceptive effects of endomorphin-1 and endomorphin-2 in the mouse. *J Pharmacol Exp Ther*. 2000; 292: 576-583.
25. Czaplá MA, Gozal D, Alea OA, et al. Differential cardiorespiratory effects of endomorphin 1, endomorphin 2, DAMGO, and morphine. *Am J Respir Crit Care Med*. 2000; 162: 994-999.
26. Hung KC, Wu HE, Mizoguchi H, Tseng LF. Acute antinociceptive tolerance and unidirectional cross-tolerance to endomorphin-1 and endomorphin-2 given intraventricularly in the rat. *Eur J Pharmacol*. 2002; 448: 169-174.
27. Chen JC, Tao PL, Li JY, et al. Endomorphin-1 and -2 induce naloxone-precipitated withdrawal syndromes in rats. *Peptides*. 2003; 24: 477-481.
28. Kastin AJ, Fasold MB, Smith RR, et al. Saturable brain-to-blood transport of endomorphins. *Exp Brain Res*. 2001; 139: 70-75.
29. Della Valle A, Stefanucci A, Scioli G, et al. Selective MOR activity of DAPEA and Endomorphin-2 analogues containing a (R)- γ -Freidinger lactam in position two. *Bioorg Chem*. 2021 Jul 28;115:105219.
30. Sufka KJ, Watson GS, Nothdurft RE, Mogil JS. Scoring the mouse formalin test: validation study. *Eur. J. Pain* 2 1998, 351–358.
31. Gentilucci L, De Marco R, Cerisoli L. Chemical modifications designed to improve peptide stability: incorporation of non-natural amino acids, pseudo-peptide bonds, and cyclization. *Curr. Pharmaceutical des*. 16 2010, 3185–3203.
32. Brogi S, Ramalho TC, Kuca K, et al. Editorial: *In silico* Methods for Drug Design and Discovery. *Front Chem*. 2020 Aug 7;8:612.
33. Chavkin C, James IF, Goldstein A. Dynorphin is a specific endogenous ligand of the κ opioid receptor. *Science*. 1982;215:413–415.
34. Carlezon WA, Thome J, Olson VG, et al. Regulation of Cocaine Reward by CREB. *Science*. 1998;282:2272–2275.
35. Pfeiffer A, Brantl V, Herz A, Emrich HM. Psychotomimesis mediated by kappa opiate receptors. *Science*. 1986;233:774–776.
36. Stefanucci A, Iobbi V, Della Valle A, et al. *In silico* Identification of Tripeptides as Lead Compounds for the Design of KOR Ligands. *Molecules*. 2021 Aug 6;26(16):4767.
37. Befort K. Interactions of the opioid and cannabinoid systems in reward: Insights from knockout studies. *Front Pharmacol*. 2015 Feb 5;6:6.

38. Pertwee RG. Receptors and channels targeted by synthetic cannabinoid receptor agonists and antagonists. *Curr. Med. Chem.* 2010; 17, 1360–1381.
39. Maldonado R, Valverde O, Berrendero F. Involvement of the endocannabinoid system in drug addiction. *Trends Neurosci.* 2006; 29, 225–232.
40. Fox A, Bevan S. Therapeutic potential of cannabinoid receptor agonists as analgesic agents. *Expert Opin Investig Drugs.* 2005;14:695–703.
41. Carella AM, Conte M, Melfitano A, et al. Neuroendocrine Mediators, Food Intake and Obesity: A Narrative Review. *Int. J. Cardiol. Lipidol. Res.* 2014;1:18–32.
42. Dimmito MP, Stefanucci A, Pieretti S, et al. Discovery of Orexant and Anorexant Agents with Indazole Scaffold Endowed with Peripheral Antiedema Activity. *Biomolecules.* 2019 Sep 16;9(9):492.
43. Slomski A. THC for Chronic Pain. *JAMA.* 2018;320:1631.
44. Moffat AC, Osselton MD, Widdop B. Clarke's Analysis of Drugs and Poisons: In Pharmaceuticals, Body Fluids and Postmortem Material, 2. Pharmaceutical Press and American Pharmacists' Association; London, UK. 2004;1125.
45. Berner G, Engels B, Vögtle-Junkert U. Percutaneous ibuprofen therapy with Trauma-Dolgit gel: Bioequivalence studies. *Drugs Exp. Clin. Res.* 2004;XV:559–564.
46. Pereira-Leite C, Nunes C, Reis S. Interaction of nonsteroidal anti-inflammatory drugs with membranes: *In vitro* assessment and relevance for their biological actions. *Prog. Lipid Res.* 2013;52:571–584.
47. Stoye I, SchrDer K, Müller-Goymann CC. Transformation of a liposomal dispersion containing ibuprofen lysinate and phospholipids into mixed micelles—Physico-chemical characterization and influence on drug permeation through excised human stratum corneum. *Eur. J. Pharm. Biopharm.* 1998;46:191–200.
48. Abdullah GZ, Abdulkarim MF, Salman IM, et al. *In vitro* permeation and *in vivo* anti-inflammatory and analgesic properties of nanoscaled emulsions containing ibuprofen for topical delivery. *Int. J. Nanomed.* 2011;6:387–396.
49. Brown MB, Hanpanitcharoen M, Martin GP. An *in vitro* investigation into the effect of glycosaminoglycans on the skin partitioning and deposition of NSAIDs. *Int. J. Pharm.* 2001;225:113–121.
50. Marzoli F, Marianecchi C, Rinaldi F, et al. Antinociceptive Effects of pH-Sensitive Niosomes Loaded with Ibuprofen in Acute and Chronic Models of Pain. *Pharmaceutics.* 2019 Feb 1;11(2):62.

CURRICULUM VITAE

Paola Minosi

Via dei Platani 110, 00171 Roma (RM)

+39 366 9563999

e-mail: pminosi@erbc-group.com

paolam1990@libero.it



EDUCATIONAL AND WORK EXPERIENCE

- March 21, 2022 - current: **ASSISTANT TO DIRECTOR OF TOXICOLOGICAL STUDY** at **ERBC (EUROPEAN RESEARCH BIOLOGY CENTER)**, Via Tito Speri, 12 POMEZIA (RM).
- September 01, 2021 - March 4, 2022: **COLLABORATIVE PHARMACIST** at **Farmacia Alessandrina, Via dei Platani, 1B/5 - ROME (RM)** and **Farmacia Casilina, Via Casilina 478 - ROME (RM)**.
- April 01, 2017 - April 01, 2021: **BORSIST** at the **National Center for Research and Preclinical and Clinical Evaluation of Drugs of the Istituto Superiore di Sanità (ISS)**.

ACADEMIC INSTRUCTION

- January 2022 - current: **SECOND LEVEL MASTER'S PROGRAM IN: PRECLINIC AND CLINICAL DEVELOPMENT OF PHARMA: ETHICAL-SCIENTIFIC, REGULATORY AND ETHICAL DISCIPLINES** at **La Cattolica University of Rome**.
- September 2018 - May 2022: **PhD in PHARMACOLOGY AND TOXICOLOGY 34th cycle** at the **Dept. of Physiology and Pharmacology 'Vittorio Ersparmer' La Sapienza University of Rome**.
- September 2009 - September 2015: **Master's degree in PHARMACEUTICAL CHEMISTRY AND TECHNOLOGY (CTF)** at **La Sapienza University of Rome**.

- September 2004 - July 2009: DIPLOMA OF CLASSICAL MATURITY obtained at. Liceo Classico "Francesca Capece," Maglie (LE).

Publications

- **In Silico Identification of Tripeptides as Lead Compounds for the Design of KOR Ligands.** *Molecules*. Stefanucci A, Iobbi V, Della Valle A, Scioli G, Pieretti S, **Minosi P**, Mirzaie S, Novellino E, Mollica A. 2021;26(16):4767. IF: 4.41.
- **Selective MOR activity of DAPEA and Endomorphin-2 analogues containing a (R)- γ -Freidinger lactam in position two.** Della Valle A, Stefanucci A, Scioli G, Szűcs E, Benyhe S, Pieretti S, **Minosi P**, Sturaro C, Calò G, Zengin G, Mollica A. *Bioorg Chem*. 2021;115:105219. IF: 5.27.
- **Ammonium Glycyrrhizinate Prevents Apoptosis and Mitochondrial Dysfunction Induced by High Glucose in SH-SY5Y Cell Line and Counteracts Neuropathic Pain in Streptozotocin-Induced Diabetic Mice.** Ciarlo L, Marzoli F, **Minosi P**, Matarrese P, Pieretti S. *Biomedicines*. 2021; 9(6):608. IF: 6.08.
- **Soy-enriched bread, a pilot study to determine its beneficial effects in menopause.** Aloisi AM, Giustarini D, Ricci C, Ceccarelli I; Pieretti; S, Andre P, Migliorini S, Massai L, **Minosi P**, Casini I. *Physiology & Behavior*. Preprints 2021, 2021010601. IF: 3.24.
- **Acupuncture decreases pain and MIF salivary levels in men and women.** Ceccarelli I, Paulesu L, Fu BT, Pieretti S, Xu L, Tan RZ, Chen Y, Yang X, **Minosi P**, Romagnoli R, Aloisi AM. *Int J Complement Alt Med*. 2020;13(2):83–89. IF: 2.57.
- **Plant-derived peptides rubiscolin-6, soymorphin-6 and their c-terminal amide derivatives: Pharmacokinetic properties and biological activity.** Stefanucci A, Dimmito MP, Tenore G, Pieretti S, **Minosi P**, Zengin G, Sturaro C, Calò G, Novellino E, Cichelli A, Mollica A. *Journal of Functional Foods*. 2020; 73, 104154. IF: 4.45.
- **Small Molecules with Anti Prion Activity.** Mustazza C, Sbriccoli M, **Minosi P** and Raggi C. *Curr Med Chem*. 2020; 27(33):5446-5479. IF: 4.18.

- **Discovery of Orexant and Anorexant Agents with Indazole Scaffold Endowed with Peripheral Antiedema Activity.** Dimmito MP, Stefanucci A, Pieretti S, **Minosi P**, Dvorácskó S, Tömböly C, Zengin G, Mollica M. *Biomolecules*. 2019, 16; 9(9) 492. IF: 4.69.
- **Polypharmacy and nutraceuticals in veterans: pros and cons.** Sciarra T, Ciccotti M, Aiello P, **Minosi P**, Munzi D, Buccolieri C, Peluso I, Palmery M, Lista F. *Frontiers in Pharmacology*. 2019,10;10:994. IF: 5.81.
- **IL-17A neutralizing antibody regulates monosodium urate crystal-induced gouty inflammation.** Raucci F, Iqbal AJ, Saviano A, **Minosi P**, Piccolo M, Irace C, Caso F, Scarpa R, Pieretti S, Mascolo N, Maione. *Pharmacol Res*. 2019, 14:104351. IF: 7.65.
- **Long-Lasting Anti-Inflammatory and Antinociceptive Effects of Acute Ammonium Glycyrrhizinate Administration: Pharmacological, Biochemical, and Docking Studies.** Maione F, **Minosi P**, Di Giannuario A, Raucci F, Chini MG, De Vita S, Bifulco G, Mascolo N and Pieretti S. *Molecules*. 2019, 24(13):2453. IF: 4.41.
- **Long-Lasting, Antinociceptive Effects of pH-Sensitive Niosomes Loaded with Ibuprofen in Acute and Chronic Models of Pain.** Marzoli F, Marianecchi C, Rinaldi F, Passeri D, Rossi M, **Minosi P**, Carafa M, Pieretti S. *Pharmaceutics*. 2019, 1;11(2) 62. IF: 6.32.
- **Design, synthesis and biological profile of mixed opioid agonist/N-VGCC blocker peptides.** Stefanucci A, Novellino E, Macedonio G, Dimmito MP, Mirzaie S, Caldas Cardoso F, Lewis R, Zádor F, Erdei AI., Dvorácskó S, Tömböly C, Benyhe S, Pieretti S, **Minosi P** and Mollica A. *New Journal of Chemistry*. 2018, 42(8). IF: 3.59.
- **Opioid receptor activity and analgesic potency of DPDPE peptide analogues containing a xylene bridge.** Stefanucci A, Novellino E, Mirzaie S, Macedonio G, Pieretti S, **Minosi P**, Szűcs E, Erdei AI, Zádor F, Benyhe S, Mollica A. *ACS Med. Chem. Lett*. 2017, 8, 4, 449–454. IF: 3.68.
- **Gender differences in pain and its relief.** Pieretti S, Di Giannuario A, Di Giovannandrea R, Marzoli F, Piccaro G, **Minosi P** and Aloisi AM. *Ann Ist Super Sanità*. 2016;52(2):184-9. IF: 1.66.

Poster and Conference presentations

- **A novel identification system for potentially counterfeit medical devices based on the visual analysis through evaluation sheet.** Minosi P, Pieretti S, Marletta M. **Poster** 40° Congresso Nazionale SIF. SIF - SOCIETÀ ITALIANA DI FARMACOLOGIA, 9-13 Marzo 2021. Pharmadvances Vol. 3 (No. 1) 218; 2021.
- **Discovery of Orexant and Anorexant Agents with Indazole Scaffold Endowed with Peripheral Antiedema Activity.** Minosi P, Dimmito MP, Stefanucci A, Pieretti S, Mollica A. **Poster** 40° Congresso Nazionale SIF. SIF - SOCIETÀ ITALIANA DI FARMACOLOGIA, 9-13 Marzo 2021. Pharmadvances Vol. 3 (No. 1) 217; 2021.
- **Pharmacological activities of plant-derived opioid peptides rubiscolin-6, soymorphin-6 and their c-terminal amide derivatives.** Minosi P, Dimmito MP, Stefanucci A, Sturaro C, Calò G, Pieretti S, Mollica A. **Poster vincitore della sessione poster**, 40° Congresso Nazionale SIF. SIF - SOCIETÀ ITALIANA DI FARMACOLOGIA, 9-13 Marzo 2021. Pharmadvances Vol. 3 (No. 1) 216; 2021.
- **pH-sensitive niosomes and liposomes: Effects on inflammation and pain in murine models.** Minosi P, Rinaldi F, Hanieh PN, Marianecchi C, Marzoli F, Ciarlo L, Carafa M and Pieretti S. **Presentazione orale** al Congresso Nanoinnovation2020, Roma 15-18 Settembre 2020.
- **Long lasting inflammatory effects of ammonium glycyrrhizinate: an integrated study of pharmacology and computational analysis".** Raucci F, Minosi P, Di Giannuario A, Chini MG, De Vita S, Bifulco G, Maione F, Mascolo N, Pieretti S. **Poster vincitore della sessione poster**, 39° Congresso Nazionale SIF. SIF - SOCIETÀ ITALIANA DI FARMACOLOGIA, Firenze, 20-23 Novembre 2019.
- **Long-lasting antinociceptive effects of Ammonium Glychirrizinate in mice.** Minosi P, Raucci F, Di Giannuario A, Chini MG, De Vita S, Bifulco G, Maione F, Mascolo N, Pieretti S. **Poster** 39° Congresso Nazionale SIF. SIF - SOCIETÀ ITALIANA DI FARMACOLOGIA, Firenze, 20-23 Novembre 2019.

- **Glycyrrhizic Acid attenuates the cytotoxicity induced by high glucose in neuroblastoma cell line.** Ciarlo L, Marzoli F, **Minosi P**, Di Giannuario A, Matarrese P and Pieretti S. **Poster** 39° Congresso Nazionale SIF. SIF - SOCIETÀ ITALIANA DI FARMACOLOGIA, Firenze, 20-23 Novembre 2019.
- **The arylpiperazinylalkyl pyridazinone ET1 as a potent antinociceptive agent after oral administration in mice.** Marzoli F, Maione F, Colucci M, **Minosi P**, Di Giannuario A, Raucci F, Mascolo N, Giovannoni MP and Pieretti S. **Poster** 39° Congresso Nazionale SIF. SIF - SOCIETÀ ITALIANA DI FARMACOLOGIA, Firenze, 20-23 Novembre 2019.
- **Opportunity to Analyze Laboratory Mice Behavior by Tracking Systems based on UHF RFID Technology: pros and cons.** Cirillo E, **Minosi P**, Marzoli F, Sergi I, Colella R, Patrono L, Catarinucci L, Pieretti S. **Presentazione orale** 10th Annual 2019 IEEE International Conference on RFID Technology and Applications RFID-TA 2019, Pisa 25-27 Settembre 2019.
- **Association of antioxidant nutraceuticals and acetaminophen (paracetamol): Friend or foe?.** **Minosi P**, Aiello P, Peluso I e Palmery M. **Poster** 2nd Conference on Innovations in Food Science & Human Nutrition (IFHN-2019). 12 – 14 Settembre 2019, Londra (Crowne Plaza London - Heathrow).
- **Flavonoids-statins interactions.** Aiello P, **Minosi P**, Ilaria P e Palmery M. **Poster** 2nd Conference on Innovations in Food Science & Human Nutrition(IFHN-2019). 12 – 14 Settembre 2019, Londra (Crowne Plaza London - Heathrow).
- **Curcumin-loaded Poly (d,l-lactide-co-glycolide) nanovesicles induce antinociceptive effects after local administration in mice.** Ciarlo L, Marzoli F, **Minosi P**, Di Giannuario A and Pieretti S. **Poster** NANOMEDICINE ROME 2018, Istituto Superiore di Sanità (Roma), 18-20 Giugno 2018.
- **Enhanced antinociceptive and anti-inflammatory effects of ibuprofen encapsulated in niosomal vesicles.** Marzoli F, **Minosi P**, Ciarlo L, Di Giannuario A, Carafa M, Marianecchi C, Pieretti S. **Poster vincitore della sessione poster** NANOMEDICINE ROME 2018, Istituto Superiore di Sanità (Roma), 18-20 Giugno 2018.

- **Prolongation of local pain insensitivity by anesthetic lidocaine loaded pH-TW20 Gly niosomes: effects on nociception in murine models of pain.** **Minosi P**, Marzoli F, Ciarlo L, Di Giannuario A, Carafa M, Rinaldi F, Pieretti S. **Poster NANOMEDICINE ROME 2018**, Istituto Superiore di Sanità (Roma), 18-20 Giugno 2018.
- **Antinociceptive effects of Curcumin-loaded PLGA vesicles.** Di Giovannandrea R, Marzoli F, **Minosi P**, Di Giannuario A, Pieretti S. **Poster NANOMEDICINE VITERBO 2016** a Viterbo, 21-23 Settembre 2016- University of Tuscia.

ACKNOWLEDGEMENTS

I would like to extend my thanks to many people who have so generously contributed in the journey of my PhD.

I am sincerely thankful to my Director of the PhD Program Prof. Maura Palmery for her support and advice throughout my PhD studies. A special thanks to my Academic Tutor, Prof. Roberta Lattanzi for her constant presence.

Special mention goes to my enthusiastic supervisor, Dr. Stefano Pieretti. My PhD has been an amazing experience and I thank Dr. Pieretti wholeheartedly, not only for his tremendous academic support, but also for giving me so many wonderful opportunities to grow up as a budding researcher under his supervision. I consider it an honor to work with him and with Dr. Di Giannuario Amalia.

Profound gratitude goes to Prof. Adriano Mollica and Dr. Azzurra Stefanucci of the Department of Pharmacy, University of Chieti-Pescara “G. d’Annunzio”, Prof. Francesco Maione and Dr. Federica Raucci of the Department of Pharmacy, University of Naples Federico II, Prof. Girolamo Calò of the Department of Medical Sciences, Section of Pharmacology, University of Ferrara, Italy and Prof. Anna Maria Aloisi of the Department of Medicine, Surgery and Neuroscience, University of Siena. I am grateful to them for the great and consistent contribution they have given to this PhD thesis work.

Therefore finally, but by no means least, thanks go to my husband, parents and my family for almost unbelievable support. They are the most important people in my world, my support and my guidance.

My time at Istituto Superiore di Sanità and at Sapienza University was made enjoyable in large part due to many friends and groups that became a part of my life.

Thank you all.